Steinar Danielsen

Electric Traction Power System Stability

Low-frequency interaction between advanced rail vehicles and a rotary frequency converter

Thesis for the degree of Philosophiae Doctor

Trondheim, April 2010

Norwegian University of Science and Technology
Faculty of Information Technology, Mathematics and Electrical Engineering
Department of Electric Power Engineering

NTNU
Norwegian University of Science and Technology

NTNU
Norwegian University of Science and Technology

Thesis for the degree of Philosophiae Doctor

Faculty of Information Technology, Mathematics and Electrical Engineering
Department of Electric Power Engineering

ISBN 978-82-471-2068-2 (printed ver.)
ISBN 978-82-471-2069-9 (electronic ver.)
ISSN 1503-8181

Doctoral theses at NTNU, 2010:56

Printed by NTNU-trykk

Abstract

Low-frequency instability in AC electric traction power systems has come to be a concern in recent years. Power oscillations in the range of 10-30 % of the system's fundamental frequency are reported from all over the world after the introduction of large numbers of rail vehicles being equipped with modern power electronic traction chain solutions. The disturbance of rail traffic has been especially noticeable in Norway, where the railway power supply contains rotary frequency converters which show a poorly damped electromechanical eigenfrequency of approximately 1.6 Hz.

The overall goal of the present thesis is to acquire knowledge concerning stability in the traction power system, focusing mainly on the low-frequency oscillations and interaction between electric rail vehicles and this particular rotary converter. An important part of this work is to establish a connection between the fields of both power electronics and power system analysis.

The problem is approached by the development and study of basic differential equations and characteristics for the two main dynamical components in the system – the synchronous-synchronous rotary frequency converter and the advanced electric rail vehicle. These simplified models are used to obtain a better understanding of the dynamical behaviour of a full converter-vehicle simulation model which is studied by the use of both time simulations and linear analysis (eigenvalues and frequency responses). The developed vehicle model is open and independent of any specific vehicle manufacturer. The model's basic validity however is investigated by comparison with measurements performed on a real-life electric rail vehicle.

This thesis focuses on the small-signal behaviour of the power system in the mentioned low-frequency range. Detailed analytical investigations of the complex single-phase AC power system is difficult, thus most of the analytical studies in present thesis focusing on the active power oscillations are carried out by several simplifications. The largest simplification is the assumption of the AC voltage and current in phase and only considering their amplitude values. This is useful for initial understanding, but is insufficient when phase angles are to be taken into account.

Therefore the simplified analytical considerations by principle are compared with the complete AC power system model in a rotating reference frame as commonly utilised for large power systems. However, for this full simulation model it has been found that traditional power system simplifications by use of standard RMS-values are insufficient in correctly representing the instability phenomenon compared with a more realistic

instantaneous value model. Fast network dynamics and vehicle current controller which are commonly neglected, have to be included as well and consequently an enhanced RMS model is proposed.

Two characteristics of the state-of-the-art electric rail vehicle are found to be of importantance. First, a control objective of the vehicle is to keep the power consumption constant and independent of the power supply conditions. This constant power load characteristic is shown to result in a positive feedback loop and basically violate a stability criterion derived for the rotary converter. Second, the time variance of a single-phase system results in several filter time constants giving dynamics in the low-frequency range. Of particular importance is the DC-link voltage control loop. These dynamics might additionally reduce the stability margins.

This study's main contribution is as a foundation for further investigation into low-frequency traction power system stability, especially in regard to the open vehicle model that is developed and discussed. A further focus should be on an understanding of more of the aspects of the AC system interaction and how to include this in a feasible method for power system study, in which the inner and commonly hidden details of the complex components are included, although not specifically disclosed.

Acknowledgements

This report completes my work carried out over the latest four years at the Department of Electric Power Engineering at the Norwegian University of Science and Technology (NTNU) in Trondheim, Norway, and constitutes my doctoral thesis.

First, I would like to thank my main supervisor, Professor Olav Bjarte Fosso at NTNU, for, with patience, contributing with his experience and knowledge. I am also grateful to my co-supervisors, Professor Marta Molinas at NTNU and research scientist Trond Toftevaag at SINTEF Energy Research, for their never ending enthusiasm and turning my 'cannot's into 'can do's.

Second, I want to thank the National Norwegian Rail Administration (Jernbaneverket (JBV)) for funding this PhD study. I appreciate the flexibility of Frode Johnsen and Christopher Schive in helping to coordinate my PhD work and regular work at JBV during these years. Hopefully, the present thesis will prove useful for the railway sector.

Third, there are three external persons without whose help this thesis would have been completely different. Through my contact with Dr. Markus Meyer at Emkamatik Gmbh in Switzerland, I received first-hand information about interaction problems in electric railways. I have also unquestionably benefitted a lot from my cooperation with Andreas Eisele at Bombardier Transportation in Switzerland in gaining a better understanding of real electric rail vehicles and investigating low-frequency instability. Thanks for all the discussions and nice 'stabilty parties' and walks. Additionally, I wish to especially thank Lars Lindquist at STRI AB in Sweden for his very valuable help with developing models in SIMPOW.

Two months during the winther of 2009 I spent at the Institute for Electrical Power Engineering and Power Electronics at Ruhr-Universität Bochum in Germany. Many thanks go to Professor Andreas Steimel and Carsten Heising, who cared well for me this time. My stay in Bochum definitely had a positive influence on my work.

I have been happy to have good colleagues at both NTNU and JBV. I especially want to thank Jon Are Suul and Emil Johansson at NTNU and Bjørn Ukkestad at JBV for their valuable discussions. I also want to thank the persons at the traction power system dispatching centres for good cooperation during the real-life tests.

Additionally, I have been lucky to learn to know and benefit from experts in my technical field. I want to thank Dr. Jonas Persson at Vattenfall in Sweden, who always

had time to discuss different problems. Further, I want to thank Lars Buhrkall from Denmark for the very enjoyable hours together watching his ‘compatibility monitor’ under several tests, valuable discussions and good cooperation in the LFSTAB project. I would also like to thank all who have answered and discussed my questions and suggestions. Among them are Dr. Stefan Menth at Emkamatik in Switzerland, Markus Pröls, Dr. Bernhard Strobl and Ingo Kosanke at Siemens in Germany, Johann Galic and Magnus Bergman at Bombardier Transportation in Sweden, Urs Ehrler at ABB in Switzerland and Edward Friman at Banverket/STRI AB in Sweden.

Finally, I want to thank Sigrid Aarbakke for supporting me through these four years. With this completion, our life can proceed. This book is for you ;-)

Steinar Danielsen

Table of contents

1 Introduction

This chapter introduces this thesis within the topic of traction power system stability. Based on the background of the work and a review of previous research, goals and research questions are established. The outline of the report is concluded with main contributions and a publication overview.

1.1 Background

Both railway systems and power systems are complex, and there are many factors which influence each other. The challenge is to make all the systems' components interact without operational disturbance. Commonly, the phrase 'electrical system compatibility' (ESC) is used to describe how electric components interact with each other in this complex system (Schmidt, et al. [154]). This system includes the electric rail vehicles (locomotives), the power supply infrastructure and the electrical telecommunication, interlocking and signalling infrastructure.

Experience has demonstrated that introducing a new electric rail vehicle into an existing railway infrastructure often leads to new and unexpected issues since the vehicle and the infrastructure may be incompatible. Many projects have experienced so-called teething trouble when the commercial operation of a new vehicle is scheduled.

One such issue is low-frequency power oscillations, which have taken place at several locations worldwide and may lead to system instability. The situation is precarious in Norway where standard European rail vehicles introduced into the railway system often do not comply with the existing power supply. A simplified sketch of the worst case Norwegian traction power system is given in Figure 1-1.

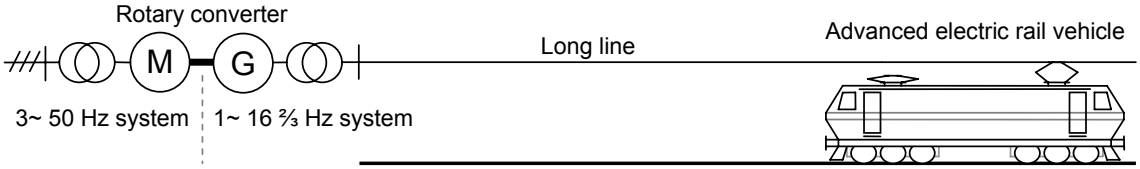

Figure 1-1: Sketch of a simple electric traction power system with a rotary converter and an advanced electric rail vehicle

Electric trains in Norway are mainly supplied via the overhead contact line from frequency converters along the railway lines. These converters are needed as the railway operates at a different power frequency than the main public grid. A long distance between the converter stations results in a relatively weak grid. Several of these

converters are rotating electric machines that show a poorly damped eigenfrequency in the range of 1.6 Hz. The Swedish electric traction power system shares this characteristic, which differs though from the typical railway power supply in continental Europe since this type of frequency converters is typically not used.

Lack of compatibility between rail vehicles and these poorly damped rotary converters may have several unfortunate consequences (Toftevaag and Pálsson [178]). As mentioned, the oscillations are a challenge for new rail vehicles and stable operation may be obstructed; the vehicles may not function properly or not operate at all. Operational problems and traffic delays are expensive in terms of time and cost for both the vehicle manufacturer and train operator, with the people who suffer the most in the end being the train passengers and taxpayers. Additionally, the infrastructure manager fears extra mechanical stress and damage to the rotary converters. Experience has shown that low-frequency oscillations also cause flickers given by voltage fluctuations in the main public grid. The first occurrence of this happened in 1998 and was largely exposed in the media (e.g. Abelsen, et al. [4]).

As an example, Figure 1-2 shows the annual delays caused by power system problems in a limited part of the Norwegian traction power system when new vehicles were gradually introduced from 2002 (Danielsen and Toftevaag [56]). The situation was improved by changes in the system.

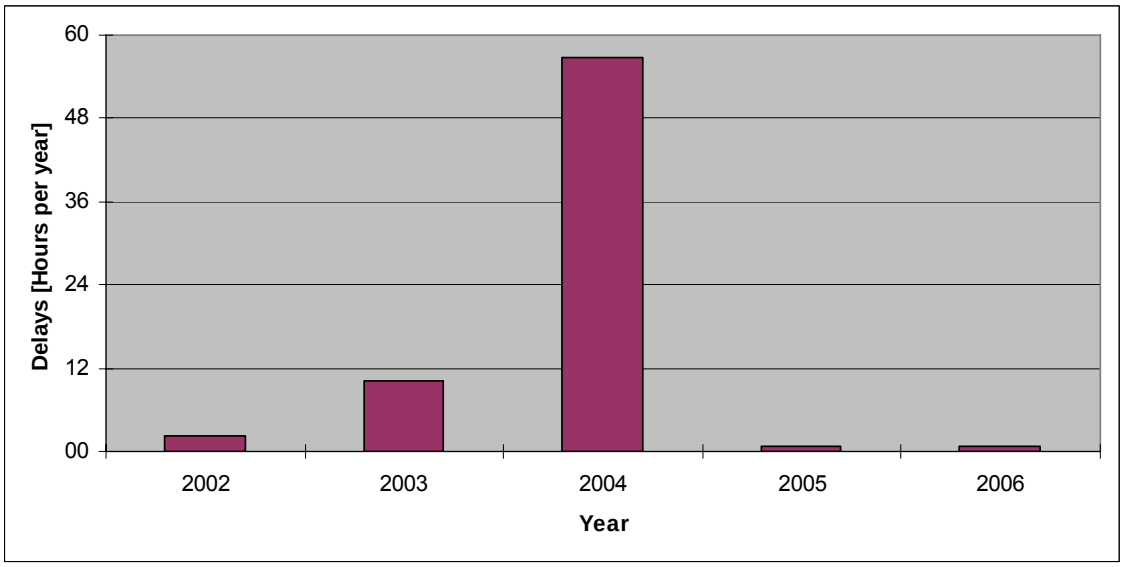

Figure 1-2: Annual delays caused by power system problems for selected years in the railway system.

New rail vehicles have become more and more technically optimised and advanced. Hence, they have often gotten the description of being ‘advanced electric rail vehicles’, though the development of new technical solutions may result in system incompatibility. In general, wide system compatibility is important due to the requirement of interoperability and cross-border rail traffic (Hill [82]). In other words,

one vehicle should be able to operate in several different countries that may contain different infrastructure characteristics.

The trains within the railway network are operated by different companies that own or rent the rail vehicles. A new rail vehicle has to be declared compatible to the existing traction power system before being put into operation. In Norway, this declaration is given by the Norwegian National Rail Administration (Jernbaneverket) which plans, builds, maintains, owns and manages the state railway infrastructure. Therefore, Jernbaneverket is also responsible for the power supply's condition. The final acceptance of the vehicle is given by the Norwegian Railway Inspectorate (Statens Jernbanetilsyn) based on this declaration.

Nevertheless, detailed information about how each new rail vehicle is designed and works internally is not given to Jernbaneverket during such a compatibility investigation. Instead, the focus is on the characteristics of the interface between the vehicle and the railway system. For low-frequency dynamics, no such interface characterisation has been commonly agreed upon, but low-frequency compatibility phenomena are still young and need more investigation and knowledge.

In order to understand the physical relationship regarding the experienced low-frequency instability and in order to be able to take action to improve the power supply conditions, Jernbaneverket decided in 2004 to support a deeper study through a PhD work.

1.2 Previous research

Even if the low-frequency oscillation issue in the railway context must be characterised as young, some research has already been published and is well-known among the experts' community. Many of these publications describe the issue from a practical point of view based on experiences from real life. These experiences are also collected and shortly described within a different context in Chapter 2. For the reader who is not familiar with traction power system stability, it might be of value to read that chapter before continuing through this section about previous research.

The first observations of heavy low-frequency oscillations in the Norwegian rotary converters caused by rail vehicles were made when introducing the NSB locomotive class El 18 back in 1996. Investigations, measurements, modelling and simulation studies have been carried out internally by the infrastructure side at Jernbaneverket in cooperation with SINTEF Energy Research, and a summary of the knowledge gained was published by Toftevaag and Pálsson [178]. The rotary converters used were found to have a poorly damped electromechanical eigenfrequency of approximately 1.6 Hz. This poor damping was explained by the absence of explicit damper windings in the converter's synchronous motor's rotor. One excitation source for these oscillations was found to be the rail vehicle's adhesion controller that on wet or slippery rails may cause the vehicle power to rapidly change in order to operate on the maximum friction limit between rail and wheel. Unfortunately, these power changes coincided with the rotary

converter's eigenfrequency, i.e., resulting in forced oscillations at a frequency where the damping is weak.

Over the past 10 years, these experiences and the emerging questions which always follow have been the source for several student master projects at the Norwegian University of Science and Technology. Garten [70] and Aschenbrenner [13] modelled the rotary converter. Stensby [168] studied and developed a power system stabiliser (PSS) together with different rotary converter excitation systems. Johannessen and Bruu [91] studied the phenomenon of self excitation effects between the poorly damped rotary converter and the series capacitors used in order to compensate the overhead contact line reactance.

On the vehicle side, work has also been conducted in order to make the advanced electric rail vehicles function within the characteristic Norwegian railway infrastructure. Meyer and Ljunggren [121] reported that there may be some interaction phenomena between the rotary converter and the electric vehicle control system, as in such a weak network they form a noticeable closed feedback loop. The powerful Iron ORE locomotive used in the Norwegian-Swedish line between Narvik and Kiruna was reported to have acted with a slight damping on the rotary converters' oscillations.

In as late as 2009, it was reported that these weak and poorly damped network characteristics present a large challenge when introducing new vehicles into the Norwegian and Swedish infrastructure (Kratz and Pawlak [105]). Some train manufacturers even bring new vehicles to Norway for pre-testing and experience collection before completion and acceptance testing in order to improve and ensure compatibility (Kaeser, et al. [99]). However, the detailed results from this recent research have not yet been published.

The field of electrical system compatibility is large and was the main impetus behind the European research project ESCARV – Electrical System Compatibility for Advanced Rail Vehicles (Schmidt, et al. [154] and Henning, et al. [81]). Meyer [119] gives an overview of all the various electrical compatibility phenomena that may result in interaction problems between an AC rail vehicle and the infrastructure. This spans from DC currents, slow transients, low-frequency oscillations, active and reactive power control and limitations, electrical resonance instability, overvoltages due to harmonics, and the influence of electromagnetic fields on track circuits.

For that reason, one of the stability issues within the ESCARV project was over low-frequency power oscillations, though electrical resonances between inductances and capacitances and the excitation of those received more focus. This instability can occur at frequencies higher than typically three times the system's fundamental frequencies. A reasonable explanation for this focus is that these oscillations were better known due to specific accidents, e.g. the 165-Hz instability case in Switzerland as reported by Meyer and Schöning [122].

The ESCARV project further focused on the interface between the rail vehicles and the power supply (Hill [82]), and the electrical resonance phenomenon even got its own stability criterion – the input admittance criterion as mathematically proven by Paice and Meyer [135]. Admittance represents the transfer function from a voltage disturbance to the current output for an electric component. The criterion guarantees a stable system if the real part of the input admittance is positive at frequencies where the imaginary part is zero. That means that a vehicle is not allowed to have a negative input admittance (i.e., inject current) at power supply resonance frequencies.

One benefit of such an interface criterion is that it is not necessary to know the details of the technical solution inside the rail vehicle in order to perform compatibility studies. As a result, the vehicle manufacturer can still keep its design secrets. A methodology for a stability study was presented by Lörtscher, et al. [114]. This methodology has been developed in such a way that it is possible to measure both infrastructure and vehicle frequency responses relatively simply (Meyer and van-Alphen [125]).

This input admittance criterion has been a template when the low-frequency qualities of rail vehicles has later been studied. For a long time due to non-linear behaviour, no methodology for investigation except time domain simulations has been established (Meyer [118]). The challenge then is to study the stability and design the system with a reasonable stability criterion that is not too conservative (Sudhoff et al. [93]).

Pröls and Strobl [148] further developed the input admittance criterion in their study of low-frequency stability together with the Nyquist criterion known from general control theory. The approach was based on so-called harmonic transfer functions (HTF) that described couplings among different frequencies as shown by Möllerstedt [130]. For non-linear and time-variant systems, these frequency couplings may have to be considered. The large advantage of this approach is claimed to be an extensive reduction in the amount of time taken to perform stability studies when each vehicle is modelled by transfer functions instead of performing time consuming time domain simulations.

As a part of the explanation of the 5-Hz oscillation and instability in Zürich (Switzerland) which occurred, Menth and Meyer [116] proposed another approach. An advanced rail vehicle is explained to have dynamics below the fundamental system frequency due to the power time variance that is inherent in all single-phase systems. This time variance limits the bandwidth of the vehicle's active power control. The study showed that it was sufficient to model the power supply system as an ideal voltage source and the network impedance was mainly determined by the line impedance and short circuit impedance of the substation. It was also claimed that a situation with more than one vehicle could be modelled by multiplying the line current from one vehicle so that the voltage drop over the network impedance of n vehicles is n times the voltage drop caused by one single vehicle.

These low-frequency dynamics by Menth and Meyer [116] are proposed to be represented by four transfer functions in a two-axis (d and q) system, such as is commonly considered for three-phase systems with the methodology summarised by

Harnefors [72]. Harnefors, et al. [74] propose how this two-axis approach can be used for stability investigations of a three-phase voltage source converter (VSC) based on input admittance considerations. The references [116] and [74] both represent an important input for present thesis, especially when it comes to development of the vehicle model in Chapter 5 and the input admittance considerations in Chapter 8.

Debruyne [60] reports on a 3-Hz oscillation and instability in the railway area of Washington, DC in the US. The reason for this instability is explained as the negative dynamic impedance the rail vehicle represents in the power system when the vehicle aims to keep the power demand constant. That is, when the line voltage decreases, the vehicle line current has to increase correspondingly in order to keep their product constant. As a solution, a simple but effective dynamic impedance compensation algorithm was implemented for all rail vehicles in the network and stability was achieved. This compensation ensured that the sign of the current change always equals the sign of the voltage change at given frequencies, i.e., making the vehicle act like a passive component such as a resistor at the oscillation frequency.

Most published research in advanced rail vehicle control concerns the motor side in favour of the line side. Consequently the there are only a few detailed publications describing the vehicle in this low-frequency phenomena in existence. Unfortunately, many of the publications reporting on practical experience do not include basic detailed theoretical explanations which could help readers who are inexperienced in the field to get started working on it. None of the referred publications reports a stability analysis of the complete vehicle and rotary converter system and explains why this system is vulnerable to instability. Furthermore, the publications proposing input admittance considerations for low-frequency instability in railway AC systems are short in interpretation and examples.

1.3 Scope of work

1.3.1 General

The low-frequency instability may be investigated in several ways. There are two main groups of engineers working in this field who have different backgrounds and will thus choose different approaches. The rail vehicle is designed by engineers with a background in the field of power electronics, who have deep insight into electric motor drives. The infrastructure manager's engineers who operate the power system may have an overview of the system, but they do not have a detailed knowledge of all the system's components. As a consequence, the exchange of information and an understanding of each other's publications may prove to be difficult.

1.3.2 Objective

The overall goal of this PhD study is to obtain knowledge about the stability of traction power systems, with a primary focus put on low-frequency power oscillations and interaction between electric rail vehicles and the rotary frequency converter. An important part of the work will be to establish a connection between the field of power

electronics and the field of power system analysis. Based on these studies and the acquired knowledge, a concept or methodology for an integrated stability analysis of traction power systems should be investigated. Through the use of this methodology, possible remedies to improve or stabilise the power system will be studied.

1.3.3 Research questions

Based on this background, previous research and the general problem formulation mentioned above, the following research questions may be established:

- Is it possible to use traditional power system analysis tools and methods to study the low-frequency instability in traction power systems?
- How and what influences the synchronous-synchronous rotary frequency converter's low-frequency electromechanical swing equation?
- How does an advanced rail vehicle work in view of the observed low-frequency instability?
- How do input admittance considerations work in terms of low-frequency instability?

These questions will be discussed in Section 9.2.

1.3.4 Limitations

This study is to be carried out on power system analysis level. A detailed study of the various power system components such as the synchronous machines and rail vehicles is not the main topic. However, some detailed knowledge with regard to some of these components is required, especially in fulfilling the goal of increasing knowledge about rail vehicles.

Furthermore, a focus has been put on the interaction between the rotary converter and the rail vehicle. Investigations on remedies for the rotary converter side, e.g. power system stabilisers are leaved out, as this is a topic for another internal project to be carried out with the cooperation of both the Norwegian and Swedish National Rail Administrations.

This thesis also focuses on the field of small-signal stability, i.e., the inherent attributes of the entire dynamical power system that are normally studied and described by use of small-signal linear methods such as eigenvalue analysis. The analyses are also limited to phenomena in the low-frequency range, i.e., below the system's fundamental frequency. Due to non-linearities and non-continuous controllers in the power supply and rail vehicles, compatibility issues related to larger disturbances may also occur. Yet before treating these phenomena, sufficient small-signal stability has to be ensured.

1.3.5 Approach

The present study is a combination of theoretical derivation, modelling, simulation, measurements and experience from real life. On every topic, there has been a way of working chosen that best illustrates the point with less effort. Often, simplified expressions which describe the points in an easily understandable way are established instead of using detailed, complex and fully correct expressions which make the topic more difficult to interpret.

The practical experience originates from measurements and observations on real-life vehicles. The author of the present thesis has participated at 17 days/nights of testing in the role of test leader, power supply organiser, project staff or observer. Several of the tests are connected to the LFSTAB (Low-Frequency STABility) project, a joint venture between Bombardier Transportation and the Norwegian and Swedish National Rail Administrations.

1.4 Main contributions

The main contributions of this thesis are:

- A collection and short presentation of reported traction power system instability events and stability studies published during recent years. These events are categorised in view of traditional power system stability classification. Such a review has not been published before and is given in Chapter 2.

- The development and study of a second-order electromechanical swing equation for a synchronous-synchronous rotary frequency converter. This simplified model describes the main characteristics of the rotary converter's low-frequency oscillations, and comparisons to more detailed models and measurements are performed. Publication attempted in [59] and reported in Chapter 3

- The development, evaluation and stability analysis of advanced electric rail vehicle models in view of their low-frequency behaviour. The detailed development and description of the line-side of a rail vehicle is based on fragments found in the available literature which is compiled into a complete model. Such a comparison between a single-phase power electronic converter in instantaneous value mode and RMS mode has not previously been found. This is published in [52] and reported in Chapter 5.

- An analytical development and study of the basics of the advanced electric rail vehicle's low-frequency DC-link voltage control eigenmode. The results are compared with the detailed vehicle model by use of small-signal stability analysis. Detailed information about this phenomenon is not found published before. Partly published in [54] and reported in Chapter 6.

- Study of the low-frequency interaction between an advanced rail vehicle and the power supply with a rotary converter, by use of both time simulations and small-

signal stability analysis (linear analysis). Models of the two components, respectively, are merged into one common system. Such a study is not reported before and is partly published in [58]/[57] and [53] and reported in Chapter 7.

- The application of the analytically derived simplified second-order rotary converter's swing equation and rail vehicle's DC-link voltage control mode models in an input admittance and output impedance consideration for low-frequency dynamics. Such a qualitative explanation of one possible reason for the low-frequency instability phenomena experienced in traction power systems has not been reported before. Partly published in [54]/[55] and [34] and reported in Chapter 8.

1.5 Outline of the thesis

The outline of the thesis is as follows:

- Chapter 1 introduces this thesis within the topic of traction power system stability. Based on the background of the work and a review of previous research, goals and research questions are established. An outline of the report is concluded with main contributions and a publication overview.

- Chapter 2 gives an introduction to electric traction power supply, electric rail vehicles and power system stability that might prove useful to read before continuing in this thesis. Different instability events and stability studies reported from traction power systems are categorised according to traditional power system instability classifications.

- Chapter 3 presents the development of a second-order swing equation for a synchronous-synchronous rotary converter which describes the main characteristic of the converter oscillations that have been experienced. The results from this equation are compared with measurements and more detailed higher-order models. A stability criterion in view of single-phase load voltage dependency is proposed.

- Chapter 4 explains various concepts of power system modelling that will be compared in the stability studies later in this thesis. An enhanced RMS mode is proposed as a compromise between instantaneous value modelling and standard RMS mode modelling.

- Chapter 5 presents a complex and fully developed model of the line-side part of an advanced electric rail vehicle. Step-by-step, each controller is explained and a comparison between time-variant instantaneous-value modelling and time-invariant RMS modelling is investigated. The complete models are evaluated in view of the dynamics observed by a load step response and a long line stability test.

- Chapter 6 develops the main characteristics of the low-frequency eigenmode for the DC-link voltage control of an advanced electric rail vehicle. A simple second-order model is compared with the fully developed model of the vehicle and measurements on a real-life vehicle. The eigenmode's sensitivity to vehicle parameters and operating point is studied.

- Chapter 7 chapter reports on a study of the interaction between the rotary converter and the developed advanced rail vehicle model conducted by use of traditional power system stability investigations, i.e., linear analysis and time simulations. Various methods for stability improvement are investigated and a reason for the observed instability is proposed. The main principles are compared with measurements on a real rail vehicle.

- Chapter 8 introduces considerations in the frequency domain of system stability based on input admittance of the rail vehicle and output impedance of the rotary converter. Simplified analytical frequency responses are discussed in view of a derived stability criterion. Input admittances of the full vehicle simulation models are also calculated and discussed.

- Chapter 9 includes a discussion of the results obtained in the previous chapters and presents answers to the research questions, conclusions and suggestions for further work.

The majority of the chapters contain a discussion and conclusion of the work performed and the results gained in each respective chapter. An overall discussion and conclusion of the work in this thesis is given in Chapter 9.

In order to support the understanding of modelling and stability study carried out in this thesis, introduction to linear analysis is given in Appendix C.

1.6 List of publications

Parts of the work reported in this thesis have been described in the following publications (listed chronologically):

Journal paper with peer review:

[52] **S. Danielsen,** O. B. Fosso, M. Molinas, J. A. Suul and T. Toftevaag, Simplified models of a single-phase power electronic inverter for railway power system stability analysis – development and evaluation, *Electric Power System Research*. 80 (2), pp. 204-214, 2010.

International conference papers presented:

[56] **S. Danielsen** and T. Toftevaag, Experiences with respect to low frequency instability from the operation of advanced electric rail vehicles in a traction

power system with rotary converters. *MET2007 8th International Conference 'Drives and Supply Systems for Modern Electric Traction'*. Warsaw, Poland, pp. 51-57, 2007.

[58] **S. Danielsen**, T. Toftevaag and O. B. Fosso, Application of linear analysis in traction power system stability studies. *Computers in Railways XI: Computer System Design and Operation in the Railway and Other Transit Systems*. Toledo, Spain, pp. 401-410, 2008.

[53] **S. Danielsen**, O. B. Fosso and T. Toftevaag, Use of participation factors and parameter sensitivities in study and improvement of low-frequency stability between electrical rail vehicle and power supply. *13th European Conference on Power Electronics and Applications, 2009. EPE '09.* pp. 1-10, 2009.

[54] **S. Danielsen**, M. Molinas, T. Toftevaag and O. B. Fosso, Constant Power Load Characteristic's Influence On The Low-Frequency Interaction Between Advanced Electrical Rail Vehicle And Railway Traction Power Supply With Rotary Converters. *MET 2009 9th International Conference 'Modern Electric Traction'*. Gdansk, Poland, pp. 89-94, 2009.

The following papers have been submitted for publication:

[59] **S. Danielsen**, T. Toftevaag and O. B. Fosso, Swing equation for synchronous-synchronous rotary frequency converters. *Electric Power System Research*. Submitted in 2009.

[57] **S. Danielsen**, T. Toftevaag and O. B. Fosso, Application of linear analysis in railway power system stability studies, *Power Supply, Energy Management and Catenary Problems*. Invited for publication in 2009.

[55] **S. Danielsen**, M. Molinas, T. Toftevaag and O. B. Fosso, Constant Power Load Characteristic's Influence On The Low-Frequency Interaction Between Advanced Electrical Rail Vehicle And Railway Traction Power Supply With Rotary Converters. *Electromotion*. Invited for publication in 17 (1). 2010.

Additionally, the author of present thesis has contributed to the following publications:

[14] H. Y. Assefa, **S. Danielsen** and M. Molinas, Impact of PWM switching on modeling of low frequency power oscillation in electrical rail vehicle. *Power Electronics and Applications, 2009. EPE '09. 13th European Conference on*. pp. 1-9, 2009.

[80] C. Heising, M. Oettmeier, V. Staudt, A. Steimel and **S. Danielsen**, Improvement of Low-Frequency Railway Power System Stability Using an Advanced Multivariable Control Concept. *35th Annual Conference of the IEEE Industrial Electronics Society (IECON)*. Porto, Portugal, pp. 560-565, 2009.

[34] L. Buhrkall, **S. Danielsen**, A. Eisele, M. Bergman and J. Galic, Low-frequency oscillations in the Scandinavian railway power supply – Part 1: Basic considerations, *Elektrische Bahnen*. 108 (1-2) pp. 56-64, 2010

[35] L. Buhrkall, **S. Danielsen**, A. Eisele, M. Bergman and J. Galic, Low-frequency oscillations in the Scandinavian railway power supply – Part 2: Tests of traction units, *Elektrische Bahnen*. Accepted for publication in 108 (3), 2010

The author has also been invited to give the following presentations (title was free to choose):

[50] **S. Danielsen**, Vehicle related low frequency oscillations in the Norwegian rail traction power system with rotating converters. *Interaction Workshop 2006*. Thun, Switzerland, 2006.

[49] **S. Danielsen**, Low-frequency instability and oscillations in railway power systems. *Interaction Workshop 2009*. Thun, Switzerland, 2009.

The author has been a member of the CENELEC TC9 X Railway applications working group C11 '*Technical Criteria for Coordination: Power Supply / Rolling stock*' since fall 2009.

2 Electric traction power systems and stability

This chapter gives an introduction to electric traction power supply, electric rail vehicles and power system stability that could be useful to read before continuing in this thesis. Different instability events and stability studies reported from traction power systems are categorised according to traditional power system instability classifications.

2.1 Introduction

This chapter could be useful for the reader who is not familiar with electric traction power systems or power system stability. Additionally, the collection and review of work already performed and published within this narrow field may be valuable for those who want to go into deeper detail or perform further research in this area.

In this thesis, the term 'electric traction power system'[1] is used to describe the total system of components used for the generation/conversion, transmission and consumption of energy for electric railway transport. This is based on the definition of the 'electric traction system' as the 'railway electrical distribution system network used to provide energy for rollings stock' in EN50163 [40]. Kiessling, et al. [102] use the term 'traction power supply system' for the same system. The majority of energy consumed in the system is used for the propulsion of electric trains, i.e., for traction purposes, though, part of the energy is used for auxillaries in both the infrastructure and the trains (comfort and control equipment). It is not explicitly clear from the two referred definitions that the electric trains are included as a part of the traction system or not, but in this thesis they are.

An electric train may consist of one or several physical units. They may be locomotives which purpose is to move the rail cars that carry the train's load, i.e., passenger or freight wagons, although the cars can also be self-powered so that no locomotive is needed. These are often called electric single or multiple units. In this thesis, the term 'vehicle' is generally used to describe the mobile traction power consuming load. The power needed for the propulsion of the vehicle is focused on in this thesis.

Thus, the electric traction power system consists of the power supply (fixed installations) being the generation/conversion and transmission equipment, and the loads being the electric rail vehicles (rolling stock). Other loads in the system are not treated in this thesis.

[1] Though the word 'railway' may be more self-explanatory for the unexperienced reader than 'traction'.

2.2 Electric traction power supply

2.2.1 Electrification systems

Electrified railway systems have benefits in terms of both transport capacity and the environment compared with railway systems based on fossil energy carriers such as oil and coal. The history of railway electrification and its extensiveness is well documented in the technical literature, i.e., by Kiessling, et al. [102], Steimel [163] or Östlund [188]. In the context of this thesis, it can however be summarised that the Norwegian State Railway's first electrified railway was the line between Christiania (now Oslo) and Drammen that opened in 1923.

The electrical system chosen in Norway was an AC single-phase system which had a nominal voltage of 15 kV and a fundamental frequency of 16 ⅔ Hz. This system was considered to be better both economically and technically for conventional railways than the concurrent proposed DC systems. Austria, Germany, Sweden and Switzerland also chose to electrify their rail systems in the beginning of the 20th century, and selected the same system. The low fundamental frequency made it possible to both transfer power over longer distances by use of transformers and to maintain relatively easy control of the speed of the vehicle by the use of AC series commutator motors.

Due to the enormous progress in power electronics for vehicle control, countries that started to employ AC electrification typically after World War II chose the single-phase 25-kV 50-Hz system. Today, international standards allow only 25 kV 50 Hz or 3 kV DC for new systems, though existing 15-kV 16 ⅔-Hz systems are allowed to be extended.

An overhead contact line is commonly used for transferring the electric energy to the moving rail vehicle. Continuous and reliable transmission of energy from the contact line is ensured by a sliding current collector on the vehicle's roof. In order to close the current loop, the so-called return current flows through the vehicle's wheels and the rails back to the feeding or generation point. In some cases, the return current is collected into special return conductors by the use of booster transformers.

Figure 2-1 shows a principle sketch of the Norwegian national railway power supply. The development from 1923 to today and further plans can be vaguely seen along the horizontal axis. The details will be introduced in the following sections.

2.2.2 Centralised feeding

From the beginning, the electrified line between Christiania and Drammen was supplied via a high voltage transmission line from a hydro power station that generated directly on the railway's frequency (Blacutts, et al. [28]) as shown on the picture's left side. Such a direct generating system is still used today to a large extent in Austria, Germany and Switzerland where large power stations supply the rail network by use of 110 or 130-kV lines. This is called centralised feeding. Such a network may also be partially fed by a frequency conversion from the public 50-Hz network. The traction power

system is not necessarily synchronised to the rest of the country's main power system, and asynchronous-synchronous frequency converters can be used. The frequency-coupling between the main public network and the asynchronous railway network is said to be elastic and allows for an active power control through the converters by use of speed-droop characteristics. In order to avoid direct current in the asynchronous motor's rotors under low-load conditions, the reference frequency in the centralised railway power supply is changed to 16.70 Hz (Linder and Heinze [111]).

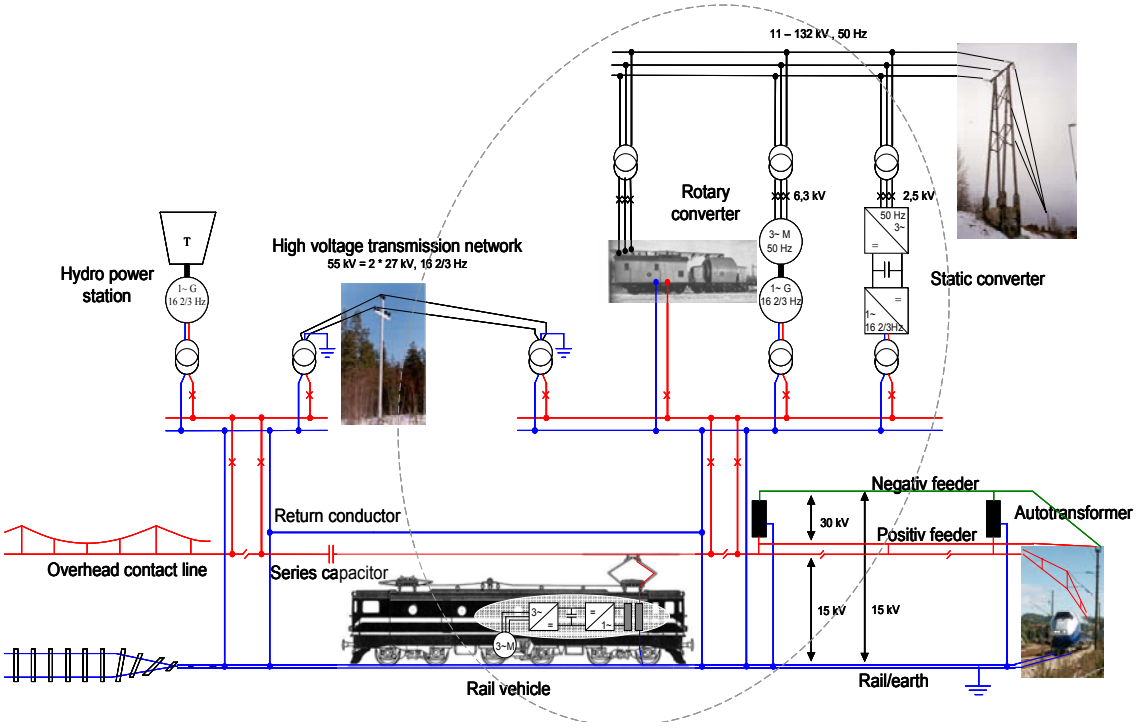

Figure 2-1: Principle sketch of the Norwegian electric traction power system and its supply.

2.2.3 Decentralised feeding

In Norway and Sweden, it was found to be beneficial to feed the railway from the overall interconnected three-phase 50-Hz public grid by use of rotating synchronous-synchronous converters. This is called decentralised feeding and includes a stiff frequency coupling between the two networks as the railway's fundamental frequency is exactly 50/3 = 16 ⅔ Hz. The majority of the energy consumed by rail traffic in Norway and Sweden today is converted from 50 Hz in a number of converter stations along the railway lines (Johnsen and Nyebak [95]).

The rotary converter can be found in the middle of the picture in Figure 2-1, and will be further explained and investigated in Section 2.2.4 and Chapter 3. To a lesser extent, synchronous-synchronous converters are also used in the eastern part of Germany which is not connected to the rest of the German traction power system. These converters have been studied by Biesenack [24] and Stoltze [169] in view of steady-state and dynamic operation, respectively.

In such a frequency-stiff system, the possibilities for controlling the power flow are limited to the use of the automatic voltage regulators on the converters' motor and generator. Active and reactive power flow is difficult to control independently of each other as both are influenced by the voltage amplitude.

On some lines, series capacitors have been used to compensate for the line's reactance, reducing the impedance between the feeding point and the train.

Over the last 20 years, static frequency converters have been put into service, sometimes in addition to, and sometimes as a replacement for rotary converters. The static converters will not be a further topic in this thesis.

In the future, Jernbaneverket is aiming at introducing the so-called autotransformer (AT) system for the long radial lines in Norway, as can be seen in the lower right corner of Figure 2-1. This system utilises a negative feeder with the potential of −15 kV in addition to the overhead contact line and positive feeder at +15 kV. The auto transformers located every ~10 km along the line make it possible to transfer power at 30 kV closer to the train, thus reducing the equivalent line impedance and voltage drop. The AT system is in use on some lines in Sweden (Bülund, et al. [39]), and is also being discussed for use in Germany (Zynovchenko, et al. [187]). Due to the high number of tunnels and cuttings in Norway, the Norwegian system will be designed differently in order to maintain a balanced impedance for the different phases (Varju [180]).

2.2.4 Rotary converters and their operation

The Norwegian and Swedish rotary synchronous-synchronous frequency converters are discrete motor-generator sets and are in present thesis referred to as rotary converters. They consist of one single-phase 16 ⅔-Hz synchronous generator (SG) that is driven directly by a three-phase 50-Hz synchronous motor (SM) as shown in Figure 2-2. The typical rating is 3-10 MVA per unit. Frequency conversion is obtained due to the ratio between the number of the machine's rotor poles which is 4/12 = 1/3. Both motor and generator are equipped with their respective excitation system that includes both an automatic voltage regulator (AVR) and DC or AC brushless field machines.

The rotary converters in Norway are located in converter stations along the electrified railway lines at a distance of 20 to 90 km apart, with two or three converter units frequently located at each station. The number of converters in service is adapted to the hourly variation of power demand dictated by the amount of train traffic. Most of the converter units are placed on rail carriages in order to simplify maintenance and adapting the capacity to the long-term power demand.

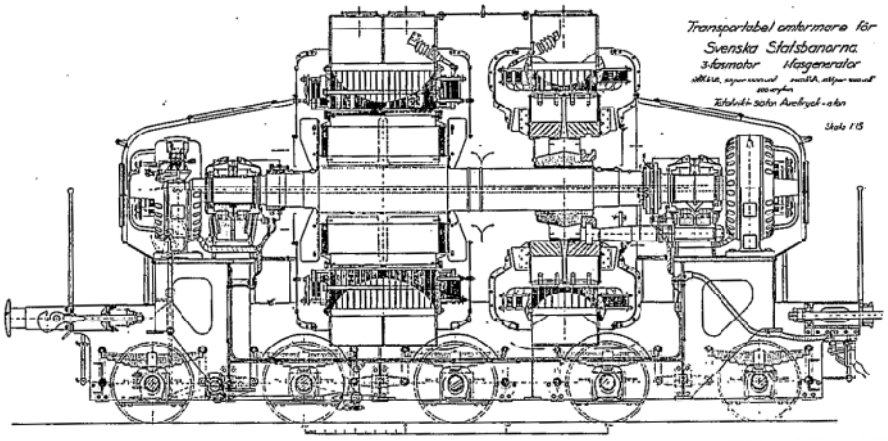

Figure 2-2: A drawing from Lundberg [113] of a transportable rotary converter with a synchronous motor (right) and a synchronous generator (left). In both ends of the shaft, there are corresponding field machines.

Such a rotary converter can be operated in three different modes:

- *Interconnected mode:* In normal operation, both three-phase utility grid and single-phase traction power systems are interconnected as shown in Figure 2-3. The power supply to one train is then supported by several converters in parallel.
- *Islanded mode:* The sectioning in the three-phase network and railway line maintenance frequently requires the overhead contact line to be sectioned. This causes the island operation of one converter (station) to directly feed the trains on the specific section. There is no connection between the single-phase generator and other generators as shown in Figure 1-1.
- *Reactive compensation mode:* A rotary converter may also be used as a synchronous condenser to support the single-phase voltage by the use of reactive power production without a three-phase power supply (Berggren [20]). However, it is seldomly used and is not in the focus of this work.

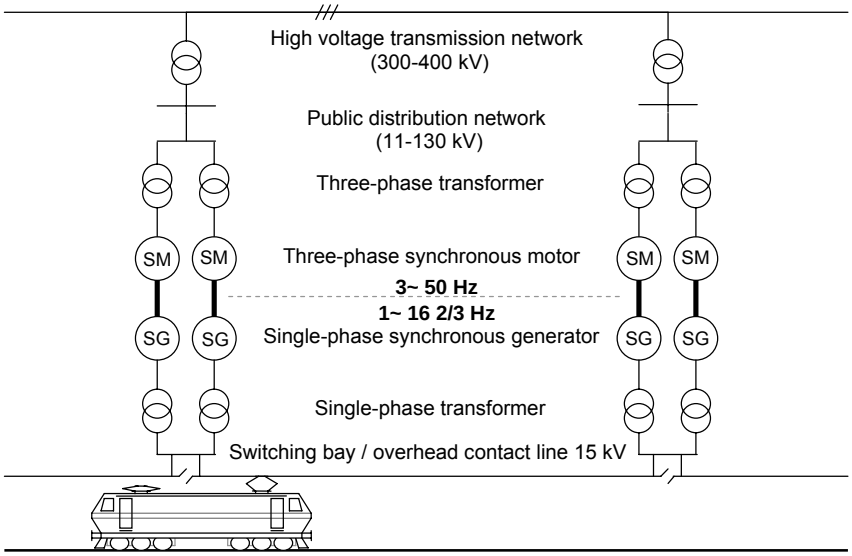

Figure 2-3: Single line diagram of a traction power system with rotary converters connected to the public utility grid.

The island operating mode as shown in Figure 1-1 is known to represent the most severe operating conditions regarding low-frequency instability (Danielsen and Toftevaag [56]). Hence, such conditions are focused on in this thesis. A reference case will be used for the majority of the analysis, and is described in detail in Appendix B.1.

The rotary converters used in Austria, Germany and Switzerland, where the frequency coupling between the 50-Hz and 16 ⅔-Hz networks is elastic, utilises an asynchronous motor instead of the synchronous motor previously mentioned. Such rotary converters were still available in 1997 (Pfeiffer, et al. [147]), but today the marked is too small for supplying new single-phase generators (Steimel [165]) and power-electronic solutions are increasingly used.

2.3 Electric AC rail vehicles

The basics of electric rail vehicles and their historical development is well documented in the technical literature, e.g. by Steimel [163] and Östlund [188]. However, a short summary follows.

Electric rail vehicles differ from most other types of vehicles such as electric cars and busses[2], electric aircrafts and all electric ships in one important respect which is that rail vehicles are constantly connected to the power supply system during operation, while these other modes of transport carry the energy needed for propulsion onboard. Therefore, rail vehicles are more bound to the railway infrastructure, and interaction issues are more likely to arise.

2.3.1 Tap-changer rail vehicles

The selected traction power system's fundamental frequency has historical roots and is related to the available technology at the beginning of the previous century. It relates to the principle normally used for the speed control of an electric motor and thereby the train. This principle was based on a single-phase AC series commutator motor operating on a low frequency which is essentially equal to a DC motor that has armature and field winding in series. When the magnetic flux in both windings simultaneously changes direction due to current alternation, the motor torque direction remains unchanged. To avoid commutation problems, the motor is operated on low fundamental frequencies, which explains the need for frequency conversion as described in Section 2.2. The rotational speed of such a DC motor is proportional to its armature voltage. Speed control is therefore carried out by tap-changing on the vehicle's main step-down transformer's secondary or primary side. Rail vehicles from this category are still strongly in use.

[2] Trolley buses excepted.

2.3.2 Phase angle controlled or thyristor controlled rail vehicles

The progress of power electronic development introduced new solutions for control of the traction motor. The first application of power electronics was the diode-bridge rectification of the motor voltage, but the speed control of the DC motor was still carried out by transformer tap-changing.

The large benefits of power electronics however was realised by the thyristor. Thyristor vehicles, or the phase angle controlled vehicles, have dominated the Swedish rail network since the 1970s. The voltage applied on the DC motors is rectified by a half controlled thyristor bridge, making the torque control of the motor continuous instead of stepwise. The large disadvantage of this technology is a large reactive power consumption and harmonic current production as studied by Olofsson [134].

2.3.3 Advanced electric rail vehicles

The vast technological developments of the last 20 years within the field of power electronics and digital control has resulted in the state-of-the-art use of the robust and compact three-phas)e induction motor in traction drives. Such vehicles with advanced power semiconductors and modern microcomputer control systems are often called 'advanced rail vehicles'. Other descriptions of these vehicles may be 'inverter vehicles', 'asynchronous motor vehicles' or 'four-quadrant converter (4QC) vehicles'.

A principal sketch of this type of vehicle showing its main electrical components is given in Figure 2-4. There is a line side and motor side of the intermediate DC-link. The vehicle's interface to the rest of the power system is a voltage-source converter (VSC), mentioned as the 'line-side converter'[3], behind a step-down transformer. The line-side converter's task is to supply the DC-link capacitance with energy from the overhead contact line in order to keep the DC-link voltage constant. The DC-link capacitance is the energy source for the motor VSC, often called the motor-side inverter[4], and the induction motor.

For high-power locomotives, Gate Turn-Off (GTO) thyristors as semiconductors has been common until recently, but the use of Insulated-Gate Bipolar Transistors (IGBT) is increasing as the development proceeds. In order to reduce harmonics the semiconductors are commonly switched with a pulse-width modulated (PWM) pattern. Typical rating of such a four-axle universal locomotive is up to 6.4 MW measured on wheel (Steimel [163]).

[3] Can also be seen referred to as 'line converter', 'line inverter', 'four-quadrant converter' or 'active rectifier unit'.
[4] Can also be seen referred to as 'motor inverter', 'motor converter' or 'traction converter'

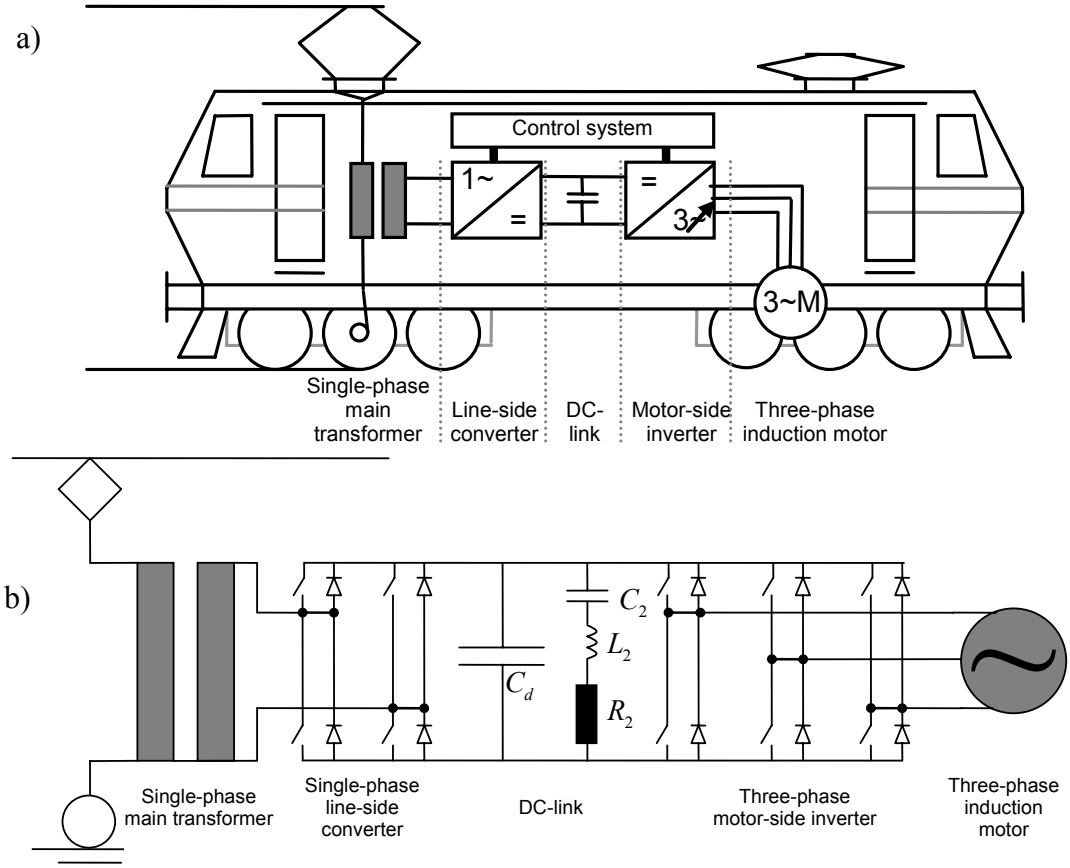

Figure 2-4: a) Sketch of an electric advanced rail vehicle with its main electrical components. b) More detailed sketch of the traction chain including the semiconductors and DC-link filters.

The line-side converter is able to operate in all four quadrants, independently controlling active and reactive power. Great features of this technology are the possibility for feeding power back into the network when regenerative braking and improving active power flow by inductive and capacitive reactive power (Appun and Lienau [12]). By adaption, such an advanced electric rail vehicle can be capable of operating in both 15-kV 16 ⅔-Hz and 25-kV 50-Hz power systems ('two-system vehicle') and even on 1.5 and/or 3 kV DC supply ('multisystem vehicle').

Further development and research this type of vehicle focuses on reduction of energy consumption, weight, noise, life-cycle costs and engineering effort together with improved reliability (Bakran [16] and Mermet-Guyennet [117]). Technologies of interests in this relation are e.g. the medium frequency line-side transformer and permanent magnet synchronous traction motor.

This category of rail vehicles is focused on in this thesis and studied more in detail in Chapters 5 and 6.

2.4 Stability in traction power systems

In this section, a proposed power system stability definition and classification is referred to. Further, this classification is applied on reported traction power system events and studies regarding stability. A further discussion of the classification is given in Section 9.1.4.

2.4.1 Power system stability definition and classification

Kundur, et al. [107] propose the following definition of power system stability:

> *Power system stability is the ability of an electric power system, for a given initial operation condition, to regain a state of operating equilibrium after being subjected to a physical disturbance, with most system variables bounded so that practically the entire system remains intact.*

Thus, the stability of an electric power system is a property of the system's motion around an equilibrium set, and is a balance between opposing forces. If the system is unstable, it will result in a runaway or run-down situation.

Power system stability is classified based on the physical nature of the resulting mode of instability as indicated by:

- the main system variable in which instability can be observed;
- the size of the disturbance considered; and
- the time span that must be taken into consideration in order to assess stability.

The three main classes of power system stability are:

- *Rotor angle stability* - refers to the ability of synchronous machines of an interconnected power system to remain in synchronism after being subjected to a disturbance. Rotor angle stability may be lost if the synchronising torque component or the damping torque component are too small, which can result in aperiodic or non-oscillatory instability or oscillatory instability, respectively.
- *Voltage stability* - refers to the ability of the power system to maintain steady-state voltages at all buses after being subjected to a disturbance. As a last consequence, voltage instability may result in a blackout or abnormally low voltages for a significant part of the system, also called a voltage collapse.
- *Frequency stability* - refers to the ability of the system to maintain a steady-state frequency following a severe upset resulting in a significant imbalance between the power generation and load.

Rotor angle instability is referred to as generator driven while voltage instability is often considered as load driven (Van Cutsem and Vournas [179]).

2.4.2 Rotor angle stability

2.4.2.1 Synchronising torque

Based on reported work, it seems as if stability against rotary converters stepping out of synchronism due to large disturbances previously has been the stability question of major concern. Short circuits on the single-phase side were first investigated by Biesenack [24], who found that a loss of synchronism would not be of any danger because of the fast action taken by the relay protection and circuit breaker.

This main conclusion is supported by Olofsson [133], who investigated the rotary converter connected to the Swedish 130-kV high-voltage transmission line. He concluded that the rotary converter speed will not increase dramatically with a single-phase side short circuit like a hydro power generator, because the motor only gives the power that the generator requires. This conclusion is stated as being valid for the first swing and is based on simplified converter-motor simulation models.

Eitzmann et al. [65] performed a dynamic system study of the Amtrak 25-Hz traction system in the US. This system contains synchronous-synchronous rotary converters, and the study showed that the expected faults did not cause a loss of synchronism. Of special interest is that the study includes dynamical models of the trains in operation (phase angle controlled vehicles) as well as the rotary and static frequency converters.

Biesenack and Schmidt [25] studied how the converter finds a new stable working point after a short time of oscillation when the power flow direction changes, due to regenerative feedback from trains.

In the only study on a lack of steady-state synchronising torque found, Biesenack [23] concludes that there is little or no risk for a step out of phase for rotary converters in parallel operation. Details about the calculation and the base inputs however are not known.

2.4.2.2 Damping torque

Only studies originating from Norway focus on the lack of damping of synchronous machines as an issue for traction power systems. Nonetheless, in other studies in which the time plot of transients or oscillations are provided, it is possible to extract information that can be compared with the Norwegian results. A comparison of the relative damping in these cases is given in Table 2-1. As far as the available information shows, the cases in the table refer to a rotary converter operating in an islanded single-phase network. However, the loading of the converter may differ from case to case.

Table 2-1: Comparison of reported low-frequency oscillation frequencies and damping[5] in the traction power supply with rotary converters.

Case	Eigenvalue of swing mode	Relative damping	Source
Germany	-1.4 1/s $\pm j1.6$ Hz	14 %	Biesenack and Schmidt [25]
Germany	-1.0 1/s $\pm j1.9$ Hz	8 %	Stoltze [169]
US	-1.6 1/s $\pm j1.2$ Hz	21 %	Eitzmann, et al. [65]
Norway	-0.6 1/s $\pm j1.6$ Hz	6 %	Toftevaag and Pálsson [178]
Norway	-0.3 1/s $\pm j1.6$ Hz	3 %	Danielsen and Toftevaag [56]

Biesenack [24] showed that such oscillations must be expected due to the basic swing equation that describes the electromechanical behaviour which is characteristic for all synchronous machines. In power system stability literature such as written by Kundur [106] and Machowski, et al. [115], this behaviour is classified as the synchronous machine's electromechanical eigenfrequency. Relative damping smaller than 5 % is generally considered as poor. It is this poor damping that is the background and one of the topics of this thesis.

For the Norwegian rotary converters, Johannessen and Bruu [91] report about sustained 1.6-Hz oscillations. It is believed that these oscillations are caused by sub-synchronous resonance, due to the interaction with line reactance compensation by use of series capacitors in the overhead contact line.

2.4.3 Voltage stability

In traction power system studies, e.g. by Aeberhard and Lörtscher [9], a voltage drop is often treated as a question of the voltage level or voltage quality rather than being a concern about voltage instability and collapse. In a traction power system without any reactive power support, the critical voltage for collapse is below the required voltage level for the opening of the vehicle's main circuit breaker as required by the European standard EN50388 [41]. This standard even describes a recommended maximum current ramp-down as a function of the line voltage characteristic to be implemented in vehicle software in order to avoid such a breakdown in weak networks.

The standards EN50388 and EN50163 [40] set requirements for the permanent and temporarily maximum and minimum voltage levels on the vehicle and power supply side. Too low voltage may result in train delays, as enough power to keep the scheduled speed cannot be consumed or delivered. This is studied by Biedermannn [22]. A requirement to reduce the power demand when the line voltage drops then becomes a requirement to the power supply.

The infrastructure managers often study these voltage levels together with the system's power flow in specially designed simulation software that includes models of moving trains in the power system. Examples of such software are described by Kaiser, et al. [100] and Stefan [162]. These time simulations are very time consuming to perform;

[5] A short introduction of the eigenvalues is given in Appendix C.

hence, Abrahamsson [7] proposes methods for faster simulation based on neural networks and Ho, et al. [84] propose investigations based on probabilistic methods.

2.4.4 Frequency stability

Frequency instability has never been reported as an issue in Norway and Sweden, where the networks are operated synchronously to the overall public power system by a stiff frequency coupling. However, in the frequency-elastic 16.7-Hz systems, two events of frequency instability are known.

In Austria, a large number of new electric rail vehicles with regenerative breaking and energy feedback facility were introduced into the railway system. Due to the mentioned demand for maintenance, sectioning of the railway network is frequent and necessary. If a network island is fed from a hydro power station only and there are large trains feeding energy back on their way down the hilly Alps, the excess energy not used by other trains may accelerate the hydro generators. A large increase in the island's fundamental frequency has been observed. Pechlaner, et al. [139] describe this problem and propose a frequency droop characteristic to be implemented in the vehicle's software in order to limit the power consumption when the fundamental frequency is low and to limit the power feedback when the fundamental frequency is high.

In the summer of 2005, the Swiss railway network experienced a large blackout ([153]). This event must be considered as a classic power system collapse, and it started with one high-voltage transmission line that was disconnected for maintenance. The remaining line between the generating part and the loaded part of the network became overloaded and disconnected as well. Due to insufficient operational routines, the part having a surplus of power production was allowed to accelerate until different generators were tripped by their own protection devices. The remaining and heavy loaded part collapsed[6] in the end, as import from Germany was not enough to cover the demand, and all electric rail traffic stopped completely.

Jian, et al. [90] reports a simulation study of the German 110-kV railway grid in view of stability when an increasing number of rotary frequency converters are replaced by static frequency converters. The worst case is reported to be outage of a 150-MW generation unit which results in a deficit in power production. Instability is prevented since the power production from other units is increased due to the 'active-power-frequency-characteristic' implemented, and overload of the static converters is prevented by a predictive current limiter. Eventually the system finds a new steady-state operating point.

[6] It may be difficult to classify this collapse as clearly being frequency instability or voltage instability. For the context, it is presented together with the rest of the reported event.

2.4.5 Other types of (in)stability

There are two types of traction power system instabilities that have been experienced which do not easily fit into the classification proposed by Kundur, et al. [107]. Both of them include a lack of damping of closed feedback control loops, but at different frequencies, and do not necessarily include synchronous generators.

2.4.5.1 Electrical resonance stability

Series and shunt resonances between inductances and capacitances in an electric network seem to not be commonly treated as a power system stability issue, but more as a phenomenon of travelling waves in high-voltage transmission networks. However, in 1995, the Swiss railways experienced mysterious disturbances in the local commuter train traffic in the area of Zürich ([2]). Meyer and Schöning [122] explained the observed 165-Hz oscillations to be resonances in the Swiss 132 kV high-voltage networks which were excited by the control system of the advanced electric rail vehicles of class Re 460 in its effort to shape the vehicle line current as a perfect sine wave. The combination of a high-voltage network, low system auxiliary power demand (normally trains parked for heating representing shunt resistances), and the low operation of passive tap-changer vehicles was explained to reduce the damping of these resonances. If a vehicle behaves like negative incremental impedance at the system resonance frequencies, i.e., a decrease in line voltage results in an increase of line current and vice versa, the closed feedback loop between the vehicle and the power supply may be unstable. A mathematical description of what occurred in Switzerland is given by Möllerstedt and Bernhardsson [131].

This phenomenon is called ‘electrical resonance instability’, or ‘linear instability’, since linear methods are often used for study and explanation, and may be experienced from three times the system’s fundamental frequency and above. It appears to be a severe problem in large traction power systems and was an important part of the aforementioned ESCARV project. The issue still gets a lot of attention when power system resonances are low, e.g. when introducing cables in connection to tunnels (Meyer, et al. [123]). The design of the vehicle control system now seems to also take this issue into account as e.g. shown by Jansson, et al. [89]. Paice and Meyer [135] define a stability criteria, and the needed information for compatibility and stability investigations can be measured by frequency sweeps as proposed by Meyer, et al. [120] and Meyer and van-Alphen [125].

This instability phenomenon must now be considered as well known within the railway community. Recent stability studies are reported from the high-voltage networks in both Austria (Wallnberger, et al. [182]) and Switzerland (Aeberhard, et al. [8]).

2.4.5.2 Low-frequency power oscillations

Of more concern in the electric railway expert's community today[7], is the oscillatory instability that advanced electric rail vehicles have caused below the system's fundamental frequency. The local commuter train system in Zürich, Switzerland experienced disturbing 5-Hz oscillations in 2004 (Menth and Meyer [116]), Amtrak has experienced 3-Hz oscillations in their 25-Hz network in the area of Washington, DC in the US (Debruyne [60]), and Pröls and Strobl [148] have recreated similar instability in the Siemens test centre's 50-Hz network as 7-Hz oscillations. In addition, as already introduced, low-frequency instability has been observed when advanced rail vehicles are fed from the poorly damped rotary converters in Norway and Sweden. Meyer and Thoma [124] report that low-frequency oscillations may also be an issue with static frequency converters.

Table 2-2 summarises a comparison of reported low-frequency oscillations which have been experienced in various traction power systems with different advanced rail vehicles. From the table, it can be observed that most of the oscillations are in the frequency range of 0.1 to 0.3 times the system's fundamental frequency.

Table 2-2: Comparison of reported low-frequency oscillations in traction power systems, together with the system's fundamental frequency and the oscillation frequency relative to the fundamental frequency

Case	Osc. freq. [Hz]	Fund. freq. [Hz]	Relative osc. freq.	Reference
Rotary conv., Nor.	1.6	16 ⅔	0.10	Danielsen and Toftevaag [56]
Thionville, France	5	50	0.10	Courtois, et al. [45]
Datong, China	5	50	0.10	No reference found
Washington, DC, US	3	25	0.12	Debruyne [60]
Siemens test, Germ.	7	50	0.14	Pröls and Strobl [148]
Zürich, Switzerland	5	16.7	0.30	Menth and Meyer [116]

The instability in France and China took place where several rail vehicles were at a standstill in depot or workshop areas with their line-side converters still active and switching. For that reason, this has sometimes been mentioned as the 'depot problem'.

This thesis focuses on this low-frequency instability in general and the interaction between the advanced electric rail vehicle and the poorly damped rotary converter in particular.

[7] At least eight of the presentations at the workshop 'Interaction' in Thun, Switzerland, in 2006 and 2009 dealt with this.

3 Rotary converter electromechanical modelling and eigenmode

This chapter presents the development of a second-order swing equation for a synchronous-synchronous rotary converter which describes the main characteristic of the converter oscillations that have been experienced. The results from this equation are compared with measurements and more detailed higher-order models. A stability criterion in view of single-phase load voltage dependency is proposed.

3.1 Introduction

Some AC power systems containing different fundamental power frequencies may be interconnected by rotary frequency converters or changers (Blalock [29]), and such is the case for the electric railway power supply in some countries as introduced in Section 2.2. A system frequency of 16.7 Hz is used in Austria, Germany, Norway, Sweden and Switzerland, where the utility frequency is 50 Hz. Railway supply at 25 Hz can be found in the US (Eitzmann, et al. [65]), where the utility frequency is 60 Hz. When interconnecting AC power systems, different types of converters may be used such as a synchronous-synchronous type, an induction-synchronous type, an adjustable-ratio induction-synchronous type and a fixed-ratio induction-synchronous type (Burnham [36]).

In this work, the synchronous-synchronous type is of interest. Stability studies for such converters used for railway applications are referred in Chapter 2.2.4 and 2.4.2. For non-railway applications, stability limits, e.g. load limits for remaining in synchronism when one out of two motor-generator sets operated in parallel is disconnected, has been studied by LeClair and Krupy [109]. Selenochat, et al. [156] report studies of the interaction between synchronous-synchronous converters and surrounding power station generators when the system is subjected to a short circuit. Furthermore, Bizjak, et al. [26] apply a digital simulation tool for analysing rotary converters in industrial networks in view of voltage stability, active power swings after disturbances and loading limits.

Among others, Fowler [68] states that hunting, which term is used for the synchronous machine alternately speeding up and slowing down, is found to some extent in AC synchronous motor DC generator sets. These were for example used for feeding of DC railways from the American 60-Hz main grid. Considerations about hunting of synchronous-synchronous motor-generator sets have not yet been found, though Selenochat, et al. [155] investigate the small-signal stability of an isolated power-transmission link with synchronous-synchronous converters. They conclude that the

system is stable and that the stability margins can be increased further by use of automatic field-current regulators on both machines.

Therefore, this chapter aims to present the basic swing equation for a synchronous-synchronous rotary converter in order to make a simplified platform for studying the nature of the observed oscillations introduced in Chapter 1.1. By having knowledge of this fundamental characteristic of the converter, countermeasures are easier to develop and judge.

A short introduction of eigenvalue analysis, which is used in this chapter, is given in Appendix C.

3.2 The swing equation

The swing equation is a well-known dynamic representation of synchronous machines, characterising the fundamentals of the machine's dynamical electromechanical behaviour (Kundur [106], Machowski, et al. [115]). The important parameters are the rotating mass and electrical connection of the machine to the rest of the electric network, together with information about the machine's damping, thereby the name 'electromechanical'. The resulting oscillation involves both changes of the machine's rotational speed and the rotor angular displacement relative to a fixed reference.

3.2.1 Single-machine infinite-bus system

A single-machine infinite-bus (SMIB) system is a commonly used term in the literature (e.g. Kundur [106]), which describes a single synchronous machine (normally a generator) connected to a stiff voltage source via an impedance (normally the line and transformer). The stiff voltage source is an aggregation and therefore a representation of all the other voltage sources in the network.

In general, Newton's 2nd law for a rotating body tells that the product of a mass of inertia J and rotational acceleration α equals the sum of torques $\sum \tau$ applied:

$$J\alpha(t) = \sum \tau(t) \tag{3.1}$$

This law can be expanded into Equation (3.2) for a synchronous machine rotating in a stationary reference system. The angle θ_m describes the rotor displacement relative to a stationary reference and can, by its double and single time derivatives, express angular acceleration and speed, respectively. The damping impact is reflected by the parameter D_d. The torque subscript m denotes mechanical and e denotes electromagnetic or electrical, respectively:

$$J\frac{d^2\theta_m(t)}{dt^2} + D_d\frac{d\theta_m(t)}{dt} = \tau_m(t) - \tau_e(t) \tag{3.2}$$

If there is a deviation between the mechanical and electromagnetic torques it will lead to a change in the machine's rotating speed by acceleration or deceleration. Any deviation from the synchronous speed will be opposed by the damping expressed by the damping constant *D*. For the sake of simplicity, all losses are neglected

Working with electric power systems, it is often convenient that quantities are expressed in:

- a reference system rotating at the synchronous angular speed ω_{sm} [rad/s] instead of being stationary, therefore $\theta_m(t) = \delta_m(t) + \omega_{sm}t$ where δ_m is the angular displacement relative to such a rotating reference;
- electrical speed and angles instead of mechanical speed and angles, $\omega(t) = \frac{p}{2}\omega_m(t)$ and $\delta(t) = \frac{p}{2}\delta_m(t)$ where *p* is the number of rotor poles;
- power instead of torque, $P(t) = \tau(t) \cdot \omega(t)$; and
- a common per unit (subscript *pu*) system relative to a common base, S_N [MVA]. The rotating mass of the machine in per unit is expressed by the mass inertia constant *H* [MWs/MVA].

The consideration of power instead of torque does not imply that the machine rotor torque balance is replaced by a power balance. It is only a multiplication of $\omega_{pu}(t)$ that temporarily simplifies the following considerations of the machine-grid interaction.

After these transformations, the final expression is given in Equation (3.3). It can be termed as the per unit swing equation of a synchronous machine. This equation describes the instantaneous power balance of the machine.

$$2H\omega_{pu}(t)\frac{d\omega_{pu}(t)}{dt} + D\omega_{pu}(t)\frac{d\delta(t)}{dt} = P_{mpu}(t) - P_{epu}(t) \tag{3.3}$$

3.2.2 Rotary converter

A synchronous-synchronous rotary frequency converter of the type used in the Norwegian and Swedish traction power supply consists of two electric machines – the synchronous generator and motor.

3.2.2.1 Synchronous generator

The single-phase 16 ⅔-Hz synchronous generator has $p_G = 4$ poles. Its swing equation (3.4) can be directly derived from Equation (3.3). Capital letter *G* refers to the generator and positive power flow direction is defined out from the machine and into the network.

$$2H_G\omega_{Gpu}(t)\frac{d\omega_{Gpu}(t)}{dt} + D_G\omega_{Gpu}(t)\frac{d\delta_G(t)}{dt} = P_{mGpu}(t) - P_{eGpu}(t) \tag{3.4}$$

A deviation from synchronous speed leads to a change in δ_G, which is the angle between the internally induced voltage in the generator and a synchronously rotating reference in the single-phase network as expressed in Equation (3.5). This is also known as the generator power angle.

$$\frac{d\delta_G(t)}{dt} = \omega_{sG}\omega_{Gpu}(t) - \omega_{sG} = \omega_{sG}\left(\omega_{Gpu}(t) - 1\right) \tag{3.5}$$

The fundamental angular frequency is $\omega_{sG} = 2\pi f_G = 2\pi \cdot 16\frac{2}{3}$ [1/s].

3.2.2.2 Synchronous motor

The three-phase 50-Hz synchronous motor has $p_M = 12$ poles. Since the power transfer for a motor is opposite from a generator, the swing Equation (3.3) should changed from generator to motor reference. Capital letter *M* refers to motor and positive power flow direction is defined from the network into the machine. This means that the signs of the mechanical and electrical power should be inverted.

$$2H_M\omega_{Mpu}(t)\frac{d\omega_{Mpu}(t)}{dt} - D_M\omega_{Mpu}(t)\frac{d\delta_M(t)}{dt} = P_{eMpu}(t) - P_{mMpu}(t) \tag{3.6}$$

While a synchronous machine operating as a generator has a power angle leading the stiff network voltage, a synchronous machine operating as motor has a power angle lagging the stiff network voltage. Since the positive rotating direction is kept as for the generator because the two machines are mechanically connected, also the sign of the power angle is inverted. As for the generator, the following relation applies then for the speed deviation:

$$\frac{d\delta_M(t)}{dt} = \omega_{sM} - \omega_{sM}\omega_{Mpu}(t) = \omega_{sM}\left(1 - \omega_{Mpu}(t)\right) \tag{3.7}$$

where $\omega_{sM} = 2\pi f_M = 2\pi \cdot 50$ [1/s]. The angle δ_M is the angle between the internally induced voltage in the motor and a synchronously rotating reference in the three-phase network, also known as the motor power angle.

3.2.2.3 Rotary converter

The shaft connecting these two machines may be considered as stiff for the frequency in question (low-frequency oscillations below the fundamental frequency). The lowest torsional eigenfrequency of the shaft is expected to be approximately 70 Hz for one of the types of converters used (Sabery [149]).

This means that the two machines can be considered as one lumped mass in which the following applies:

- the total inertia constant is the sum of the two machines' inertia constants, $H_{MG} = H_M + H_G$;
- the mechanical power delivered from the motor is equal to the mechanical power delivered to the generator, $P_{mMpu}(t) = P_{mGpu}(t)$;
- the per unit speed of the motor is equal to the per unit speed of the generator, resulting in a common per unit speed, $\omega_{pu}(t) = \omega_{Mpu}(t) = \omega_{Gpu}(t)$; and
- the power angle of the motor and the power angle of the generator have common origins in the rotor displacement, resulting in an expression of a common per unit power angle having a generator reference sign, $\delta_{pu}(t) = \frac{\delta_M(t)}{-\omega_{sM}} = \frac{\delta_G(t)}{\omega_{sG}}$, since the relation $\frac{d\delta_{pu}(t)}{dt} = \omega_{pu}(t) - 1$ applies.

The two last items on the list above are based on the assumption that the speed of both the synchronous references is constant. The mechanical power balance implies a mechanical torque balance as well.

Merging the two machines into one lumped mass, the final swing equation for a synchronous-synchronous rotary converter reduces to:

$$2H_{MG}\omega_{pu}(t)\frac{d\omega_{pu}(t)}{dt} + \omega_{pu}(t)\left(D_M\omega_{sM} + D_G\omega_{sG}\right)\frac{d\delta_{pu}(t)}{dt} = P_{eMpu}(t) - P_{eGpu}(t) \quad (3.8)$$

A block diagram describing the swing Equation (3.8), together with Equation (3.5) and (3.7) is given in Figure 3-1. The letter *s* is the Laplace operator. Positive power flow direction is still into the motor and out from the generator, i.e., from the three-phase side to the single-phase side.

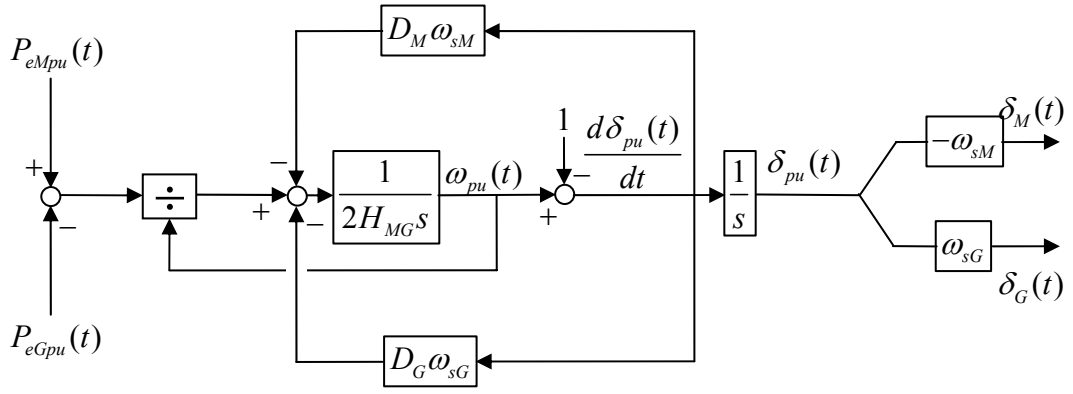

Figure 3-1: A block diagram for the rotary converter non-linear swing equation.

It can be seen from the block diagram that the machines share the same rotating mass and speed. The system also has two inputs, the motor and generator active power, respectively, and two outputs, the motor and generator power angle, respectively. The electrical power P_{epu} for the machines can be divided into two main categories:

- power transfer as a function of the power angle relative to the stiff network voltage (i.e., the rest of the power system) P_{etpu}; and
- power supply to/from a local load/production P_{elpu}. This one is not relevant for the motor in practice, and will be neglected in all of the following practical considerations. The generator local load will be discussed in island operating mode only.

3.3 Linearisation and eigenvalue expression

3.3.1 Operating point

In order to study the low-frequency eigenmode, the swing equation (3.8) should be linearised. Linearisation is performed and valid for a given operating point only. The electrical operating point will be considered later, while the mechanical operating point is at a rotational speed $\omega_{pu}(t) \approx 1.0$, thus the per unit electrical power equals the per unit electromagnetic torque.

The above is a common simplification that is often included in the linearisation process in the literature (e.g. Machowski, et al. [115] page 143 and Andersson and Fouad [11]) without further significant notice (Kundur [106] page 175), probably due to simplicity, and has no influence in no-load. However, one should be aware that this simplification of keeping the turbine power constant instead of the turbine torque, exerts an influence on the eigenvalues calculated for a governor driven generator (Johansson, et al. [93]; Kaberere, et al. [98]).

In a rotary synchronous-synchronous converter, both of the balancing torques have the same origin in being machine electromagnetic torques. The simplification by assuming a unity speed consequently treats them equally.

3.3.2 Linearisation

These two differential equations have to be linearised:

$$f_1(\delta_{pu}, \omega_{pu}, t) = \frac{d\delta_{pu}(t)}{dt} = \omega_{pu}(t) - 1 \tag{3.9}$$

$$\begin{aligned} f_2(\delta_{pu}, \omega_{pu}, t) &= \frac{d\omega_{pu}(t)}{dt} \\ &= \frac{1}{2H_{MG}}\left(\frac{P_{eMpu}(t)}{\omega_{pu}(t)} - \frac{P_{eGpu}(t)}{\omega_{pu}(t)} - \frac{d\delta_{pu}(t)}{dt}\left(D_M\omega_{sM} + D_G\omega_{sG}\right)\right) \end{aligned} \tag{3.10}$$

Linearisation of f_1 results in $\Delta\dot{\delta}_{pu} = \Delta\omega_{pu}$. Linearisation of f_2 introduces the linearisation constants K_{1M} and K_{1G}. These constants describe the motor respective generator power transferred to the stiff network as a function of the machines' power angles and are commonly referred to as the transient synchronising power coefficients (Machowski, et al. [115]). They are identical to the transient synchronising torque coefficients if unity speed is considered and machine armature resistance is neglected, since the air-gap torque and power are equal (Kundur [106] page 174).

This results in the following linear expressions in which the coefficients' values will depend on the electrical operating point:

$$\begin{aligned} \Delta\tau_{etMpu} &= K_{1M}\Delta\delta_M \\ \Delta\tau_{etGpu} &= K_{1G}\Delta\delta_G \end{aligned} \tag{3.11}$$

The previously introduced notation used for transferred power and locally supplied power is used for torque as well.

The linearised swing equation for a rotary converter connected to both stiff networks should then be as in Equation (3.12). This linear equation is also illustrated by the block diagram in Figure 3-2.

$$2H_{MG}\Delta\dot{\omega}_{pu} + \left(D_M\omega_{sM} + D_G\omega_{sG}\right)\Delta\omega_{pu} + \left(K_{1M}\omega_{sM} + K_{1G}\omega_{sG}\right)\Delta\delta_{pu} = \Delta\tau_{elMpu} - \Delta\tau_{elGpu} \tag{3.12}$$

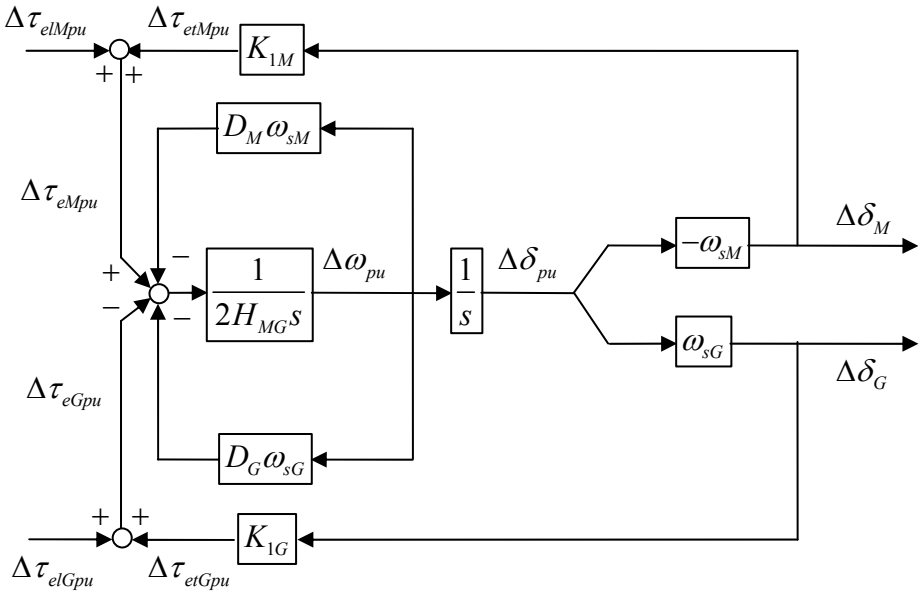

Figure 3-2: A block diagram for a rotary converter linear swing equation.

In the final step, the linear model represents the characteristic second-order differential Equation (3.13) which describes the inherent properties of the rotary converter in regard to the low-frequency electromechanical eigenmode:

$$2H_{MG}\Delta\ddot{\delta}_{pu} + \left(D_M\omega_{sM} + D_G\omega_{sG}\right)\Delta\dot{\delta}_{pu} + \left(K_{1M}\omega_{sM} + K_{1G}\omega_{sM}\right)\Delta\delta_{pu} = 0 \qquad (3.13)$$

Power to/from the local load/production is as a first step assumed to be unaffected by the power angles' change, and can then be treated as disturbance variables in a state space model. The single-phase network load's influence will be studied in Section 3.4.5.

3.3.3 Eigenvalue expression

Calculating the eigenvalues for Equation (3.13) yields the expression Equation (3.14). For reasonable values of the D, the eigenvalues will be a complex pair in which the real part describes the damping of the mode and the imaginary part describes the angular oscillation frequency $\omega_{osc} = 2\pi \cdot f_{osc}$.

$$\lambda_{1,2} = -\frac{D_M\omega_{sM} + D_G\omega_{sG}}{4H_{MG}} \pm \sqrt{\left(\frac{D_M\omega_{sM} + D_G\omega_{sG}}{4H_{MG}}\right)^2 - \frac{K_{1M}\omega_{sM} + K_{1G}\omega_{sG}}{2H_{MG}}} \qquad (3.14)$$

It is possible to develop this Equation (3.14) without the reduction of state variables from two different power angles for the two machines into one common angle as performed in Section 3.2.2.3. These two angles are not independent, and due to a consequent over specification of the system by three state variables, an additional zero-valued eigenvalue will result.

3.4 Analytical considerations

3.4.1 Electromechanical eigenmode

In the previous section, it was shown how the non-linear swing equation, the characteristic equation, and the analytical expression for the eigenvalues describing the low-frequency electromechanical eigenmode for a synchronous-synchronous rotary converter can be developed. All these equations have a similar structure as the equations known from the literature for a SMIB system, with the only exception being that the damping and transient synchronising torques for both the synchronous machines adds together, respectively. That means that the total damping of the electromechanical oscillations is the sum of the damping from both motor and generator and similarly for the synchronising torque.

However, it should be noted that the contribution from each of the machines to the characteristic dynamic behaviour are weighted by their fundamental frequency due to the ω_s factor. The reason for this is that ω_s is the connection between the common physical speed and displacement of the rotor, here expressed in per unit, and the respective electrical angular speeds and angles. A higher electrical speed or frequency

leads to a larger power angle for the same per unit displacement and hence a larger torque and power flow.

For the rotary converter considered here, the ratio between the three-phase and single-phase fundamental electrical frequencies is three. This means that if the motor and generator have equal coefficients, the machine with the highest fundamental frequency (i.e., the motor) will dominate and determine both the damping and the oscillation frequency. This also implies that two per unit identical machines with different fundamental frequencies will have different damping and electromechanical oscillation frequencies. This can be demonstrated by Equation (3.15) in which the undamped natural ω_{nat} eigenfrequency for a SMIB system (Kundur [106]) is proportional to the square root of the fundamental frequency.

$$\omega_{nat} = \sqrt{\frac{K_1 \omega_s}{2H}} \tag{3.15}$$

The real part of the eigenvalue for a SMIB system is proportional to the fundamental frequency. The imaginary part is, if the damping impact is neglected, proportional to the square root of the fundamental frequency. Therefore, the damping ratio ζ in Equation (C.4) will be proportional to the square root of the fundamental frequency, as well as shown in Equation (3.16).

$$\zeta \approx \frac{D\sqrt{\omega_s}}{2\sqrt{2HK_1}} \tag{3.16}$$

3.4.2 Power oscillations in interconnected mode

When the power flow through the rotary converter is from the three-phase to the single-phase network and the converter has a connection to both the network stiff references (i.e., not the island mode and no local load or production is considered), a phasor diagram such as Figure 3-3 can be drawn. This is valid for both steady state considerations and dynamical considerations.

The converter can be excited to oscillations by for example a change in one of the stiff voltage references' angle. During such an oscillation, the rotor rotational speed increases and decreases periodically. This means that the rotor rotates faster and slower than the synchronous reference. Equation (3.9) and Figure 3-3 show that the power angles also change, which again influences the power oscillations according to Equation (3.11). The power angle change referred to the motor or generator's fundamental frequency is given by a reading of the respective scale on the figure.

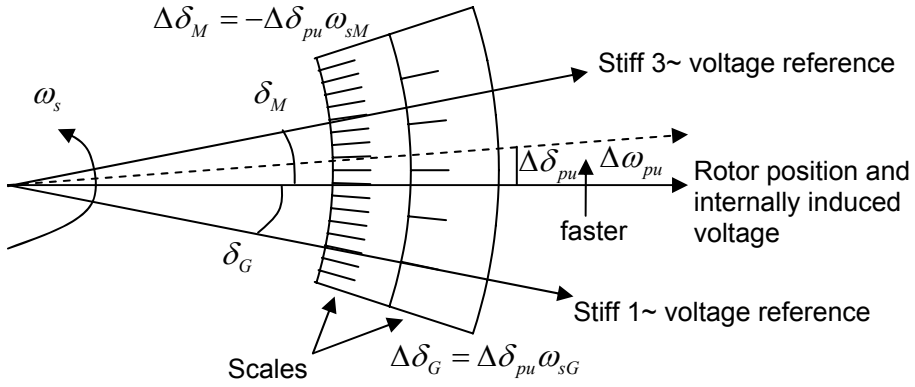

Figure 3-3: A phasor diagram for a rotary converter connected to stiff network voltages on both three-phase and single-phase side.

When the rotor rotates faster than the synchronous rotating references ($\omega_{pu}(t) > 1$), the following holds:

- the motor power angle decreases, the three-phase network will deliver less electrical power to the motor, and the electromagnetic torque will decrease and decelerate the rotor;
- the generator power angle increases, the generator will deliver more electrical power to the single-phase network, the electromagnetic torque will increase and decelerate the rotor;
- motor rotor induced eddy currents result in a damping torque that will decelerate the rotor to the synchronous speed; and
- generator damper winding currents result in a damping torque that will decelerate the rotor to the synchronous speed.

This means that the motor and generator power (ΔP_{etMpu} and ΔP_{etGpu}) will oscillate opposite each other in anti-phase, i.e., motor power decreases when generator power increases. If the transient synchronising torque coefficients for the two machines are equal, the three-phase power oscillations will have three times the amplitude of the single-phase power oscillations due to a frequency ratio of three. In general, the ratio between the three-phase and single-phase power oscillation amplitudes is expressed by Equation (3.17):

$$R_{\Delta p} = \frac{\Delta\left(\Delta P_{etMpu}\right)_{p-p}}{\Delta\left(\Delta P_{etGpu}\right)_{p-p}} = \frac{K_{1M}\omega_{sM}}{K_{1G}\omega_{sG}} \tag{3.17}$$

These relationships are illustrated by the time simulation in Figure 3-4 based on Equation (3.13), in which the generator power is changed due to a step in the single-phase stiff network voltage phase. When the generator power angle changes, there is no longer an electromagnetic torque balance which consequently results in acceleration of the rotating mass until a new equilibrium between the motor and generator

synchronising torques is reached. But because of the moment of inertia, the rotor overshoots the final position, speeding up more than it should. Due to increasing power angle, the synchronising torque stops the acceleration and rotor starts to decelerate. Again, the rotor overshoots the final position, but with a smaller amplitude because of the energy losses in the system given by machines' damper windings. Eventually, the successive oscillations die down and the rotary converter reaches its new steady state.

However, if the torque which brings the rotor back from the position ahead or behind the equilibrium is larger then the torque which opposes the deviation of the rotor from this equilibrium, each swing tends to exceed the preceding one in amplitude. The energy losses are insufficient and the oscillation thus increases in amplitude and becomes cumulative; this is called hunting (Steinmetz [166]).

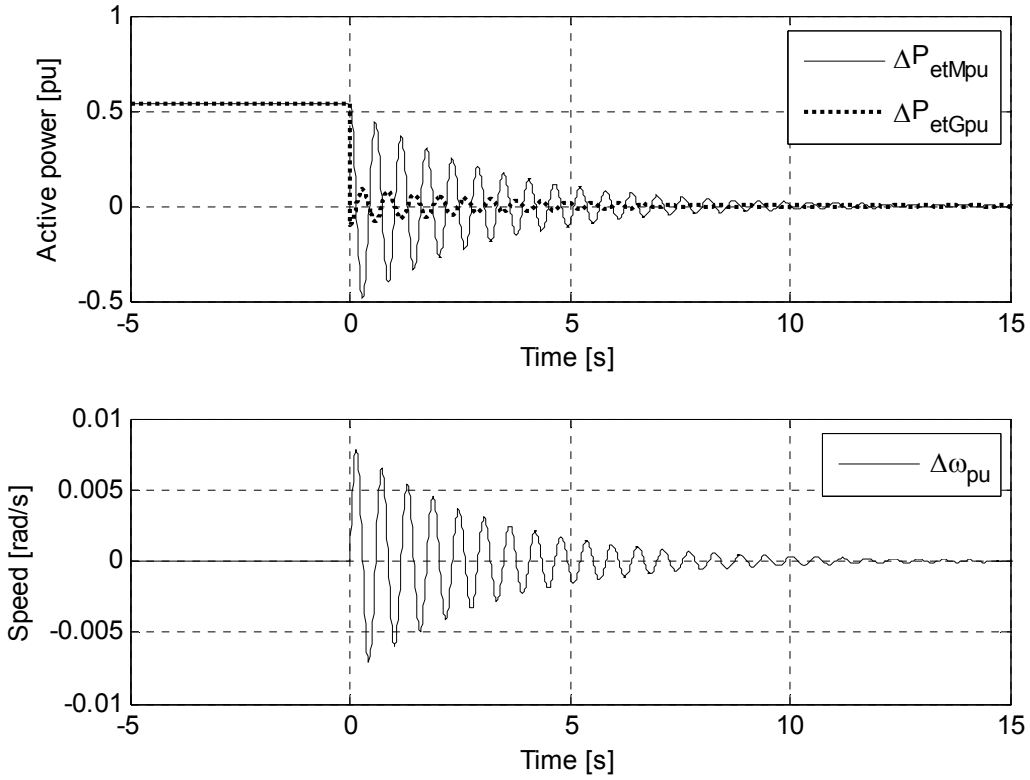

Figure 3-4: Response in active power and speed when single-phase stiff network voltage phase is changed in a step to zero, resulting in no-load.

The figure also shows that the three-phase and single-phase power oscillations are 90 degrees leading and lagging the rotor speed oscillations, respectively, as expected by the integrators and signs in Figure 3-2. However, 90 degree phase shifts relative to the speed create power oscillations against the stiff networks having a zero or neutral damping impact. The damping of the oscillation is caused by power having components oscillating in phase with speed such as the second term in Equation (3.13), which expresses both the motor and the generator damping. The exact phase of the torques

given by the synchronizing power and damper windings is influenced by the design of the machine (Steinmetz [166]) and may not in real life be that perfectly orthogonal as these simplified considerations indicate.

It can also be observed that the motor power oscillation shows larger amplitude than the generator power oscillation as indicated by Equation (3.17)

3.4.3 Power oscillations in island mode

In island operating mode, the generator electrical power flows to a local load. Temporarily assuming this load to be neutral, the generator damping and transient synchronising torque coefficients disappear in the previously shown equations, $D_G = K_{1G} = 0$. The influence of the local load on the damping will be discussed in the next sections. A new block diagram describing the transfer function from single-phase generator power to three-phase motor power for island operation is shown in Figure 3-5.

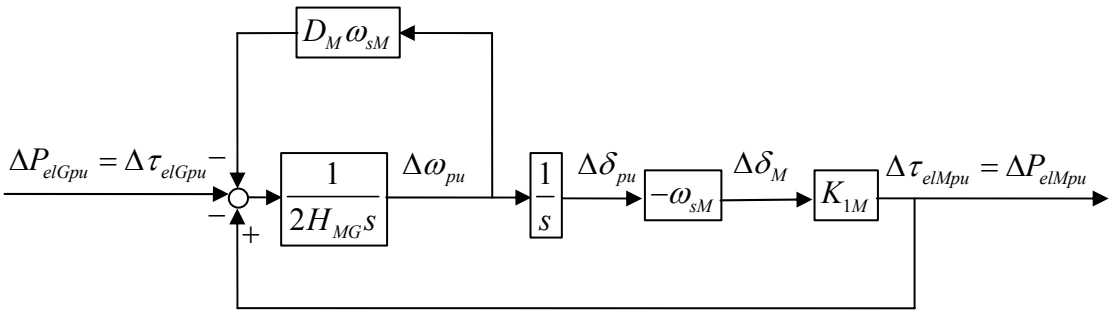

Figure 3-5: A block diagram for island mode operation of the rotary converter.

The transfer function from single-phase power disturbance to three-phase power oscillation is consequently Equation (3.18). A change in generator power requires a change in motor power in order to maintain electromechanical torque balance in steady state. Changed motor power and torque requires a change in the motor power angle, and due to the inertia of the rotating masses, this cannot be obtained instantly as alreaddy discussed in Section 3.4.2 and oscillations will result.

$$\frac{\Delta P_{elMpu}(s)}{\Delta P_{elGpu}(s)} = \frac{1}{2H_{MG}s^2 + D_M \omega_{sM} s + K_{1M} \omega_{sM}} \tag{3.18}$$

The roots of the closed-loop transfer function yield the following eigenvalues:

$$\lambda_{1,2} = -\frac{D_M \omega_{sM}}{4H_{MG}} \pm \sqrt{\left(\frac{D_M \omega_{sM}}{4H_{MG}}\right)^2 - \frac{K_{1M} \omega_{sM}}{2H_{MG}}} \tag{3.19}$$

There is no longer a generator power that is related to the machine's power angle, as there is no connection to the single-phase stiff voltage. This analytical expression is also

known for a regular SMIB system, but in present case it is the motor of the rotary converter that determines the electromechanical mode, and not the generator. This is different from a non-electric prime mover driven synchronous generator in island operating mode, which does not have such an electromechanical eigenmode at all.

The frequency ratio of 3 between the two machines no longer has any influence on the amplitude of the power oscillations as in interconnected operating mode. On the other hand, based on the fundamentals for such a second order transfer function, it is clear that there will be an amplification of a periodic single-phase power disturbance through the converter to the three-phase power if its frequency is close to the converter's electromechanical eigenfrequency. This amplification can easily exceed 3 and even reach 10 if the damping is poor as illustrated by Toftevaag and Pálsson [178].

3.4.4 Single-phase side voltage oscillation

The induced voltage in generator stator windings are due to Faraday's law of induction related to the machine's rotational speed. An increase in speed leads to an increase in generator voltage as will be discussed regarding Equation (4.15). The factor k_u represents the relation between the speed oscillation and the generator voltage oscillation ΔU_G used in these simplified considerations such that:

$$U_G(t) = k_u \cdot \omega_{pu}(t) = U_{G0} + \Delta U_G(t) = U_{G0} + k_u \cdot \Delta\omega_{pu}(t). \tag{3.20}$$

U_{G0} is the nominal or initial load voltage amplitude (RMS) in per unit.

It can be initially assumed that k_u is approximately 1 per unit for an unregulated generator. However, the generator's excitation system may exert an influence on this resulting in k_u being frequency dependent. A fast voltage controller may keep the voltage constant independent of the rotor oscillations, thus resulting in $k_u = 0$. On the other hand, an unfortunate tuned voltage controller may amplify the voltage oscillation and result in $k_u > 1$.

During an oscillation, the rotary converter speed will oscillate with a given oscillation frequency $\omega_{osc} = 2\pi \cdot f_{osc}$, which most likely correspond to its eigenfrequency. Based on the above analytical considerations, the instantaneous value single-phase output voltage from the generator is both:

- amplitude modulated due to Equation (3.20); and
- frequency/phase modulated due to the speed/phase oscillation as seen in block diagrams Figure 3-2 and Figure 3-5.

The resulting single-phase instantaneous value voltage is shown in Equation (3.21). Note that if the frequency/phase modulation is neglected, the instantaneous value voltage consists of three frequency components, the fundamental frequency ω_{sG} and two sidebands given by the fundamental frequency plus/minus the oscillation frequency $\omega_{sG} \pm \omega_{osc}$. The resulting voltage does not contain a frequency component equal to the oscillation frequency ω_{osc} (Buhrkall [32]). When the oscillation frequency is low, as is

the case here, the sidebands are close to the fundamental frequency. E.g. for the 1.6-Hz oscillation the sidebands are at 15.0 and 18.3 Hz. Hence, characterising low-frequency oscillations, it must be distinguished between the modulation frequency and the instantaneous value frequency component as the first one is close to zero and the second one is close to the fundamental frequency[8].

$$\begin{aligned} u_G(t) &= \left(\sqrt{2}U_{G0} + \sqrt{2}\Delta U_G \sin\left(\omega_{osc}t\right)\right)\sin\left(\left(1+\Delta\omega_{pu}(t)\right)\omega_{sG}t\right) \\ &= \sqrt{2}U_{G0}\sin\left(\left(1+\Delta\omega_{pu}(t)\right)\omega_{sG}t\right) \\ &+ \frac{\sqrt{2}\Delta U_G}{2}\cos\left(\left(\left(1+\Delta\omega_{pu}(t)\right)\omega_{sG} - \omega_{osc}\right)t\right) \\ &- \frac{\sqrt{2}\Delta U_G}{2}\cos\left(\left(\left(1+\Delta\omega_{pu}(t)\right)\omega_{sG} + \omega_{osc}\right)t\right) \end{aligned} \tag{3.21}$$

Amplitude modulation in instantaneous values appears as beating (see Young and Freedman [184] pages 654-656) between the fundamental frequency and the side bands. Beats are fluctuations in amplitude produced by to waves of slightly different frequency. These expressions are mostly known for sound waves.

3.4.5 Single-phase load characteristic influence

A common way to describe electric loads in power systems are by their characteristic voltage and frequency dependency for both active and reactive power (Kundur [106]). In this context, only the voltage dependency of the single-phase generator active power load will be considered without any dynamic behaviour. The actual active power demand from the load, P, is given by the exponential model in Equation (3.22) where P_0 is the initial, reference or desired power, U is the actual load voltage amplitude and U_0 is the nominal or initial load voltage amplitude.

$$P(t) = P_0\left(\frac{U(t)}{U_0}\right)^{MP} \tag{3.22}$$

The exponent MP is called the active power voltage exponent. The most commonly used values are:

- MP = 0: Load power demand is independent of voltage amplitude, and the load may be referred to as a constant power load (CPL).
- MP = 1: Load power demand is proportional to voltage amplitude, and the load may be referred to as a constant current load.
- MP = 2: Load power demand is proportional to voltage amplitude squared, and the load may be referred to as a constant impedance or resistance load.

[8] From the field of signal processing, this shift in frequency is mentioned as 'frequency translation', 'frequency transformation' or 'frequency shift'.

This load model, however, involves several simplifications. First, the voltage dependency has to be considered within the time frames of the dynamical phenomena studied. In this case, these are the low-frequency oscillations which last from 1 to 15 seconds with a frequency of 1.5 to 4.5 Hz. Second, a constant power load in a single-phase system does not exist in reality (see Section 4.6). The power has to be considered as an average over a fundamental period, i.e., RMS values.

The power demand from a local single-phase load fed from the generator can be expressed as in Equation (3.23) by inserting (3.20) into (3.22).

$$P_{elGpu}(t) = P_{elGpu0}\left(\frac{k_u \cdot \omega_{pu}(t)}{U_{G0}}\right)^{MP} \tag{3.23}$$

Neglecting the motor local load/production P_{elMpu} and the generator power-transfer P_{etGpu} to the stiff single-phase voltage source, the differential Equation (3.10) that was linearised in Section 3.3 has to be replaced by Equation (3.24). This equation represents the rotary converter that operates islanded on the single-phase side, supplying a local load connected to the generator's terminals.

$$\begin{aligned} f_2(\delta_{pu}, \omega_{pu}, t) &= \frac{d\omega_{pu}(t)}{dt} \\ &= \frac{1}{2H_{MG}}\left(\frac{P_{etMpu}(t)}{\omega_{pu}(t)} - \frac{P_{elGpu0}}{\omega_{pu}(t)}\left(\frac{k_u \cdot \omega_{pu}(t)}{U_{G0}}\right)^{MP} - \frac{d\delta_{pu}(t)}{dt}\left(D_M\omega_{sM} + D_G\omega_{sG}\right)\right) \end{aligned} \tag{3.24}$$

The initial voltage U_{G0} may be assumed to be 1 pu and therefore omitted. Remember also that the speed operation point is close to the nominal speed 1 pu. The expression for the generator torque given by Equation (3.23) ($\tau_{eGpu} = P_{elGpu}/\omega_{pu}$) is linearised to Equation (3.25). The exponential expression is in the linearisation process replaced by a first-order Taylor series.

$$\Delta\tau_{eGpu} = \Delta\tau_{elGpu} = \left(P_{G0} \cdot k_u^{MP}\left(MP - 1\right)\right)\Delta\omega_{pu} \tag{3.25}$$

From Equation (3.25) and the corresponding block diagram in Figure 3-6, it can be seen that a constant current load having $MP = 1$ will give no speed dependent torque variation and have neutral damping impact.

A constant power load having $MP = 0$ will yield a torque opposite to the speed variation which has the impact of decreasing the damping. The constant power load may be said to contribute a negative damping. If the rotor speed slows down, the constant power load will increase the generator electromagnetic torque in order to keep the product of speed and torque constant. Increased generator torque reduces the speed even more, but

a total stop is prevented by the motor synchronising torque that increases when the power angle increases due to the decreased speed. These opposing forces will cyclically accelerate and decelerate the rotor resulting in the low-frequency oscillations in study. If the system is unstable, e.g. by the loads negative damping impact being larger than the motors own damping, the oscillation amplitudes will increase as time lapses.

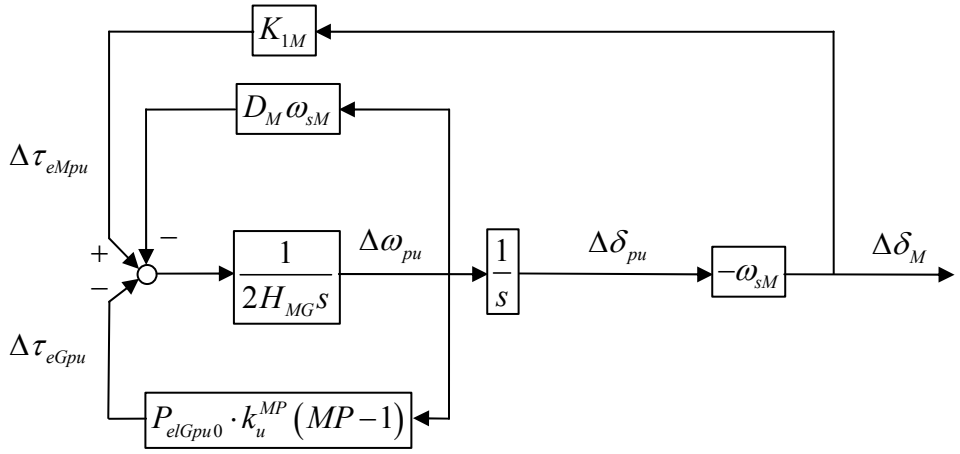

Figure 3-6: A block diagram for a rotary converter linear swing equation with load characteristic influence.

In contrast, a constant resistance load having $MP = 2$ will result in a torque oscillation in phase with the speed, thus increasing the damping, which is called positive damping. The larger the generator voltage variation is, described by k_u, the larger the damping impact will be. The influence is zero in no-load, and increases as the initial load becomes larger.

Equation (3.26) is an explicit expression of the eigenvalue describing the converter electromechanical eigenmode in single-phase island operation when the influence of the local single-phase load's voltage dependency is taken into consideration. The above considerations of the torque variation relative to the speed oscillation are directly reflected in the eigenvalue's real part and hence the damping of the mode:

$$\lambda_{1,2} = -\frac{D_M \omega_{sM} + P_{elGpu0} \cdot k_u^{MP} \cdot (MP-1)}{4H_{MG}} \pm \sqrt{\left(\frac{D_M \omega_{sM} + P_{elGpu0} \cdot k_u^{MP} \cdot (MP-1)}{4H_{MG}}\right)^2 - \frac{K_{1M} \omega_{sM}}{2H_{MG}}} \quad (3.26)$$

The understanding of k_u when $MP = 0$ is however not obvious since $k_u^0 = 1$ cancels its influence. An explanation for this is not found. It might well be due to the simplifications performed when establishing Equation (3.23). A better representation of k_u in an explicit eigenvalue expression than in Equation (3.26) will be given for a constant power load in Equation (8.15).

3.4.6 Stability criterion

Based on the load characteristic considerations in Section 3.4.5, a general criterion to the torque variation relative to the speed oscillation as shown in Equation (3.27) can be established. The transfer function from speed oscillation to torque oscillation must have a phase less than or equal to ± 90 degrees, i.e., a zero or positive real part.

$$\left|\arg\left(\frac{\Delta\tau_{eGpu}(s)}{\Delta\omega(s)}\right)\right| \leq 90° \Rightarrow \mathrm{Re}\left(\frac{\Delta\tau_{eGpu}(s)}{\Delta\omega(s)}\right) \geq 0, \quad s = j\omega_{res} \tag{3.27}$$

The criterion is stated in the frequency domain and is generally valid for all frequencies. From a stability point of view only, such behaviour is safe and advantageous. But for practical applications such a wide frequency requirement is too stringent and unnecessary. In this context however, the requirement is of importance in relation to the rotary converter's eigenfrequency $\omega_{res} = 2\pi \cdot f_{res}$. It is at this frequency that the system shows its dynamical behaviour with poor damping and amplification of frequency components nearby.

A load that satisfies the criterion by having a positive real part transfer function may be classified as 'passive', meaning that the energy transferred from the load to the rotary converter is less than or equal to the energy transferred originally from the converter to the load. The energy at the frequency of interest is then dissipated in the load (Brogliato, et al. [31]). The opposite of being 'passive' is being 'active', i.e., injecting energy into the system at the oscillation frequency.

This criterion does not imply that the system becomes unstable if it is not fulfilled. Violation only reduces the total damping of the rotary converter. The degree of violation determines whether the system will be unstable or not, with the opposite being a load as modelled here that cannot make the rotary converter unstable if this criterion is satisfied.

3.4.7 Generalisation

The characteristic swing equation and the analytical expression for the electromechanical mode as shown in Equations (3.13) and (3.14), respectively, are not valid for a railway rotary frequency converter only. They can be generalised to be valid for any number of n synchronous machines operating on their respective synchronous networks, stiffly mechanically connected. The characteristic equation for each of these n machines is added together in Equation (3.28), resulting in the expression for the eigenvalues shown in Equation (3.29). Such a machine may, for example, be a prime mover powering two synchronous generators connected to two networks having different fundamental frequencies[9].

[9] Such a configuration with one turbine powering two synchronous generators connected to respective networks with different ω_s was said to exist at Kjosfoss hydro power station in Norway before the recent refurbishment. However, a connection to both the interconnected 16 ⅔-Hz traction network and 50-Hz utility network at the same time, was never experienced.

$$\sum_n \left(2H_n \Delta\ddot{\delta}_{pu} + D_n \omega_{sn} \Delta\dot{\delta}_{pu} + K_{1n} \omega_{sn} \Delta\delta_{pu} \right) = 0 \tag{3.28}$$

$$\lambda_{1,2} = -\frac{\sum_n D_n \omega_{sn}}{4\sum_n H_n} \pm \sqrt{\left(\frac{\sum_n D_n \omega_{sn}}{4\sum_n H_n} \right)^2 - \frac{\sum_n K_{1n} \omega_{sn}}{2\sum_n H_n}} \tag{3.29}$$

3.4.8 Mechanical analogy

Mechanical analogies of electric systems may facilitate the basic understanding of power system dynamics. Samuelsson [151] develops analogies for several power system phenomena.

A mechanical mass-spring analogy to the electric rotary converter for the low-frequency electromechanical eigenmode can be established as shown in Figure 3-7:

- The rotating solid mass of the converter is illustrated as a mass that can slide back and forth without friction, corresponding to a mass rotating faster and slower than its synchronous rotating reference system.
- This sliding mass is connected to fixed points or walls in both ends, corresponding to the stiff network voltages.
- The mass is connected to the walls by springs which have spring constants that correspond to the transient synchronising torque coefficient multiplied by the fundamental frequencies for the two electric machines. From the basics of mechanical vibration (e.g. Thomson [177]), it is known that two springs in parallel yield a resulting spring constant $K_{sum} = K_a + K_b$, as illustrated by the development of the electrical equations in previous sections.
- The mass is also connected to the walls by dampers which have damping constants that correspond to the respective damper coefficients multiplied by the fundamental frequencies of the two electric machines, respectively.

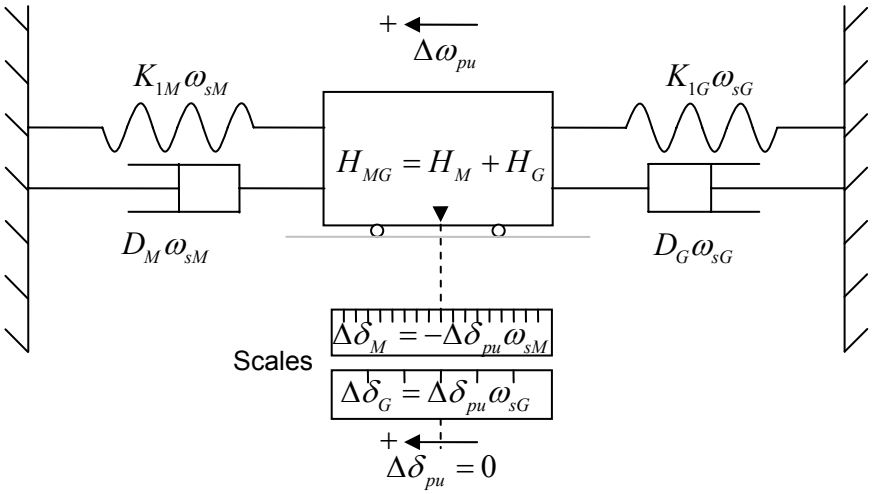

Figure 3-7: A mechanical mass-spring analogy for the rotary converter connected to stiff network on both three-phase and single-phase side.

- The mechanical distance the mass moves when oscillating is a change in displacement relative to the fixed walls corresponding to the per unit power angle for the rotary converter.
- The per unit mechanical distance can be converted to actual displacement relative to the two different references using different scales that correspond to the two different fundamental network frequencies.

3.5 Numerical example and comparison with measurements

This section includes a numerical example on how the characteristics of the electromechanical oscillations are calculated for the three operating modes. Finally, the calculations are compared with measurements performed and reported by Danielsen [48]. The nomenclature for the angles, impedances and time constants used here is given in Appendix B.2.

3.5.1 Operating conditions

For the calculations and measurements given in this section, operating in no-load has been chosen. This choice has the advantage of having no current and hence no voltage drops, making all calculations easier, i.e., the expression of the damping constant shown in Section 3.5.5. Additionally, there will be no influence by the dynamical qualities of the loads in the system, which excludes some uncertainty in both the calculation and the measurements.

3.5.2 Network model

The network under study is a railway rotary converter rated at 4 MVA, connecting two synchronous networks as shown in Figure 3-8. This is the most typical converter type used in Norway (Banverket/Jernbaneverket [17]). Between the motor and the stiff voltage source $U_{3s,}$ there is a 22-kV three-phase network having a short-circuit capacity of 248 MVA at node U_3 and a 22-kV/6.3-kV transformer. Between the generator and the artificial stiff voltage $U_{1s,}$ there is a 4.0 kV/16.6 kV step-up transformer and 92 km of overhead contact line.

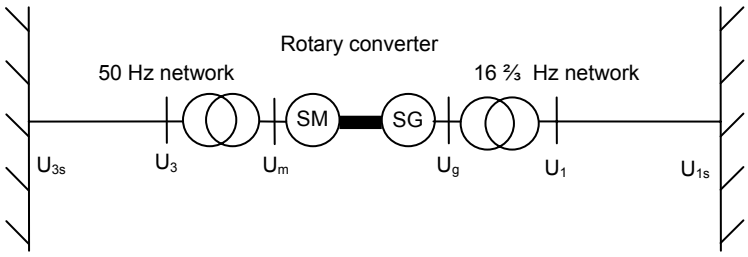

Figure 3-8: A single-line diagram of a network under study.

For the calculations, all resistances for the purpose of simplicity are neglected together with the influence from the automatic voltage regulators. The stiff network voltages are assumed to be 1 per unit and the converter is in no-load, i.e., power angles are zero. Numerical figures for the networks and synchronous machines are given in Appendix B.2, which also includes an explanation of the synchronous-machine parameters in use.

3.5.3 Synchronous-machine parameters

Synchronous-machine parameters are received from the former manufacturer of these up to 50-year-old machines. However, calculation by use of these parameters does not result in such a poor damping of the electromechanical eigenmode as shown in Table 2-1. The poor damping experienced in Danielsen and Toftevaag [56] is confirmed for measurements in which the automatic voltage regulator and excitation system are not active.

In the literature as per Dahl [46], Bonfert [30] and Machowski, et al. [115], the linear damping D proportional to the machine slip or deviation from synchronous rotational speed is expressed as Equation (3.30). The parameter abbreviations are explained in Appendix B.2.

$$D = U_s^2 \left(\frac{X'_d - X''_d}{\left(x_e + X'_d\right)^2} T''_{d0} \sin^2 \delta + \frac{X'_q - X''_q}{\left(x_e + X'_q\right)^2} T''_{q0} \cos^2 \delta \right) \tag{3.30}$$

This damping consists of two terms: the d-axis and the q-axis contribution. Among others things, each of these is proportional to the difference between the respective transient and sub-transient reactances. The d-axis parameters are relatively easy to find as they are given by a short-circuit test (Bonfert [30], Kundur, et al. [107]). Tests requiring more effort are needed to determine the q-axis data. The damping impact from the converter motor is provided by eddy currents in the massive poles. Massive pole rotors increases the X_q'' compared with machines having damper windings (Bonfert [30]).

Based on this, it has been chosen to increase the value of X_q'' until the poor damping that has been experienced in reality is reached in the model, i.e., an increase from 0.24 to 0.34 pu, which corresponds to an increase of 42 %. The X_q'' over X_d'' ratio is increased from 1.45 to 2.0. A typical ratio for machines with massive poles is 1.2 to 1.8 (Bonfert [30]).

Additionally, the given inertia constants (H) do not include the rotating mass of the field machines. Hence, the received values for the inertia constants are increased by 5 %.

3.5.4 Transient synchronising torque coefficient

The transient synchronising torque coefficient is a linearisation constant reflecting the change in the electromagnetic torque of the synchronous machine in relation to a change in the electrical power angle, and has the unit per unit torque per radian. An expression for this coefficient is shown in Equation (3.31) found by a partial differentiation in the equation for the salient-pole synchronous-machine transient power-angle characteristic:

$$K_1 = \frac{\partial \tau_{etpu}\left(\delta'_0\right)}{\partial \delta'} = \frac{E'_q U_s}{x_e + X'_d} \cos \delta'_0 + U_s^2 \frac{X'_d - X'_q}{\left(x_e + X'_d\right)\left(x_e + X'_q\right)} \cos 2\delta'_0 \tag{3.31}$$

3.5.5 Damping coefficient

The damping coefficient is an expression of the damping torque given by electrical damping per speed deviation from the synchronous reference rotational speed. Its value is both dependent on the construction of the machine (such as damper windings) and the operating point in study (especially the power angle). The determination of the exact damping impact from the electrical damping may be a difficult task. A common and simplified expression for the damping constant D is shown in Equation (3.30). However, this equation is found to be insufficient when dealing with the large generator sub-transient quadrature axis time constant, due to the low-resistance damper windings needed for single-phase machines. Pal [136] (page 6-21) provides a more detailed expression that takes such time constants into account, together with the oscillation frequency ω_{osc} to be damped.

$$\begin{aligned} D = {} & U_s^2 \left(\frac{\left(X_d - X_d'\right) T_{d0}'}{\left(x_e + X_d\right)^2 + \omega_{osc}^2 \left(x_e + X_d'\right)^2 T_{d0}'^2} + \frac{\left(X_d' - X_d''\right) T_{d0}''}{\left(x_e + X_d'\right)^2 + \omega_{osc}^2 \left(x_e + X_d''\right)^2 T_{d0}''^2} \right) \sin^2 \delta \\ & + U_s^2 \left(\frac{\left(X_q - X_q'\right) T_{q0}'}{\left(x_q + X_q\right)^2 + \omega_{osc}^2 \left(x_q + X_q'\right)^2 T_{q0}'^2} + \frac{\left(X_q' - X_q''\right) T_{q0}''}{\left(x_e + X_q'\right)^2 + \omega_{osc}^2 \left(x_e + X_q''\right)^2 T_{q0}''^2} \right) \cos^2 \delta \end{aligned} \tag{3.32}$$

In the calculation in this section, Equation (3.33) is used. This is a simplification of Equation (3.32) when the following simplifications are made:

- The converter is studied in no-load, i.e., with power angles that are equal to zero. The direct axis damping impact is then zero.
- $X_q' = X_q$. Such a simplification is common for salient pole machines (Machowski, et al. [115]).

$$D = U_s^2 \frac{\left(X_q' - X_q''\right) T_{q0}''}{\left(x_e + X_q'\right)^2 + \omega_{osc}^2 \left(x_e + X_q''\right)^2 T_{q0}''^2} \tag{3.33}$$

3.5.6 Measurements

The measurements are performed for a case in which a local single-phase load is shut off by use of two multiple operated locomotives that open their main circuit breakers when consuming power. The stiff single-phase voltage is in the interconnected operating mode represented by the rest of the single-phase network, including a rotary converter at a distance of 92 km. This second rotary converter represents a dynamic behaviour that is not included in the calculation model in Section 3.5.2. A perfectly stiff single-phase voltage reference was due to practical reasons not available.

The measurements include active automatic voltage regulators for both synchronous machines. An example of the results for motor (*P3*) and generator (*P1*) power for interconnected and island operation, respectively, is shown in Figure 3-9.

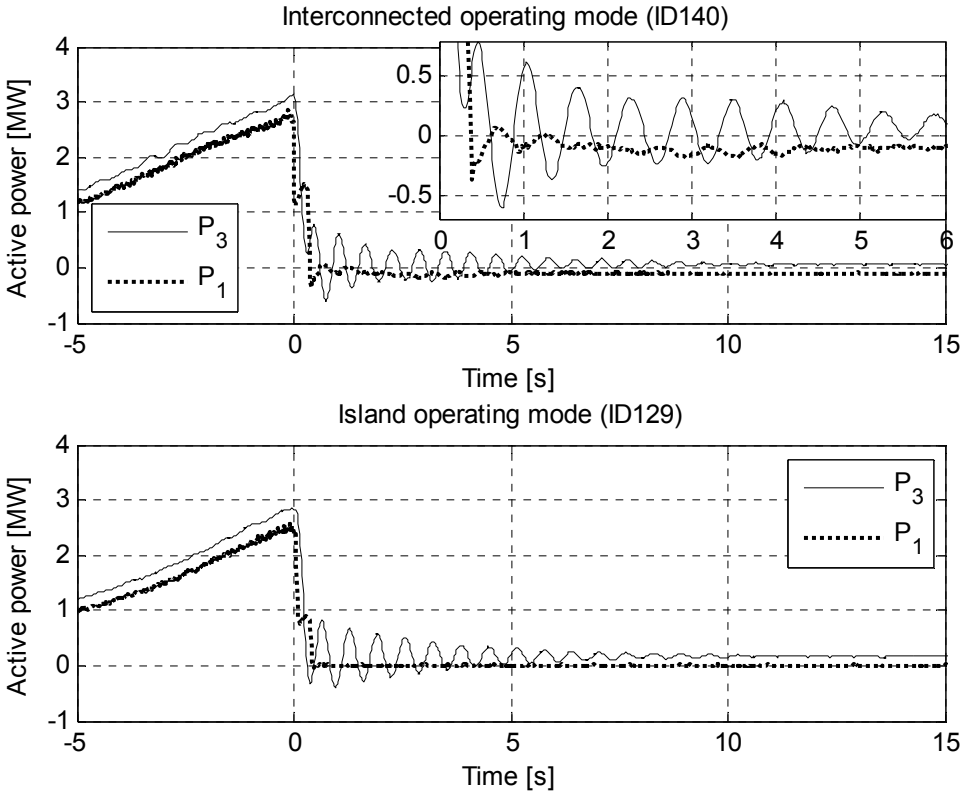

Figure 3-9: An example of test results for single-phase active power shut-off in interconnected and island operating mode, respectively.

In interconnected mode there are motor and generator power oscillations, while in island mode there is no generator power since there are neither local loads nor single-phase connection to other converters.

The damping and frequency of the oscillation are extracted from the converter step response by use of the three-phase active power (*P3*) as input to Equation (C.3) in order to calculate an apparent eigenvalue. This is done for the 10 first oscillation periods, and then an average is created.

It can be observed in Figure 3-9 that three-phase and single-phase active power roughly oscillates in anti-phase as predicted for interconnected operation. Comparing the amplitude of the power oscillations in Figure 3-9 gives a ratio $R_{\Delta p}$ of (0.5/0.1=) 5. A similar calculation for the numerical values in Table 3-1 by use of Equation (3.17) gives $R_{\Delta p} = 5.26$.

3.5.7 Comparison between calculations and measurements

The low-frequency electromechanical eigenvalues calculated and measured are compared in Table 3-1 together with the calculated coefficients for the two machines in the three different operating modes.

Table 3-1: A comparison between the calculated and measured electromechanical eigenvalues. See Section 2.2.4 for explaining of operating modes.

Operating mode	Motor		Generator		Calculated mode	Measured mode
	K_{1M}	D_M	K_{1G}	D_G	[1/s] ± *j* [Hz]	[1/s] ± *j* [Hz]
Interconnected	2.27	0.014	1.27	0.005	– 0.32 ± *j*1.69	– 0.32 ± *j*1.66
Island	2.27	0.015	0.00	0.000	– 0.31 ± *j*1.55	– 0.33 ± *j*1.57
Reactive comp.	0.00	0.000	1.27	0.032	– 0.23 ± *j*0.67	Not measured

Inserting the numerical coefficients into Equation (3.14) clearly shows that the three-phase motor dominates the low-frequency behaviour resulting in an eigenfrequency f_{res} in the vicinity of 1.6 Hz. The coefficients are larger for the motor than for the generator, both in interconnected and island operation. In addition, the coefficients are weighted three times more due to the frequency ratio. Despite the large generator damper windings, its contribution to the damping is low due to the weak line connection to the rest of the single-phase system. Islanding the single-phase side creates no significant change in the mode. The change in damping coefficients among the different modes is due to the frequency-dependent damping. The measurements show similar values to the calculations.

3.5.8 Comparison with higher order models

The developed swing equation of the second order describes in a simplified way the basics of the low-frequency eigenmode. Real synchronous machines are more complex, and a common way of representing these in power system studies is by the use of 5th order models (Kundur [106] and Machowski, et al. [115]). Such a model includes the rotor speed and power angle, as in the second-order model developed. In addition, three differential equations describing the dynamics for the field winding and the *d*-axis and *q*-axis damper windings are included. Additionally, the real power system impedances also have a resistive part.

Modelling the simple power system as described in Section 3.5.2 by means of 5th order machine models reveals the eigenvalues shown in Table 3-2 when using the linear analysis tool in SIMPOW. The simulated eigenvalues are compared with the calculated and measured eigenvalues in Section 3.5.7.

Table 3-2: A comparison between simulated, calculated and measured electromechanical eigenvalues. Units are [1/s] and [Hz]

Operating mode	Simulated mode with 5th order model	Calculated mode with 2nd order model	Measured mode
Interconnected	– 0.39 ± *j*1.77	– 0.32 ± *j*1.69	– 0.32 ± *j*1.66
Island	– 0.34 ± *j*1.59	– 0.31 ± *j*1.55	– 0.33 ± *j*1.57
Reactive compensation	– 0.12 ± *j*0.76	– 0.23 ± *j*0.67	Not measured

The table shows similarities between the eigenvalues found in island operation. In interconnected and reactive compensation mode, larger differences can be observed. These differences are not studied further, though some deviation due to a different level of model detailing must be expected as described by Johansson, et al. [93].

3.6 Mode sensitivity to surrounding networks and loads

It could be of interest to study how the damping and frequency of the rotary converter's low-frequency electromechanical mode is influenced by changes in the surrounding three-phase and single-phase networks. The calculation of the eigenvalues is done by the simple second-order model developed in this thesis. Only one rotary converter unit in each converter station is considered.

3.6.1 Three-phase network

The characteristics of the three-phase network may be divided into two categories: its nominal voltage U_N and short-circuit capacity S_{sc}. The minimum, typical and maximum figures for the Norwegian power supply can be found in the document which describes the characteristics of the infrastructure (Banverket/Jernbaneverket [17]). The apparent short-circuit power is related on the network side of the converter-station three-phase transformer, and is assumed to be without contribution from the rotary-converter motor itself. The results for the islanded single-phase network are shown in Table 3-3:

Table 3-3: A comparison of low-frequency mode for different three-phase networks. Units are [1/s] and [Hz].

S_{sc}	Min: 11 kV	Typical: 66 kV	Max: 132 kV
Min: 70 MVA	$-0.27 \pm j1.49$	$-0.26 \pm j1.47$	$-0.21 \pm j1.39$
Typical: 250 MVA	$-0.31 \pm j1.55$	$-0.30 \pm j1.54$	$-0.24 \pm j1.45$
Max: 2500 MVA	$-0.33 \pm j1.58$	$-0.32 \pm j1.57$	$-0.26 \pm j1.47$

This table indicates no large differences in the electromechanical mode for the different combinations of three-phase network nominal voltage and short circuit capacity, and the essential poor damping is kept. However, we observe that the increased short-capacity results in increased damping and oscillation frequency of the mode as the network impedance Z_{l3}, is as indicated by Equation (3.34) proportional to S_{sc} inverse. A change in U_N alone when S_{sc} is kept constant has no influence, but a higher primary voltage requires another transformer with a higher inductance which reduces both damping and oscillation frequency accordingly.

$$Z_{l3} = \frac{U_N^2}{S_{sc}} \tag{3.34}$$

3.6.2 Single-phase network

The single-phase network can be characterised by the distances to the next converter stations and the type of line used. Two line types are compared, the conventional 15-kV overhead contact line and the new proposed autotransformer system on +15/–15 kV. The distance between the two following converter stations is varied in the normal steps

of 40, 80, 120 and 160 km for both systems. An equivalent stiff single-phase network bus is considered to be the combination of the next stations in both directions. That is, the distance to the stiff network bus is 40 km in a system in which the distance is 80 km between two stations.

A typical three-phase network of 66 kV/250 MVA is used. The typical line impedance for conventional overhead contact line is given in Banverket/Jernbaneverket [17], and the expected line impedance between positive and negative feeder inclusive autotransformers is found in Varju [180]. The results are shown in Table 3-4.

Table 3-4: A comparison of low frequency mode for different single-phase networks. The units are [1/s] and [Hz].

Distance between converter stations	**Conventional overhead contact line 15 kV**	**Autotransformer system +15/–15 kV**
40 km	$-0.42 \pm j1.73$	$-0.50 \pm j1.75$
80 km	$-0.36 \pm j1.71$	$-0.46 \pm j1.74$
120 km	$-0.34 \pm j1.70$	$-0.43 \pm j1.73$
160 km	$-0.32 \pm j1.69$	$-0.40 \pm j1.73$

The results indicate a tendency for an increased damping as the distance between converter stations decreases or an AT-system is introduced. In both cases, the line impedance is decreased, though no large increase in the converter damping can be expected. The results are based on the simplification of modelling the next stations as voltage sources without internal impedance, which overestimates the damping. Detailed modelling may reduce the differences between the cases even more.

3.6.3 Single-phase load characteristic

The single-phase load voltage-dependency characteristic in Equation (3.26) is found to have an influence on the converter's damping. This contribution to the eigenvalue's real part is shown in Equation (3.35).

$$D_{MP} = -\frac{P_{elGpu0} \cdot k_u^{MP} \cdot (MP-1)}{4H_{MG}} \tag{3.35}$$

Table 3-5 shows a comparison between the three main types of load characteristic and their influence on the eigenvalue in question. The generator is supplying a nominal load, and an automatic voltage regulator is not being used. The influence calculated by use of Equation (3.35) is compared with the eigenvalue calculated in SIMPOW with the 5th order synchronous-machine models introduced in Section 3.5.8. The neutral constant-current load is used as a reference.

Table 3-5: The eigenvalues for different single-phase load voltage dependency characteristics. The units are [1/s] and [Hz].

MP	Eigenvalue 5^{th} order model	Load characteristic influence 5^{th} order model	Load characteristic influence Equation (3.35)
0	$-0.3627 \pm j1.6164$	$+0.0694$	$+0.0668$
1	$-0.4321 \pm j1.6164$	0.0000	0.0000
2	$-0.5099 \pm j1.6161$	-0.0777	-0.0668

The direction and size of the influence calculated by Equation (3.35) are reflected by the differences between the eigenvalues based on the 5^{th} order machine models. The constant power load is reducing the system's damping of the rotary converter's eigenfrequency. It should be commented though that the influence is low (15%) compared with the actual value of the eigenvalues' real parts, even for this poorly damped converter.

By comparing the eigenvalues for the 5^{th} order models at neutral nominal constant current load in Table 3-5 with the no-load case in Table 3-2, it can be observed that the mode damping has increased. This is due to the increased load and changed motor power angle resulting in an increase in *d*-axis damping corresponding to Equation (3.30). This more than compensates for the corresponding decrease in *q*-axis damping.

3.7 Discussion and conclusion

3.7.1 Discussion

3.7.1.1 Measurement considerations

The measurements reported support the theoretical development and considerations presented in this chapter. However, it is not immediately clear that Figure 3-4 and Figure 3-9 show the same response. The measured responses have oscillation amplitudes that are much lower than the initial values. This is due to an imperfect step in single-phase power, as the main circuit breakers of the two multiply operated locomotives did not open at exactly the same instant, but instead there was an unfortunate time delay. A closer study though, as in Table 3-1, reveals that the oscillation damping and frequency correspond.

The measurements also confirm that three-phase and single-phase powers oscillate against each other in anti-phase in interconnected operating mode. It should be noted, however, that even if the power oscillations in low-frequency electromechanical mode are in anti-phase, the steady state or quasi-stationary power varies in phase, i.e., an increase in generator power increases the motor power as shown in the figures.

The measured oscillation in the interconnected mode does not have a perfect exponential decay as in the island mode. This is probably due to the excitation of and interaction with the next rotary converter on the line, as the single-phase power is much distorted. When single-phase power oscillation is more than 180 degrees phase shifted

relative to three-phase power, as seen from 2 to 4 s in Figure 3-9, the oscillation amplitude decay is low. The damping is then also low due to single-phase power containing a component in anti-phase of the speed oscillations. When single-phase power is less than 180 degrees phase shifted relative to three-phase power, as seen from 1 to 2 s, the oscillation amplitude decay and damping is high due to a component in phase with the speed. Hence, the damping found based on the measurement is calculated as an average over 10 oscillation periods.

3.7.1.2 Reason for poor damping

Experience and measurements (e.g. Toftevaag and Pálsson [178] and Danielsen and Toftevaag [56]) shows that the rotary converter has a poorly damped eigenfrequency. However, calculations based on the synchronous machine parameters received from the former converter manufacturer do not reflect this poor damping. It has not been possible to explain as to why the converter shows such a poor damping in real life and the received parameters do not.

One suggestion for the reduction of the machine damping that has been proposed and introductorily studied by Garten [70] is the fact that most of the converters are placed on railway carriages which includes leaf springs as shown in Figure 2-2. Therefore, the machine stators may not be expected to be fixed as if they were placed directly on a fixed foundation (e.g. the floor). Mechanical oscillations in the carriage are reported when the converter oscillates at electromechanical eigenfrequency. This proposal for damping reduction in this work has not been followed-up on any further. Instead, the quadrature axis sub-transient reactance has been increased as described in Section 3.5.3 to reflect the poor damping quality.

The reason for this poor motor damping is investigated and discussed more in detail by Danielsen [48]. Kundur [106] describes how damping may be reduced in some situations. At page 752, the field flux variation due to the armature reaction for a hydraulic generator without damper windings operating at light load and connected to a line of relatively high resistance to reactance ratio to a large system is explained. At page 766, the destabilising effect of the AVR is explained for high values of external system reactance and high generator output. The fact that the rotary converter shows poor damping in no-load and island mode (motor active only) without active AVR does not obviously correspond to these described situations. The supplying three-phase grid has not been considered to have a special high resistance to reactance ratio. Deeper investigations are needed in order to tell for sure if these phenomena really have influence on the rotary converter damping or not.

3.7.2 Conclusion

An extended and simplified swing equation for synchronous-synchronous rotary frequency converters is developed and numerical calculations are supported by measurements. The converters studied here have a poorly damped electromechanical eigenfrequency. It has though not been possible to recreate this poor damping based directly in the models based on the synchronous-machine parameters received from the

manufacturer. A tuning of the quadrature-axis sub-transient time constant has been found to be necessary.

The converter's low-frequency behaviour is dominated by the motor due to its higher fundamental frequency and stiffer connection to the three-phase network. The interconnected operating mode resembles a single-machine infinite-bus (SMIB) system for a prime mover driven generator. However, the island operating mode for the converter generator differs from the similar operation of a prime mover driven generator, as the converter motor is still connected to a stiff network on the three-phase side, and the characteristic second-order electromechanical dynamics is still present.

The two synchronous machines' oscillation and damping properties come together when both are connected to their respective power networks. This can be generalised for any number of synchronous machines connected together as a lumped mass, and their contribution to the electromechanical mode is weighted by the fundamental frequencies of their respective networks.

An important characteristic of the rotary converter is that a positive electromagnetic torque imbalance results in acceleration of rotor, and opposite when negative imbalance. The voltage characteristic of a local single-phase load supplied from the rotary converter is found to have an influence on the damping of the converter's low-frequency electromechanical eigenmode since it has an impact on the generator electromechanical torque during a speed oscillation. A constant power load is reducing the damping and a constant resistance load is increasing the damping, and a constant current is considered to be neutral. An important qualitative stability criterion is that the single-phase load should not show a constant power load behaviour at the eigenfrequency where the converter's damping is poor. Additionally, it has been observed that increased loading also increases the motor damping of the eigenmode.

The numerical sensitivity analysis regarding three-phase and single-phase network parameter variations shows that the stiffness of the networks cannot be expected to have an influence on the damping of the eigenmode to any serious extent.

3.7.3 Further work

Based on the work in this chapter, further work may be proposed even though nothing here is new:

- The rotary converter shows a poorly damped electromechanical eigenfrequency. A common way to damp such oscillations is by use of a power system stabiliser (PSS). The development and implementation of such a PSS for the rotary converter should be futher focused on, especially in regard to the motor.

- The damping of the rotary converter eigenfrequency is influenced by the single-phase load by the generator voltage on speed variation ratio k_u as shown in

Equation (3.26). This negative influence could be reduced by use of the generator AVR, perhaps together with an additional PSS.

- The exact reason for the poor damping of the rotary converter eigenfrequency has not been found. It might be of interest to further investigate this reason by a more exact determination of the synchronous-machine parameters and the influence from the rail carriage oscillations. This activity is however of more as a curiosity, as the converters are old and no large hardware changes may be expected.

- The measurement in interconnected operating mode shown in Figure 3-9 is not illustrating the single-phase power oscillation very well. When opportunity, a new measurement with a stiffer equivalent single-phase voltage should be performed and the step disturbance should be performed by one vehicle only.

4 Power system modelling

This chapter explains various concepts of power system modelling that will be compared in the stability studies later in this thesis. An enhanced RMS mode is proposed as a compromise between instantaneous value modelling and standard RMS mode modelling.

4.1 Introduction

In a traditional three-phase power system with mainly electric machines and passive loads, it can be argued that low-frequency stability studies by time-domain simulations and linear analysis can be performed in fundamental frequency (or RMS (root-mean-square)) mode instead of in time-domain simulations with instantaneous values of voltage and current values (Kundur [106]). For electromechanical transients it is normally sufficient to consider the power frequency component of voltages and currents in an AC network and the mean value of the voltages and currents in a DC network, as for power flows ([3] page 1228 for a full power converter wind turbine, page 1265 for a doubly-fed induction generator, page 1455 for a HVDC converter, page 1541 for a HVDC Light converter, page 1517 for a STATCOM, page 1620 for a railway line voltage converter, page 1641 for a railway PWM and page 1747 for a rotary converter).

In a power system with dominating non-linear components, particularly in a single-phase system, these traditional tools may not however be fully valid any more (Möllerstedt [130]). It would be of great interest and benefit though if already established and traditional methods for the study of power system stability could be used in systems with power-electronic components as well. Thus, one objective of this thesis is to investigate to what extent traditional power system modelling of a power electronic component reflects low-frequency phenomena in a single-phase system.

4.2 Instantaneous values of voltage and current

The instantaneous value modelling of a power system is close to being reality, and all experienced phenomena can be represented and tested most realistically. Hence, time domain modelling and simulation, e.g. in Matlab/Simulink (Menth and Meyer [116]), is often used in studies of advanced electric rail vehicles in which complex phenomena may be of interest.

Among the vehicle manufacturers, so-called real-time-simulators (RTS) as described by Terwiesch, et al. [176] are considered to be a powerful tool. The vehicle digital control system with all its non-linearities is simulated in real-time together with a power system model and/or a motor side model. This is often called hardware-in-the loop or software-

in-the-loop simulations, depending on one's point of view. On the other hand, Staudt, et al. [161] describe a method for a high-speed simulation of the same phenomena.

The instantaneous voltages and currents in an AC system in instantaneous value mode can, if harmonics are neglected and the system is in steady-state, be described as sinusoidal waves as functions of time t, as in Equations (4.1) and (4.2). The fundamental angular speed is $\omega_s = 2\pi \cdot f_s$ where the fundamental (or synchronous) frequency is given as $f_s = 16\ ⅔$ Hz in the traction power system considered in this thesis. A_u and B_u in Equation (4.1) and A_i and B_i in Equation (4.2) together describe the individual amplitude and phase of the voltage u and current i, respectively.

$$u(t) = A_u \cos(\omega_s t) + B_u \sin(\omega_s t) \tag{4.1}$$

$$i(t) = A_i \cos(\omega_s t) + B_i \sin(\omega_s t) \tag{4.2}$$

These instantaneous signals, with fundamental frequency only, can be written in their complex form (rectangular or exponential form) as rotating phasors as shown in Equations (4.3) and (4.4) where θ_{u0} and θ_{i0} are initial displacement angles for the voltage and current, respectively. Yet, it is common to choose a reference, θ_u and θ_i, for instantaneous values such that the imaginary parts disappear. $\hat{U}$ and $\hat{I}$ express the peak values of the voltage and current, respectively.

$$\begin{aligned} u(t) &= A_u \cos(\omega_s t + \theta_{u0}) + jB_u \sin(\omega_s t + \theta_{u0}) \\ &= \hat{U} \cos(\omega_s t + \theta_u) \\ &= \sqrt{A_u^{\,2} + B_u^{\,2}}\, e^{j(\omega_s t + \theta_{u0})} \\ &= \hat{U} e^{j(\omega_s t + \theta_u)} \end{aligned} \tag{4.3}$$

$$\begin{aligned} i(t) &= A_i \cos(\omega_s t + \theta_{i0}) + jB_i \sin(\omega_s t + \theta_{i0}) \\ &= \hat{I} \cos(\omega_s t + \theta_i) \\ &= \sqrt{A_i^{\,2} + B_i^{\,2}}\, e^{j(\omega_s t + \theta_{i0})} \\ &= \hat{I} e^{j(\omega_s t + \theta_i)} \end{aligned} \tag{4.4}$$

4.3 Reference frames

From a sideline perspective as in Figure 4-1a), the phasors in Equations (4.3) and (4.4) are seen rotating with the angular speed ω_s in the complex plane. This is called the stationary reference frame, and the direction of these phasors is then time-variant, i.e., depending on the instant it is considered – even in steady-state.

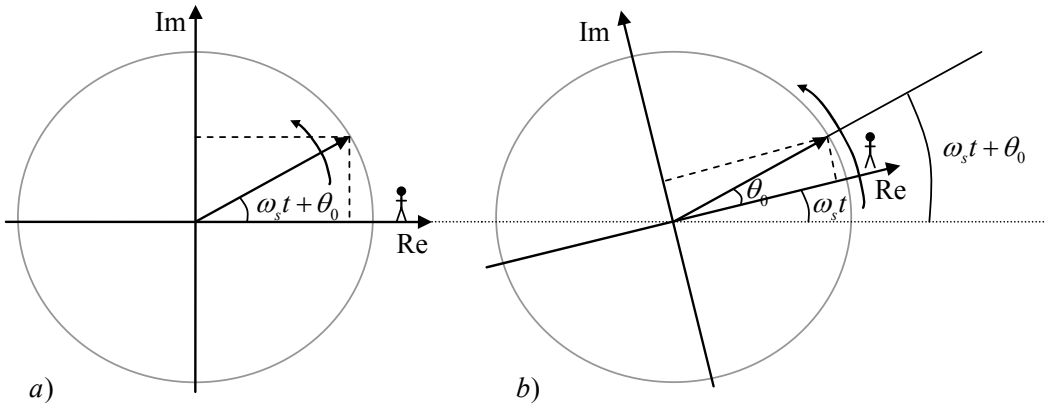

Figure 4-1: a) Stationary reference frame
b) Rotating reference frame

In order to simplify hand calculations and increase simulation speed for power system analysis, it is common to make use of root-mean-square (RMS) values and a reference frame rotating at a synchronous speed ω_s as seen in Figure 4-1b). Hence, this is called the rotating reference frame, and all steady-state fundamental AC values can in this frame be expressed by DC values. The arguments of the phasors describe their mutual displacement from the reference only, and the signals are now time-invariant in steady state.

Using standard RMS values also implies neglecting fast network transients in synchronous-machine stators and corresponding series network components (Kundur [106]). The influence of the changed network frequency in reactance values is also neglected, thus the number of differential equations describing the network can be considerably reduced. Using this simplification, the corresponding voltages and currents are as formulated in Equations (4.5) and (4.6) in which there is no time dependency in steady state.

$$\vec{U} = \frac{1}{\sqrt{2}}\left(A_u \cos\left(\theta_{u0}\right) + jB_u \sin\left(\theta_{u0}\right)\right) = U_{\mathrm{Re}} + jU_{\mathrm{Im}} = Ue^{j(\theta_{u0})} = \frac{\hat{U}}{\sqrt{2}}e^{j(\theta_{u0})} \tag{4.5}$$

$$\vec{I} = \frac{1}{\sqrt{2}}\left(A_i \cos\left(\theta_{i0}\right) + jB_i \sin\left(\theta_{i0}\right)\right) = I_{\mathrm{Re}} + jI_{\mathrm{Im}} = Ie^{j(\theta_{i0})} = \frac{\hat{I}}{\sqrt{2}}e^{j(\theta_{i0})} \tag{4.6}$$

The equations have become time-invariant as the $\omega_s t$ term of the angle is omitted. That does not however mean that the voltage and current cannot change as time goes. They are still a function of time, and will change when the power system operating state changes or during transients. It is common to leave out the time dependency (t) for the variable notations in rotational reference frame, which is adopted in the following.

The synchronously rotating phasor coordinate system can be considered as a global synchronously rotating DQ system, in which the direct (D) axis is aligned with the real (Re) axis and the quadrature (Q) axis is aligned with the imaginary (Im) axis.

In a multi-phase system, a transform between the stationary and the rotating reference frame can be done instantaneously. For example, a symmetric three-phase system (abc) might first be transformed to a two-phase stationary $\alpha\beta$ reference frame by use of $abc/\alpha\beta$ or Clarke's transform and then to the rotating reference frame by use of $\alpha\beta/dq$ or Park's transform. The latter is essential in this thesis, and is shown in Equation (4.7).

$$\begin{bmatrix} u_D \\ u_Q \end{bmatrix} = \begin{bmatrix} \cos\omega_s t & \sin\omega_s t \\ -\sin\omega_s t & \cos\omega_s t \end{bmatrix} \begin{bmatrix} u_\alpha \\ u_\beta \end{bmatrix} \tag{4.7}$$

Nevertheless, in a single-phase system, an instantaneous transform from one phase to two phases in stationary reference frame is not possible. The orthogonal β-signal simply does not exist as there is only one phase. A back transformation from a rotating to a stationary reference frame is possible though by use of the inverse transformation matrix used in Equation (4.7), e.g. Equation (4.13).

4.4 Series impedance voltage drop

4.4.1 Instantaneous value and standard RMS

The voltage drop $\Delta u(t)$ or $\Delta\vec{U}$ over a resistor R and an inductor L can be described as in Equation (4.8) for instantaneous values and (4.9) for standard RMS values, respectively.

$$\Delta u(t) = R \cdot i(t) + L\frac{di(t)}{dt} \tag{4.8}$$

$$\begin{bmatrix} \Delta U_{\mathrm{Re}} \\ \Delta U_{\mathrm{Im}} \end{bmatrix} = \begin{bmatrix} R & -\omega_s L \\ \omega_s L & R \end{bmatrix} \begin{bmatrix} I_{\mathrm{Re}} \\ I_{\mathrm{Im}} \end{bmatrix} = \begin{bmatrix} R & -X \\ X & R \end{bmatrix} \begin{bmatrix} I_{\mathrm{Re}} \\ I_{\mathrm{Im}} \end{bmatrix} \tag{4.9}$$

The term $\omega_s L$, called the reactance X, leads to the rotationally induced voltage drop given by the fundamental current alternation. In the model of series inductors implemented in this thesis such as power lines and transformers the fundamental frequency is assumed to be constant, i.e., $\omega_s = 1$ pu. Note that RMS current in Equation (4.9) is no longer a state variable, i.e., it is allowed to change with an infinite time-derivative.

The amplitude of the voltage drop is given by Equation (4.10), while the amplitude of the current is given by Equation (4.11). This similarly applies to other complex values such as node voltages and changes in voltages and currents.

$$\Delta U = \left|\Delta U_{\mathrm{Re}} + j\Delta U_{\mathrm{Im}}\right| = \sqrt{\Delta U_{\mathrm{Re}}^2 + \Delta U_{\mathrm{Im}}^2} \tag{4.10}$$

$$I = \left|I_{\mathrm{Re}} + jI_{\mathrm{Im}}\right| = \sqrt{I_{\mathrm{Re}}^2 + I_{\mathrm{Im}}^2} \tag{4.11}$$

4.4.2 Enhanced RMS

For instantaneous-value modelling of three-phase systems, a synchronous rotating reference frame is often used when synchronous machines are present, as described by Persson, et al. [145]. This is called *dq0*-representation of the power system. Additionally, for the study of three-phase power electronic components, a similar local synchronously rotating *dq* reference frame is often established, as shown by for example Harnefors [72].

An important difference from traditional power system modelling and standard RMS is that the current is kept as a state variable, including the fast line current dynamics given by the term $L \cdot di/dt$. Consequently, the voltage drop over the inductive reactance becomes as shown in Equation (4.12) when considered in the real and imaginary axis coordinate system already introduced. In this thesis, this introduction of current as a state variable is called the 'enhanced' RMS mode or 'RMS $L \cdot di/dt$' (in contrast to 'standard' RMS mode):

$$\begin{bmatrix}\Delta U_{\mathrm{Re}} \\ \Delta U_{\mathrm{Im}}\end{bmatrix} = \begin{bmatrix} R + L\dfrac{d}{dt} & -\omega_s L \\ \omega_s L & R + L\dfrac{d}{dt}\end{bmatrix}\begin{bmatrix} I_{\mathrm{Re}} \\ I_{\mathrm{Im}}\end{bmatrix} = \begin{bmatrix} R + L\dfrac{d}{dt} & -X \\ X & R + L\dfrac{d}{dt}\end{bmatrix}\begin{bmatrix} I_{\mathrm{Re}} \\ I_{\mathrm{Im}}\end{bmatrix} \tag{4.12}$$

In the stationary reference frame, Equation (4.8) includes one state variable which results in one non-oscillatory mode, i.e., a real valued eigenvalue. The rotating reference frame Equation (4.12) includes two state variables which results in two eigenvalues that together form a complex conjugate pair with an oscillation frequency equal to the rotational speed of the reference frame (Harnefors [73]). This means that a DC component in the stationary reference frame will appear as a fundamental frequency AC component in the rotating reference frame, and vice versa.

In the rotating reference frame the fundamental voltages and currents are as mentioned time invariant in steady state, i.e., they can be understood as DC values. Note that the impedance in the diagonal elements of the transfer matrix in Equation (4.12) resembles the impedance in a DC system as well. The two axes can be understood as two DC systems that are connected by the reactance $\omega_s L$. This relationship is utilised further as a simplification in the analytical considerations in this thesis (Chapters 6 and 8).

Sun [174] clearly distinguish between modelling in the rotating *dq* coordinate system by instantaneously reference frame transformation and phasor-based average modelling based on RMS values for three-phase systems. The proposed enhanced RMS modelling for the single-phase system here is a combination of these to approaches.

4.4.3 Comparison

Figure 4-2 shows a comparison of the calculated current by instantaneous values and RMS values, both with and without including the dynamic voltage term $L \cdot di/dt$ during a transient. A sinusoidal voltage is imposed to an inductive impedance at voltage zero, crossing by means of a short circuit at the end of a line connected to an ideal voltage source. That means that Equations (4.8), (4.9) and (4.12) are used for calculating the voltage drop over the inductance, respectively.

The RMS mode results are expressed as instantaneous value currents by use of the transform in Equation (4.13). In standard RMS mode the DC component is absent, as the current is allowed to change with an infinite time-derivative. The extent of the DC component of the current in instantaneous value mode is known to be time-variant, i.e., dependent on the voltage phase for when the voltage disturbance is imposed, which in this case at maximum. In enhanced RMS mode, the DC component is time-invariant and always present at maximum.

$$i(t) = I_{Re}(t)\cos(\omega_s t) - I_{Im}(t)\sin(\omega_s t) \tag{4.13}$$

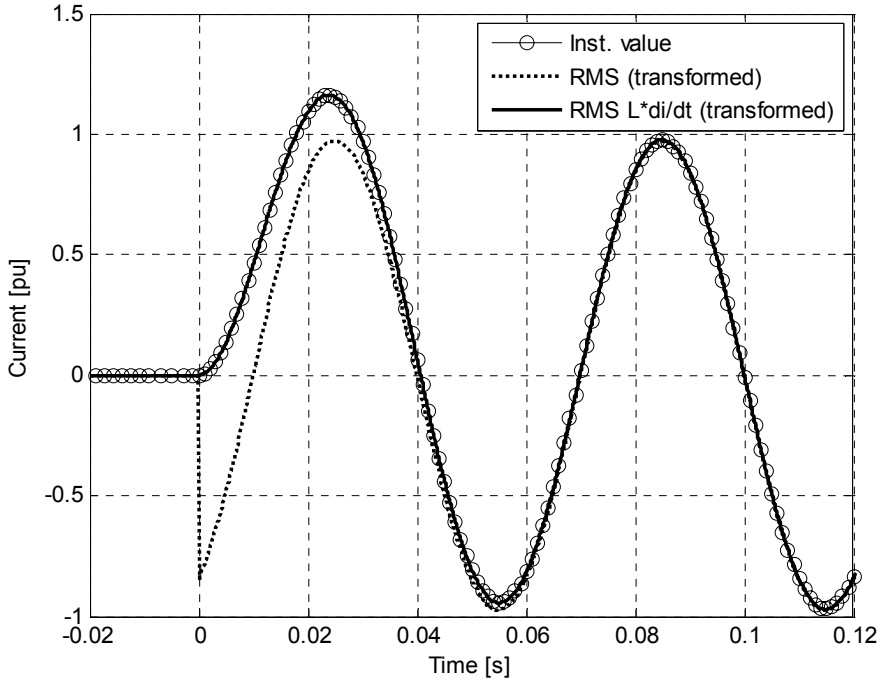

Figure 4-2: Current *i(t)* simulated in instantaneous value mode and RMS mode with and without *L·di/dt* when a sinusoidal voltage is applied to an inductive impedance.

4.5 Synchronous-machine stator flux linkages

4.5.1 Standard RMS

As described in the previous section, the time derivative current is commonly neglected in the network equations for power system studies. To make the system consistent, it is also common to neglect the voltage drop given by the time derivative of the synchronous-machine stator flux Ψ. This simplification is shown by Kundur [106] to be counterbalanced by neglecting the machine speed variation's influence on the stator winding induced voltage e. That means that the stator-voltage two-axis equations are often simplified to Equation (4.14). R_a is the stator resistance.

$$\begin{bmatrix} E_d \\ E_q \end{bmatrix} = \begin{bmatrix} -\psi_q \\ \psi_d \end{bmatrix} - R_a \begin{bmatrix} I_d \\ I_q \end{bmatrix}. \tag{4.14}$$

The simplification of neglecting the influence of the machine's speed variation implies fixing it to $\omega_{pu}(t) = 1.0$.

4.5.2 Enhanced RMS

In enhanced RMS, the simplifications for the stator-voltage equations explained in Section 4.5.1 are reversed. Equation (4.15) shows these complete equations in the rotating reference frame.

$$\begin{bmatrix} E_d \\ E_q \end{bmatrix} = \frac{1}{\omega_s}\frac{d}{dt}\begin{bmatrix} \psi_d \\ \psi_q \end{bmatrix} + \omega_{pu}\begin{bmatrix} -\psi_q \\ \psi_d \end{bmatrix} - R_a \begin{bmatrix} I_d \\ I_q \end{bmatrix} \tag{4.15}$$

For the practical implementation of the synchronous machines in this thesis, the 5th order model described and developed by Johansson [92] is used, with the only change that of replacing Equation (4.14) with (4.15)[10]. The resulting synchronous-machine models are therefore of the 7th order.

4.5.3 Comparison

Figure 4-3 shows a comparison of the calculated current by instantaneous values and RMS values, both with and without including the voltage term $L \cdot di/dt$ when a short circuit at voltage zero crossing is applied at the end of a line fed from a synchronous generator. The line is modelled as described in Section 4.4.3. For the normal and enhanced RMS modes, the stator induced voltage is calculated according to Equations (4.14) and (4.15). As there is no instantaneous single-phase synchronous-machine model available but a three-phase one, the simulations are performed with a three-phase machine and the results are shown for phase A. The results for the rotating reference frame models are transformed by use of Equation (4.13).

[10] The standard fifth order synchronous-machine model in SIMPOW represents a compromise between these two equations since the first term in Equation (4.15) is excluded while the speed influence in the second term is included.

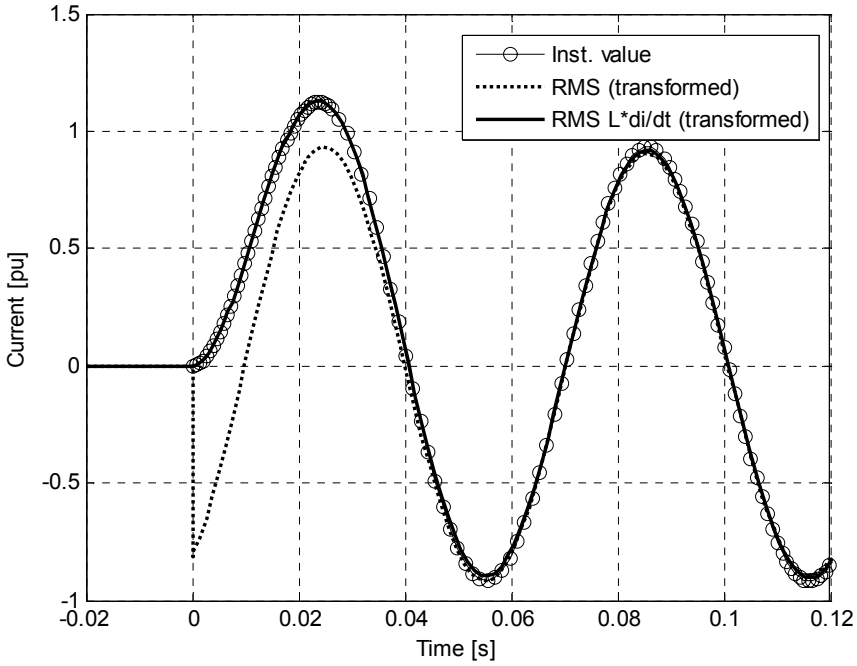

Figure 4-3: Current *i(t)* simulated in instantaneous value mode and RMS mode with and without *L·di/dt* when short circuit is applied.

The result, including the synchronous machine, shows an equal pattern as in the case with the line only.

4.6 Single-phase power availability

The instantaneous electric power $p(t)$ is known as the product of voltage $u(t)$ and current $i(t)$:

$$\begin{aligned} p(t) &= u(t) \cdot i(t) \\ &= \hat{U}\cos(\omega_s t + \theta_u) \cdot \hat{I}\cos(\omega_s t + \theta_i) \end{aligned} \tag{4.16}$$

By selecting $\varphi = (\theta_u - \theta_i)$, the instant power can be expressed as:

$$\begin{aligned} p(t) &= \frac{\hat{U}\hat{I}}{2}\cos(\varphi) \\ &+ \frac{\hat{U}\hat{I}}{2}\left(\cos(\varphi)\cos(2\omega_s t) - \sin(\varphi)\sin(2\omega_s t)\right) \end{aligned} \tag{4.17}$$

From this we can see that the instantaneous single-phase power is time-variant, having a frequency equal to twice the fundamental frequency. One may say that the terms with frequency $2\omega_s = 2 \cdot 2\pi f_s$ describe the second harmonic 'packages' in which the energy is delivered (Menth and Meyer [116]). In contrast to three-phase systems in which the sum

of the time-variant power in all three phases cancels this second-harmonic pulsation, in single-phase systems it remains.

In RMS mode, the active power P in Equation (4.18) is time-invariant since both U and I are time-invariant.

$$P = UI\cos(\varphi) \tag{4.18}$$

As an illustration, imagine the voltage $u(t)$ with $\hat{U} = 1$ pu applied to a $R = 1$ pu resistor at time $t = 0$. The resulting current $i(t)$ has $\hat{I} = 1$ pu, and is in phase with the voltage. The instantaneous power transferred is described by Equation (4.17) and the RMS power is described by Equation (4.18). The energy $e(t)$ dissipated in the resistor for the previous half fundamental period $T_s/2$ can be calculated by Equation (4.19).

$$e(t) = \int_{t-\frac{T_s}{2}}^{t} p(t)\,dt \tag{4.19}$$

Figure 4-4 shows $u(t)$, $i(t)$ $p(t)$ and $e(t)$ as a function of time for different values ([0, 45, 90, 135] degrees) of the voltage-displacement angle θ_{u0} after voltage zero crossing. As φ is kept constant, θ_{i0} is varied correspondingly. From this, it can be understood that the power availability is time-variant as given by the phase of the voltage and the current. Close to the voltage zero-crossing there is no power available while at the voltage peak there is large power available. The corresponding energy from RMS values is shown for the sake of comparison.

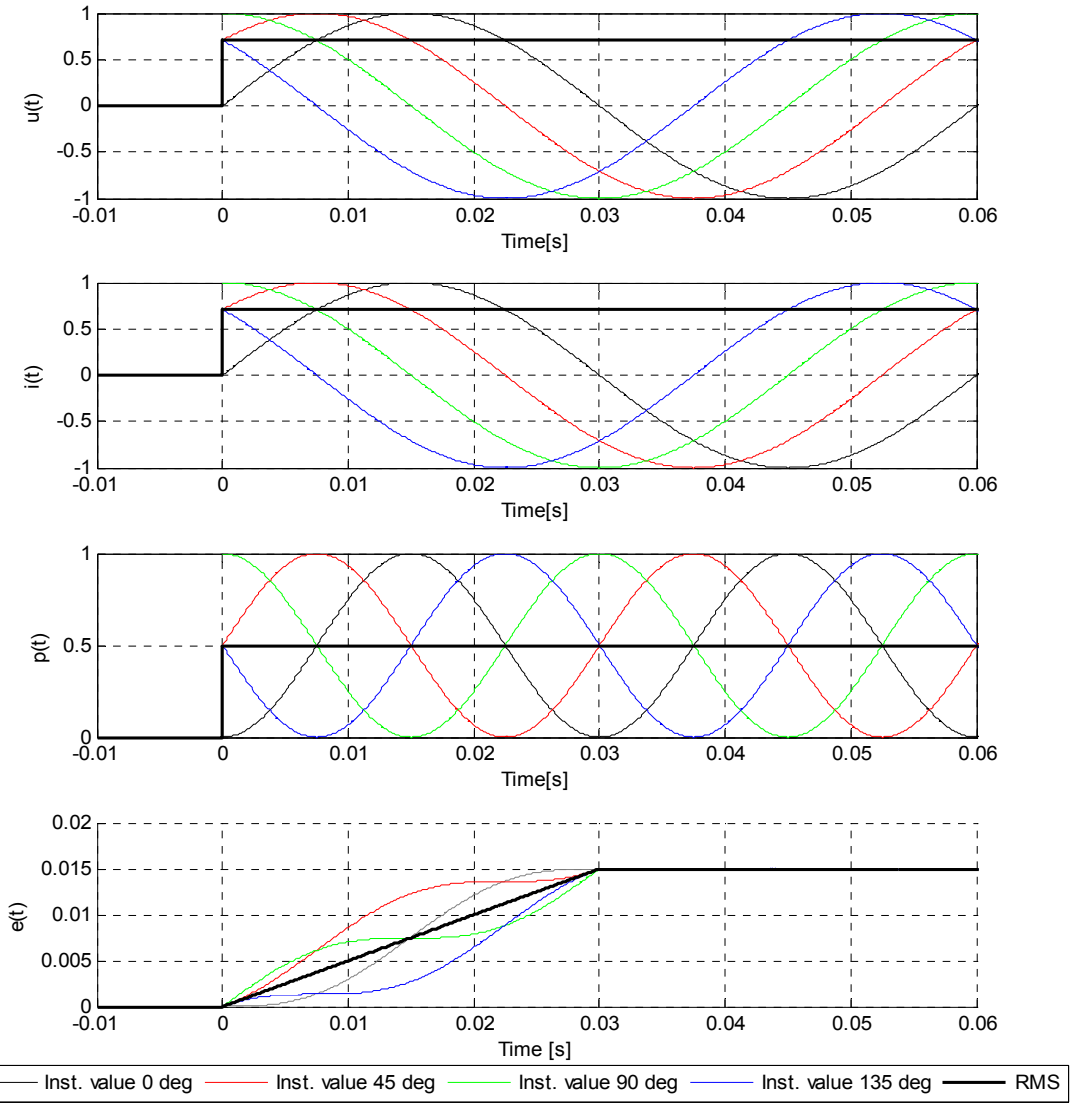

Figure 4-4: Voltage $u(t)$, current $i(t)$, power $p(t)$ and energy $e(t)$ as a function of time when voltage is applied at $t = 0$ for different values of voltage-displacement angles.

4.7 Summary

In this chapter, the fundamentals of power system modelling in stationary and rotating reference frames are explained. Instantaneous value modelling is commonly used for the single-phase study of advanced electric rail vehicles, while a rotating reference frame using RMS values is commonly used for larger power systems. For single-phase systems, modelling in the rotating reference frame is a simplification and an imitation of the formally allowed reference frame transformation commonly used for three-phase systems. The big advantage of using this method of modelling is time-invariance and constant power availability. Two different rotating reference frame models are shown, both with and without the fast current and flux dynamics in the network inductance and synchronous-machine stator. The proposed enhanced RMS mode takes the fast current dynamics of inductors into account, while this is commonly neglected in standard RMS modelling.

5 Electric rail vehicle modelling

This chapter presents the full and complex developed model of the line-side part of an advanced electric rail vehicle. Step-by-step, each controller is explained and a comparison between time-variant instantaneous-value modelling and time-invariant RMS modelling is investigated. The complete models are evaluated in view of dynamics observed by a load step response and a long line stability test.

5.1 Introduction

In this chapter a full and complex model of the line side electric solution of an advanced electric rail vehicle is developed. It is as far as possible based on fragmental descriptions found in literature and publications, but the assembly of the different components and solutions is believed to be new. A complete description of the line side of an electric rail vehicle like this has not been found published before, thus this model is a corner stone of present thesis.

The vehicle model is based on the literature and is not related to one specific real vehicle. This means that the model can be published independently of any vehicle manufacturer's industrial secrets. However, it also introduces uncertainty, as there is no real-life vehicle to compare the model with.

The vehicle model development focuses on the single-phase instantaneous value solutions since it is under these circumstances a real vehicle has to operate. These solutions are further represented in a rotating reference frame in order to be used for the corresponding RMS models that are developed in parallel. Instantaneous value variables are commonly written with lowercase letters and RMS variables are commonly written as phasors with uppercase letters. The paralell modelling in both instantaneous values and RMS values in this chapter may challange this convention, even if it is aimed to use the letter case that illustrates the each point, equation or figure best according to the context.

Important parts of the vehicle model in view of low-frequency power oscillations are more deeply studied and discussed in Chapter 6. An overall discussion of the vehicle model relevance in this thesis is given in Section 9.1.

5.2 Overview

5.2.1 Block and phasor diagram

The main task for an electric rail vehicle is to convert electric energy delivered from the overhead contact line into mechanical energy in order to run the train. A more detailed single-line and signal-flow diagram on how the control system of an advanced electric rail vehicle in Figure 2-4 may look like is shown in Figure 5-1. The voltage u_{ac1} in the lower left corner is the line voltage at the vehicle's current collector.

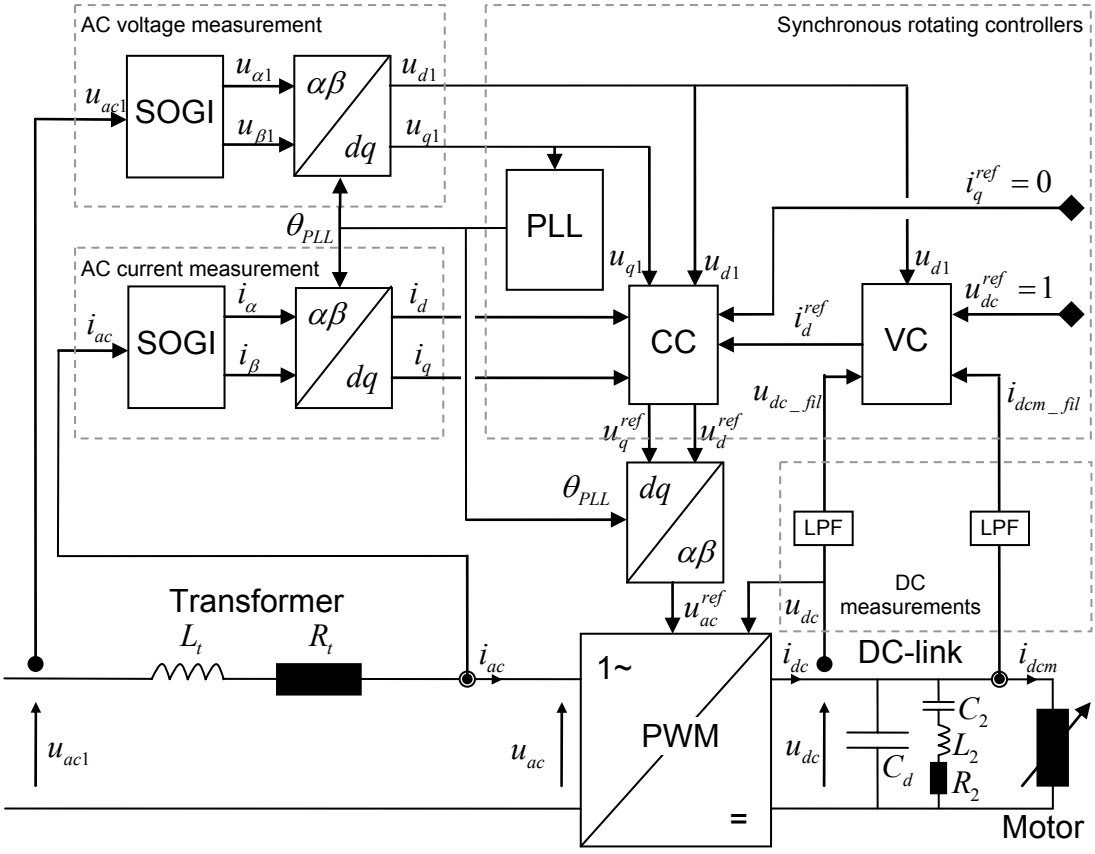

Figure 5-1: A single line and signal flow diagram of the vehicle model.

In real life, the motor-side load consists of a three-phase induction machine fed by a motor-side inverter controlling the motor's torque and, consequently, the train's speed. The required electric power is taken from the energy storage in the DC-link. It is the main task of the line-side converter to maintain this energy storage by controlling the active power inflow, or outflow if regenerative braking, from/to the line (Menth and Meyer [116]). Additionally the line-side converter is used to control the power factor at the transformer upside.

The line-side converter (PWM) and its control system are of primary interest for these studies. The active power flow is controlled by the voltage controller (VC), keeping the

DC-link voltage u_{dc} to its reference value u_{dc}^{ref} = 1 pu by calculating the reference active current i_d^{ref} for the current controller (CC). Based on the active and reactive current references i_d^{ref} and i_q^{ref} and the measured actual line current i_{ac} and voltage u_{ac1}, the current controller gives the reference voltage u_{ac}^{ref} for the inverter to pulse-width modulate u_{dc} into an AC voltage u_{ac}. This voltage is referred to as the 'actuated voltage' since it is this voltage that the vehicle actually controls. The phase θ_{ac1} of u_{ac1} is estimated by the synchronisation controller, the phase-locked loop (PLL), into the angle θ_{PLL}.

The resulting voltage difference, both in amplitude and phase, between u'_{ac} (′denotes transformation to the transformer primary side) and the line voltage u_{ac1} over the vehicle's main transformer inductance L_t and resistance R_t gives the resulting current i_{ac} flowing into the DC-link, as shown by the phasor diagram in Figure 5-2. In no-load should i_{ac} be zero and consequently the vehicle controlled u'_{ac} should be equal to the line voltage u_{ac1}.

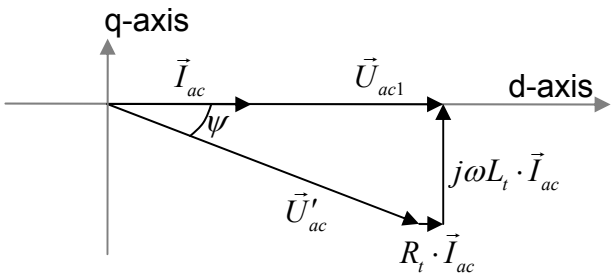

Figure 5-2: A principle phasor diagram for vehicle voltage and current when operating in power consumption.

Assuming a lossless line-side converter without any energy storage allows the instantaneous power balance between the AC side and the DC side to be expressed as:

$$u_{ac}(t) \cdot i_{ac}(t) = u_{dc}(t) \cdot i_{dc}(t). \tag{5.1}$$

The DC-link capacitance (C_d) stores the previously mentioned (Section 4.6) time-variant second-harmonic energy packages from the line side in order to provide the three-phase motor-side inverter with time-invariant power. The corresponding second-harmonic ripple in the DC-link voltage is reduced by an LCR filter (L_2, C_2 and R_2) tuned to a resonance of approximately 33.4 Hz as described by Heising, et al. [77].

Buhrkall [33], Steimel [163] and Östlund [188] describe aspects to consider when designing the vehicle main transformer and DC-link.

5.2.2 Overall control objective

To run the train, the power equal to the product of speed and torque is to be kept constant at its reference. The vehicle's mechanical power is independent of the line voltage in steady state when no line power limitation is active. Consequently, from a power system point of view, the vehicle is seen as a constant power load as the electrical power demand is kept constant independent of the line voltage. This means that if the line voltage decreases, the line current must be increased. For a single-phase system, such a constant power load characteristic cannot be understood as instantaneous, but as an average, for example, over one fundamental frequency period. One fundamental question that will be studied further in this thesis is if this constant power load characteristic is also valid for the vehicle in the low-frequency range described in Section 2.4.5.2.

Because such compensation of a voltage change cannot be done immediately due to transformer and line inductance (Equation (4.8)) and time-variant power availability (Equation (4.17)), the vehicle must have some type of dynamic behaviour by charging and discharging its DC-link like any other continuous feedback system, and with a bandwidth lower than the fundamental frequency of the supplying grid (Menth and Meyer [116]). This low-frequency dynamic behaviour is of special interest in this thesis.

In this work, the displacement power factor of the vehicle is controlled to be unity at the interface between the vehicle and the rest of the power system at the transformer upside. That is to say, i_{ac} is controlled to be in phase with u_{ac1} by setting the reference current $i_q^{ref} = 0$. Hence, the vehicle's reactive power is controlled to zero at all line voltage levels. A line voltage dependent line power limitation is neither implemented in the model.

5.2.3 Electric AC circuit

The vehicle is studied in a simplified railway network based on the reference case described in Section B.1. Here, the difference to the reference case is that the rotary converter, its single-phase transformer and three-phase feeding is replaced by an ideal voltage source, illustrated by the electric AC circuit in Figure 5-3.

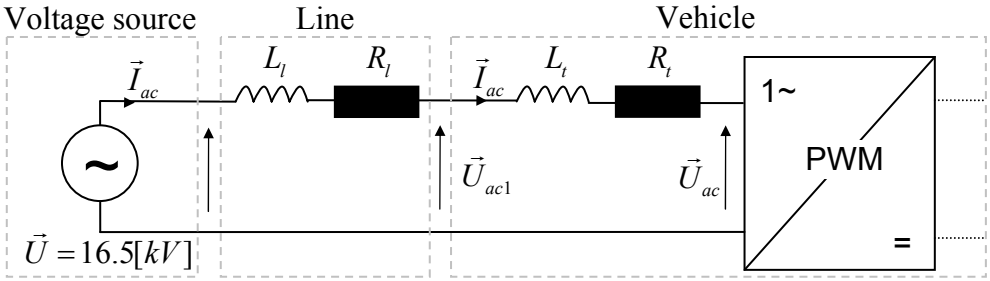

Figure 5-3: An electric system in which the vehicle model is tested.

5.2.4 Simulation and test approach

When comparing the different developed models, a load step response is used. Such a step-up in load rarely happens in the railway, as most vehicles ramp up their power in order to avoid jerks[11] in the train. However, for investigating the dynamical performance of the system, such steps are used for rail vehicles as well, e.g. by Heising, et al. [78], Menth and Meyer [116], Mikus [127] and Stanke [160]. In these previous works, the DC-link voltage u_{dc} has been found to be a good monitor for the vehicle's behaviour. In regarding to low-frequency stability and power oscillations, the DC-link voltage is a measure of the vehicle's power exchange and is monitored by both Debruyne [60], Menth and Meyer [116] and Pröls and Strobl [148].

A second method to compare the different models is by the 'long line stability test' in Section 5.7. The vehicle is operated in no-load and the overhead contact line's length is increased until the system becomes unstable. This test may be understood as a special case of the 'depot problem' reported in Section 2.4.5.2, in which several rail vehicles together at a standstill started to oscillate. As described in Section 1.2, Menth and Meyer [116] report that a situation with several vehicles together may be simplified by multiplying the current from one single vehicle by the number of vehicles. A practical interpretation of this is to study one vehicle, but multiply the impedance of the original overhead contact line length by the number of vehicles instead (Kaeser, et al. [99]).

The time simulations are compared with eigenvalue analysis that is given a short introduction in Appendix C.

5.3 The model and its simplifications

5.3.1 Electrical components

The model developed in this thesis represents a 6.4 MW universal locomotive with an overall structure as shown in Figure 2-4. Several hardware frames for such a locomotive are given in example 17.8 in Steimel [163]. These main frames are adopted here and include the rating, nominal DC-link voltage, main transformer impedance and ratio, switching frequency, and the second-harmonic resonance tank resistance and inductance (L_2 and C_2).

The second-harmonic resonance-tank resistance R_2 is adopted from a vehicle model with the same rating and control system structure described by Mikus [127]. The value of R_2 will be an influence on the damping of the second-harmonic filter and its total impedance, which is a trade-off between damping and the resulting DC-link ripple amplitude in steady state.

The DC-link capacitor C_d has been selected based on the impression of typical discharge times for this capacitor on a rail vehicle being 26 ms. This choice is further discussed in Section 6.2.1.

[11] 'Jerk' is the derivative of acceleration with respect to time, the second derivative of velocity and the third derivative of position.

The electrical DC-link components are identical for the instantaneous value and the RMS mode models. For the main transformer, the internal voltage drop is calculated by the use of Equations (4.8), (4.9) and (4.12) for the respective simulation models.

The PWM in instantaneous value mode acts as a power balance as shown by Equation (5.1). The corresponding RMS or rotating reference frame equation is Equation (5.2):

$$\mathrm{Re}\left(\vec{U}_{ac}(t)\right)\cdot\mathrm{Re}\left(\vec{I}_{ac}(t)\right)+\mathrm{Im}\left(\vec{U}_{ac}(t)\right)\cdot\mathrm{Im}\left(\vec{I}_{ac}(t)\right)=u_{dc}(t)\cdot i_{dc}(t) \tag{5.2}$$

The switching of the PWM and the motor side is further explained with its simplifications in Section 5.3.4.

5.3.2 Control system

Despite of the thorough description of the motor side and its control system in the literature (e.g. Steimel [163]) and available papers, only a limited amount of information is provided on how the complete line-side converter control may actually look like (e.g. Steimel [163] and Östlund [188]). It has therefore been a major task in this work to collect the different information available and combine this into a complete system. It is believed that there might be large variations between the different manufacturers and the different rail vehicles within what can be considered as state-of-the-art structure that comprises a proportional-integral controller for keeping the DC-link voltage constant as a basis.

For the control system, the concept of vector control is chosen in a way in which the controllers are implemented in a local synchronously rotating *dq* reference frame as shown for a rail vehicle, e.g. by Busco, et al. [37]. This choice has the benefit of the control system being identical for both models in instantaneous value mode and RMS modes, respectively. A block diagram illustrates this in Figure 5-4. The challenge is how to transform from the instantaneous value measured single-phase AC voltages and currents into a vehicle local rotating reference frame. In this work, this is solved by use of a second-order generalised integrator (SOGI), as will be more deeply explained together with its imitation as a first-order low-pass filter for use in RMS mode in Section 5.4.3.

The different controllers and their parameters will be studied more in-depth in the next sections one by one, with the exception of the DC-link voltage and motor current measurements which are pure first-order low-pass filters (LPF). Their bandwidth is selected to 100 Hz[12].

[12] A variation between 20 and 500 Hz has been observed in real rail vehicles.

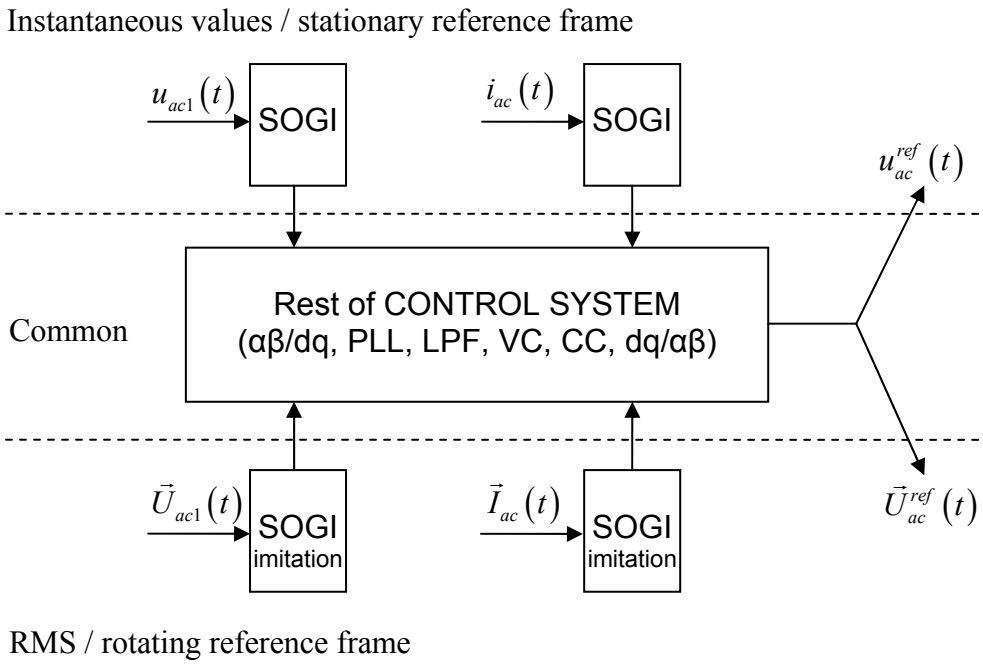

Figure 5-4: The principle for the vehicle control system model for both the instantaneous value and RMS value simulation.

5.3.3 Implementation

The single-phase electric circuit, the PWM and the control system have all been implemented by use of the Dynamic Simulation Language in SIMPOW. The code for the vehicle dynamical model implementation is found in Appendix D.

In order to allow a simulation with the described dynamical vehicle model to start at an arbitrary load operating point, a power flow model of the vehicle is developed as well. This static model is not explicitly described in this thesis, as the dynamical behaviour is the focus.

5.3.4 Major simplifications

5.3.4.1 PWM switching

The PWM switching of the semiconductors in instantaneous value mode is not included; hence the voltage $u_{ac} = u_{ac}^{ref}$ is averaged over one switching period (T_{sw}). It is usual to consider a time delay from u_{ac}^{ref} to u_{ac} being equal to half a switching period ($T_{sw}/2$) due to the switching itself (Buso and Mattavelli [38]). This delay may be compensated for by a modification of the *dq/αβ* transform as proposed by Harnefors [73]. Since this delay and the proposed compensation both ideally cancel each other, they are both neglected in the present model.

Assefa, et al. [14] perform introductory studies of the PWM switching impact on low-frequency power oscillations. A comparison between a model that includes the

switching and a model that averages over one switching period is performed. The work presented indicates a difference between the models, but no conclusive explanation for this difference is provided. Nevertheless, it has been chosen in the present thesis to not include semiconductor switching.

The assumption of $u_{ac} = u_{ac}^{ref}$ also imply that the modulation index (Mohan, et al. [128]) is calculated based on the actual DC-link voltage and not the DC-link voltage reference. This ideally cancels the influence of the modulation index and results in a linear relationship between u_{ac} and u_{ac}^{ref}.

The vehicle model does not include any filters other than the main windings of the main transformer itself for reduction of switching harmonics. Neither extra filter for attenuation of switching harmonics in the DC-link is included in this model.

5.3.4.2 Motor side

Only a simple representation of the motor side is included in present model. In a quasi-stationary state the motor has to keep its power constant. If not, the torque and further speed reference cannot be fulfilled. However, a motor side acting as a constant power load for all frequencies, i.e., always increase the motor-side current if the DC-link voltage drops, will reduce the stability of the DC-link (Mosskull [129]).

There are different ways of manipulating the motor torque in order to stabilise the DC-link. One such way, which is considered as state of the art, was proposed by Jänecke [97] and Sudhoff, et al. [171] in which the torque reference is given as a DC-link voltage dependent characteristic. Equation (5.3) expresses this characteristic in terms of motor-side power p_{Motor} where p_{Motor}^{ref} is the reference power. MP is the voltage dependency where $MP = 0$ leaves the motor as a CPL for all frequencies as explained in Section 3.4.5. Increased MP increases the voltage dependency. The actual DC-link voltage u_{dc} is compared with a voltage u_{dc_filt} filtered by a first-order low-pass filter having time constant T_{CPL} (Equation (5.4)). In this work $MP = 2$, giving the motor side a quadratic voltage dependency for frequencies higher than the low-pass filter bandwidth is used based on a similar choice by Sandberg [152].

$$p_{Motor}(t) = p_{Motor}^{ref}\left(\frac{u_{dc}(t)}{u_{dc\_filt}(t)}\right)^{MP} \tag{5.3}$$

$$u_{dc\_filt}(s) = \frac{u_{dc}(s)}{Tf_{CPL}s + 1} \tag{5.4}$$

The influence of the motor side and its control system cannot always be neglected as it might be a source of instability (Yanhong and Shaotang [183]). However, as the line-side converter has the main influence on the interaction between the vehicle and the rest

of the power system (Menth and Meyer [116]), the line-side converter and its control system is the main focus of this thesis.

This motor power consumption is the only load in the vehicle model. Auxiliary power consumption for heating, cooling, battery charging, control system power supply etc. is not included neither from the DC-link nor from a separate transformer winding.

5.3.4.3 Type of controllers used

The control system is implemented with analogue continuous controllers only.

5.3.4.4 Inverter and DC-link structure

The structure of an advanced electric rail vehicle in real life may be more detailed than shown in Figure 2-4. There may be several DC-links per vehicle and several line- and motor-side inverters in parallel to each DC-link. In this model, all the vehicle's DC-links are aggregated into a large one.

5.4 Synchronisation controller (PLL and SOGI)

In order to ensure the required power flow, the line-side converter has to synchronise the PWM actuated voltage u_{ac} to the phase of the line voltage u_{ac1}. This section explains this synchronizing controller, called the phase-locked loop (PLL), and compares the instantaneous value model with the corresponding RMS model. Such a simple representation of the synchronisation controller in the rotating reference frame and comparison to the stationary reference frame implementation has not been found reported before.

5.4.1 Fundamental voltage phase tracking

A local *dq* coordinate system has to be created in order to establish the synchronously rotating reference frame utilised for the vehicle control system. The rotational speed and phase of this internal *dq* system is determined by use of a phase-locked loop (PLL) (Best [21]) that continuously tracks the phase of the line voltage u_{ac1} as shown by the block diagram in Figure 5-5.

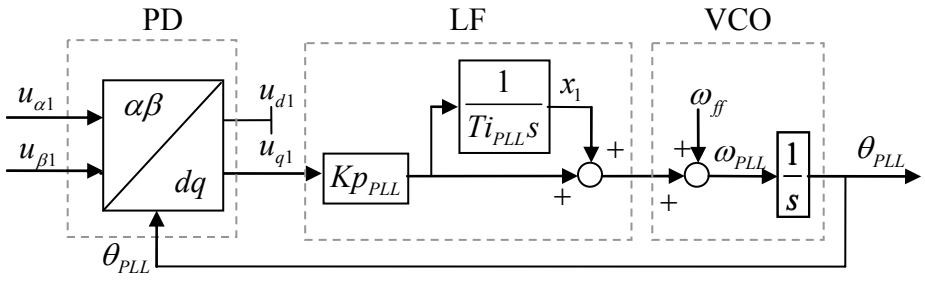

Figure 5-5: A block diagram for PLL.

The PLL consists of a proportional-integral (PI) controller also called a loop filter (LF) that controls the quadrature (*q*) component of the measured line voltage u_{q1} to zero. This means that the direct (*d*) axis in steady-state is oriented in phase with the line voltage u_{ac1} (Harnefors, et al. [74]). Referring to Figure 4-1, the phase of u_{ac1} and thus u_{d1} is

$\omega_1 t+\theta_0$ in instantaneous value mode and θ_0 in RMS mode. However, during transients, there might be a difference between the real phase θ_{ac1} of the line voltage and the phase θ_{PLL} due to the dynamics of the entire synchronisation system which will be further studied in Section 5.4.5.

More information and an explanation of phase-locked loops in general can be found in the literature by Best [21] and Gardner [69]. For power system applications in particular, see Ciobotaru, et al. [43] and Karimi-Ghartemani [101].

A feed-forward fixed frequency ω_{ff} of the voltage controlled oscillator (VCO) is used to reduce the pull-in time of the PLL, i.e., it starts the simulation in steady-state and the PLL does not need to detect the network frequency itself. In instantaneous value mode $\omega_{ff} = \omega_s$, but in RMS modes $\omega_{ff} = 0$ since the entire system is rotating at synchronous speed ω_s. The frequency of the line voltage in per unit values can then be calculated for instantaneous value mode by Equation (5.5) and for RMS modes by Equation (5.6).

$$\omega_{pu} = \frac{d\theta_{PLL}}{dt} \cdot \frac{1}{\omega_s} = \frac{\omega_{PLL}}{\omega_s} \tag{5.5}$$

$$\omega_{pu} = \frac{d\theta_{PLL}}{dt} \cdot \frac{1}{\omega_s} + \frac{\omega_s}{\omega_s} = \frac{\omega_{PLL}}{\omega_s} + 1 \tag{5.6}$$

The phase detector (PD) here in fact is equal to Park's *αβ/dq* transform in Equation (4.7). In RMS mode, this is a transform between the global synchronously rotating coordinate system introduced in Section 4.3 and the vehicle internal rotating coordinate system. In instantaneous value mode, it is a transform between the stationary reference frame and the vehicle internal rotating reference frame and coordinate system. Hence, exactly the same structure of the PLL can be used in both modelling modes, with the only difference being ω_{ff}.

5.4.2 PLL parameters

The parameters for the PLL, i.e., the gain and time constant Kp_{PLL} and Ti_{PLL}, are selected based on the same pattern as in Ciobotaru, et al. [44] in which the relative damping is 1 and the settling time is three fundamental periods.

5.4.3 Orthogonal signal generation

In order to perform such a reference frame transform from instantaneous value mode, two orthogonal instantaneous value signals, α and β, are needed (Ciobotaru, et al. [43]). However, in a single-phase system, two orthogonal signals as input to the PLL do not exist. As a result, the second and orthogonal β signal has to be artificially generated. The simplest method for generating such a signal may be to shift the existing α signal 90 degrees, corresponding to a delay of a quarter of a fundamental period $T_s/4$. For the orthogonal signal generation in this single-phase model, a second-order generalised integrator (SOGI) as described by Ciobotaru, et al. [44] is used. This solution has not

been found to be reported for use in electric rail vehicles. The most common solution used in railways is as a Discrete Fourier Transform (DFT) as described by e.g. Kindell [103] and Bartelt, et al. [18]. For the instantaneous value simulations in this work, the SOGI is simpler to implement than a DFT.

The SOGI is a second-order band-pass filter having a transfer function from u_{ac1} to $u_{\alpha 1}$ as in Equation (5.7) and from u_{ac1} to $u_{\beta 1}$ as in Equation (5.8). As seen in the block diagram in Figure 5-6, an orthogonal signal $u_{\beta 1}$ 90 fundamental degrees delayed with respect to $u_{\alpha 1}$ can be achieved by an integrator. For simplicity, only the transfer functions regarding the α-output will be described here, though the same applies to the β-output.

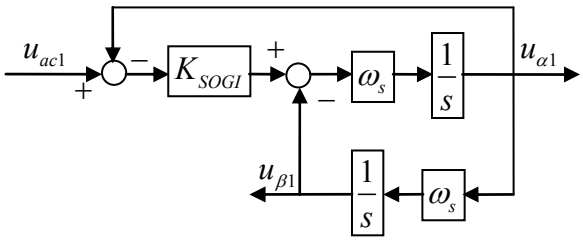

Figure 5-6: A block diagram of SOGI.

$$H_{\alpha s}(s) = \frac{u_{\alpha 1}(s)}{u_{ac1}(s)} = \frac{K_{SOGI}\omega_s s}{s^2 + K_{SOGI}\omega_s s + \omega_s^2} \tag{5.7}$$

$$H_{\beta s}(s) = \frac{u_{\beta 1}(s)}{u_{ac1}(s)} = \frac{K_{SOGI}\omega_s^2}{s^2 + K_{SOGI}\omega_s s + \omega_s^2} \tag{5.8}$$

The SOGI's resonance frequency is tuned to the fundamental frequency ω_s and the width of the pass band can be adjusted by the parameter K_{SOGI}. Decreased K_{SOGI} narrows this band and increases filtering of harmonics, as well as slowing down the dynamic behaviour during a transient.

Ciobotaru, et al. [44] propose to feed the frequency detected by the PLL, ω_{PLL}, to retune the SOGI resonance when the grid frequency has fluctuations. Here, such a direct feedback is found to introduce an undesirable additional dynamic impact and is not used. However, it might be useful in frequency-elastic 16.7-Hz grids if heavily filtered in order to tune the SOGI for better steady-state behaviour.

The voltage and current signals u_{ac1}, i_{ac} and u_{ac}^{ref} are sinusoidal in instantaneous value mode and phasors in RMS mode. The α and β outputs from the SOGIs are also sinusoidal in instantaneous value mode and they are DC-values in RMS mode.

The SOGI in instantaneous value mode has both a band-pass impact and an orthogonalisation impact. The dynamics of both these impacts must be represented in RMS mode models, even though two orthogonal signals are already present: the real and the imaginary part of the phasor signal.

It can be shown by performing frequency mapping (Kraniauskas [104]) that a low-pass filter having a transfer function equal to Equation (5.9) in the rotating reference frame can be transformed into a band-pass filter having a transfer function equal to Equation (5.7) in the stationary reference frame.

$$H_r(s) = \frac{u_{\alpha 1}(s)}{u_{ac1}(s)} = \frac{K_{SOGI}\omega_s}{s + K_{SOGI}\omega_s} \tag{5.9}$$

Orthogonalisation can be considered as a delay of the instantaneous signal a quarter of a fundamental period (T_s/4). Its transfer function shown in Equation (5.10) has been found here by a simple curve fitting of its frequency response (see Figure A-3). A similarity to the first order Padè polynomial approximation for time delay transfer function ($e^{-s\tau}$) (Dorf and Bishop [61]) can be seen in the denominator.

$$H_{Delay}(s) = \frac{u_{\alpha 1}(s)}{u_{ac1}(s)} = \frac{1}{\frac{T_s}{4 \cdot 2}s + 1} \tag{5.10}$$

For the total SOGI transfer function in RMS mode, a combination of the transfer functions (5.9) and (5.10) has by curve fitting empirically been found in present work to result in Equation (5.11). The recorded frequency responses for the instantaneous value mode SOGI from line voltage amplitude and phase, D = Re(u_{ac1}) and Q = Im(u_{ac1}), to the filtered, orthogonalised and Park-transformed line voltages phase and amplitude, $d = u_{d1}$ and $q = u_{q1}$, are shown in Figure 5-7 together with the frequency response of Equation (5.11).

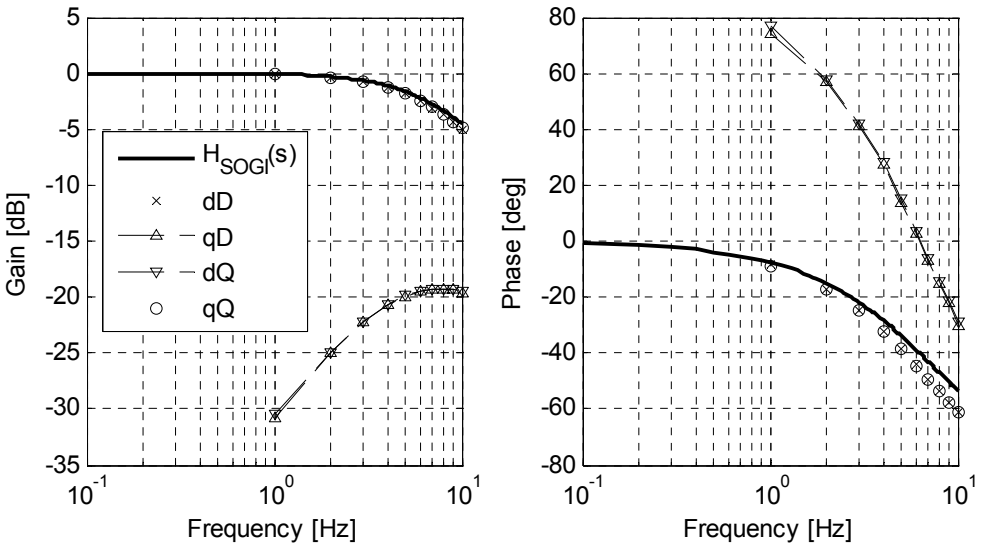

Figure 5-7: Frequency response of instantaneous value SOGI (dD, qD, dQ and qQ) compared with the low pass filter transfer function found for the RMS mode SOGI (H_{SOGI}(s)). K_{SOGI} = 0.8.

$$H_{SOGI}(s) = \frac{u_{\alpha 1}(s)}{u_{ac1\_Re}(s)} = \frac{u_{\beta 1}(s)}{u_{ac1\_Im}(s)} = \frac{1}{\frac{1}{K_{SOGI}}\left(\frac{1}{\omega_s} + \frac{T_s}{8}\right)s + 1} \tag{5.11}$$

The cross-coupling terms *qD* and *dQ* are found to have low gain and are thereby neglected in this continuing work. Furthermore Equation (5.11) is only investigated in the vicinity of K_{SOGI} = 1. For larger deviations, and especially for K_{SOGI} > 1, the equation may not be as accurate as Figure 5-7 indicates. Despite this, a low-pass filter with a transfer function equal to Equation (5.11) is used for the imitation of the SOGI in RMS mode, as illustrated in Figure 5-4, for both the real and imaginary parts of the complex signal that is considered.

5.4.4 SOGI parameters

For the SOGI used for line voltage measurements, Ku_{SOGI} = 0.8 is chosen in order to filter the large extent of harmonics that can be experienced in railway networks, for example up to 33 % THD is observed (Banverket/Jernbaneverket [17]).

For the SOGI used for line current measurements, an increase of the bandwidth has been necessary and Ki_{SOGI} = 3 is chosen for better damping of the DC-link second-harmonic resonance. Consequences of this choice are discussed in Section 7.7.1.1.

5.4.5 Step response and time-variance

The response in both the measured line voltage phase θ_1 and amplitude $u_1 = \sqrt{u_{d1}^2 + u_{q1}^2}$ of the synchronisation system (SOGI+PARK+PLL) has been recorded for three different disturbances:

1. Step in line voltage phase $\Delta\theta_{ac1}$ = –13 degrees
2. Step in line voltage amplitude $\Delta\hat{U}_{ac1}$ = –0.27 pu
3. Step in line voltage phase $\Delta\theta_{ac1}$ = –13 degrees and amplitude $\Delta\hat{U}_{ac1}$ = –0.27 pu

The system is in no-load, i.e., PWM is turned off, giving a current i_{ac} = 0. Disturbance no. 3 corresponds roughly to the voltage change when a load with a unity power factor is stepped from 0 to 3.67 MW on a 60 km long single-side fed overhead contact line. In instantaneous value mode, the disturbances are imposed with different voltage-displacement angles θ_{u0} = [0, 45, 90, 135] of voltage u_{ac1}.

The angle θ_1 in instantaneous value mode is calculated by $\theta_1 = \theta_{PLL} - \omega_s t$ and in RMS mode is given by $\theta_1 = \theta_{PLL}$.

The results are presented in Figure 5-8. As can be seen, the θ_{ac1}-to-θ_1 (plot a)) and $\hat{U}_{ac1}$-to-u_1 (plot e)) response is essentially time-invariant and the instantaneous value and RMS simulations are very similar. There is, however, some time variance in the cross

coupling θ_{ac1}-to-u_1 (plot b)) and $\hat{U}_{ac1}$-to-θ_1 (plot d)), but in the total disturbance (plot c) and f)), this is found to be small. The time-variant response in instantaneous value mode repeats every 180 degrees.

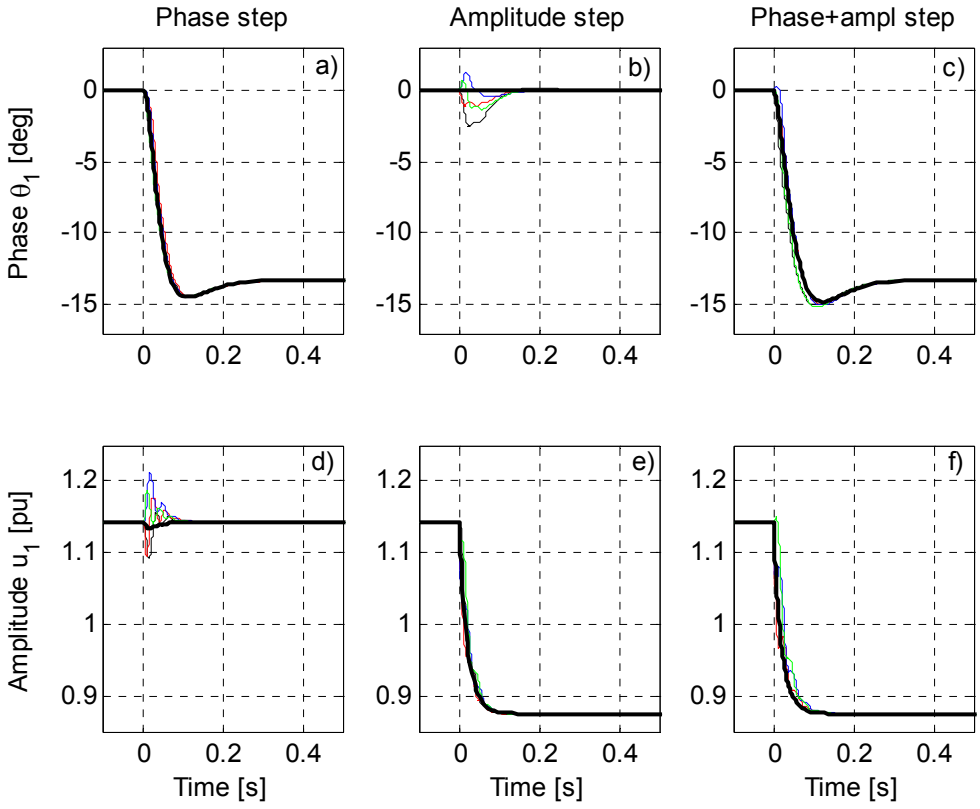

Figure 5-8: The response of synchronisation system for step in line voltage phase and amplitude, and comparison between instantaneous value mode (thin curves) and RMS mode (thick curve). The thin curves represent different time delays for the step after voltage zero crossing in the order black, red, green and blue for increasing voltage-displacement angles.

The apparent overshoot in the phase θ_1 due to change in the phase θ_{ac1} is assumed to be caused by a zero in the PLL's equivalent transfer function.

5.5 Active power controller / DC-link voltage control (VC)

5.5.1 Control structure

The control of active power consumption from the line is performed by the DC-link voltage controller (VC), which is a proportional-integral controller (PI) aiming to keep the DC-link voltage u_{dc} constant on its reference value u_{dc}^{ref} as shown in the block diagram in Figure 5-9. Such a PI controller for the DC-link voltage control is applied for example by Appun and Lienau [12], Busco, et al. [37], Heising, et al. [79], Mikus [127], Stanke [160], Steimel [163], Östlund [188] and Venkatesh, et al. [181] and can therefore be considered as the state of the art.

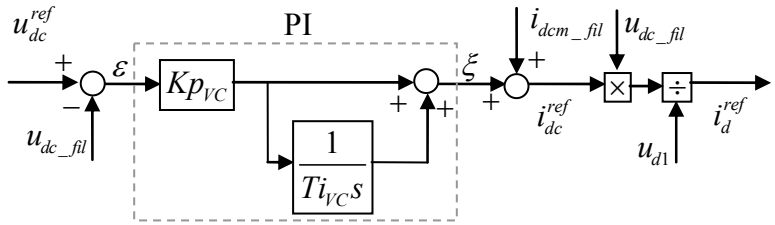

Figure 5-9: A block diagram for DC-link voltage controller (VC).

The filtered motor current i_{dcm_fil}, whether measured or calculated, is fed forward and added to the regulator output ξ resulting in a needed DC current i_{dc}^{ref} to close the voltage deviation. This DC current is recalculated to a needed AC current i_d^{ref} given by the ratio between the measured DC voltage u_{dc_fil} and line voltage u_{d1}. This is the direct-axis current component in the local rotating *dq*-system, i.e., the amount of current needed in phase with the line voltage u_{ac1}.

The design of the DC-link voltage controller raises the need for choosing between several possible solutions:

- For simplicity, the DC-link voltage reference is kept constant during all simulations in this thesis. However, some vehicles increase the DC-link voltage when the motor speed increases in order to improve the torque control and similarly decrease the voltage at low speed in order to reduce the wear of the semiconductors.
- The feed forward of the motor current is used to improve the performance, as a load change is directly compensated for instead of resulting in a change in DC-link voltage which has to be compensated by the controller itself. This is used in some vehicles, e.g. by Östlund [188], Stanke [160] and Mikus [127], but not in others, e.g. by Busco, et al. [37] and Steimel [163].
- The conversion from i_{dc}^{ref} to i_d^{ref} here is performed based on the actual measurement of the DC and AC voltages as in Mikus [127]. This introduces extra feedback loops in the system. Alternatively, this conversion may be based on a constant factor for the nominal DC and AC voltages as shown by Bajracharya, et al. [15]. Another option is to not compensate at all. If the motor current feed forward is not used, this conversion factor might be included in the VC gain Kp_{VC}.
- Transformer losses are not included in this calculation of i_{dc}^{ref} such as by Busco, et al. [37] and have therefore to be taken care of by the VC integral part.

5.5.2 Parameters

The DC-link voltage controller and the selection of its parameters are further studied and discussed in Chapter 6.

5.5.3 Step response

A step in the motor power from 0 to 3.67 MW is imposed when the model is connected to a stiff voltage source through a 60 km long line. The PWM is modelled as a current

source which injects the required active AC current i_d^{ref} given by the VC into the power system, and the required reactive AC current i_d^{ref} is still zero. This means that the current controller (CC) can be considered as being ideal; it is extremely fast and strong without dynamics. This of course is not physical, as it will result in a close to infinite high current time derivative and consequently need a very high and short-term voltage peak. However, this case is used to illustrate the dynamics when CC is ideal as is common for traditional power system stability analysis.

In instantaneous value mode, the power step is imposed with different voltage-displacement angles θ_{u0} = [0, 45, 90, 135] degrees of voltage u_{ac1} in order to see the influence from the time-variant power availability as shown in Figure 4-4.

As mentioned, the DC-link voltage u_{dc} is a good monitor for vehicle stability regarding power oscillations, as it is a measure of the vehicle's power exchange. Its response is shown in Figure 5-10 for both instantaneous value mode and RMS mode (with and without fast line current dynamics, Equations (4.9) and (4.12), respectively). In order to reduce the influence to the plotting of the second harmonic ripple in instantaneous value mode, all results are filtered by a sliding averaging window of $T_s/2$ before being presented in the plots. The dominant low-frequency mode in the instantaneous mode step response is found to be essentially time-invariant, but the time responses show a difference in oscillation amplitude.

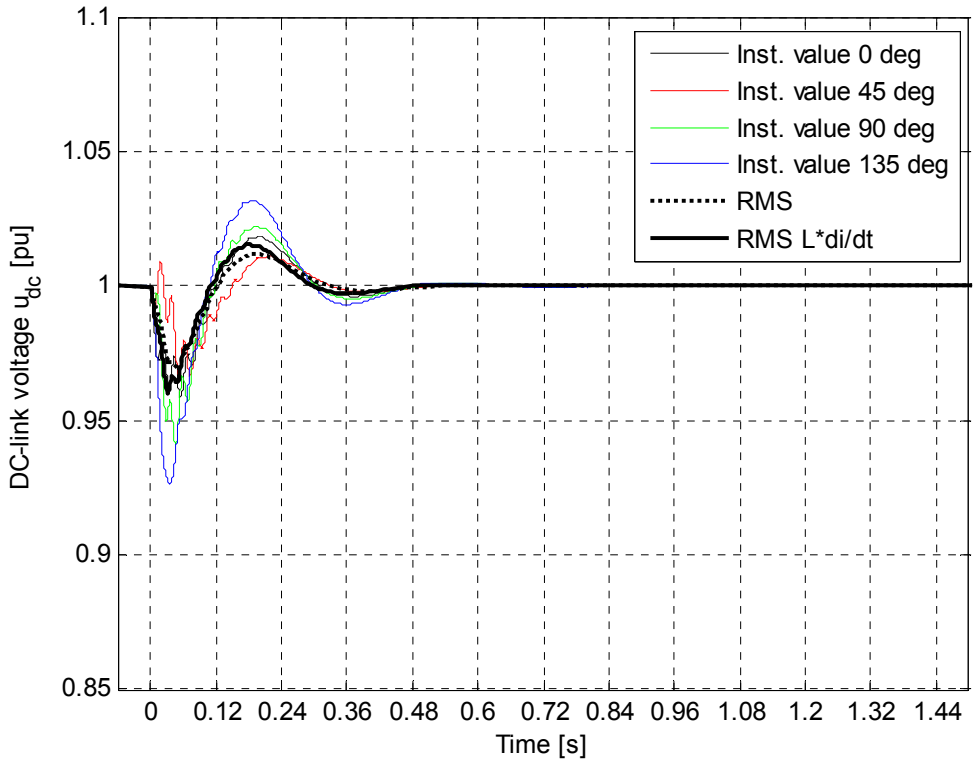

Figure 5-10: The response in DC-link voltage u_{dc} when a 3.67 MW step in motor power is imposed on a 60 km line with ideal current controller. The ticks on the time scale are adapted to the fundamental system frequency, i.e., two fundamental periods.

5.5.4 Linear analysis

The step response in Figure 5-10 showed one dominating low frequency mode. Based on the time plot using Equation (C.3) and linear analysis in SIMPOW, the corresponding eigenvalues (λ) are found for both instantaneous value mode and RMS modes. The pole placements are shown in Figure 5-11, and the linearisation is performed in steady-state. In instantaneous value mode, linearisation is performed at different voltage-displacement angles θ_{u0} = [0, 45, 90, 135] degrees of line voltage u_{ac1}. Instantaneous mode is time-variant in steady state, and the state variables' time derivative might not be zero. Hence, linearisation is not formally allowed and results in eigenvalues circulating with the double fundamental frequency. They are therefore shown with a trajectory and a label with a corresponding θ_{u0}. In some cases, they might even be difficult to identify at all. The eigenvalues in numerical values are listed in Appendix E.

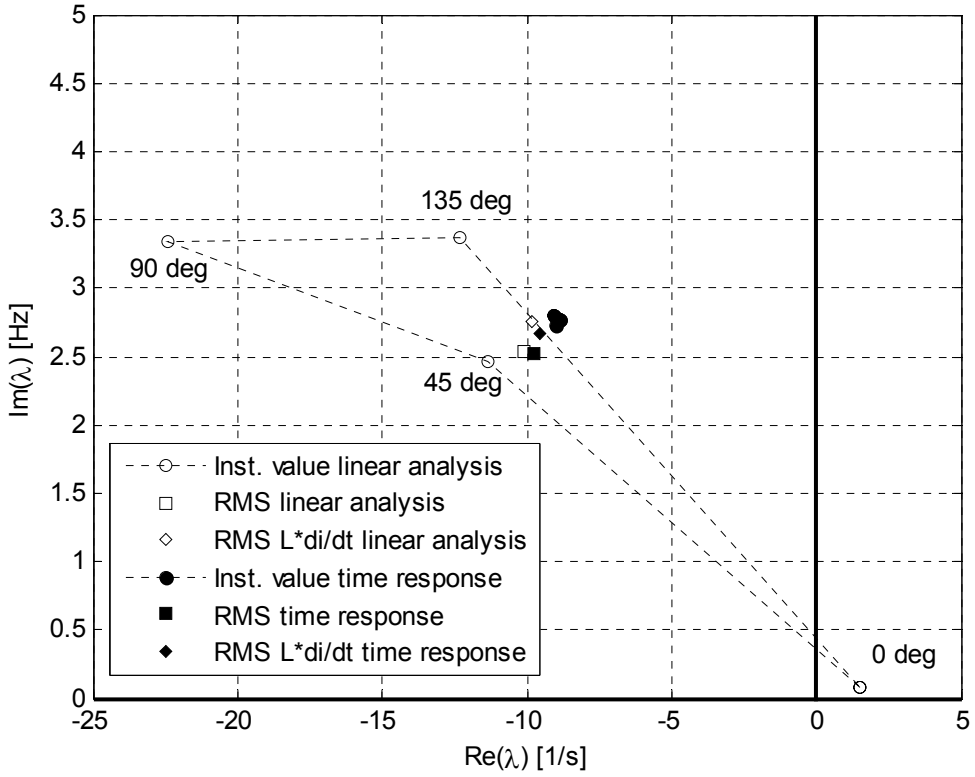

Figure 5-11: A comparison of low frequency mode from linear analysis (unfilled) and a response from time-domain simulation (filled) for instantaneous value mode (circles), standard RMS mode (squares), and RMS mode with *L·di/dt* (diamonds).

The RMS mode eigenvalues calculated from the time simulation correspond essentially to the eigenvalues calculated by linearization.

5.6 Current controller (CC)

5.6.1 Control structure

The current controller (CC) converts the reference currents given from the active and reactive (if present) power control into a voltage reference for the PWM and its internal modulation. Different controller topologies exist, i.e., current control with sinusoidal reference as shown by Steimel [163] and Östlund [188] and vector control or two component control as shown by Busco, et al. [37] and Stanke [160]. The latter is adopted here with some simplifications, and its block diagram is shown in Figure 5-12.

This choice of vector control has one large advantage – it simplifies the parallel modelling in instantaneous value mode and RMS mode, as they can use the same implementation. Even though Zmood, et al. [186] claim to transfer a current controller from the stationary to the rotating reference frame and vice versa, modelling both modes equally reduces uncertainty when comparing them.

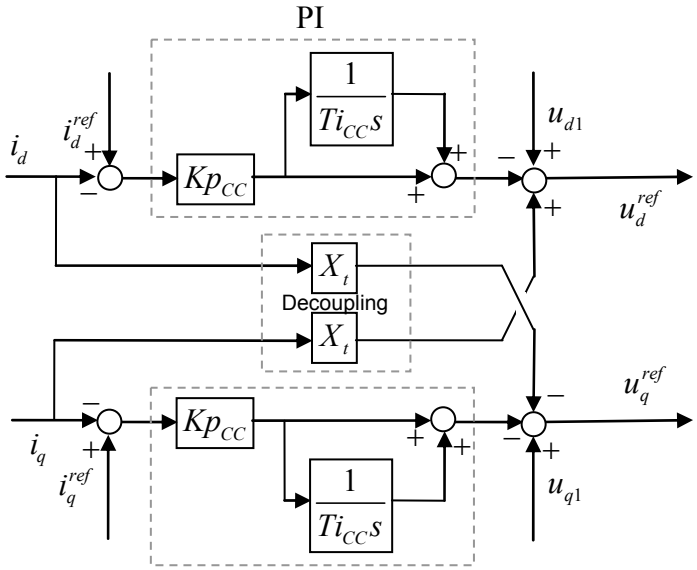

Figure 5-12: A block diagram for current controller (CC).

The idea of vector control is to let the controllers work with DC-valued signals in the already introduced rotating reference frame. In such a frame, the active and reactive power can ideally be controlled independently. Thus the two paths, *d* and *q*, in the block diagram. The integrator outputs in steady state correspond to the resistive voltage drop over the vehicle's main transformer and are subtracted from the measured line voltages, u_{d1} and u_{q1}, resulting in the reference voltages, u_d^{ref} and u_q^{ref}, for the PWM. The two control loops are decoupled through the cross feeding of the main transformer inductive voltage drop $i_{d/q} \cdot X_t$ to cancel the coupling of the two axis introduced by Equations (4.9) and (4.12). The decoupling used here is simplified since a perfect decoupling during transient conditions might also be difficult to obtain. The integral part is also used to remove the steady-state impact of the mismatch between the actual and the control system parameter given inductances, leading to an imperfect decoupling (Harnefors, et

al. [74]). The DC-valued voltage references are converted to AC values by use of the inverse Park's transform ($dq/\alpha\beta$).

The network shown in Figure 5-12 is often mentioned as the vehicle control system transformer model. From this, it is possible to understand how the vehicle controls its line power flow by controlling the voltage drop over the main transformer.

5.6.2 Parameters

The CC gain Kp_{CC} is chosen by the internal control model method as applied to a voltage-source converter with vector control as shown by Harnefors, et al. [74]. However, the same method for the CC integration time Ti_{CC} results in a time constant of several seconds, which is assumed to be too large for this application. A traditional tuning technique such as the modulus optimum (Bajracharya, et al. [15]) has not resulted in optimal parameters. A possible reason is the relatively large time constant for the current measurements (SOGI) which is necessary in single-phase systems, but not present in three-phase systems. Stanke [160] also observes difficulties in applying such traditional techniques. A time constant equal to the one selected by Stanke [160] has been chosen.

5.6.3 Step response

A step in the motor power from 0 to 3.67 MW is again imposed when the model is connected to a stiff voltage source through a 60 km long line as described for the active power control in Section 5.5.3, with the results shown in Figure 5-13.

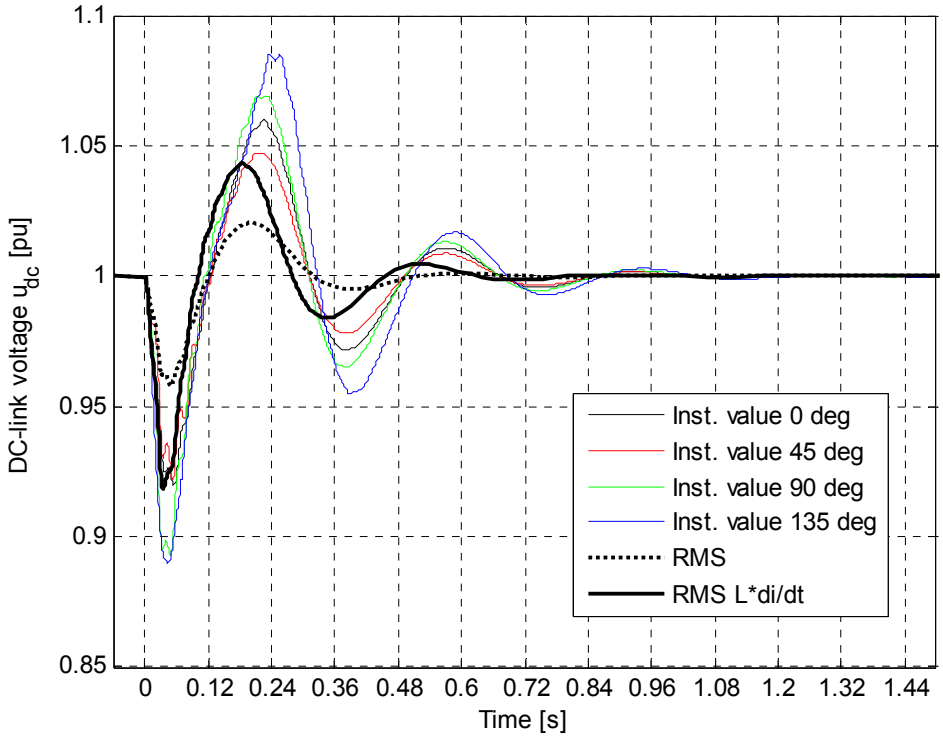

Figure 5-13: A response in DC-link voltage u_{dc} when a 3.67 MW step in motor power is imposed at a 60 km line with modelled current controller (CC).

The frequency and damping of the dominant mode remains essentially time-invariant, but there is a noticeable difference in the amplitude. The standard RMS mode response is very different from the instantaneous value mode response. The enhanced RMS mode with the *L·di/dt*-term reflects the instantaneous value mode response better, but still with noticeable deviation.

5.6.4 Linear analysis

Corresponding eigenvalues for the dominating mode for the model including the current controller are calculated from the time plot (where it is possible) and shown in Figure 5-14. It was not possible to identify all the eigenvalues by linear analysis. The differences between the three models seen in the step response are reflected in the eigenvalues. The eigenmode for the instantaneous value model reflect smaller damping than the enhanced RMS model. The standard RMS model shows largest damping. These results are further discussed in Section 5.8.1. The eigenvalues in numerical values are listed in Appendix E.

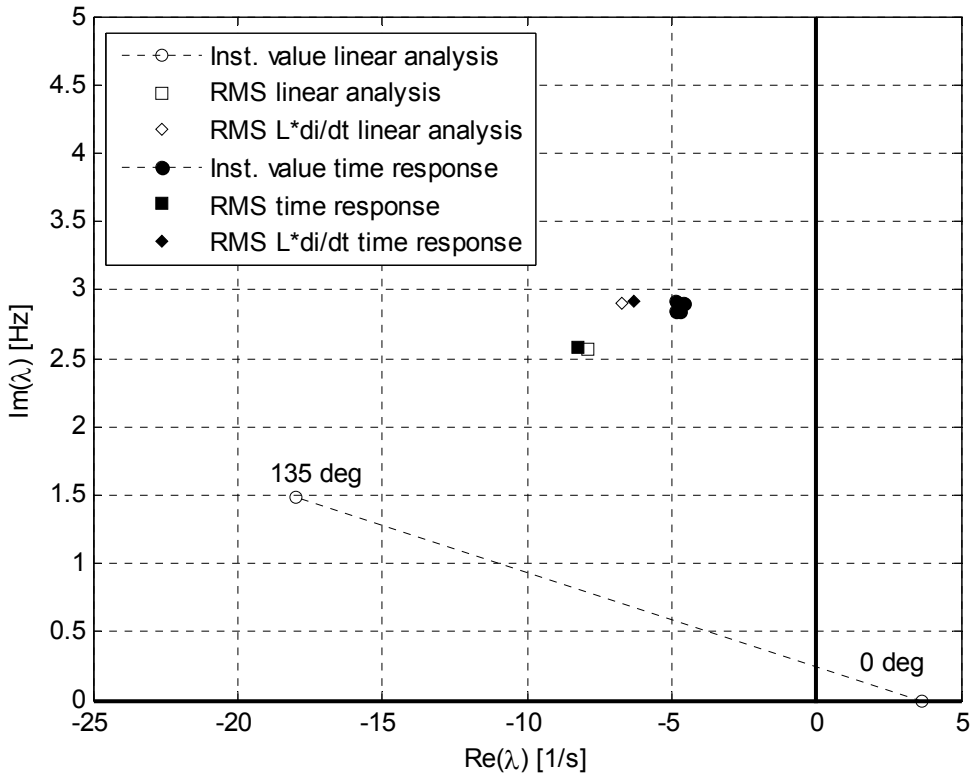

Figure 5-14: A comparison of low frequency mode from linear analysis (unfilled) and response in time plot (filled) for instantaneous value mode (circles), standard RMS mode (squares) and RMS mode with *L·di/dt* (diamonds).

5.6.5 Parameter sensitivity

For the operation point reached after the 3.67 MW load step at a 60 km line length, the dominant mode has been tested for sensitivity against changes in the current-controller parameters, i.e., gain Kp_{CC} and integration time Ti_{CC}. The root loci curves from such a linear data scanning in RMS mode with *L·di/dt* is shown in Figure 5-15. This figure

shows that current-controller parameters have a significant impact on low-frequency stability. By reduction of the controller's gain it is even possible to turn the system unstable.

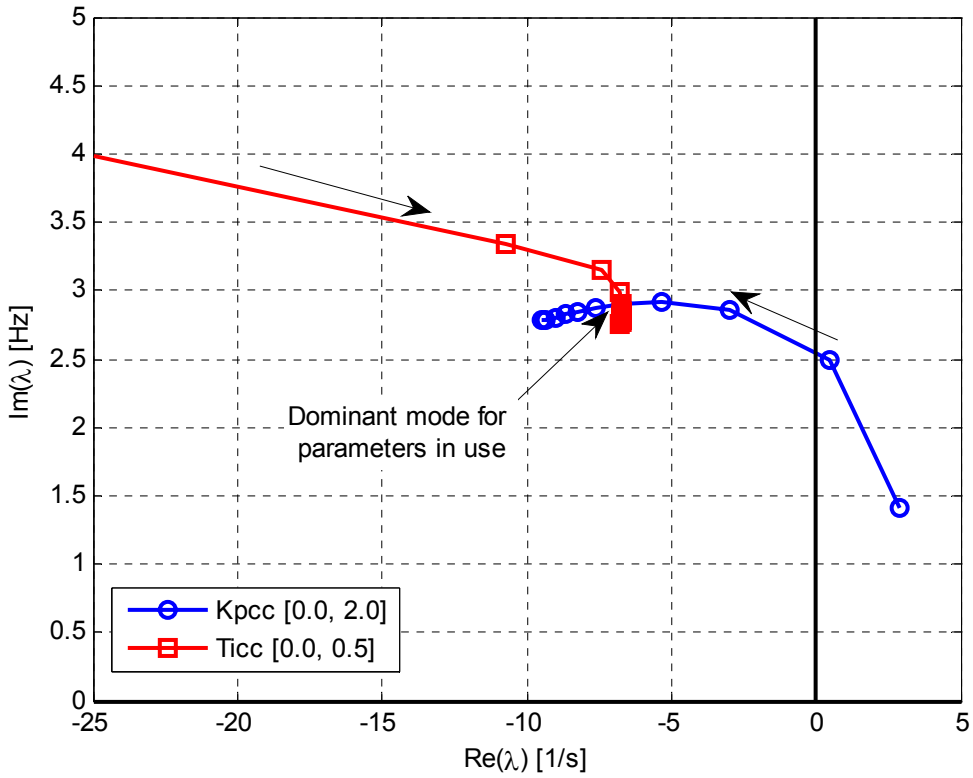

Figure 5-15: Data scanning on dominant mode for the current-controller parameters. Note an increase of parameter in the direction of the arrows.

5.7 Long line stability test

The stability limit of the different models has been found by gradually increasing the line length between the voltage source and the vehicle model until the system becomes unstable. The vehicle is operated at no-load, i.e., motor current $i_{dcm} = 0$ in order to avoid a voltage collapse due to a high line-voltage drop.

The models that assume the current controller to be ideal as described in Section 5.5 are stable until infinite line length, as they are simply imposing $i_{ac} = 0$. There is no feedback from the line voltage to the current.

However, the models with the current controller as modelled in Section 5.6 behave different. They have to balance the PWM actuated voltage u'_{ac} equal to the line voltage u_{ac1} in both amplitude and phase in order to keep $i_{ac} = 0$. If there is a difference, there will be a voltage drop over the transformer and a current flowing into or out of the DC-link. This forms a closed feedback loop; line voltage – DC-link voltage – vehicle control system – line current – line voltage that at a finite line length results in a sustained low-frequency oscillation. The system then becomes marginally stable.

Further increase in line length results in instability which corresponds to a pole (eigenvalue) moving into the right half of the complex plane.

The instantaneous value models are simulated in time-domain until instability occurs. The stability limits for the RMS models are found by increasing the line length in linear analysis as shown in Figure 5-16. Such a sensitivity analysis for line length is simple to perform when the system is in no-load since there is no initial voltage drop and the line length does not exert an influence on the power-flow operating point. The oscillation frequency when damping is zero (Re(λ) = 0) is observed and shown together with the corresponding line length in Table 5-1.

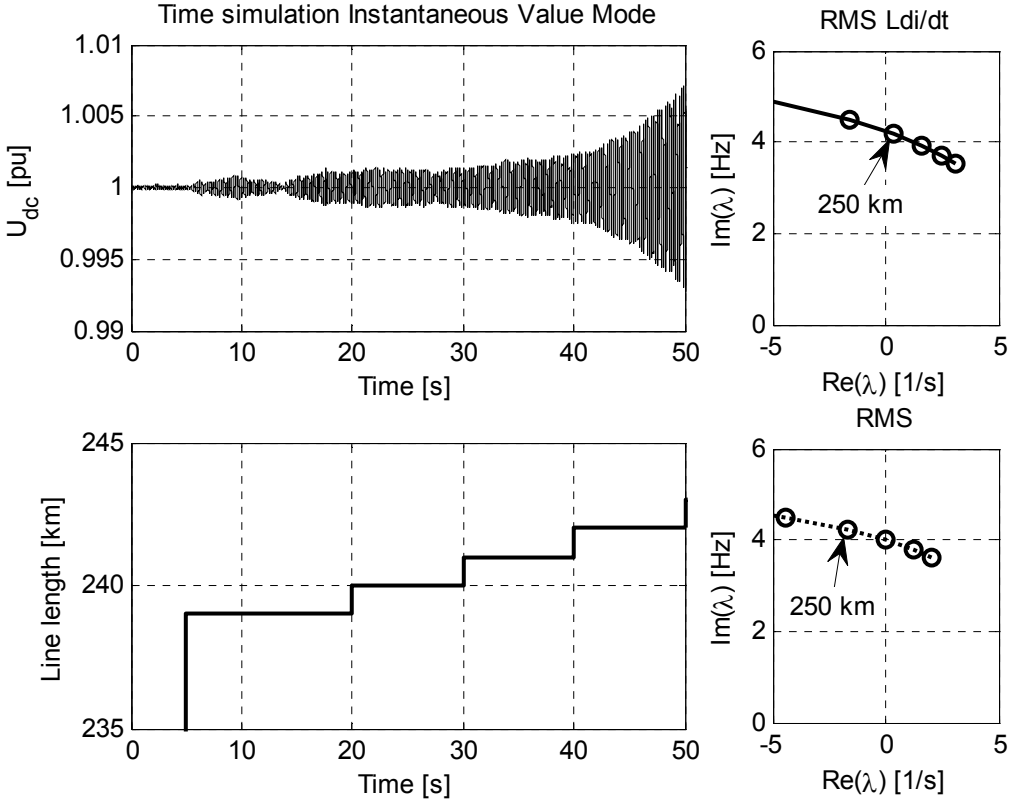

Figure 5-16: The stability limit for the three different models that includes current controller, and time simulation for instantaneous value mode (left) and linear analysis in steps of 50 km for the RMS modes (right).

Table 5-1: The stability limit for the different models.

Model	**Current controller**	**Stability limit [km]**	**Oscillation frequency f_{osc} [Hz]**
Instantaneous value	No	∞	-
Standard RMS	No	∞	-
Enhanced RMS L·di/dt	No	∞	-
Instantaneous value	Yes	240	3.93
Standard RMS	Yes	299	4.02
Enhanced RMS L·di/dt	Yes	238	4.26

The results show that the instantaneous value model with current controller is stable until a line length of 240 km. The standard RMS mode model is stable until 299 km, while introducing the *L·di/dt* term makes the model more conservative and stable until 238 km.

5.8 Discussion and conclusion

5.8.1 Discussion

5.8.1.1 Modelling phenomena and simulation approach

Stability studies should be performed with models reflecting relevant phenomena for the study. In this chapter, six different models for the single-phase source-line-vehicle system have been developed and described with different degrees of simplification:

- *Models 1 and 2:* Instantaneous value mode *without* and *with* current controller, respectively.
- *Models 3 and 4:* Standard RMS mode *without* and *with* current controller, respectively.
- *Models 5 and 6:* Enhanced RMS mode including *L·di/dt*-term *without* and *with* current controller, respectively.

Model no. 2, the instantaneous-value model with current controller, is considered to be closest to a single-phase real-life solution since this model has the lowest degree of simplification. Its main simplification is the neglect of the semiconductor switching and the resulting harmonics. The other five models are therefore compared and discussed with respect to model no. 2.

5.8.1.2 Control structure and parameters

One task of this work has been to develop and evaluate a representative model of an electric rail vehicle for introductory studies of low-frequency traction power system stability. To ensure electrical compatibility between a new electric vehicle and the power supply, a number of requirements have to be met. Constraints related to harmonics, transient behaviour, running performance, etc., in addition to space/weight restrictions onboard the vehicle, may imply non-optimal low-frequency behaviour, whether intended or not. The focus in the development and testing in this thesis has been on the low-frequency behaviour and general performance of a vehicle that could be considered as typical.

As shown, there are several choices to be made in making a control structure. The chosen solution with a DC-link PI-controller must be considered as state of the art. However, Heising, et al. [78] propose a different concept based on multivariable control, but this solution has not been studied here. It has not been the goal of this present work to develop a control structure or set of parameters which guarantees stable operation. In fact, a typical vehicle resulting in an unstable power system as experienced in reality would be more interesting in order to increase the knowledge about the phenomena. The interaction between the developed vehicle model and the power supply

is further studied in Chapters 6 and 7. Additionally, the relevance of the vehicle model is discussed in Section 9.1.2.

5.8.1.3 Influence of current loop dynamics

Traditional power system modelling implies neglecting current dynamics (Kundur [106]). For example, Bjorklund, et al. [27] claim that the current control of their three-phase HVDC Light system is very close to ideal and that standard RMS mode can then be utilised for dynamical studies of active power modulation and damping in a three-phase system. Such installations are used for the damping of oscillations up to at least 1 Hz (Johansson, et al. [94]), which represents 2 % of the fundamental frequency in a 50-Hz system. By contrast, it is found in the present work that this traditional neglect has had a big influence on the simulation results for oscillations in the range of 10-30% of fundamental frequency. This is shown in Figure 5-13, Figure 5-15 and Table 5-1.

The current controller is a dynamical component that interacts with the dynamics of the series line and transformer impedance in a closed loop. Therefore, an enhanced RMS mode is tested. Including the voltage drop given by the $L \cdot di/dt$-term influences the damping and gives better correspondence to the instantaneous value mode than neglecting it. For a more detailed study of the current control loop influence, see Section 6.2.6.

The observed importance of the current controller is in accordance with the conclusions by Liserre, et al. [112] for grid-connected inverters used for renewable energy sources, though their conclusions cover phenomena at higher frequencies.

5.8.1.4 Influence of state-space averaging on harmonics

Despite the better correspondence of the enhanced RMS model (6) to the instantaneous value model (2), there is some inconsistency. With load, the enhanced RMS model is better damped than the instantaneous model, but without load in the long line stability limit test, it is less damped. Therefore, it is not easily given that the enhanced RMS model is too optimistic or too pessimistic.

The instantaneous value model is state-space averaged for one switching period, while the RMS models are state-space averaged for one, alternatively half a, fundamental period. This is referred to as double averaging (Chen and Sun [42]). Consequently, the influence from phenomena at higher frequencies than the fundamental may be disregarded in RMS modes. One difference between RMS mode and instantaneous value mode is the second-harmonic ripple in the DC-link voltage due to the time-variant power availability. This ripple is difficult to totally avoid and may spread through the control system and filters, and influence on the line current in real life and hence the line-voltage harmonics. The impact from these harmonics on low-frequency behaviour has not been studied here. In no-load, neither this second-harmonic ripple nor line current harmonics are present.

Emadi [66] compares two different degrees of simplification due to state-space averaging in the modelling of power electronic loads that have a constant power load

(CPL) characteristic in combined AC-DC power systems. In that work, it was concluded that neglecting DC values on the AC side of an AC-DC converter influenced the calculated stability margins. This supports the findings in the present work by including the $L \cdot di/dt$-term. Emadi additionally found that ripples on the DC-side also influenced the stability margins. This is interesting with regard to the differences observed, but not explained, between the instantaneous value model and the enhanced RMS model.

5.8.1.5 Time-variant versus time invariant modelling

The time-variant power availability in single-phase system is in this work not found to have a significant impact on the dominating low-frequency power eigenmode as observed from the time-domain simulations. The oscillation frequency and damping of this mode remain essentially unchanged independent of the instance of disturbance. This observation is essential and the justification for making time-invariant simplifications. For small-signal instability such as the long line stability test, there is no explicit disturbance and oscillation starts due to the inherent properties of the system. From this it becomes obvious that the exact time instant of a disturbance is of low importance.

Figure 5-11 and Figure 5-14 confirm though that the results from linear analysis in a single-phase instantaneous value system are difficult to interpret. The instantaneous value system is time periodic due to the sinusoidal voltages and currents (Möllerstedt [130]), and there is formally no steady state, i.e., time derivatives of all state variables are not zero. Circulating eigenvalues have also been observed in three-phase instantaneous value system studies by Persson and Söder [146].

The impact of the state-space averaging in RMS mode incorporates more than the DC-link voltage ripple. This averaging applies to all state variables resulting in a real steady state, and accordingly, linearisation is formally allowed.

Linear analysis with eigenvalues is a powerful tool for power system stability analysis, even for systems with non-linearity up to a certain degree. In this study, the low-frequency eigenvalues reflect the time-domain simulation results, even when the current dynamics are included. Additionally, the simulation time is considerably reduced compared with instantaneous value mode when the system is in steady-state and the simulation tool utilises variable simulation time steps (step length is only small when small time constants are active during transients, etc.).

A disadvantage of the concept of RMS mode is that it may be difficult to represent time-domain functions correctly in the rotating reference frame, e.g. the SOGI as shown in Section 5.4.3. The deviation between the instantaneous value SOGI and its rotating reference frame representation influence on the measured line voltage and current that are input to the vehicle control system. These measurements are important differences between the instantaneous value model (2) and the enhanced RMS model (6) as shown in Figure 5-4. This affect the current measurement especially since the gain used (see

Section 5.4.4) are on the limit of the rotating reference frame model's validity. As a result of this difference, it might be expected slightly different results as well.

Harnefors [72] describes a methodology that transforms components between the three-phase stationary and the rotating reference frame. This approach can be a candidate for further and more detailed work.

5.8.1.6 Motor-side modelling

The motor side of the vehicle in this thesis is simplified and modelled as described in Section 5.3.4.2, though in a real-life vehicle, the motor side must be expected to include more advanced dynamics. The motor-side inverter's task is to provide an AC voltage with an amplitude and phase that results in the required motor torque, and consequently, the demanded rotational speed. This can be compared with the line-side converter task, even in no-load (coasting). If the inverters fail to synchronise its actuated voltage to the line or motor voltage, an undesired exchange of power results which consequently influences the DC-link voltage. Thus, there is a closed feedback loop between the DC-link and induction motor through the motor control system. The impact from this control on the low-frequency behaviour may be focused in further work.

5.8.1.7 Comparison with other models

The dynamic studies of the different models of the rail vehicle here is performed with the described control structure and parameters. For comparison, the same study is reported in Danielsen, et al. [52] with a slightly different vehicle model parameters (e.g. $Ki_{SOGI} = 1$). The overall control structure is kept, but the main transformer, DC-link, measurement filter and VC and CC controller parameters are changed. The motor side is also modelled as a pure resistor only, i.e., infinite Tf_{CPL}.

These changes results in a change in both the vehicle step responses and long line stability limits. The observations and main conclusions, however, remain the same. For example, the enhanced RMS model (6) is better damped than the instantaneous value model in the load step test, but opposite in the long line stability test.

5.8.2 Conclusion

Simplified models of a single-phase power electronic component representing an advanced electric rail vehicle have been developed and implemented in a simulation tool for a power system analysis. Even though the available power in an instantaneous value mode single-phase system is time-variant, it is found to have only minor influence on the low-frequency eigenmode of the vehicle, as both the oscillation frequency and damping remain essentially unchanged. Traditional simplifications used for power system analysis based on RMS values and the neglecting of a fast current dynamic are found to be unable to guarantee a correct representation of the dynamic behaviour of the power-electronic component in this study. An enhanced RMS mode model including this current dynamics in both the power-electronic component itself and the series inductances has been developed and proposed. These improvements are found to yield results that better correspond to the results from instantaneous value mode in both time-

domain simulations and linear analysis, i.e., eigenvalue calculations. The accuracy is considered sufficient enough to utilise the enhanced RMS mode model for further low-frequency stability studies and will be used in Chapter 6 and 7 this thesis.

5.8.3 Further work

The modelling of the advanced electric rail vehicle in this thesis includes several simplifications as described in Section 5.3.4. Some of these should be investigated further:

- The influence on low-frequency behaviour from the inverter PWM semiconductor switching is not completely understood in the work described by Assefa, et al. [14]. The importance of any possible impact should be judged in view of a future increase in switching frequency.

- The motor-side influence on low-frequency behaviour as discussed in Section 5.8.1.6. An extension of the model to also include the motor side in more detail is a possible future task, both with today's induction motor and with possible future's permanent magnet synchronous motor.

- The present model does not include a line-voltage dependent reactive power control as can be of benefit in weak railway networks together with a line-voltage line power limitation (e.g. according to EN50388 clause 7 [41]). Implementation of such controllers is also a possible future task.

- The methodology for rotating reference frame modelling as described by Harnefors [72] is interesting. A further task could be to investigate this more in detail with focus on single-phase systems. For the deviation between the instantaneous value model (2) and enhanced RMS model (6) observed in this specific case, the SOGI used for measurements of line voltage and current should be investigated further. This component represents an important difference between these two models.

6 Vehicle DC-link voltage control low-frequency eigenmode

This chapter develops the main characteristics of the low-frequency eigenmode for the DC-link voltage control of an advanced electric rail vehicle. A simple second-order model is compared with the fully developed model of the vehicle and measurements on a real-life vehicle. The eigenmode's sensitivity to vehicle parameters and operating point is studied.

6.1 Introduction

The testing of the developed vehicle model in Chapter 5 revealed that the vehicle shows a dominating low-frequency dynamical behaviour. This behaviour, which is observed in time-domain simulations when imposing a load step, is also reflected by the eigenvalue calculations for the corresponding RMS models. It was also observed that the current controller and the fast current dynamics ($L \cdot di/dt$) had an influence on this low-frequency dynamic behaviour.

Table 6-1 shows an overview over all the calculated eigenvalues for the full enhanced RMS vehicle model when consuming 3.67 MW on a 60 km long line (reference case). The table shows these 18 eigenvalues, their damping ratio and the state variables that have a participation factor larger than 0.1 ($P_i > 0.1$). A participation factor is measure of the relative participation of one state variable in one specific eigenmode or vice versa and is more introduced as a part of linear analysis of power systems in Appendix C.

It can be observed that eigenvalues numbers 12 and 13 have the lowest damping ratio, and their oscillation frequency corresponds to the dominating mode observed in the time simulations in Chapter 5. The mode's main participants are the DC-link voltage controller, together with the DC-link capacitor and second-harmonic filter-capacitor voltages. This eigenvalue pair will be focused on later in this chapter.

In this chapter, this low-frequency eigenmode is further studied, first by considerations made on a simple second-order model, and then by linear analysis of the full vehicle model from Chapter 5.

Table 6-1: Full vehicle model eigenvalues, including main participating state variables.

No.	Eigenvalue [1/s], [Hz]	Damping ratio [%]	Main participation (participation factor in parenthesis)
1	$-678 \pm j0.00$	100	DC-link voltage-measurement filter (2.28) and Motor current-measurement filter (1.29)
2, 3	$-15.4 \pm j43.3$	5.65	Second-harmonic filter inductance current (0.49), Second-harmonic filter capacitance voltage (0.29) and DC-link capacitor voltage (0.20)
4, 5	$-111 \pm j31.7$	48.7	Line current (0.20+0.22), AC current measurement (SOGI) (0.17+0.22) and Transformer current (0.14+0.17)
6	$-667 \pm j0.00$	100	DC-link controller (1.19), Motor current-measurement filter (0.61) and DC-link voltage-measurement filter (0.48)
7, 8	$-99.6 \pm j11.1$	81.9	AC current measurement (SOGI) (0.53+0.44), AC voltage measurement (SOGI) (0.20+0.16), Line current (0.22+0.15) and Transformer current (0.11+0.08)
9, 10	$-32.2 \pm j5.55$	67.9	AC voltage measurement (SOGI) (0.28+0.71), PLL angle (0.57), AC current measurement (SOGI) (0.15+0.10), Line current (0.12+0.07), PLL loop filter (0.18) and DC-link voltage controller (0.11)
11	$-29.7 \pm j0.00$	100	Second-harmonic filter-capacitor voltage (0.30), AC voltage measurement (SOGI) (0.10+0.18), DC-link damping filter (0.22), PLL angle (0.21) and PLL loop filter (0.16)
12, 13	$-6.69 \pm j2.90$	34.5	*DC-link voltage controller (0.53), AC voltage measurement (SOGI) (0.36+0.06), DC-link capacitor voltage (0.24), Second-harmonic filter-capacitor voltage (0.17) and AC current measurement (SOGI) (0.11)*
14	$-16.1 \pm j0.00$	100	PLL loop filter (1.21), AC voltage measurement (SOGI) (0.06+0.25), PLL angle (0.33), DC-link voltage controller (0.21), DC-link damping filter (0.13) and DC-link capacitance voltage (0.11)
15,16	$-5.46 \pm j0.08$	99.6	AC current controller (0.59+0.48) and DC-link damping filter (0.23)
17	$-6.47 \pm j0.00$	100	DC-link damping filter (0.67), AC current controller (0.24+0.51) and AC voltage measurement (SOGI) (0.18+0.12)
18	$-10.0 \pm j0.00$	100	DC-link damping filter (0.82), AC voltage measurement (SOGI) (0.40+0.04) PLL angle (0.12) and PLL loop filter (0.15)

6.2 DC-link voltage control

6.2.1 DC-link capacitance

6.2.1.1 Typical DC-link design

An important task for the DC-link is to act as a filter for the time-variant supply of single-phase power in order to supply time-invariant power to the three-phase motor side. Its presence is important for the selected back-to-back inverter topology chosen, and the total DC-link energy storage capacity is related to the rated power of the vehicle.

However, any published complete description for choosing the size of the main capacitor has not been found and public numbers are rare. Östlund [188] describes that the accepted DC-link voltage ripple due to the line-side converter switching influences the main capacitor size. Furthermore, this capacitance has also to be selected so that the DC-link contains an amount of energy such that the motor-side inverter control is stable. According to Steimel [164], motor-side and line-side harmonics and controllers' response, the main transformer design, the presence of overvoltage-limiting of DC-link chopper, the sensitivity of force-commutated thyristor converters to DC-voltage ripple, the range of motor field weakening, and the response of wheel slip-slide control also influence the selection of the DC-link components.

Steimel [163] and Östlund [188] describe how the specific second-harmonic filter capacitor and inductor may be chosen in order to reduce the second-harmonic voltage ripple.

Table 6-2 shows key information for 10 different vehicles from various vehicle manufacturers. Most of the vehicles in the list are electric locomotives, only one of them is an electric multiple unit. The information is given per DC-link if the vehicle consists of several traction units or traction chains. Together with the physical electrical values for each vehicle, a normalised or per-unit capacitance equal to the capacitor rated discharge time T_C is given and will be explained in the following. Nominal DC-link voltage is typically 2.4-2.8 kV due to the rating of available semiconductors (GTO thyristors) (Steimel [163]).

Even if the DC-link design with one main capacitor and a second-harmonic resonance tank may be considered as typical, other designs exist as well. Dahler, et al. [47] describe a vehicle in which the tuned second-harmonic DC-link filter is omitted due to a significant increase in the DC-link main capacitor. This solution is claimed to be advantageous for DC-link voltage stability.

Table 6-2: DC-link key information for 10 vehicles.

Vehicle	f_s [Hz]	P_{dcN} [MW]	U_{dcN} [kV]	C_d [mF]	C_2 [mF]	T_{Cd} [ms]	T_{C2} [ms]	T_C [ms]
A	50	0.610	0.900	18	3.16	24	4	28
B	16 ⅔	3.200	2.600	8.28	7.13	18	15	33
C	50	2.150	2.800	7.8	3.4	28	12	41
D	16 ⅔	3.200	2.800	9	7.67	22	19	41
E	16 ⅔	2.000	2.800	6.2	4.75	24	19	43
F	16 ⅔	1.980	1.500	24	15.2	27	17	45
G	16 ⅔	3.000	2.800	10.6	7	28	18	46
H	16 ⅔	3.200	2.800	11	7.67	27	19	46
I	16 ⅔	2.400	2.400	12	8	29	19	48
J	16 ⅔	3.595	3.500	13.8	5.57	47	19	66

6.2.1.2 Normalisation

The per unit capacitance for a capacitor in a DC-system may be defined as the time needed to discharge the capacitor from nominal voltage U_{dcN} to zero by drawing constant nominal current I_{dcN}. This nominal current is given by the rated power (P_{dcN}) of the component in study or the base power (S_{Base} or S_N) of the system as $I_{dcN} = P_{dcN}/U_{dcN}$. Rated power in this context is the maximal power of the converters and DC-link, and may be up to 15-30 % higher than the continuous power on wheel that is normally found in the datasheets for rail vehicles.

Solving the basic differential equation for a capacitor $i(t) = C \cdot du(t)/dt$ for the time T_C when $i(t)=-I_{dcN}$ results in Equation (6.1). The discharge time is dependent on the DC-link voltage, the capacitance and the rating of the vehicle.

$$T_C = C\frac{U_{dcN}}{I_{dcN}} = C\frac{U_{dcN}^2}{P_{dcN}} = C_{pu} \tag{6.1}$$

Table 6-2 compares the normalised discharge times or per-unit DC-link capacitances C_d for the 10 vehicles. For the 16 ⅔-Hz vehicles, the main capacitor discharge time typically lies in the range of 24-29 ms, i.e., up to half a fundamental period time, with an average of 26 ms.

In focus in this thesis are oscillations in the DC-link voltage at low frequency. For low frequencies, the time derivative of the second-harmonic filter series-inductor current will be low. Hence, most of the DC-link voltage will stay over the second-harmonic filter capacitor C_2, and Equation (6.1) can then with sufficient accuracy be applied to this capacitor as well. The typical discharge time according to Table 6-2 is 15-20 ms.

Based on this, the total DC-link capacitance typically is $C=C_d+C_2$ and the two capacitors' discharge times can be added to a total of 39-49 ms.

6.2.1.3 Selection of DC-link parameters

For the vehicle model developed in Chapter 5, the nominal power and DC-link voltage, together with the second-harmonic resonance filter are given in example 17.4 by Steimel [163]. The DC-link capacitor C_d is chosen for modelling purposes in this thesis based on the typical DC-link values in Table 6-2. Final parameter values are given in Appendix B.4.

6.2.2 DC-link voltage controller (VC)

The proportional-integral DC-link voltage controller (VC) as explained in Section 5.5 aims to keep the DC-link voltage at its reference. Its output is the active current reference for the current controller.

The active power control of the vehicle cannot be infinitely fast. Its bandwidth is limited by the single-phase time-variant power availability and consequently the system's fundamental frequency f_s. Close to the line voltage zero crossings, the power availability is absent. At that instant, there is no reason to have an active power control increasing the current very quickly if more power is needed. On the other hand, at line voltage peaks, the power availability is high. Within one half of a period, both one voltage zero crossing and one voltage peak have surely passed. The average time to wait for the next zero crossing or peak is a quarter of a fundamental period, which restricts the maximum bandwidth of the active power control loop.

For dimensioning of the active power control loop, the power availability for simplicity is approximated by a first-order filter between the demanded direct current I_{dc}^{ref} and the resulting current I_{dc} into the DC-link. The filter has unity stationary gain K_{eq} and a time constant T_{eq} equal to the average delay or waiting time.

A block diagram of this simple DC-link voltage-control system, including the artificial filter for power availability, is shown in Figure 6-1. The motor current I_{dcm} is a disturbance drawing current out from the DC-link. Therefore, the DC-link energy storage is a net current integrator. The total DC-link capacitance is represented by its rated discharge time T_C (equal to the per unit capacitance) as the integration time. The resulting DC-link voltage U_{dc} is compared with the reference, and the difference is input to the PI controller.

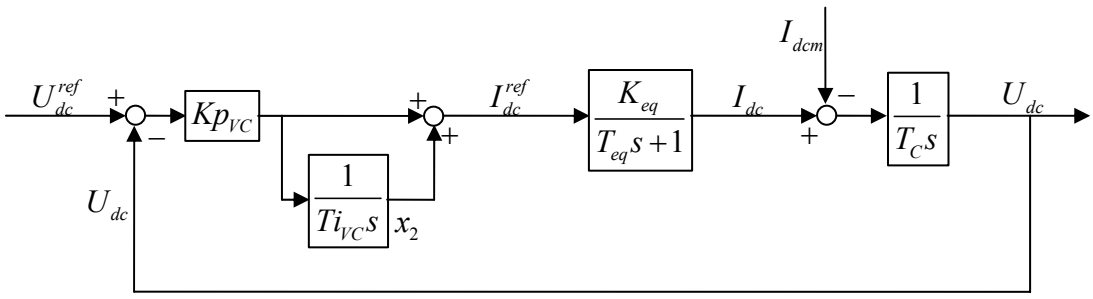

Figure 6-1: A block diagram for DC-link voltage and active power control loop assuming single-phase power availability

For selecting the VC gain Kp_{VC} and integration time Ti_{VC}, the symmetrical optimum method can be used. This method is used for control systems in which the open loop transfer function $A(s)$ (Equation (6.2)) has two poles close to origin, e.g. as in similar VSC-HVDC systems (Bajracharya, et al. [15]). Optimum phase is reached when $Ti_{VC} = 4T_{eq}$ and $Kp_{VC} = T_C/(2K_{eq}T_{eq})$ when a damping ratio of 0.5 is requested.

$$A(s) = \frac{Kp_{VC}\left(1 + Ti_{VC}s\right)}{Ti_{VC}s} \cdot \frac{K_{eq}}{T_{eq}s + 1} \cdot \frac{1}{T_C s} \tag{6.2}$$

Based on symmetrical optimum design criteria, the VC parameters are given by the single-phase power availability and the total DC-link capacitance. Thus, the controller's integration time is equal to one fundamental line period.

6.2.2.1 Selection of controller parameters

In a real vehicle, there might be a motivation to alter these parameters in order to improve the vehicle's transient response. For example, if a vehicle is consuming power and the motor load is suddenly reduced or cut off or a vehicle in regenerative braking is exposed to a 'pantograph bounce'[13], the DC-link voltage will rapidly raise. It is then important to have a fast DC-link voltage control in order to protect the semiconductors from DC-link overvoltage. Additionally, a DC-link chopper which discharges the DC-link over a resistor may be used. However, extensive use of this chopper may lead to the resistor being overheated and should consequently be avoided. Such a DC-link chopper is not included in the present model. In this thesis, controller parameters as calculated here are used further with only a slight (15%) increase of Kp_{VC}. Final parameter values are given in Appendix B.4.

6.2.3 DC-link voltage control eigenmode

In order to find a simple analytic expression for the DC-link eigenmode, only two state variables are considered: the DC-link voltage (U_{dc}) and the VC integration part (x_2). The artificial filter for power availability is neglected and the current controller (CC) is temporarily considered to be ideal, as introduced in Section 5.5. Hence, the line-side converter is representing a current source that instantly delivers current according to the calculated active current reference without any delay, i.e., $I_d^{ref} = I_d$.

As the VC output is the demanded direct current, a conversion to d-axis current is needed by multiplying with the DC/AC voltage ratio as discussed in Section 5.5.1. The opposite conversion is physically performed by the line-side converter due to the power balance in Equation (5.1). Simply and ideally, these two conversions cancel each other and are consequently neglected, i.e., $U_{dc\_fil} = U_{dc}$ and $U_{d1} = U_d$. In reality, they are not a perfect inverse as the first is performed in the control system based on measured voltages and the second is physical. Additionally, $U_{d1} \neq U_d$ in load conditions due to the transformer voltage drop. These simplifications are illustrated in Figure 6-2.

[13] The current collector temporarily looses contact to the overhead contact line along which it is sliding.

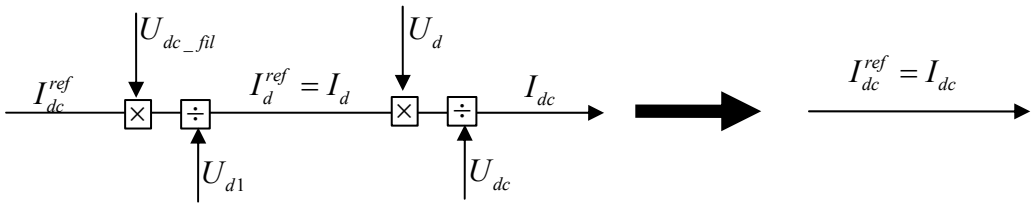

Figure 6-2: A simplification of the control loop.

The system in question after these simplifications is shown by the block diagram in Figure 6-3. It is assumed nominal DC-link voltage giving $U_{dc} = U_{dc}^{ref} = 1$ pu and for simplicity, the initial value of the state variable $x_2 = 0$.

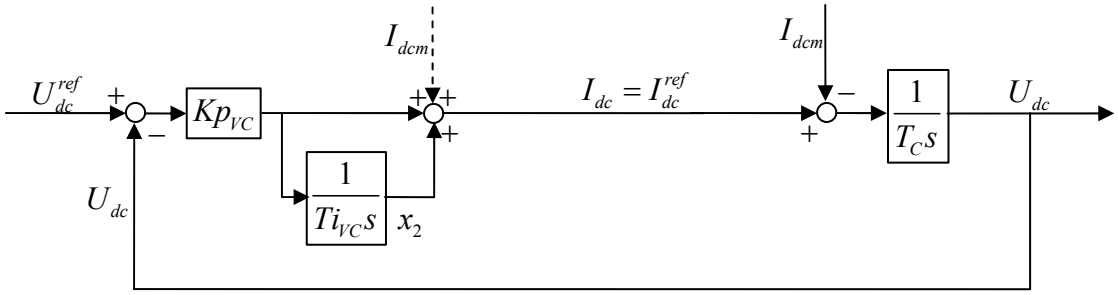

Figure 6-3: A block diagram for DC-link voltage and active power control loop assuming perfect power availability.

6.2.3.1 No-load

In no-load, the motor current I_{dcm} = 0. No feedback from the motor due to DC-link voltage variations is assumed. This results in the following two linear differential Equations (6.3) and (6.4) to be considered:

$$f_1\left(x_2, U_{dc}, t\right) = \frac{dx_2}{dt} = \frac{Kp_{VC}}{Ti_{VC}}\left(U_{dc}^{ref} - U_{dc}\right) \tag{6.3}$$

$$f_2\left(x_2, U_{dc}, t\right) = \frac{dU_{dc}}{dt} = \frac{1}{T_C}\left(x_2 + Kp_{VC}\left(U_{dc}^{ref} - U_{dc}\right)\right) \tag{6.4}$$

Based on the differential equation, an explicit expression for the eigenvalues describing this second-order system can be found in Equation (6.5). Analytical considerations of this equation can be found in Section 6.2.4.

$$\lambda_{1,2} = -\frac{Kp_{VC}}{2T_C} \pm \sqrt{\left(\frac{Kp_{VC}}{2T_C}\right)^2 - \frac{Kp_{VC}}{Ti_{VC}T_C}} \tag{6.5}$$

6.2.3.2 Influence from motor load

Under load conditions the motor current $I_{dcm} \neq 0$. If I_{dcm} is fed forward, as indicated in Figure 6-3, it ideally cancels its influence and can be neglected. Equation (6.5) then ideally applies in load as well.

If I_{dcm} is not fed forward, the motor voltage dependence characteristic has an influence on the eigenmode. In Section 5.3.4.2, the simplified modelling of the motor side is explained, and the motor power is given a characteristic dependence on the DC-link voltage in order to stabilise the DC-link voltage. This characteristic is further simplified into the different load characteristics introduced for the rotary converter in Section 3.4.5 in order to avoid a third state variable. The motor side may then act as a constant power load independent of the DC-link voltage or act as a constant current load, or as a constant resistance load dependent on the DC-link voltage given by the parameter *MP* equal to 0, 1 and 2, respectively. The differential equation describing the change in the system compared with no-load is Equation (6.6). The initial load $P_{m0} = U_{dc0}/I_{dcm0}$ of the motor has to be taken into consideration as well. Equation (6.7) explicitly expresses the eigenvalues for the vehicle DC-link eigenmode when the influence of motor load characteristic is taken into account.

$$f_2\left(x_2, U_{dc}, t\right) = \frac{dU_{dc}}{dt} = \frac{1}{T_C}\left(x_2 + Kp_{VC}\left(U_{dc}^{ref} - U_{dc}\right) - I_{dcm}\right) \tag{6.6}$$

$$\lambda_{1,2} = -\frac{Kp_{VC} + P_{m0}\left(MP-1\right)}{2T_C} \pm \sqrt{\left(\frac{Kp_{VC} + P_{m0}\left(MP-1\right)}{2T_C}\right)^2 - \frac{Kp_{VC}}{Ti_{VC}T_C}} \tag{6.7}$$

6.2.4 Analytical considerations

In the following, Equations (6.5) and (6.7) will be discussed in order to increase the understanding of them.

A comparison to the corresponding expressions for the rotary converter, Equations (3.19) and (3.26), reveals several similarities. First, the rated discharge time T_C equal to the per-unit capacitance for the DC-link appears in the denominator, as the normalised mass inertia constant *H* does. They both reflect the energy stored in the system. According to the equations, increased energy storage will decrease the oscillation frequency.

Second, the load characteristic has an influence on the eigenvalues in the same manner. Constant power load decreases the damping, constant current load is neutral, and a resistance increases the damping. The influence is also proportional to the steady-state or initial power consumed; however, the size of the influence is different.

In some vehicles, the VC output is an alternating current reference and not a direct current reference as used for this vehicle, e.g. $I_{dc}^{ref} = I_d^{ref}$. This means that the

simplification and cancellation of the AC/DC conversions shown in Figure 6-2 are not valid. Equation (6.6) becomes non-linear and consequently has to be linearised. This results in a load influence changing from *(MP*-1*)* to *(MP*-0), meaning a constant power load being neutral. Alternating current *VC* output hence has consequently a damping impact.

Selection of the VC parameters is a compromise between transient response and damping. As described, the fast response may be desired in order to avoid high DC-link voltage damaging the semiconductors. A larger Ti_{VC} will not directly result in a better damping of the DC-link mode described in this simple second-order system, though it will increase the damping ratio as the oscillation frequency is reduced.

Note that only considering the main capacitor C_d as the DC-link capacitance and not including the second-harmonic filter when choosing control parameters will result in a lower gain Kp_{VC} and consequently reduce the damping and also possibly lower oscillation frequency.

6.2.5 Numerical example

Based on Equation (6.7), the eigenvalues describing the DC-link eigenmode are calculated for the vehicle model parameters in Appendix B.4. For a comparison, the corresponding eigenvalues for the full vehicle RMS model with an ideal current controller (CC) introduced in Section 5.5 are calculated by the use of linearisation functionality in SIMPOW. In addition, the full model used here disregards the motor current feed forward, has a motor damper filter time $Tf_{CPL} = \infty$ (see Equation (5.4)), and considers a short line length of only 1 km in order to comply with the analytical calculations. This means that the full model still includes all measurement filters and the synchronisation controller PLL. The eigenvalues are shown in Table 6-3.

Table 6-3: Comparison between eigenvalues for DC-link voltage control eigenmode calculated by simplified model and full model. Units are [1/s] and [Hz].

P_{m0}	*MP*	Calculated by Equation (6.7)	Calculated for full simulation model
0	-	$-19.2 \pm j2.62$	$-17.0 \pm j2.73$
1	*0*	$-7.68 \pm j3.84$	$-5.47 \pm j3.52$
1	*1*	$-19.2 \pm j2.62$	$-15.6 \pm j2.65$
1	*2*	$-13.3 / -47.9$	$-13.8 / -37.8$

The table shows a correspondence between the eigenvalues calculated based on the simplified second-order model and the full simulation model with ideal CC. The motor load characteristic has a significant influence on the damping and frequency of the vehicle's eigenmode.

The vehicle mode is largely influenced by the motor characteristic, while the rotary converter mode in Section 3.6.3 is less influenced by respective load characteristics for the same relative loading. This can be seen as $Kp_{VC} \ll D_M \omega_{sM}$, while the load power is given in pu and is equal for the two expressions.

6.2.6 Influence from current control loop and line impedance

In the simplified approach used in Section 6.2.3, the vehicle line-side converter was assumed to be an ideal direct current source. In the present section, this assumption will be studied by means of a simplified model of the current control loop.

6.2.6.1 Simplification

The model under study is shown in Figure 6-4. No measurement filters or synchronisation controller are included. This means that there are no dynamic deviations between the voltages and currents in the electric system and the respective measured voltages and currents used by the control system. The system is fed from an ideal voltage source. For simplicity, the line and vehicle transformer impedances are aggregated into one lumped sum. As a consequence, the vehicle interface point between the vehicle and power supply is moved to the ideal voltage source. This means that the vehicle line voltage u_{ac1} can be considered as being identical to the stiff voltage source voltage, but the total physical impedance in the AC network remains unchanged.

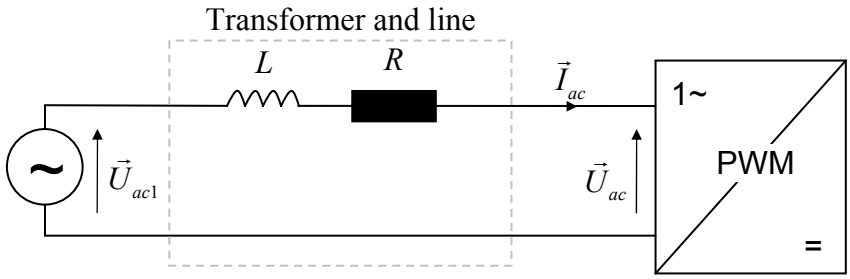

Figure 6-4: A simple circuit with interface between the vehicle and power system at the voltage source, i.e., the line impedance is lumped together with the vehicle transformer impedance.

The actuated voltage u_{ac} at the vehicle line-side converter (PWM) terminals is given by $\vec{U}_{ac} = \vec{U}_{ac1} - \vec{I}_{ac}\left(R + j\omega_s L\right)$. Transformed into the vehicle's internal rotating reference frame, U_d and U_q are given by Equation (6.8) where s is the Laplace operator d/dt.

$$\begin{bmatrix} U_d \\ U_q \end{bmatrix} = \begin{bmatrix} U_{d1} \\ U_{q1} \end{bmatrix} - \begin{bmatrix} R + sL & -\omega_s L \\ \omega_s L & R + sL \end{bmatrix} \begin{bmatrix} I_d \\ I_q \end{bmatrix} \tag{6.8}$$

The current controller (CC) is described in Section 5.6.1. Its task is to provide a voltage reference u_{ac}^{ref} to the line-side converter pulse-width modulator by comparing the reference current i_{ac}^{ref} to the measured i_{ac} and calculating the necessary voltage drop over the transformer impedance based on the line voltage u_{ac1}. For the CC in Figure 5-12, the calculation of U_d^{ref} and U_q^{ref} is shown in Equation (6.9). The integral part of the CC is neglected for simplicity in the present section in order to decrease the number of state variables, with only the proportional part represented by the gain Kp_{CC} remaining.

Accordingly, the transformer model voltage drop calculated is purely inductive, as the resistive part was assumed to be taken care of by the integrator.

$$\begin{bmatrix} U_d^{ref} \\ U_q^{ref} \end{bmatrix} = \begin{bmatrix} U_{d1} \\ U_{q1} \end{bmatrix} - Kp_{CC} \begin{bmatrix} I_d^{ref} - I_d \\ I_q^{ref} - I_q \end{bmatrix} - \begin{bmatrix} 0 & -\omega_s L \\ \omega_s L & 0 \end{bmatrix} \begin{bmatrix} I_d \\ I_q \end{bmatrix} \tag{6.9}$$

Assuming the PWM and its modulator to be perfect and without any delays results in $u_{ac} = u_{ac}^{ref}$. Equations (6.8) and (6.9) can thereby be combined into Equation (6.10).

$$\begin{bmatrix} I_d \\ I_q \end{bmatrix} = \frac{Kp_{CC}}{R + sL} \begin{bmatrix} I_d^{ref} - I_d \\ I_q^{ref} - I_q \end{bmatrix} \tag{6.10}$$

These simplifications of the current control loop are illustrated by the block diagram in Figure 6-5. Due to the above simplifications, the transfer function from reference currents I_d^{ref} and I_q^{ref} to actual currents I_d and I_q in the rotating reference frame consists of two decoupled first-order transfer functions. The dotted lines in the diagram show the cross coupling between the *d*- and *q*-axis introduced by Equation (6.8) which are cancelled by the decoupling in Equation (6.9). It has also been observed that the assumption to lump the line impedance into the transformer impedance results in the cancellation of the line voltage influence. The two current control loops may therefore be considered as independent, at least for the simplified considerations made here. Each of the two loops now resembles a DC system as discussed in Section 4.4.2.

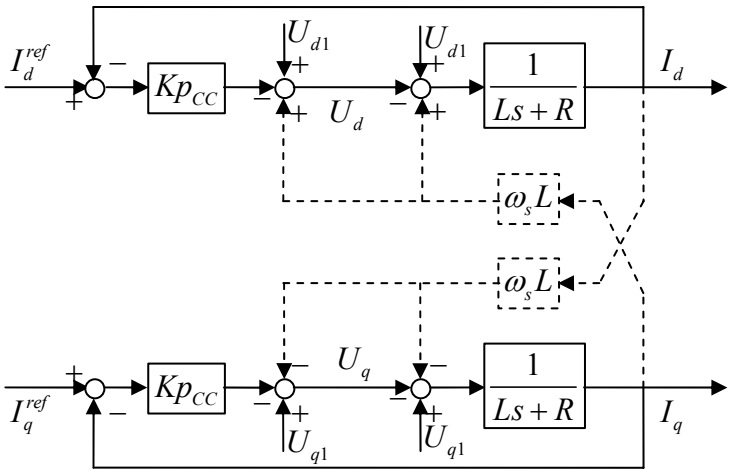

Figure 6-5: Decoupled current control loops.

When the reactive power is controlled to be zero, the vehicle reactive current reference $I_q^{ref} = 0$ as well. Additionally, the PLL orients the vehicle internal rotating reference frame by controlling the voltage $U_{q1} = 0$ as described in Section 5.4.1. As a result, a major part of the active power consumed by the vehicle in steady state is given by the *d*-

axis loop (ref. Equation (5.2): $P = U_{d1}I_d + U_{q1}I_q \approx U_{d1}I_d$). For reasons of simplicity here, this is assumed to be valid for low-frequency oscillations as well. Based on this, the simplified block diagram for the active power control loop in Figure 6-3 is now combined with the *d*-axis part of Equation (6.10) and Figure 6-5 to give the DC-link voltage control block diagram as shown in Figure 6-6.

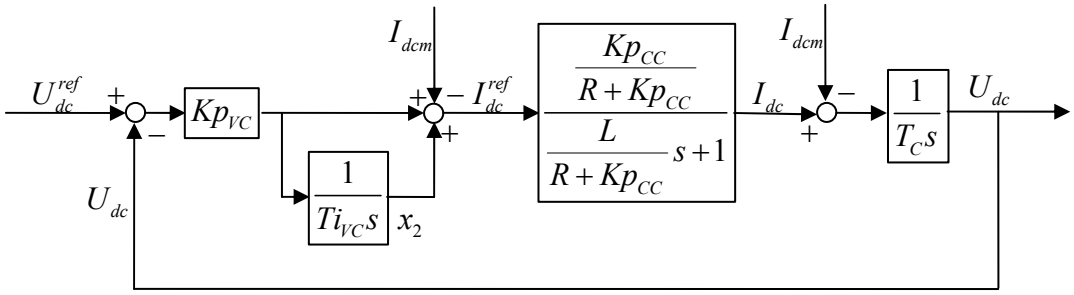

Figure 6-6: A block diagram for the DC-link voltage and active power control loop, including the simplified current control loop

The simplified vehicle inverter control consists of two cascaded control loops. The outer loop controls the DC-link voltage and active power, and the inner loop controls the vehicle's AC current. The *d*-axis current control loop in Figure 6-5 is expressed in Figure 6-6 as an equivalent first-order filter where the gain K_{eq} and time constant T_{eq} are shown in Equations (6.11) and (6.12).

$$K_{eq} = \frac{Kp_{CC}}{R + Kp_{CC}} \tag{6.11}$$

$$T_{eq} = \frac{L}{R + Kp_{CC}} \tag{6.12}$$

6.2.6.2 Eigenvalue expression

From the roots of the closed loop transfer function $H(s) = A(s) / (1 + A(s))$ where the open loop transfer function $A(s)$ is given by Equation (6.2), application of Equation (6.11) and a further assumption of $T_{eq} = 0$ in order to avoid an extra state variable, a similar eigenvalue expression as Equation (6.5) may be established as in Equation (6.13).

$$\lambda_{1,2} = -\frac{Kp_{VC} \cdot \frac{Kp_{CC}}{R + Kp_{CC}}}{2T_C} \pm \sqrt{\left(\frac{Kp_{VC} \cdot \frac{Kp_{CC}}{R + Kp_{CC}}}{2T_C}\right)^2 - \frac{Kp_{VC} \cdot \frac{Kp_{CC}}{R + Kp_{CC}}}{Ti_{VC}T_C}} \tag{6.13}$$

This expression shows that increased resistance *R* and decreased current controller gain Kp_{CC} reduces the damping of the DC-link voltage control mode and to some extent also the oscillation frequency.

6.2.6.3 Considerations

The inductance in the loop represents a counter force the current controller has to fight in order to change the line current. An increased inductance increases the control loop time constant and decreases its bandwidth. The time constant may be reduced by increasing the resistance, but that also reduces the loop gain. Table 6-4 shows a comparison of the low-frequency eigenmode calculated with the second-order model in Equation (6.5) and the third-order model in Figure 6-6 for 0 and 60 km line. An increase in impedance reflects a decrease of K_{eq} and an increase of T_{eq}, and leads to a reduction of mode damping and frequency as partly explained by Equation (6.13).

Table 6-4: A comparison between eigenvalues for the DC-link voltage control eigenmode calculated by second- and third-order models for different values for the lumped impedance. The units are [1/s] and [Hz].

Inductance	**2nd order model**	**3rd order model**
Vehicle transformer only	$-19.2 \pm j2.62$	$-19.2 \pm j3.05$
Vehicle transformer and 60 km line	$-19.2 \pm j2.62$	$-13.0 \pm j2.90$

The current controller gain Kp_{CC} both decreases the time constant and increases the loop gain at the same time. Hence, Kp_{CC} increases the current control loop bandwidth, resulting in a faster fulfilment of the DC-link voltage controller's requirement for active current. A reduction of Kp_{CC} will reduce the apparent line power availability and consequently reduce the damping of the mode as shown in Figure 5-15. Nonetheless, the bandwidth is limited by the PWM switching frequency. Harnefors and Nee [75] recommend that the current control loop bandwidth should be smaller than 0.2 times the switching frequency f_{sw}.

Based on these simplified considerations, we understand that increased line side impedance has an influence on the power availability seen from the DC-link, with large impedance causing a reduction in the loop gain. This reduction is compensated by the current controller by an increased gain.

When including the current control loop in the block diagram in Figure 6-6, we also understand that feed forward of the motor current cannot perfectly cancel the disturbance caused by the motor as assumed in Section 6.2.3. How well this disturbance is cancelled depends on how close the current control loop is to unity. Harnefors and Nee [75] propose to compensate for imperfections by manipulating the feed forward signal.

The simplified third-order model described in Section 6.2.6.1 fails to represent the instability observed in Sections 5.6.5 and 5.7, since the instability phenomenon is not completely modelled. In Section 8.2.5, the constant power load characteristic's influence is introduced and explained.

6.3 Sensitivity analysis

In this section, the low-frequency eigenmode's sensitivity to changes in operating point, control system structure changes and parameter changes for the full electric vehicle model is studied. The analysis is performed by use of the enhanced RMS model, including the $L \cdot di/dt$ voltage term and current controller (CC) as developed in Chapter 5. The reference operating point of the vehicle is 3.67 MW motor power consumption at 60 km line.

6.3.1 Parameter sensitivity

The low-frequency eigenmode's sensitivity to change in the various control system parameters has been calculated and is shown as root-loci curves in Figure 6-7. The study also includes the DC-link main capacitance C_d. Each parameter is changed one at a time from half to double the original value in 10 equal steps. Arrows indicate the direction of movement when the value is increased and the centre point corresponds to mode (12,13) in Table 6-1.

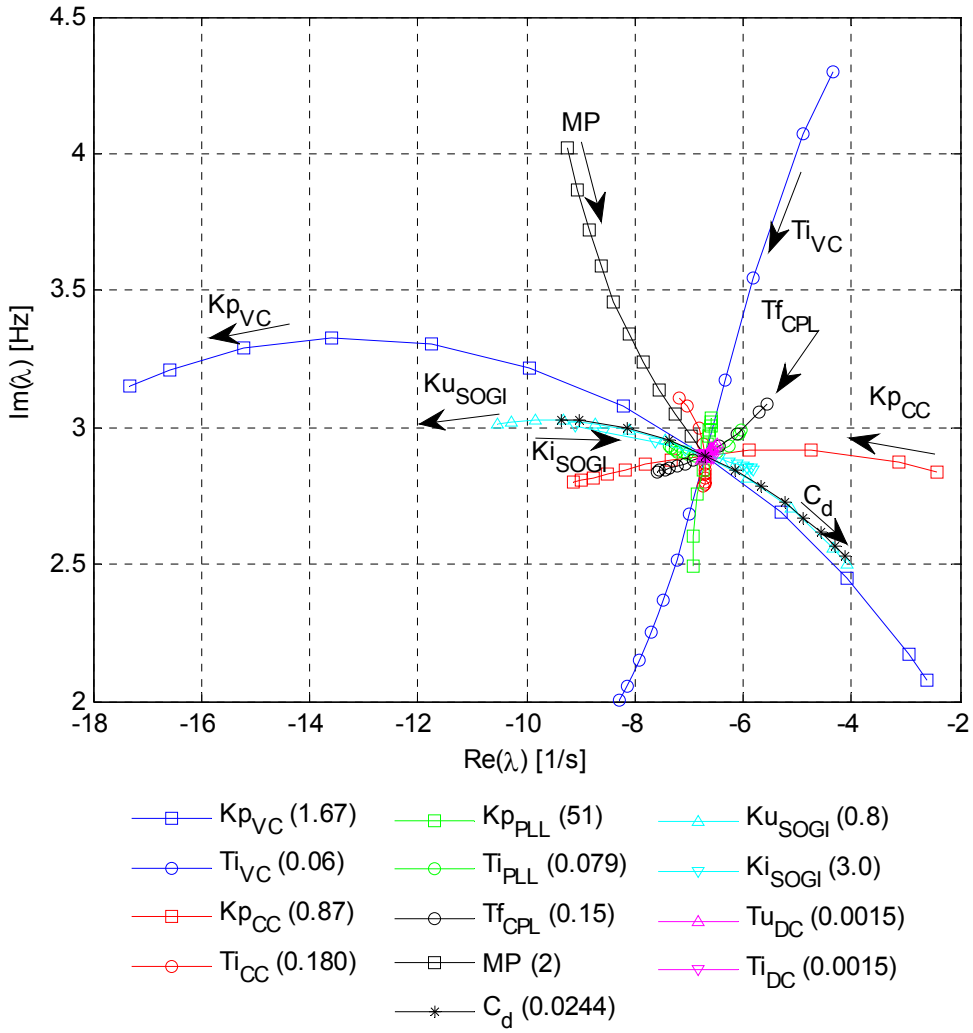

Figure 6-7: Root loci for change in vehicle parameters.

The plot shows a decrease in both the real and imaginary part of the eigenvalue when the DC-link capacitance C_d is increased. An increased DC-link voltage controller gain Kp_{VC} increases the real part and an increased integration time Ti_{VC} decreases the imaginary part. This is according to the simplified analytic expression for the low-frequency resonance in Equation (6.5).

Increased current controller gain Kp_{CC} shows an increase in the eigenvalue's real part, which corresponds to Equation (6.13). If increased damping of the DC-link low-frequency mode is a demand, then the VC and CC gains should be increased.

Additionally, it may be observed that the gain of the line voltage and current measurement SOGI's have an influence on the root-loci as well. A larger gain means a smaller filter time constant according to Equation (5.11) and consequently an increased bandwidth. This may be interpreted as being an advantage to have an accurate line voltage measurement, while it is an advantage to filter the line current.
The rest of the parameters, i.e., the PLL and DC measurement filters, show a minor influence here. The motor characteristic has an influence as well, and will be studied further in the next section.

6.3.2 Motor load characteristic and current feed forward sensitivity

In Section 6.2.3.2, the basic impact from the motor voltage characteristic and the feeding forward of the motor current on the DC-link voltage control eigenmode was shown. Table 6-5 shows corresponding information via the eigenvalues found for the full vehicle model together with the damping ratio. The motor-current feed forward almost cancels the influence from the motor characteristic, while this characteristic has a significant influence when not feeding forward. A constant current characteristic shows equal eigenvalues both with and without feed forward.

Table 6-5: Low-frequency mode eigenvalues for different motor load voltage characteristics. Units are [1/s], [Hz] and [%], respectively

Case	*MP*	Tf_{CPL} [s]	With I_{dcm} feed forward	Without I_{dcm} feed forward
Constant power	0	∞	$-9.23 \pm j4.02$ (34.3)	$-2.98 \pm j3.77$ (13.9)
Constant current	1	∞	$-9.27 \pm j3.35$ (40.3)	$-9.27 \pm j3.35$ (40.3)
Constant resistance	2	∞	$-8.58 \pm j2.83$ (43.5)	$-13.1 \pm j2.57$ (63.0)
U_{dc} filter eqn. (5.4)	2	0.15	$-6.69 \pm j2.90$ (34.5)	$-10.0 \pm j2.12$ (60.0)

For the sake of comparison, the eigenvalues when the DC-link stabilisation filter (Equation (5.4) is used are shown. This characteristic represents a compromise. Zero filter time constant (Tf_{CPL}) corresponds to a constant power characteristic and infinite filter time corresponds to a constant resistance characteristic.

6.3.3 Operating point sensitivity

The eigenvalue of the poorest damped low-frequency eigenmode of the vehicle is calculated for different operating points. The motor power consumption is increased in steps of 1 MW from no-load to 8 MW. In addition, the line length is increased from

zero until instability in terms of a voltage collapse or heavy oscillations, in steps of 10 km. For 2 MW load and lower, the steps in line length are 20 km. An increase in line length represents an increase in both inductance and resistance on the inverter AC side.

Figure 6-8 shows the eigenvalues connected with lines showing an equal load and equal line length. The eigenvalues (12,13) from the reference case of 3.67 MW are shown as well. The plot shows a trend in which increased line length and increased load both decrease the damping and oscillation frequency. This is true for long line and high load, but is not clear for short line and low load, due to interaction with another eigenmode outside the diagram. It is only at no-load and 1 MW load that the vehicle shows oscillatory instability before voltage collapse.

At high load power, the poorest damped low-frequency eigenmode is recognised as the DC-link voltage control mode, with eigenvalues (12,13) as discussed. At no-load, the other vehicle low-frequency mode, the eigenvalues (9,10) which have the main participation from the vehicle control system in general, dominate. In between, there is interference between these two modes. This interference is the reason for the large clockwise bow shown by the root loci in Figure 6-8. For other vehicle control system parameters, the separation of these two resonances at low load and short line length may be even more visible. Yet, this does not mean that the DC-link and its controller are not important participants at low load. The time simulations for the long line stability test in Section 5.7 confirm that the DC-link voltage oscillates in no-load as well.

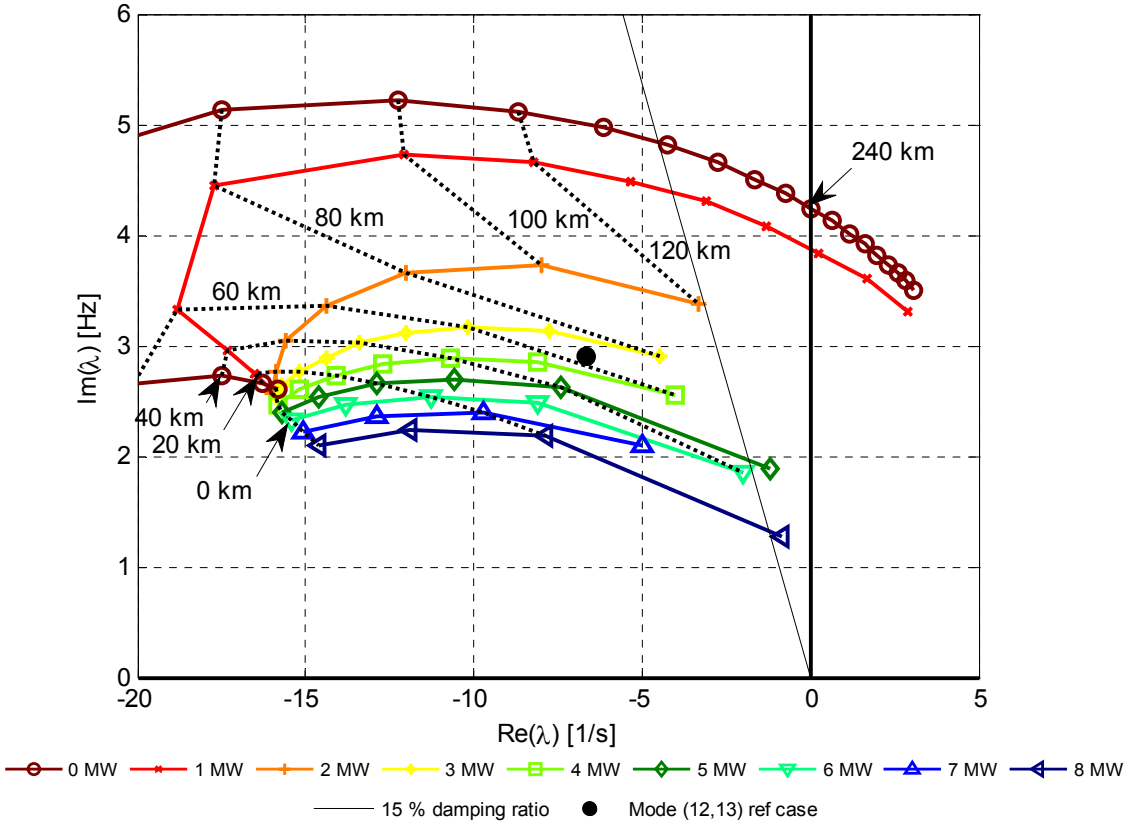

Figure 6-8: Vehicle low-frequency eigenmode sensitivity to change in operating point in terms of motor power and line length.

6.4 Participation of state variables

6.4.1 Participation factors

The participation factor for all state variables in the system is calculated according to Equation (C.7) for the low-frequency eigenmode (12,13). Their amplitudes are compared in the bar diagram in Figure 6-9.

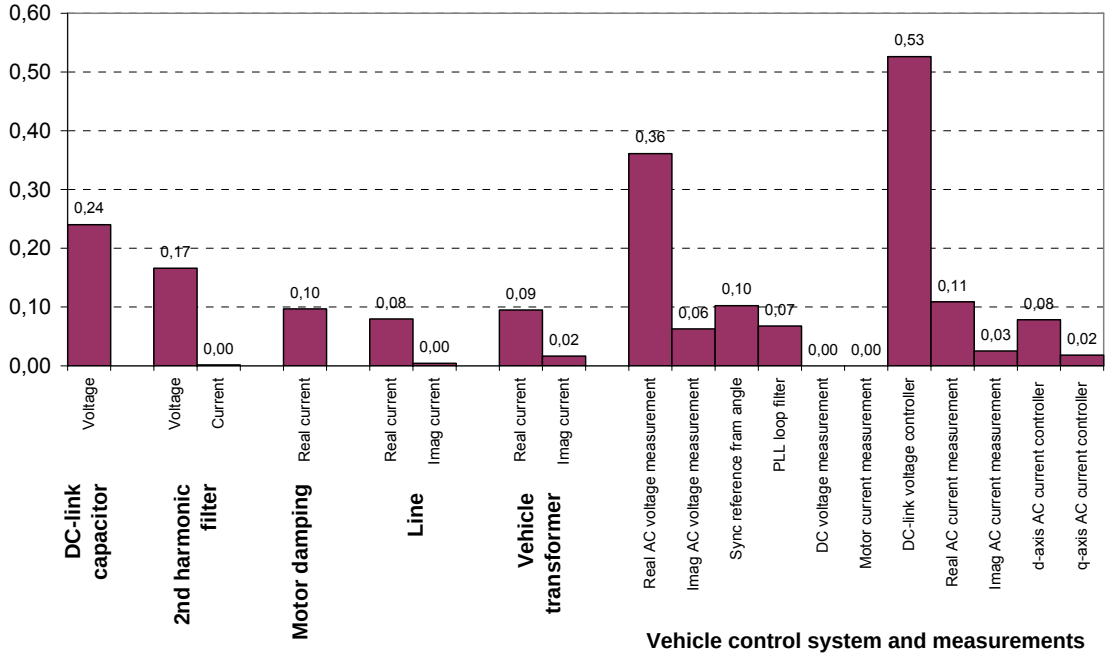

Figure 6-9: Participation factors for all state variables in vehicle low-frequency eigenmode.

The most participating state variable is the DC-link voltage controller integrator x_2. Together, the capacitor voltage over C_d and C_2 forms a second large participant. This indicates that it is the DC-link voltage controller mode as described by Equation (6.5) that is found as mode (12,13). The mode's eigenfrequency also corresponds to the expectation from the calculations with the second-order model in Section 6.2.5. Additionally, the line voltage measurement filter participates significantly. The rest of the state variables have a medium to low participation.

6.4.2 Time constants

The dynamical system contains several time constants. Some of them are physically given, some are chosen for the control system, some are chosen for measurement filtering, and one is the artificial and limiting single-phase power availability. They are all shown as bars relative to the logarithmic scale in Figure 6-10.

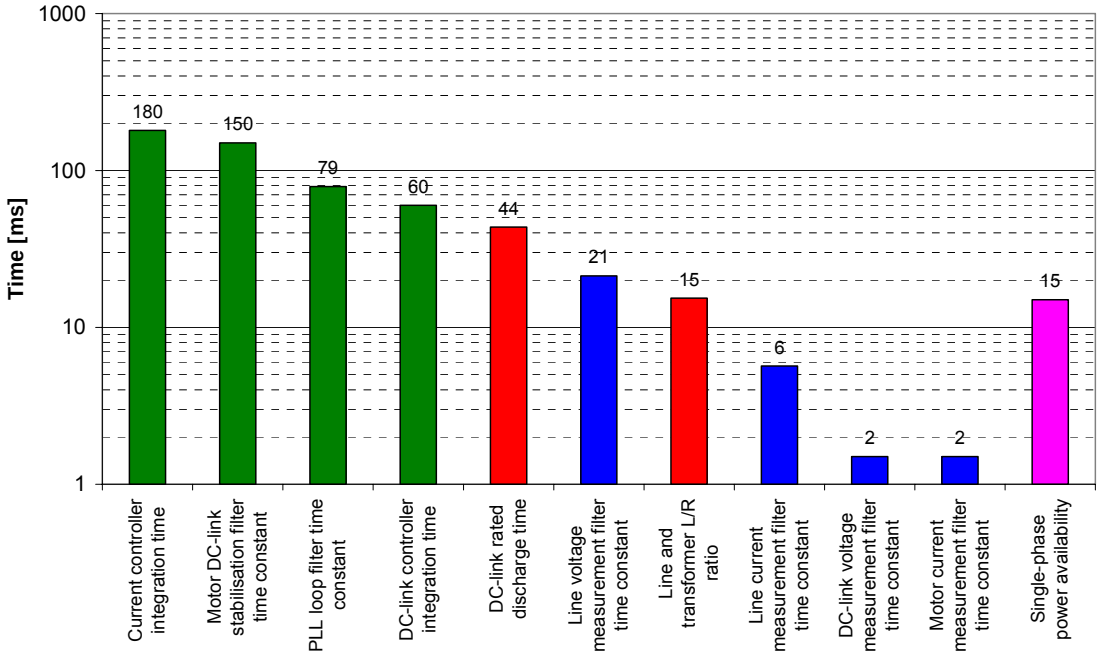

Figure 6-10: Physical (red), control system chosen (green), measurement filter chosen (blue) and artificial (pink) time constants in the dynamical system.

The diagram reveals that there are six time constants within the same decade 10-100 ms. If these were time constants in first-order low-pass filters, they would have all resulted in a bandwidth of 1.6-16 Hz. The single-phase power availability limits the active power control loop to a bandwidth of 10 Hz. Based on this consideration, the vehicle has to have a dynamic behaviour below the fundamental frequency of 16 ⅔ Hz as stated by Menth and Meyer [116].

Some correlation between the state variables that participate in the low-frequency DC-link voltage controller eigenmode and the proximity of the state variable's time constant to the DC-link rated discharge time and voltage controller integration time may be observed.

6.5 Measurements on a real-life vehicle

Measurements have been performed on a real advanced electric rail vehicle (Danielsen, et al. [51]). It is a 5.6 MW (wheel power) four axle freight train locomotive. Its line-side converter control system software is equal to the standard configuration when the locomotive is operated in continental Europe 16.7 Hz system, i.e., in Germany and Switzerland. The control system structure and parameter values differ from the simulation model developed in this thesis. However, the main structure with a DC-link voltage PI-controller is present. The DC-link data is among the typical values shown in Table 6-2.

The vehicle is operated in steady state 2.8 MW power consumption at 10 km from a single rotary converter in island operating mode. At this stage, sustained oscillations are

observed in the vehicle DC-link voltage, as well as the line active power. The vehicle DC-link voltage, together with the line active power is shown in Figure 6-11. Both the application of Equation (C.3) and an FFT analysis resemble a significant 4 Hz component.

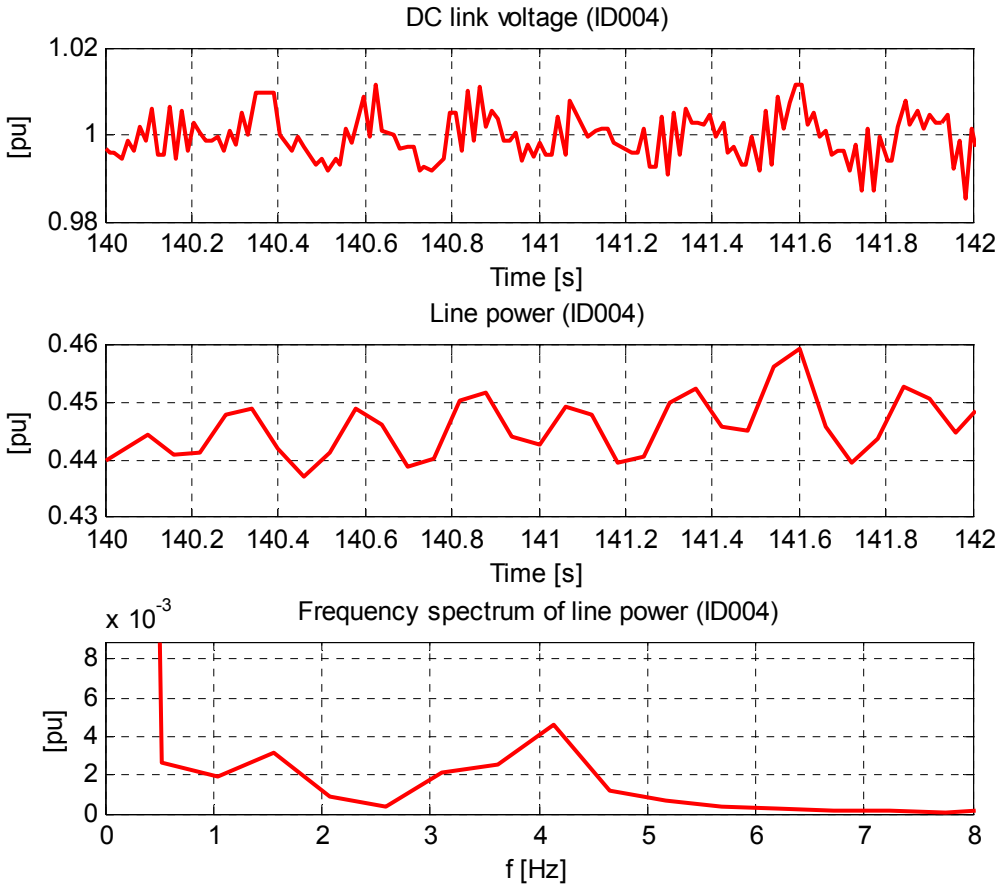

Figure 6-11: Measured vehicle DC-link voltage and line active power at stability limit, together with the frequency spectrum of the line power signal.

Equation (6.5) is applied for the same vehicle when the DC-link voltage controller parameters (Ti_{VC} = 0.04 s and Kp_{VC} = 1.5 pu[14], Eisele [64]) are given. As the oscillations are sustained, the real part is zero, and the damping impact on the oscillation frequency can be neglected. The corresponding undamped eigenfrequency is calculated to approximately 4.6 Hz by use of Equation (6.14).

$$f_{nat} = \frac{1}{2\pi}\sqrt{\frac{Kp_{VC}}{Ti_{VC} \cdot T_C}} \tag{6.14}$$

[14] The gain is given in physical values and converted to per unit by the author of present thesis.

6.6 Discussion and conclusion

6.6.1 Discussion

6.6.1.1 Participating components in low-frequency dynamics

In this chapter, some of the fundamentals of the vehicle low-frequency dynamics are studied by both simplified analytical considerations and an analysis on the full simulation model. Of major importance are the DC-link energy storage and its voltage controller which have been modelled according to state-of-the-art for the design and control of the back-to-back converter solution used in electric vehicles today. These components form the basis of the observed low-frequency eigenmode. Additional system time constants in the vicinity of the DC-link voltage controller integration time and the DC-link rated discharge time both participate in and exert an influence on this mode.

Several of the time constants in the vehicle are determined by the single-phase power availability which restricts how fast the power control can actually be. Hence, some of these time constants are difficult to 'move out' from the low-frequency range. Additionally, the time-invariant characteristic of the single-phase system results in a need for measurement filters, both on the AC- and DC-side of the line-side converter. For that reason, selection of values for time constants may become a trade-off between filtering harmonics and low-frequency behaviour. A demand for fast control action to disturbances has an influence on this selection as well.

This filtering, together with the current control loop, is expected to have a large influence on the results of the long line stability test (as shown in Section 5.7). Figure 6-8 indicates interaction between the DC-link voltage control mode and another low-frequency mode when the load power is low (9,10). Here, the measurement filters show a higher participation. It has also been observed, although not shown, during the present work, that when the system is at its long line stability limit, the relative participation is more evenly distributed among the state variables than in the reference case. Still, the details in filter and current control loop influence remain for further studies.

A new control system is proposed however by Heising, et al. [78] based on a multivariable control of the line-side converter, where the DC-link voltage controller has no integral part. One of the important and basic time constants for the low-frequency mode studied here is thus removed. This solution shows larger stability margins than does the conventional PI-controller in the long line stability test (Heising, et al. [80]), though there will still be some time-constants in the low-frequency range given by physics and measurement filters that will result in some low-frequency dynamics.

The vehicle model studied here includes only control of the active power to be constant as given by the motor's demand. Yet, real vehicles may include a voltage dependent line active power limitation (as required by EN 50388 [41]) and a voltage dependent on line

reactive power control (Appun and Lienau [12]), both for supporting operation in weak networks (high line impedance). These controllers cannot be much slower or faster than the basic active power control bandwidth of the vehicle, and must observe the same input signals (measurement of voltage and current) and influence the same physical variables (voltage and current). Hence, their controller time constants are possibly located in the low-frequency range, and they may exert an influence on the low-frequency dynamics and stability as well. Details of this topic remain for further studies.

6.6.1.2 Mode sensitivity to change in paramters value

Change in parameter values, motor characteristics and control structure demonstrate an influence on the oscillation frequency. There is some correlation between the components' participation and the low-frequency mode sensitivity to these components' parameters, and from this the DC-link voltage controller's parameters are important. However, the current controller gain is important as well, even without the current control loop state variables having a large participation.

The change of operating point shows even larger variations without parameter change. Additionally, if the DC-link voltage reference is dependent on the motor speed, the DC-link discharge time constant changes as well. It might therefore be too narrow to focus on the mode frequency in numbers as a distinct characteristic between different vehicles without taking the load and outer line impedance into consideration.

The numbers for the low-frequency mode presented here are based on what must be considered as a traditional design of an electric rail vehicle. The controllers' bandwidths are limited in the lower frequencies by the desire to reduce both the physical and electrical size of the DC-link and in the higher frequencies by the semiconductor's switching frequency. Technical developments resulting in other DC-link solutions and higher switching frequencies may allow for a larger bandwidth separation of the different controllers, e.g. a larger variety of time constants. This may also change the low-frequency behaviour, for example, a larger separation of the two vehicle low-frequency modes as indicated in Figure 6-8. This may also increase the frequency range of where low-frequency instability may be experienced, and should be a topic for further investigation.

One proposal for improving the situation regarding the 'depot problem' described in Section 2.4.5.2 can be to reduce the low-frequency dynamics by reducing the participation from the DC-link voltage controller's integral part. In no-load, a fast transient response is less important and the integration time can be increased. For example, by increasing Ti_{VC} to 1 s, the long line stability limit described in Section 5.7 more than doubles to 560 km.

6.6.1.3 Comparison with measurements and observations

Measurements of the low-frequency mode studied on a real rail vehicle are performed and compared with calculations of the eigenfrequency by the simplified Equation (6.5). The results correspond surprisingly well, even though other controller designs, line length, load operating point and motor-side influence are also expected to influence the eigenfrequency.

All numerical figures from both the simplified models and the full vehicle model confirm an eigenfrequency in the range of 0.1-0.3 times the fundamental frequency, which corresponds to the real life experiences listed in Table 2-2.

6.6.2 Conclusion

The state-of-the-art structure of an advanced electric rail vehicle is studied in view of low-frequency dynamics. Simplified analytical considerations, analysis on a full vehicle line-side converter model, and observations on a real-life rail vehicle all show that the vehicle has an eigenfrequency in the range of 10-30 % of the fundamental frequency.

The main participants in this mode are the DC-link energy storage and its voltage controller due to the DC-link rated discharge time and the controller's integration time being close. Furthermore, several others of the system's time constants are determined by the characteristic single-phase second-harmonic pulsating power and are hence fixed to this time range where the DC-link voltage control eigenmode is located.

Vehicle control system parameters, control system structure and electrical values have influence on this low-frequency eigenmode. Components showing time constants in the vicinity of the DC-link rated discharge time and the controller integration time participate in the mode, and their parameters show an influence on both the mode's damping and frequency. If increased damping of the DC-link low-frequency mode is a demand, then the DC-link voltage controller gain and the AC current controller gain should be increased. The eigenfrequency can be decreased by increasing either the DC-link energy storage or the DC-link voltage controller's integration time.

The motor-side DC-link voltage dependence characteristic influences both the eigenfrequency and the damping of this mode. For example; a constant power load characteristic reduces the mode's damping and increases its eigenfrequency while a constant resistance load characteristic has opposite influence. A constant current characteristic is neutral. The influence from this load characteristic can be ideally cancelled by feeding forward the motor-side current to the DC-link voltage regulator.

The vehicle low-frequency mode is until a certain degree sensitive to the operating point regarding power consumption and line length to the ideal voltage source. Increasing load and line length decreases both eigenfrequency and damping and reduces the system's stability margins and eventually leads to instability, either low-frequency oscillations or voltage collapse.

6.6.3 Further work

In this chapter, the basics of the vehicle's low-frequency dynamics are analytically studied based on a simplified approach. However, a real-life vehicle is far more advanced than the second-order model developed here reflects. Thus, further investigation of the following is of interest:

- Details in filter and current control loop influence are of importance in order to understand more of the vehicle's behaviour. Harnefors, et al. [74] perform analytical considerations, including this influence on a more general three-phase voltage-source converter. More detailed analytical investigations of the rail vehicle is important to understand more of this complex component.

- Line active power limitation and reactive compensation are features which are utilised under weak power supply conditions. Under such conditions, the stability margins are observed to be smaller and the low-frequency behaviour of these controllers is believed to be important.

- The proposed multivariable control concept described by Heising, et al. [78] should be implemented in a real vehicle and tested correspondingly to obtain more full scale experience. Outer control loops such as line power limitation and reactive power control should be added to the multivariable control system in order to adapt it to realistic operation under weak power supply conditions. In that way, the potential of this system compared with the state-of-the-art solution can be investigated.

- It should also be investigated if there are other methods than the one described by Heising, et al. [78] that can increase the damping of the vehicle low-frequency mode, e.g. reduce the dominating DC-link integral part, without compromising the control system's transient response.

- By modelling the motor side more in detail than in the present model, its low-frequency influence can and should be studied.

7 Rotary converter – vehicle interaction

This chapter reports on a study of the interaction between the rotary converter and the developed advanced rail vehicle model conducted by use of traditional power system stability investigations, i.e., linear analysis and time simulations. Various methods for stability improvement are investigated and a reason for the observed instability is proposed. The main principles are compared with measurements on a real rail vehicle.

7.1 Introduction

The traction power system in study was introduced in Chapters 1 and 2 and is sketched in Figure 1-1. It consists of a rotary frequency converter having a poorly damped electromechanical eigenfrequency as studied in Chapter 3 and an advanced electric rail vehicle as studied in Chapters 5 and 6. The components are modelled by use of the concept with enhanced RMS, including the current dynamics described in Chapter 4 and 5. The system's operating point is as per the reference case described in Appendix B.1.

7.2 Time domain simulation

A time domain simulation is performed with the simulation model explained in Section 7.1. A step in vehicle motor power of 22 kW is made until the operating point used as the basis for linearisation in the reference case is reached. The result is a 1.6-Hz oscillation increasing in amplitude as time passes, as shown in Figure 7-1. As a consequence of this, the system is therefore unstable.

The figure includes a plot of the important electrical variables in the system, together with the 'core' of the rotary converter oscillation – the rotor speed variation as shown in Section 3.2. Hence, the speed variation is here used as a reference for considering the oscillation of the other variables, and is plotted in the same sub-diagram as the vehicle DC-link voltage. These two important state variables and energy storages oscillate in anti-phase, i.e., 180 degrees shifted in phase, which indicates an exchange of energy between them.

The different sub-diagrams in the figure show the comparable variables such as voltage, current and power for the rotary converter three-phase motor, the single-phase generator, and the vehicle. The values shown are observed at the three-phase 6.3 kV busbar, the single-phase 15 kV busbar, and the vehicle's current collector and interface to the rest of the power system. The exception to the busbar values are the synchronous machines' power angles which are the internal angles in the respective machines. In addition, the electrical interface values measured by the vehicle's control system are shown. For example, the voltage phase determined by the phase-locked loop (as seen in

the step response in Section 5.5.3) is compared with the exact angle for current collector voltage. All values are plotted with their respective steady-state values as a reference, i.e., it is only the deviation from steady state referred to as zero that is shown. Positive single-phase power direction is out from the generator and into the vehicle.

The essence of the interaction may be summarised as follows:

1. When the converter oscillates due to the load step excitation, the generator voltage amplitude oscillates in phase. The internal induced generator voltage is rotor speed dependent due to Equation (4.15). The generator exciter model used here does not change this relationship; hence, the relation between the generator voltage and speed, k_u, in Equation (3.20) is positive.

2. This voltage amplitude oscillation is observable at the vehicle as well. A line voltage change will change the power flowing into the vehicle DC-link according to Equation (5.1), resulting in a change in the DC-link voltage. As the DC-link controller aims to keep the DC-link voltage constant, the line current has to be changed accordingly to keep the power input constant. The line current must therefore be changed in anti-phase to the line voltage oscillation.

3. However, despite constant power load control objective, the vehicle line active power is not kept perfectly constant. It oscillates in phase with the line current and hence in anti-phase to the voltage amplitude and converter speed. The vehicle counteracts the line voltage oscillations too much by the line current control. This active power oscillation is amplified through the line due to the losses given by $P_l = R_l \cdot I^2$. From the figure it can be observed that the vehicle active power oscillation is approximately on third of the generator active power oscillation, i.e., the line losses represents the remaining two thirds. The resulting generator electromagnetic torque oscillation violates the stability criterion in Equation (3.27). Consequently, this active power oscillation has a destabilising impact.

4. It might be observed as well that the generator reactive power oscillates in phase with the active generator power to cover the reactive line losses, which is due to the change in line current. Here, positive reactive power is the load being inductive, i.e., consuming reactive power. However, the vehicle reactive power does not constantly equal its zero-valued reference; it oscillates in anti-phase to line voltage, active power, and generator reactive power. This means that during the oscillation, the vehicle covers some of the changes in line reactive power losses. This reactive power oscillation has a stabilising impact, as inductive behaviour when voltage is high and capacitive behaviour when voltage is low reduce the line voltage oscillations.

Based on these observations, a closed feedback loop as shown in Figure 7-2 is proposed. The rotary converter oscillations influence the line voltage, which in turn influence the DC-link voltage. The DC-link voltage regulator gives the vehicle's current reference, and the current influences the generator power; thus balance in Equation (3.8).

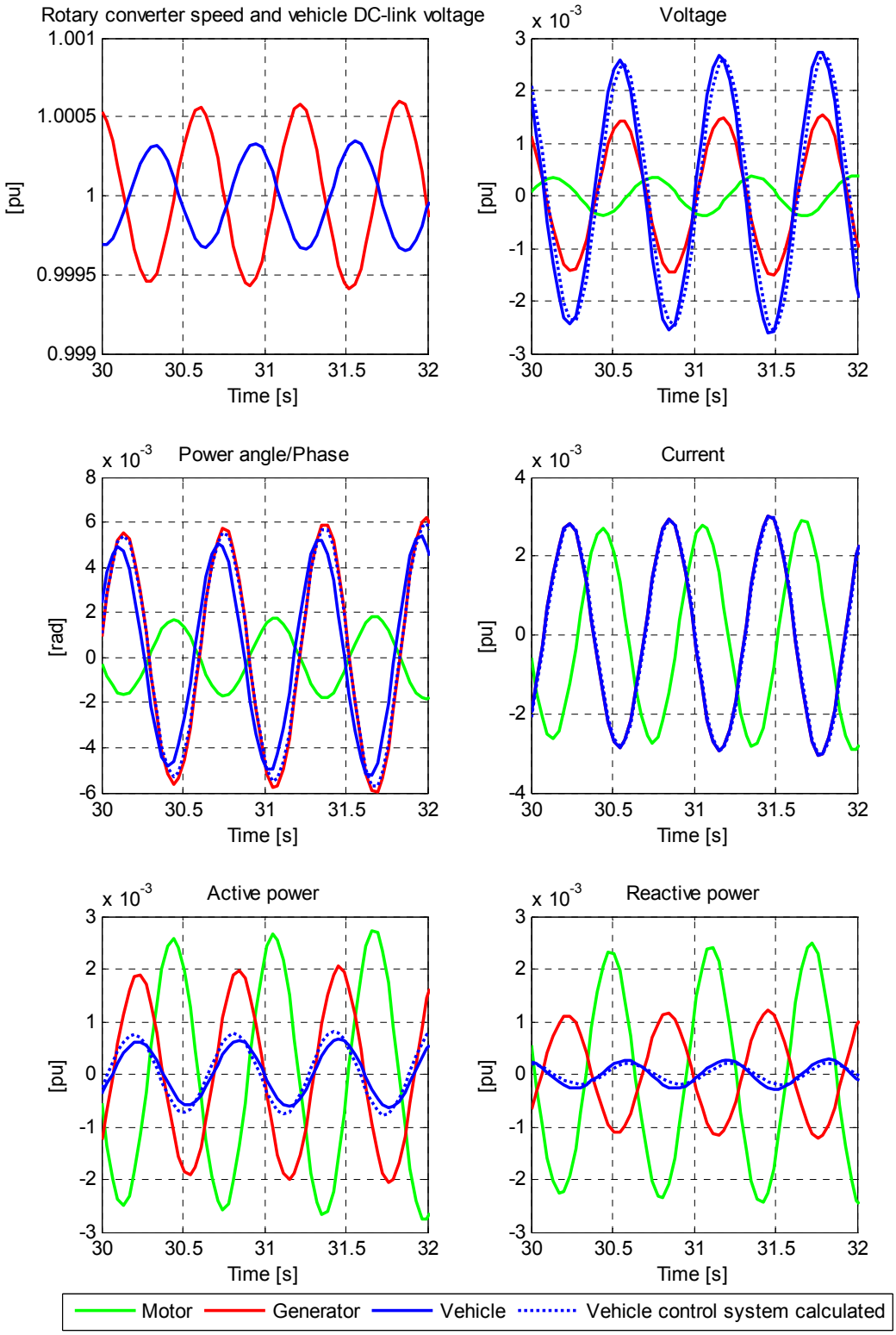

Figure 7-1: Oscillating electrical variables relative to the converter speed in the unstable reference case. Rotary converter motor active power in the diagram is divided by 10 in order to put the power values in the same scale.

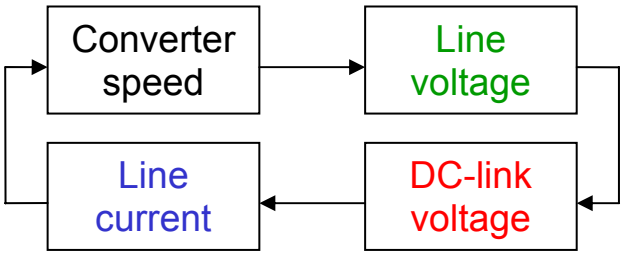

Figure 7-2: A principle sketch of a rotary converter – rail vehicle closed feedback loop.

It can be observed from Figure 7-1 that neither the voltage amplitude, current amplitude nor voltage phase measurements in the vehicle show large deviations from the real electrical values, i.e., the measurements are not out of phase with the real values. However, the lagging angle from the PLL will be studied further in Section 7.4.1.4.

7.3 Linear analysis

7.3.1 System eigenvalues

For the reference case given, the system's eigenvalues are calculated. Out of a total of 40 eigenvalues (zero-values excluded), the ones having a frequency lower than the fundamental frequency ($\mathrm{Im}(\lambda) < f_s$) and a real part larger than -100 ($\mathrm{Re}(\lambda) > -100$) are shown in Table 7-1. The table also includes the main participating components in each mode, i.e., the components having a participation factor larger than 0.1 ($|P_i| > 0.1$). Infrastructure components are marked with a '+' and the vehicle components are marked with a '*'. From these it can be observed that the vehicle, the rotary converter and both of the synchronous machines' excitation systems participate in the listed modes.

Of primary interest here are the eigenvalues with the lowest damping ratio ζ, see Equation (C.4), as they will dominate the system's dynamical response. There are two important eigenvalue pairs, numbers 21 and 22 and numbers 25 and 26, which have a damping ratio of +10.0 % and -0.58 %, respectively. The first (21,22) has a main participation from the vehicle and the second (25,26) a main participation from the rotary converter. They are recognised as the vehicle and rotary converter modes, respectively. The rotary converter mode is negatively damped which describes the system as unstable. Oscillations at the rotary converter's eigenfrequency of 1.6 Hz will increase in amplitude as time passes, as seen in the simulation in Section 7.2.

It has also been observed that the vehicle mode is now changed in comparison to the case in which an ideal voltage source is used instead of the rotary converter in Chapter 6. The relative damping is decreased from 34.2 % to 10.0 %.

Table 7-1: The eigenvalues calculated for the system, including the main participating components.

No.	Eigenvalue [1/s], [Hz]	Damping ratio [%]	Main participation (participation factor in parenthesis)
13, 14	$-21.0 \pm j6.15$	47.8	* Vehicle PLL angle (0.52), * Vehicle AC-voltage measurements (0.45+0.23), * Vehicle PLL loop filter (0.17), * Vehicle AC-current measurements (0.11+0.09) and * Vehicle DC-link controller (0.10)
17, 18	$-5.50 \pm j3.03$	27.8	+ Generator exciter field voltage (0.72) and * Vehicle DC-link controller (0.14)
19, 20	$-4.83 \pm j3.18$	23.5	+ Motor exciter field voltage (1.00)
21, 22	$-1.45 \pm j2.29$	*10.0*	** Vehicle DC-link controller (0.45),* ** Vehicle AC-voltage measurement (0.17+0.17),* ** DC-link voltage (0.16+0.11),* ** DC-link damping (0.14),* *+ Generator exciter field voltage (0.16),* ** Vehicle d-axis current controller (0.11),* *+ Generator field winding flux (0.10) and* *+ Generator damper winding d-axis flux (0.10)*
25, 26	$+0.06 \pm j1.64$	-0.58	*+ Motor power angle (0.51),* *+ Motor speed (0.27) and* *+ Generator speed (0.27)*
29, 30	$-4.85 \pm j0.13$	98.6	* Vehicle d- and q-axis current controller (0.50+0.49), * DC-link damping (0.28), * Vehicle AC-voltage measurement (0.14+0.06) and * Vehicle DC-link controller (0.12),
31, 32	$-1.73 \pm j0.30$	67.6	+ Generator exciter regulator voltage (0.81) + Generator field winding flux (0.60) and + Generator damper winding d-axis flux (0.27)
33, 34	$-0.93 \pm j0.16$	67.9	+ Motor field winding flux (0.70) and + Motor exciter regulator voltage (0.70)

7.3.2 Participation

7.3.2.1 Participation factors

Table 7-1 reveals that even if the infrastructure and vehicle modes are mostly separated, they may participate in each other's modes, e.g. as in eigenvalues (17,18) and (21,22).

Figure 7-3 shows a bar diagram with the participation factors for all of the system's state variables regarding the two modes of interest: the vehicle mode (21,22) and rotary converter mode (25,26).

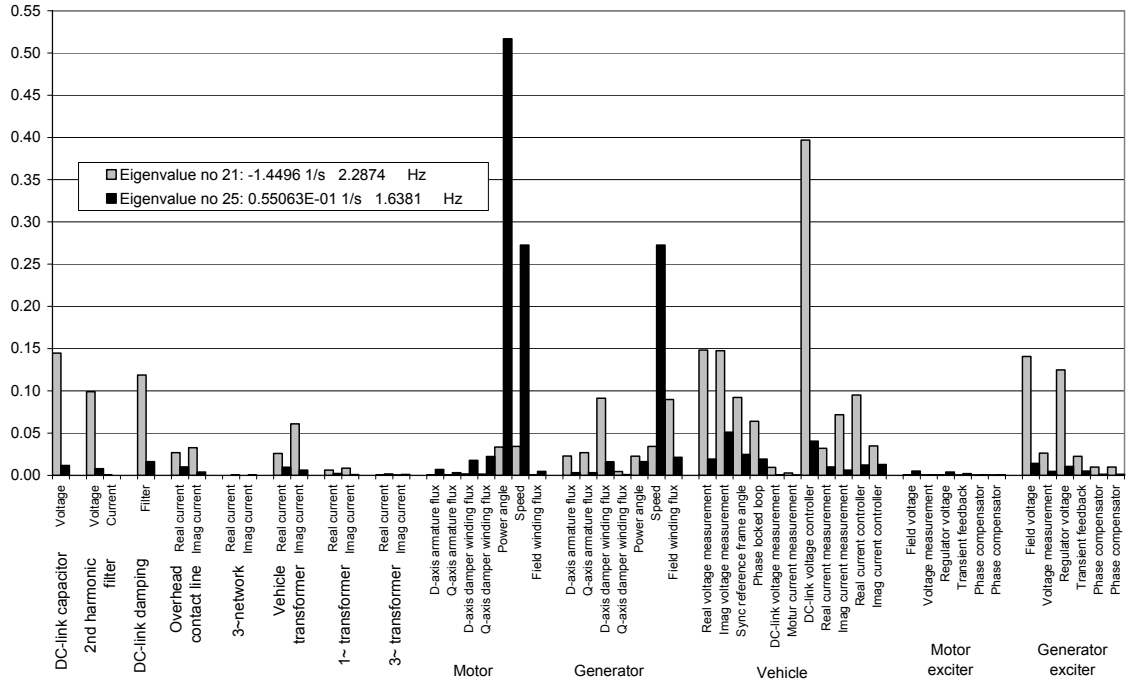

Figure 7-3: The participation factors for the vehicle and rotary converter modes.

For the vehicle mode, the pattern shown in Figure 6-9, when the vehicle was fed from the ideal voltage source, is recognised. There are several state variables participating with a factor of 0.05 to 0.15 in the vehicle control system, the vehicle DC-link, the vehicle transformer, and in the generator and its excitation system. However, the basic Equation (6.5) for the vehicle mode concerning the DC-link voltage and DC-link voltage controller integral part is still essential due to these two state variables' large participation.

The rotary converter mode is different. There are two large participants: the rotary converter speed and the motor power angle as indicated by the swing equation (3.8). The participation from other state variables compared with those is relatively low. The main participants from the vehicle control system are the DC-link voltage controller, the line voltage measurement and the phase-locked loop. This participation indicates that to some extent, the rotary converter mode is influenced by the vehicle low-frequency dynamics. The ratio between their eigenfrequencies is 2.28/1.64 = 1.39, which shows that they are in each other's vicinity.

7.3.2.2 Time constants

In line with the pattern for the vehicle when it was fed from the ideal voltage source alone, all the system's time constants when the vehicle is fed from the rotary converter, are shown in Figure 7-4. Both the synchronous machines and their excitation system add several time constants to the system. The abbreviations used in the legend correspond to an explanation of each parameter in Appendix B.

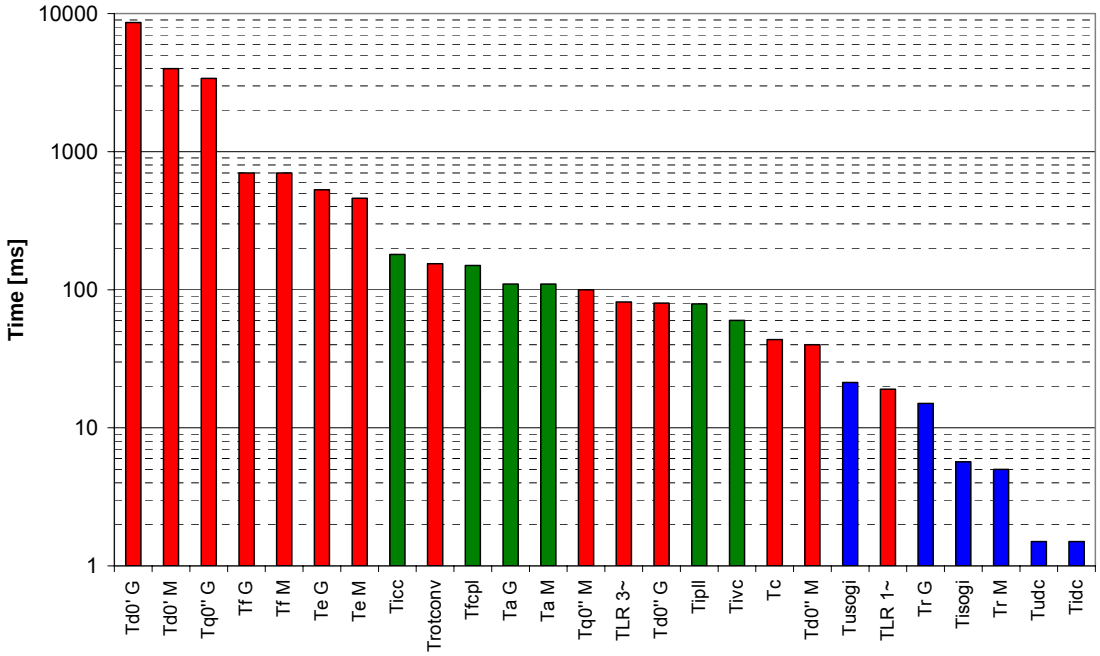

Figure 7-4: The time constants in the complete rotary converter – rail vehicle system: physical (red), control system chosen (green) and measurement filters (blue).

Of special interest, particularly in view of the low-frequency oscillations, is a time constant for the rotary converter electromechanics. For synchronous machines, different types of time constants for the rotating masses may be defined (Machowski, et al. [115] and Pal [136]). The inertia constant H and the mechanical acceleration time T_m are two such time constants. However, using Equation (3.15) for the natural oscillation frequency as a basis, the inertia coefficient $M = 2H/\omega_{sM}$ represents the mass when K_1 is interpreted as the spring constant in the analogue mass-spring-system. The inertia coefficient M has the unit s^2 and may be interpreted as the angular momentum ($M_m = J\omega_{smM}$) referred to the electrical rotational speed: $M = J\omega_{sM}$. The time constant of interest is hence the square root of the inertia coefficient, as in Equation (7.1).

$$T_{rotconv} = \sqrt{M} = \sqrt{\frac{2H}{\omega_{sM}}} \tag{7.1}$$

For the rotary converter under study, this physical time constant is in the same time range as that studied for the vehicle time constants in Section 6.4.2. $T_{rotconv}$ is two to three times the DC-link voltage controller integration time Ti_{VC} and the DC-link discharge time T_C, respectively. This vicinity indicates that the various dynamical components can interact in the low-frequency range, as has already been found by time simulation and the study of the participation factors.

7.3.3 Sensitivities

7.3.3.1 Vehicle parameter sensitivity

In Section 6.3.1, the vehicle low-frequency mode's sensitivity to the vehicle control system parameters values was studied for the reference case. A similar study is performed for the vehicle parameter value's influence on the rotary converter mode. The corresponding root-loci plot is shown in Figure 7-5.

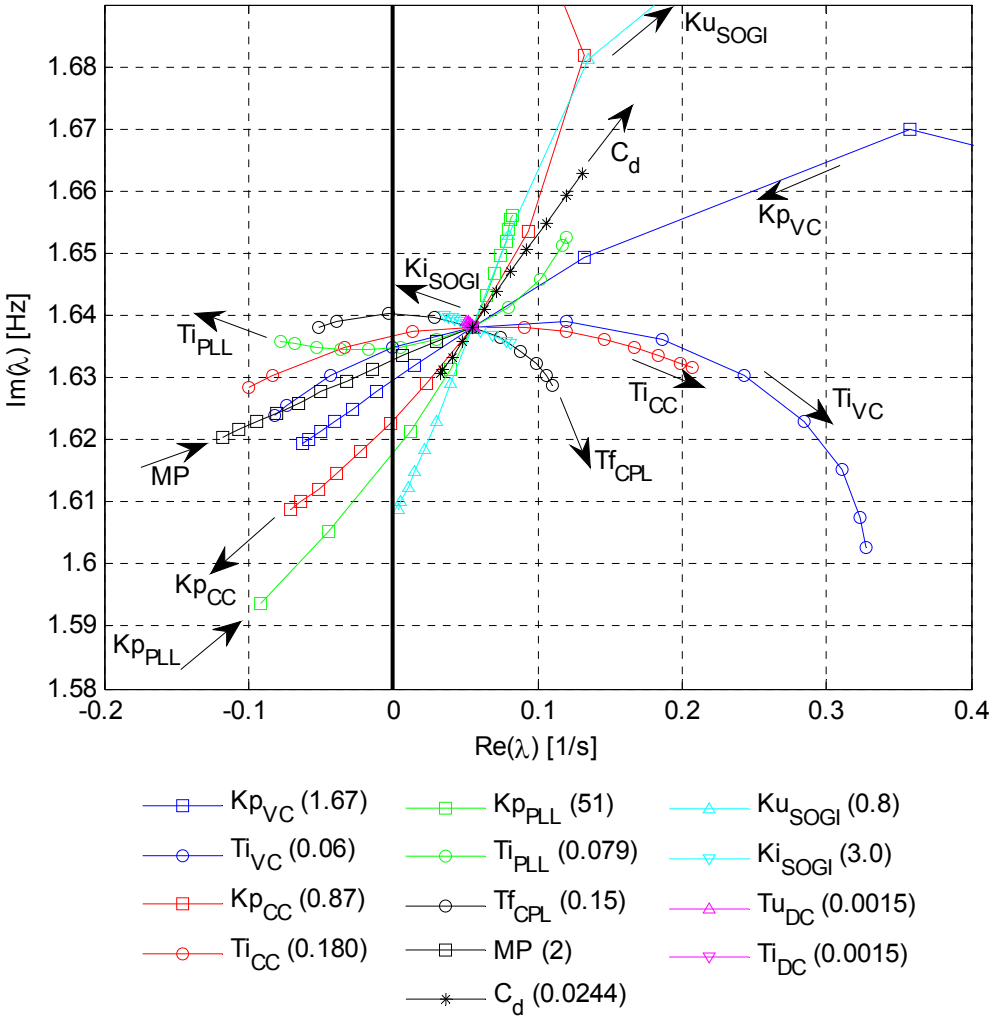

Figure 7-5: Rotary converter mode root loci plot showing sensitivities to vehicle parameter values.

It is observed from the figure that several vehicle control system parameters have an influence on the damping of the rotary converter eigenfrequency. Only small deviations from the original values used result in an even more unstable system. The vehicle control system indeed has an influence on the system's damping. It is also possible to improve the stability by altering some parameters, with such an improvement performed in Section 7.4.1.

A comparison of Figure 7-5 to the similar sensitivity plot for the vehicle mode in Figure 6-7 reveals a pattern. A change of vehicle parameters in a direction which damps the vehicle mode or increases its eigenfrequency may have a damping impact on the rotary converter mode. For example, decreasing the DC-link capacity will, as described by Equation (6.5), decrease the vehicle oscillation frequency which consequently decreases the rotary converter damping, and the same applies to the motor power DC-link voltage dependency as an increase of parameter *MP* decreases the damping of the vehicle mode and hence the damping of the rotary converter mode. For the controller (VC, CC, and PLL) parameters, this impact is further studied in Section 7.4.1. However, this pattern does not apply to the current measurement filter. An increased gain for the current SOGI reduces the damping of the vehicle resonance and increases the damping of the converter resonance.

A similar sensitivity analysis for the other power supply components, such as the synchronous-machine excitation system, may be performed in order to understand how to improve the power supply infrastructure. Such a study however is defined outside the scope of this thesis.

7.3.3.2 Operating point sensitivity

The rotary converter's electromechanical mode is studied in view of the rail vehicle's operating point in the same way as the vehicle mode was studied in Section 6.3.3. The vehicle load is increased by steps of 1 MW and the overhead contact line length is increased by steps of 10 km. The corresponding eigenvalues are shown in Figure 7-6.

From this figure, the following observations can be made. The damping is reduced when the line length is increased and when the vehicle load power is increased, but the damping is more sensitive to load than to line length. A 600 km long line in no-load has almost no influence, while the situation with 8 MW power consumption at 0 km line length is barely stable.

In some cases with a long line and low load power, it has been observed that the vehicle mode turns unstable before the rotary converter mode (this is not shown explicitly in the figure).

When comparing with the vehicle mode's sensitivity to operating point, the following pattern can be recognised:

- There is a positive correlation between reduced damping and frequency of the vehicle mode and the reduced damping of the rotary converter mode.
- But the system including the rotary converter is less damped than the vehicle only and consequently reaches oscillatory instability at shorter line lengths and lower power consumption.

One observation for both the vehicle mode in Figure 6-8 and rotary converter mode in Figure 7-6 is reduced damping when the operating point approaches the maximum transferable power indicated by the nose curves in Figure B-2.

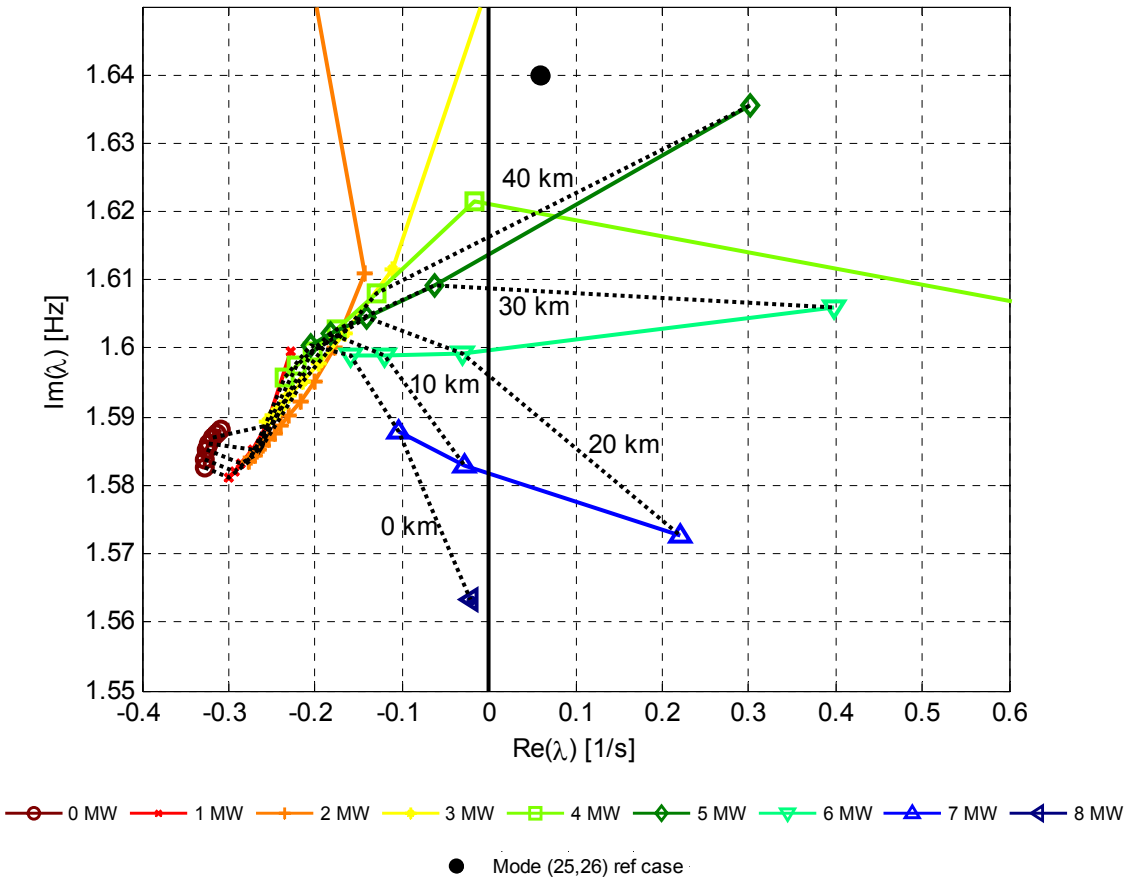

Figure 7-6: Eigenvalues describing the rotary converter mode when the vehicle operating point is varied.

7.3.4 Components and characteristics influencing damping

Both measurements and calculations reported in Chapter 3 show that the rotary converter alone is stable. Additionally, the vehicle at the studied operating point in chapter 6 was found to be well damped. However, an analysis of the complete system model in the current chapter shows that the combination of the rotary converter and the rail vehicle consuming power at long line results in an unstable system. It is of interest to obtain an impression of which components and characteristics are causing this reduction in system damping. This is investigated here by adding components and changing characteristics in the system one by one.

The load condition in the reference case results in a given mechanical torque being applied to the rotary converter rotor seen from the motor. This motor steady-state torque is retained in all the various cases tested, i.e., the motor steady-state operating point is unchanged. However, different load characteristics result in different torque variations when the converter oscillates. The results are illustrated in Figure 7-7 for the following seven cases:

1. A constant mechanical torque load is applied to the motor rotor. This means that the converter generator and the entire single-phase network, including the

vehicle as known from the previous system study, is temporarily removed. This is the reference for comparing the other cases' negative influence on damping.

2. As in Case 1, but the motor AVR is added. The difference between 1 and 2 shows the influence from the motor AVR.
3. As in Case 2, but the mechanical rotor load is changed from a constant torque to a constant power characteristic. The difference between 2 and 3 shows the influence of the changed mechanical load characteristic.
4. As in Case 3, but the mechanical constant power load on the rotor is replaced by a synchronous generator and transformer supplying a constant electric power load at the rotary converters single-phase 15 kV busbar. The difference between 3 and 4 shows the influence of changing from a mechanical constant power load to an electric constant power load, including the generator and transformer. The constant power load is modelled by Equation (3.22).
5. As in Case 4, but the generator AVR is added. The difference between 4 and 5 shows the influence of the generator AVR.
6. As in Case 5, but the electric constant power load is moved from the 15 kV busbar to the end of the 60 km long line. The difference between 5 and 6 shows the influence of the line voltage drop and losses.
7. As in Case 6, but the constant power load is replaced by the dynamical vehicle model. This is the reference case that was previously studied. The difference between 6 and 7 shows the influence of the vehicle dynamical behaviour and the vehicle transformer losses.

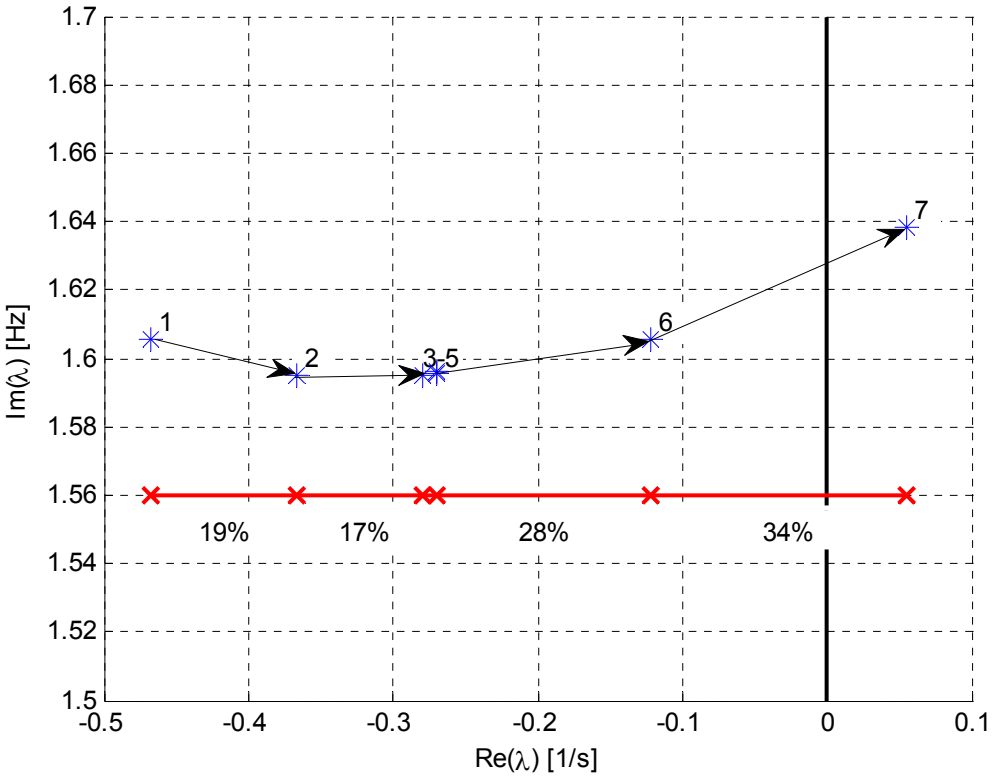

Figure 7-7: The reduction of system damping as various components and characteristics are added one by one (respective eigenvalues marked with a blue asterisk*)

The results show that approximately one-fifth of the change in damping from Case 1 to Case 7 is caused by introduction of the converter motor AVR. One-sixth of the damping is given by the characteristic of the change from constant mechanical torque to constant mechanical power. The change from a constant mechanical power load to a constant electric power load at the converter 15-kV busbar has a small influence and the generator AVR shows a negligible influence. The AVR influence however is not a central concern here.

The influence of the line voltage drop and losses have a significant influence (Case 6), above one-quarter, though a constant power load without dynamics is still not able to make the system unstable at the present operating point. The contribution from the vehicle dynamics, one-third (Case 7), is therefore of special interest since this is the change that makes the system unstable, and which is the topic of concern in this thesis.

The time simulation in Section 7.2 shows an oscillating vehicle DC-link voltage. That proves that the vehicle does not keep its active power consumption constant. The sensitivities in Figure 7-5 also show that system damping may be changed by altering the control system parameters. Hence, the contribution from the vehicle dynamics exerts a significant influence on stability. In Danielsen, et al. [57], the same power system has been linearised at the same operating point, but with another vehicle model (the one studied in Danielsen, et al. [52]). The result is a system that is even more unstable (+ 0.23 [1/s] ± j1.59 [Hz]).

7.4 Stability improvement

Both time simulations and a linear analysis of the rotary converter supplying an advanced electric rail vehicle show an unstable system in the reference case. It is thereby of interest to investigate whether the system can be made more stable.

Previous results in the present chapter show that the vehicle dynamic behaviour has an influence on the system's stability. Improving this behaviour and reduce its influence on the rotary converter mode may be solved in different ways. One method is by altering and tuning the existing control system parameters, while another is to change the vehicle characteristic from behaving like a de-stabilising constant power load to acting neutral or actively damping[15]. For components that are not synchronous machines, such a supplementary controller is often mentioned as a power oscillation damper (POD). Both these methods are investigated in the present section.

Another common method to damp synchronous-machine electromechanical oscillations is to utilise a power system stabiliser (PSS) as an add-on to the machine's AVR. This thesis, however, will focus on measures that can be made on the rail vehicle only.

[15] As opposite to passive damping, e.g. a resistor load

7.4.1 Improved vehicle parameters

The rotary converter mode's sensitivity to change in vehicle parameters was studied in Section 7.3.3.1. Here, the results regarding the vehicle controller parameters are discussed in more detail.

7.4.1.1 Control system parameter sensitivities

For the two modes of interest, the vehicle and the rotary converter mode, respectively, the sensitivities for the controller parameters are calculated and shown in the complex plane in Figure 7-8. The controllers in question are the synchronisation controller (phase-locked loop PLL), the DC-link voltage controller (VC), and the current controller (CC). They all have a proportional gain and an integration time constant. The range for each of these six parameters' variation is from 0.5 to 2.0 times the original value given in parenthesis in the figure legend. The step between the markers on the lines is 10 % of the variation range, i.e., 15 % of its original value, with an arrow indicating a mode change for increasing the parameter's value.

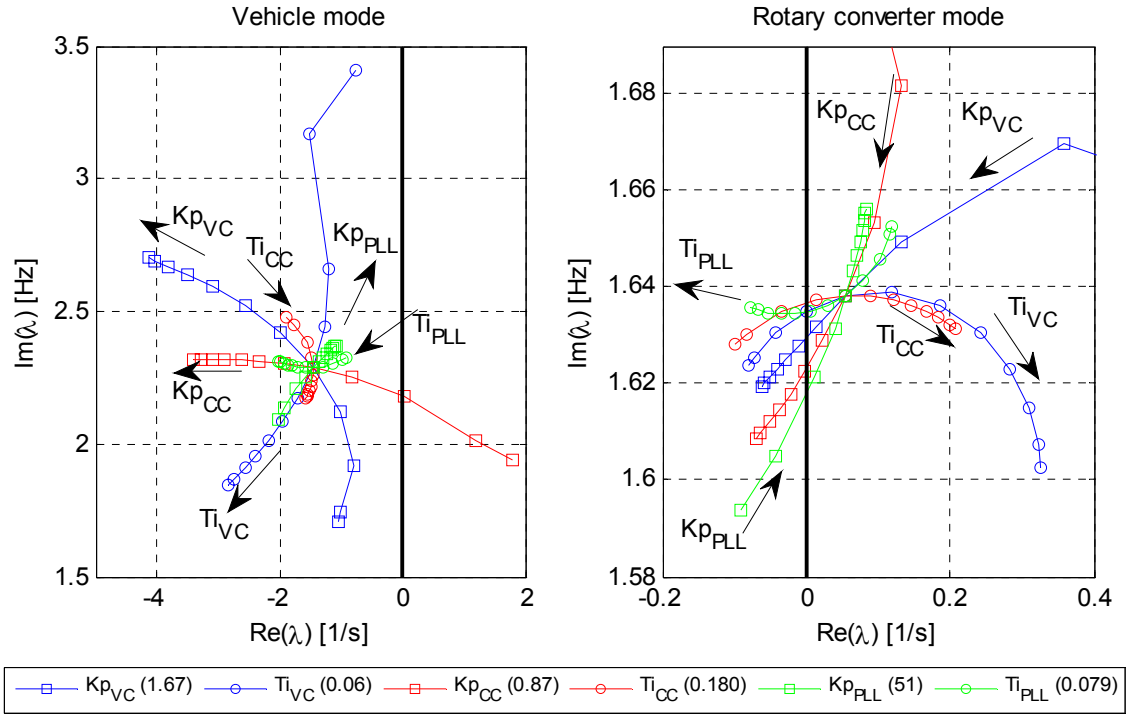

Figure 7-8: Parameter sensitivities for vehicle (left) and rotary converter (right) modes.

The main observation from the diagrams in Figure 7-8 is that the vehicle mode is more sensitive to parameter changes than the rotary converter mode. Note that the scales on the two diagrams' horizontal axes differ by a factor of 10. However, the parameter sensitivity is still sufficient to affect the converter mode damping.

Comparing the vehicle and rotary converter modes' sensitivities reveals that the change needed for each parameter in order to increase the converter damping corresponds to either, or both, increasing the damping or increasing the frequency of the vehicle mode.

This means that the rotary converter mode may be stabilised by moving the vehicle mode away from the complex plane.

7.4.1.2 Parameter change

Based on the parameter sensitivities, a change in the vehicle control system parameters may be proposed:

1. Increase of integration time and decrease of gain of the PLL loop filter. This results in a larger settling time and poorer tracking of the line-voltage phase.
2. Decrease of integration time and increase of gain of the VC. This results in a faster active power control, as both the integral part and the proportional part of the controller are increased.
3. Decrease of integration time and increase of gain of the CC. This results in a faster current control, as both the integral part and the proportional part of the controller are increased.

In the proposed improvement, these six parameters are changed simultaneously by an increase or decrease in steps of 10 %. Five steps are performed in the proposed directions from the original values (0). For comparison, one step (-1) is performed in the opposite direction.

Figure 7-9 shows the root loci plot when the control parameters are successively changed as proposed, and arrows indicates the direction of movement. The zoomed small plot shows that four-five such steps of a 10 % change are needed to increase the damping of the rotary converter mode until it is equal to the no-load case in Section 3.5, thus almost neutralising the negative contribution from the vehicle. The participation of VC and CC in the converter mode is reduced, while PLL participation is slightly increased. A step in the opposite direction (-1) makes the system even more unstable.

It can be observed that the proposed parameter change increases both the damping and the oscillation frequency of the vehicle mode, eigenvalues (21,22), as well as the generator exciter mode (17,18), while the motor exciter mode (19,20) remains unaffected. However, this parameter change results in a reduced damping of the second vehicle mode (13,14) in which, according to Table 7-1, the PLL participates to a greater extent. The same reduction in damping is observed in the 43-Hz mode ((2,3) in Table 6-1) among the DC-link components C_d, C_2, L_2 and R_2 (not included in Figure 7-9). These two modes will now dominate the vehicle dynamical response. In order to keep the vehicle low-frequency modes above a 15 % damping ratio, the parameters in Step 4 are chosen.

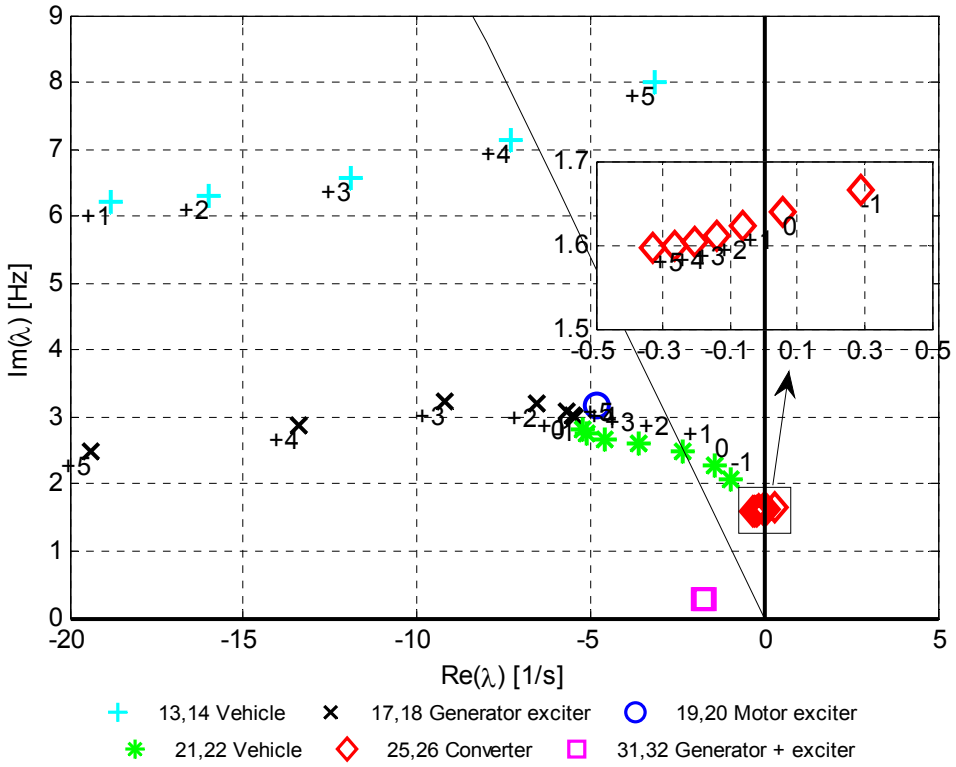

Figure 7-9: Root loci for the changed parameter sets, with the converter mode zoomed in on in the right section of the diagram. 15 % damping ratio is shown as a thin black line.

The system's low-frequency eigenvalues of interest, the rotary converter and the two vehicle modes, are shown in numbers for different steps of improvement in Table 7-2. Besides showing the reference case, the improved parameters for Step 4 are shown. Corresponding eigenvalues for the partial improvement of each of the three controllers in the study are shown as well. It can be observed that the change of PLL parameters contributes most equally to VC and CC together.

Table 7-2: The three low-frequency eigenvalues for the different steps of stability improvement. Units are [1/s] and [Hz].

Case (step no.)	Converter (25,26)	Vehicle (21,22)	Vehicle (13,14)
Original reference case (0)	$+0.06 \pm j1.64$	$-1.45 \pm j2.29$	$-21.0 \pm j6.15$
PLL improvement only (4)	$-0.14 \pm j1.61$	$-2.36 \pm j2.19$	$-14.7 \pm j5.28$
VC improvement only (4)	$-0.08 \pm j1.62$	$-4.66 \pm j4.09$	$-15.8 \pm j5.27$
CC improvement only (4)	$-0.08 \pm j1.62$	$-2.82 \pm j2.39$	$-27.1 \pm j7.91$
VC and CC improvement (4)	$-0.16 \pm j1.61$	$-9.27 \pm j3.91$	$-15.9 \pm j7.62$
Complete improvement (4)	$-0.27 \pm j1.60$	$-5.10 \pm j2.76$	$-7.31 \pm j7.15$

7.4.1.3 Time simulation

The quality of the linear analysis is tested by time simulations. In the absence of an instantaneous value single-phase synchronous-machine model, the simulation is performed by the enhanced RMS model, though an instantaneous value simulation

without a rotary converter has also been carried out (not shown here) in order to ensure that the improved parameters at least work together with an ideal voltage source.

The time simulation of the model where the vehicle is supplied from the rotary converter is performed by means of a step disturbance. A 100-kW resistor load is connected to the rotary converter 15-kV busbar. This load is suddenly disconnected in order to excite the rotary converter's electromechanical eigenmode. The system's operating point after the load rejection corresponds to the reference case.

The response in the converter's rotational speed, generator and vehicle active and reactive power, and vehicle line current and voltage together with its DC-link voltage is shown in Figure 7-10. The responses reflect results from the linear eigenvalue analysis for both the original and improved (Step 4) set of controller parameters. Mode (13,14) at 7 Hz can be observed immediately after the disturbance. The PLL is a large participant in this eigenmode.

With the proposed parameters, the line current and active power control are improved by being faster and more accurate since the active power control loop bandwidth is increased. The movement of the vehicle mode away from the rotary converter eigenfrequency reduces the vehicle dynamics at 1.6 Hz. The vehicle keeps its line voltage, line current and active power almost constant, independent of the poorly damped rotary converter oscillations; hence, the DC-link voltage is constant as well. A constant vehicle active power and a constant current giving constant line losses result in constant generator active power.

The damping of the rotary converter for an improvement in Step 4 is equal to the constant power load at generator bus damping shown in Figure 7-7. The parameter improvement resulting in a constant generator load has cancelled the negative damping given by the line voltage drop and losses, and the vehicle dynamic behaviour.

It is also important to note that the vehicle reactive power oscillation has increased, while the generator reactive power oscillation has decreased in amplitude. The vehicle reactive power oscillation opposite to the line voltage oscillations has been explained in Section 7.2 to have a damping impact. Here this impact is increased.

In Figure 7-5 it was shown a very unstable case involving a 30-km line and a 6-MW load with the original vehicle controller parameters. Applying the improved parameter values (Step 4) on this case shows a damped and still stable system.

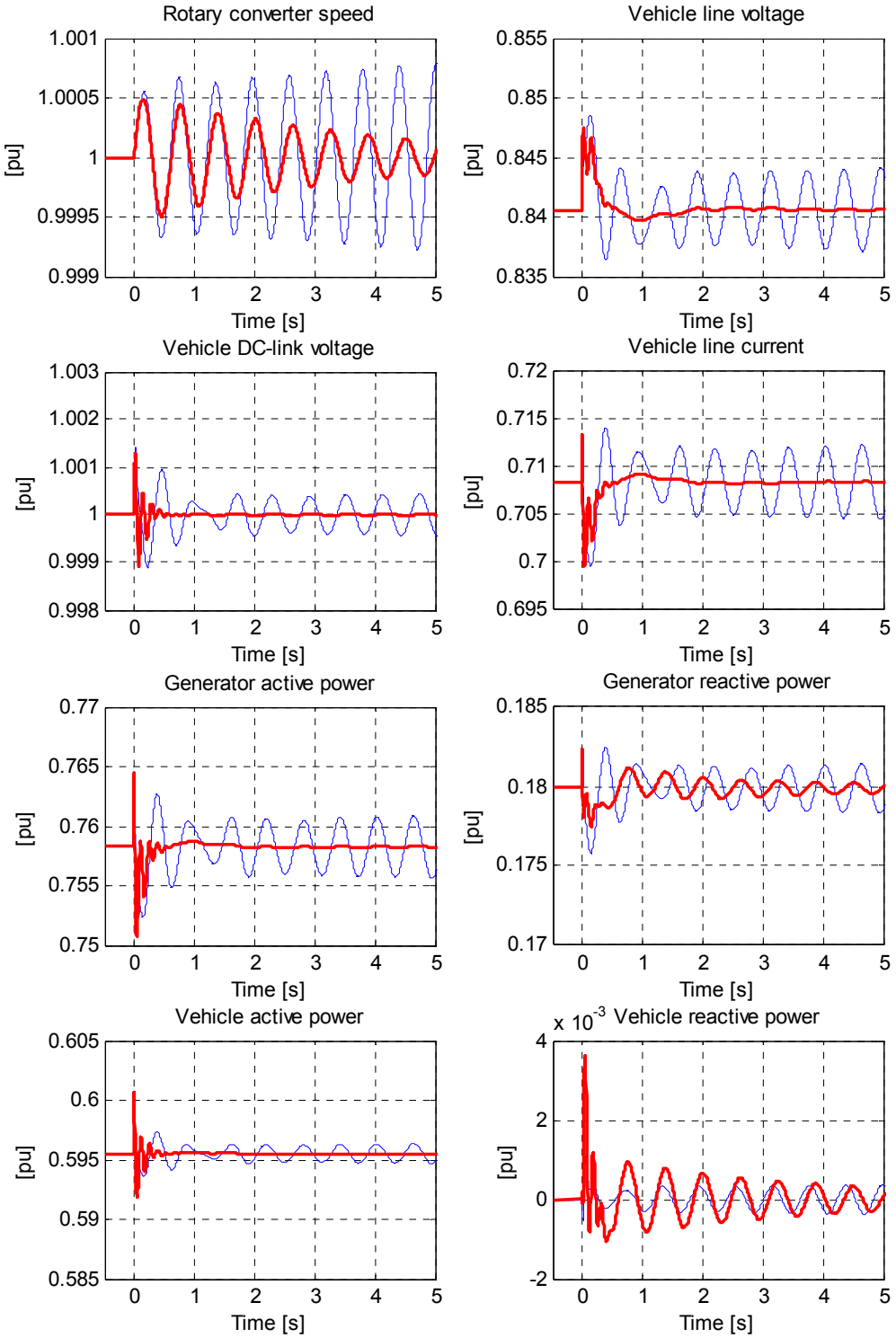

Figure 7-10: System response to a load step with original (thin blue line) and improved (thick red line) parameters.

7.4.1.4 PLL's influence on system damping

From the time simulation in Figure 7-1 it can be observed that the phase angle given by the PLL lags voltage phase it is supposed to track. The change in phase-locked loop parameter values shows in Table 7-2 to have a large influence on the damping of the rotary converter's electromechanical eigenmode. In this section this influence is principally studied.

The PLL's closed-loop transfer function in Equation (7.2), which is based on the block diagram in Figure 5-5, is shown by its frequency response in Figure 7-11 for the parameter values used in Steps 0 and 4, respectively. This parameter change results in a reduced bandwidth of the synchronisation controller. The PLL's eigenfrequency is reduced, which consequently results in a larger amplification and phase lag at the rotary converter's 1.6-Hz eigenfrequency.

$$H_{PLL}(s) = \frac{\Delta\theta_{PLL}(s)}{\Delta\theta_1(s)} = \frac{Ti_{PLL}Kp_{PLL}s + Kp_{PLL}}{Ti_{PLL}s^2 + Ti_{PLL}Kp_{PLL}s + Kp_{PLL}} \tag{7.2}$$

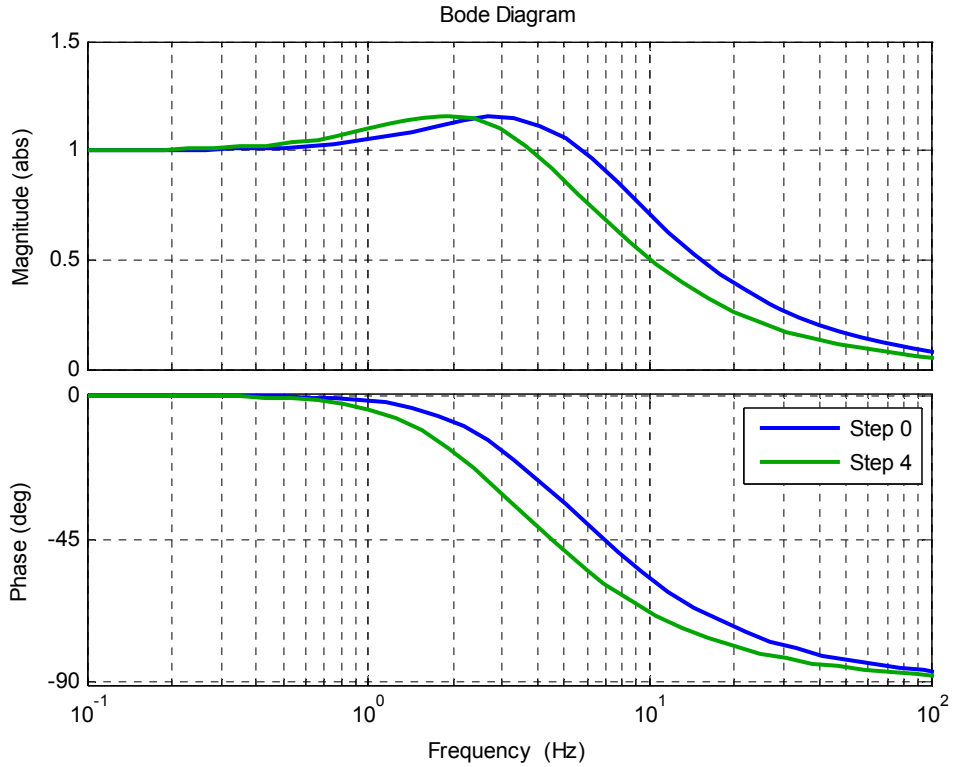

Figure 7-11: Closed loop frequency response for PLL with paramter values for Step 0 and 4.

The impact of this lagging as seen from a stability point of view is investigated by use of the basic power-flow Equations (7.3) and (7.4). They describe the active power P and reactive power Q that flow between two AC power system buses, A and B, measured on bus A. Power may flow due to voltage amplitude U and/or phase δ differences over the line impedance $R + jX$. The system in study is shown in Figure 7-12.

$$P_A = \frac{R\left(U_A^2 - U_A \cdot U_B \cos\left(\delta_A - \delta_B\right)\right) + X \cdot U_A \cdot U_B \sin\left(\delta_A - \delta_B\right)}{R^2 + X^2} \tag{7.3}$$

$$Q_A = \frac{X\left(U_A^2 - U_A \cdot U_B \cos\left(\delta_A - \delta_B\right)\right) - R \cdot U_A \cdot U_B \sin\left(\delta_A - \delta_B\right)}{R^2 + X^2} \tag{7.4}$$

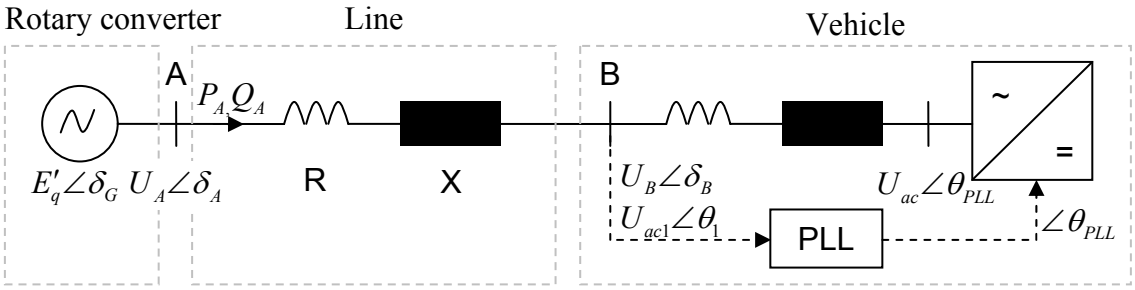

Figure 7-12: Illustration of the system used for the study of the PLL influence on the oscillations.

In most power-flow analysis, it is common to neglect the first term in the active power fraction and the last term in the reactive power fraction, as the line resistance is often assumed to be much less then the line reactance (Machowski, et al. [115]). Consequently, the power flow equations commonly simplify. Such a simplification is however not obvious in this traction power system as the line resistance is in the same range as the line reactance (See Appendix B.1).

Based on Equation (7.3), Equation (7.5) shows how the active power from bus *A* changes when the difference between the phase angle between bus *A* and *B* changes. It consists of two non-linear terms where the first is a sine function of the angle difference while the second is a cosine function. The first term will dominate for large phase differences and the second will dominate for small angles if the two constants K_{P1} and K_{P2} are equal, which they are for $R = X$.

$$\frac{\partial P_A}{\partial\left(\delta_A - \delta_B\right)} = K_{P1} \sin\left(\delta_A - \delta_B\right) + K_{P2} \cos\left(\delta_A - \delta_B\right) \tag{7.5}$$

This relation will now be applied to the interaction between the rotary converter and the rail vehicle. During a rotary converter oscillation, the generator power angle $\Delta\delta_G$ according to Equation (3.5) will oscillate 90 degrees, lagging the rotary converter speed $\Delta\omega$. The vehicle PLL will track the power system's phase oscillation, but due to the loop filter, it will show low-pass behaviour with attenuation and phase shift as seen in Figure 7-11. Hence $\Delta\theta_{PLL}$ will lag the real power system phase $\Delta\theta_1$. The PLL gives the reference phase for the *PWM* actuated voltage u_{ac}, which consequently will lag the real voltage phase oscillation as well. The difference between δ_G and θ_{PLL} now represents the

phase difference discussed in Equations (7.3) and (7.5) and will consequently cause a power flow.

Equation (7.6) shows the relationship between the oscillating angles and the resulting power oscillation and is illustrated in Figure 7-13. For the sake of readability, all variables are shown as deviations from their respective steady-state values, hence the Δ-values. Since only the influence on the power oscillations given by the phase oscillations are of interest, the voltage amplitudes are kept constant and for simplicity equal to 1. Furthermore, even if R is different from X due to the generator impedance and the converter and vehicle transformers it is assumed in this principle figure such that $R = X$ as well. These simplifications do not influence on the basic characteristic, only on the amplitude of the curves.

$$P_A = P_{A1} + P_{A2} = \left(1 - \cos\left(\delta_G - \theta_{PLL}\right)\right) + \sin\left(\delta_G - \theta_{PLL}\right) \tag{7.6}$$

The initial power flow in the reference case is shown in Figure B-1. Based on this the initial angle difference between the δ_G and θ_{PLL} in steady state is the difference between the transient internal induced voltage in the generator and the actuated vehicle voltage (U_{ac}). This steady-state angle difference is used for the non-linear functions.

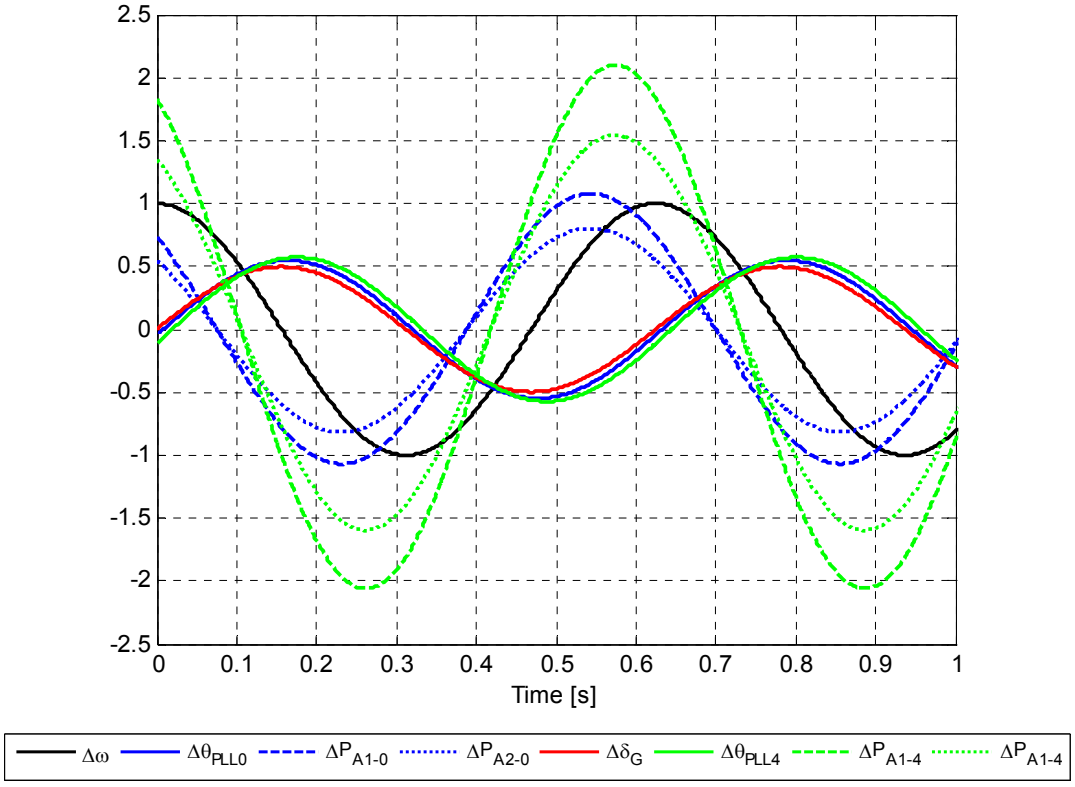

Figure 7-13: Illustration of angles and resulting active power oscillation relative to the converter speed oscillation for PLL parameters in Steps 0 and 4. The values of the angles are multiplied by a factor of 5 and the power oscillations are multiplied by a factor of 100 in order to increase the readability.

The figure shows a 1.6-Hz rotary converter rotor speed oscillation. Two PLLs are tracking the resulting phase oscillation. One PLL has the parameter values from Step 0 and the other has the values from Step 4. The slower PLL in Step 4 increases the phase lag from 6.8 to 13.5 degrees.

The corresponding active power oscillations given the phase difference between $\Delta\delta_G$ and $\Delta\theta_{PLL}$ for the two terms, P_{A1} and P_{A2}, in Equation (7.6) are shown as well. Both of them oscillate essentially in phase with the rotary converter speed and larger phase lag results in active power and speed oscillation being even more in phase. This in-phase power oscillation has according to the stability criterion in Section 3.4.6 a damping impact. Furthermore this positive impact is increased due to the PLL's amplification, which is reflected in the curves as well. The relative contribution from the two terms in Equation (7.6) depends on the initial power system operating point and impedance. When the angle difference is large and R is larger than X, then the first term will dominate.

This active power oscillation relationship is however difficult to explicitly observe in the complete closed loop system simulation, were the resulting voltage angles are a consequence of the power flow that is given by several other factors than the angle and PLL alone. The damping given by the PLL is therefore not easily quantified for the closed-loop system, but the principle consideration in this section indicates the qualitative influence.

Similar considerations as above can be performed for the reactive power oscillations caused by the PLL phase tracking deviation as well, though details remains for further work. The corresponding relationship between the phase difference and the reactive power flow will differ from Equation (7.5) with one important property; the two terms will have opposite signs. This means that it is not obviously given in what phase the net reactive power will oscillate, and it is more sensitive to the network impedance and operating point than the active power. Furthermore it also depend much on where in the system the reactive power is observed, at the rotary converter or at the vehicle, as a majority of the reactive power is due to inductive losses and is not transferred from generator to the vehicle. Introductory studies indicate that the net reactive power at the vehicle will oscillate opposite the active power, i.e., in anti-phase to the rotor speed oscillations and hence amplify the line voltage oscillations. This is, however, not possible to observe from the full system time simulation in Figure 7-10 where the reactive power oscillation in the vehicle in phase with the speed are increased due to the change of VC and CC parameter values as well.

7.4.2 Vehicle active damping

7.4.2.1 Vehicle as a damping device

Active damping of low-frequency oscillations in power systems in order to ensure stability is being increasingly utilised as the development of power electronic components proceeds (Machowski, et al. [115] and Hingorani and Gyugyi [83]). Power oscillation dampers (PODs) may be implemented in series devices such as thyristor-

controlled series capacitors (TSCS) or shunt devices as static VAR compensators (SVC) and static compensators (STATCOM), in order to damp local generator electromechanical oscillations or inter-area power oscillations between different areas of a power system.

Due to its four-quadrant line-side converter, the advanced rail vehicle is a flexible load that might be utilised for power system damping. The reactive power may be controlled independently of the active power consumption. Additionally, the vehicle represents a large amount of energy storage by both the internal DC-link and the moving train mass, which could be used for modulating the vehicle's line-side active power.

7.4.2.2 Controllability

The location to inject a damping signal into the vehicle control system must be in the summation point of a controller where the oscillations can be influenced and controlled. This controller cannot be an inner controller in which the damping impact may be counteracted by an outer controller. By studying the control scheme for the vehicle, e.g. with a basis in Figure 5-1, the following three different active damping schemes are suggested:

1. Modulation of the DC-link voltage in order to store the excess energy in the vehicle's DC-link. The idea is to increase vehicle line power and the corresponding current when the line voltage increases, which was first proposed by Debruyne [60]. The active power consumption of the vehicle is controlled by the DC-link voltage controller, and therefore the DC-link voltage reference u_{dc}^{ref} may be modulated. From the rotary converter point of view, this may be perceived as load modulation, which has been used by Samuelsson [150] to damp electromechanical oscillations in conventional power systems.

2. Modulation of the line-side converter reactive power flow in order to cancel or reduce the line voltage amplitude variations caused by the oscillating rotary converter. This may be achieved by changing the q-axis current reference i_q^{ref} shown in the block diagram for the vehicle current controller in Figure 5-12. When the rotary converter accelerates and the line voltage amplitude increases, the current reference should hence be decreased[16] in order to consume reactive power and decrease the line voltage. An opposite action applies when the converter decelerates. Table 7-3 shows the amount of reactive power needed to keep the vehicle line voltage constant when the rotary converter voltage is increased and decreased by 1 % in the reference case, with only a minor deviation from unity power factor needed. This essentially results in a constant current being consumed by the vehicle, resulting in constant line losses. The

[16] Note that increased reactive power consumption corresponds to a decrease of the q-axis current due to the definition of the rotating reference frame in Section 4.3. The q-axis leads the d-axis, while a reactive inductive current component lags the active component.

vehicle then acts as a reactive compensator at the oscillation frequency at the same time as the vehicle active power is kept constant.

3. Modulation of the vehicle's motor torque in order to store the oscillating energy in the moving masses. The motor-side inverter is commonly used to damp DC-link oscillations by use of Equation (5.3), and the motor side may be used to damp low-frequency line-voltage oscillations by modulating the power reference P_{ref} or the torque equivalent. It is expected that an efficient line-side damping by use of a motor-power modulation requires motor current feed forward as studied in Section 6.3.2. Otherwise, the motor side will be too hidden behind the line converter and DC-link. A disadvantage of this method may be that the mechanical side of the vehicle, the electrical motor side and line side become more closely connected, and power system oscillations may have an influence on longitudinal mechanical eigenmodes in the train that are observed in the 0.5-2.0 Hz range (Ehrler [62]).

Methods 1 and 2 above will be further studied in this section. Method 3, motor power or torque modulation, will require inclusion of the motor side in the vehicle model used in this thesis, and is not investigated further here.

Table 7-3: A comparison of vehicle line voltage, line current and reactive power when rotary converter voltage is changed by 1 % both with and without reactive compensation in the reference case.

Voltage at rotary converter 15 kV-busbar [kV]	**Vehicle line voltage [kV]**	**Vehicle line current [A]**	**Vehicle reactive power [MVAr]**	**Vehicle power factor**	**Line losses [MW]**
16.665 (+1 %)	13.091	280.4	0.0000	1.0000	0.8961
16.665 (+1 %)	12.865	285.7	+0.1979	0.9986 ind	0.9305
16.500 (ref)	12.845	285.7	0.0000	1.0000	0.9305
16.335 (–1 %)	12.874	285.7	–0.2438	0.9978 cap	0.9305
16.335 (–1 %)	12.594	291.4	0.0000	1.0000	0.9678

7.4.2.3 Observability

As input to the POD, a signal must be chosen in which the oscillations are observable. The vehicle acts as a current source and bases its control on, among other disturbances, the line voltage. The line voltage consists of amplitude achieved from the measurements by means of the SOGI and its phase or frequency that can be achieved from the PLL. Essentially, the voltage amplitude oscillates in phase with the converter speed, while the phase is 90 degrees lagging. It is simplest and most intuitive to base the damping signal on the measured line voltage amplitude.

7.4.2.4 Design of active damper (POD)

The intention of the active damping is to make the vehicle compliant with the stability criterion presented in Equation (3.27). This means that when the rotary converter accelerates, the vehicle should increase its line power or current demand, with the

opposite when the rotary converter decelerates. The POD must hence consist of a band-pass filter allowing the observed 1.6-Hz amplitude oscillations in the line voltage u_{ac1} to pass through. The block diagram of a general POD is shown in Figure 7-14. The summation point corresponds to the comparison between reference input x^{ref} and the measured system output x in for the DC-link controller Figure 5-9 and the q-axis current controller in Figure 5-12. The structure corresponds to a traditional PSS structure (Kundur [106]) and a proposed POD structure for a TCSC (Lin, et al. [110]), as well as for a STATCOM (Abido [5]).

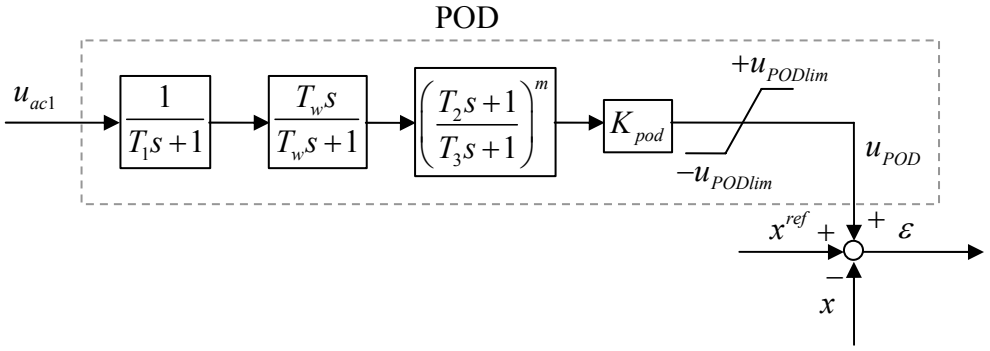

Figure 7-14: The general control structure for a power oscillation damper.

The first block in the figure represents the filtering of the line voltage u_{ac1} due to measurements, and corresponds to the SOGI low-pass filter in Equation (5.11). The second block is a wash-out filter to remove the steady-state voltage changes, so the steady-state output from the POD is zero. The third block represents the number of m lead-lag or lag-lead compensators in order to shift the input signal into an appropriate phase for the output signal. Finally, the amplification of the POD's output signal u_{POD} can be controlled by a pure gain, K_{POD}. This output is kept between the maximum and minimum limit ($\pm u_{PODlim}$) before being injected into the respective controller's summation point.

Three different power oscillation dampers are proposed and compared in the following:

- *POD1a* aims to damp the rotary converter's electromechanical mode, especially, by vehicle DC-link voltage modulation. The pass-band filter created by the measurement block and the wash-out block is chosen to be symmetrical around the rotary converter eigenfrequency which results in zero phase of the filter at 1.6 Hz. The output signal should, however, ensure that the vehicle active power oscillates in phase with the line voltage. A closer inspection of Figure 7-1 reveals that the DC-link voltage oscillation lags the vehicle line power by 50-60 degrees. Hence, the lag compensator has to add a lag of approximately 55 degrees that may be obtained by a single first-order filter. This method, in choosing the compensation signal phase, is based on the design of dampers, e.g. as by Lin, et al. [110] and Aboul-Ela, et al. [6]. The lead term in the compensator numerator may be omitted.

- *POD1b* aims to influence the range of low-frequency oscillations which are experienced as shown in Table 2-2, i.e., 10-30 % of the fundamental frequency, by DC-link voltage modulation. The pass band created by the wash-out filter is given its corner frequency equal to $0.1 \cdot f_s$ and the measurement filter together with an additional low-pass filter are given a resulting corner frequency equal to $0.3 \cdot f_s$. The lead term in the compensator numerator may be omitted.

- *POD2* aims to reduce the line voltage oscillations at the rotary converter eigenfrequency by means of reactive power modulation. The pass-band filter created by the measurement block and the wash-out block are chosen to be symmetrical around the rotary converter eigenfrequency. This results in a zero phase of the filter at 1.6 Hz, and no extra lead and lag block is used.

For a vehicle with a rating in the same range as the rotary converter, a given speed increase of the converter should result in an equal increase of the DC-link voltage in order to store the same amount of energy. A 1 % increase in the line voltage should result in an approximately 1 % increase in DC-link voltage in order to ensure that the line current is not changed in the opposite direction. For this reason, K_{POD} should be in the range of one in order to result in a neutral behaviour. However, a non-unity converter speed to terminal voltage relation ($k_u \neq 1$), the line voltage drop and losses, and the filter and lag compensator attenuation may be an influence on this. As a result, the gain may be subject to tuning.

The POD1 (*a* and *b*) output signal limiter should ensure that the resulting DC-link voltage reference ($U_{dc}^{ref} + U_{POD}$) is not too high. There is a limit of how high voltage the vehicle inverter semiconductors can withstand. Additionally, the POD1 should not interfere with non-oscillatory line voltage changes such as caused for example by load steps. This applies to both step up and step down. Small-signal damping of oscillations do not require wide limits. Still, it will be a trade-off against how much damping the vehicle should contribute with if large oscillations occur.

For POD2, the unity gain equal to POD1 is kept. Moreover, the limit is kept without further consideration in this thesis.

Table 7-4 shows the proposed parameters for the three power oscillation dampers. Figure 7-15 shows the resulting POD frequency responses, i.e., their transfer functions from u_{ac1} to u_{POD}. The output signal from POD1a is lagging as designed, while the signal from POD1b is leading. The phase of the output signal for POD2 is zero which gives the three completely different filter characteristics, and the filters' attenuation at 1.6 Hz also differs.

Table 7-4: Parameters for POD1a, POD1b and POD2.

Parameter	Unit	POD1a	POD1b	POD2
T_1	[s]	0.02	0.02	0.02
T_w	[s]	0.47	0.10	0.47
T_2	[s]	0.00	0.00	0.00
T_3 (=T_{POD})	[s]	0.14	0.02	0.00
K_{POD}	[pu]	1.00	1.00	1.00
u_{PODlim}	[pu]	0.01	0.01	0.01

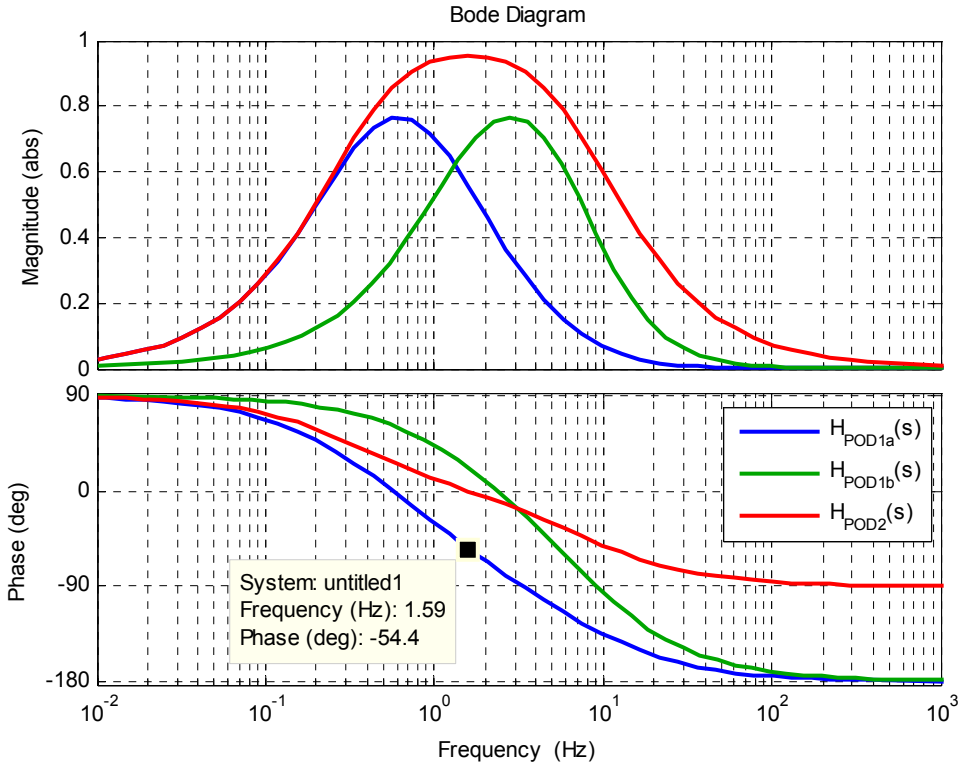

Figure 7-15: A Bode plot of POD transfer functions.

For practical implementational reasons, the POD transfer function may be simplified into Equation (7.7) (Eisele [63]) if the lead-lag blocks are not needed:

$$u_{POD}(s) = K_{POD}\left(1 - \frac{U_{ac1\_measured}(s)}{T_W s + 1}\right) \tag{7.7}$$

7.4.2.5 Linear analysis

The system's low-frequency eigenvalues when the power oscillation dampers are active are shown together with the reference case eigenvalues in Figure 7-16.

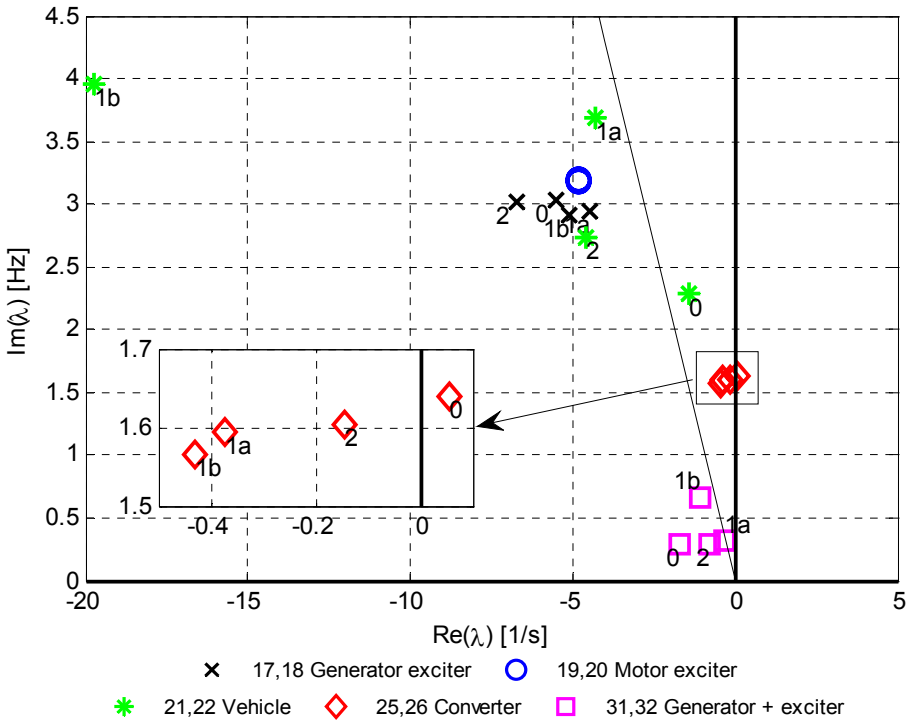

Figure 7-16: System low-frequency root loci when PODs are applied, with rotary converter mode zoomed in. The marker '0' reflects the reference case without POD. The other markers are annotated by the POD number, and the 15% damping ratio is indicated as a thin black line.

All three PODs increase the rotary converter mode damping and are able to stabilise the system. Thus, the negative damping impact that the vehicle has on the mode is reduced. A further increase of the POD gain, K_{POD}, increases the mode damping, but only to a limited extent. Despite higher filter gain, POD2 is less effective than POD1. Its potential for a further increase of the gain is also limited. A possible reason for this is that the reactive power modulation aims to cancel the line voltage oscillation, reducing the mode's observability. Any generator active power modulation is a bi-effect. This is in contrast to an active power modulation which aims to modulate the vehicle and generator active power in phase with the speed variation. A reduction of the line voltage oscillation is then a bi-effect.

In all cases, the vehicle mode is better damped when POD is introduced. This is especially visible for POD1b which was designed for also covering the vehicle mode.

It may however be observed that the vehicle interferes with other low-frequency modes within the system. This particularly concerns the eigenvalue that describes the dynamics

of the generator field and damper winding, together with the exciter regulator, no. (31,32) at 0.3-0.6 Hz. After introduction of the PODs, this mode is significantly more poorly damped and will dominate the dynamical response. An increase of K_{POD} decreases the damping of this mode even more. Analysing the participation factors for this mode reveals that the POD's filter transfer functions create a dynamic connection to the DC-link damping given by the motor power reference manipulation in Equation (5.3), since they have all time constants in the same range. A decrease of Tf_{CPL} increases the damping of mode no. (31,32). A decrease of Tf_{CPL} also increases damping of the rotary converter mode and decreases damping of the vehicle mode without POD in use (see Figure 7-5 and Figure 6-7, respectively).

A study (not shown here) of operating point sensitivity still indicates a stable system in the very unstable original case of a 30 km line and 6 MW load in Figure 7-5. However, the PODs are not able to compensate for all the negative damping impact the vehicle has on the system compared with rotary converter no-load damping.

7.4.2.6 Time simulations

Time simulations are performed for all of the three proposed PODs, with the results presented in Figure 7-17, Figure 7-18 and Figure 7-19, respectively. The same load rejection step disturbance as described in Section 7.4.1.3 is used, and the reference case without PODs is shown as a reference. In the absence of an instantaneous value model of the rotary converter, the simulations are performed with the enhanced RMS model.

There are two essential observations. First, the damping impact observed in the linear analysis is confirmed since all three PODs damp the rotary converter electromechanical oscillation. Second, there is now another frequency that dominates the response, a 0.3-0.6-Hz component. This was also foreseen by the linear analysis. Unfortunately, the presence of this mode makes detailed investigations of the 1.6 Hz behaviour difficult.

For POD1a, it is observed[17] in Figure 7-17 that the DC-link voltage no longer oscillates in an opposite manner to the rotary converter speed. When the rotary converter accelerates, the line voltage increases, although the vehicle line current shows no 1.6-Hz oscillation and the vehicle acts neutral as designed. An oscillating line voltage and a constant current result in both an active and reactive power oscillation that is in phase with the speed oscillation. This has a damping impact on the rotary converter electromechanical mode, as the behaviour is in compliance with the stability requirement in Equation (3.27).

Similar observations are made from the plot of the simulation with POD1b in Figure 7-18. The DC-link voltage is modulated at 1.6 Hz. In contrast to POD1a, the vehicle current now also contains a 1.6 Hz component. This component is in phase with the line voltage oscillation and increases the damping even more.

[17] Tip: Compare the curves at for example time = 2 s where speed is at maximum value.

POD2 shows a different behaviour. As it is the reactive power that is modulated, the DC-link voltage is allowed to still oscillate opposite to the rotary converter speed. This gives an active power oscillation in anti-phase to the speed oscillation and the stability requirement in Equation (3.27) is still violated. However, an increased vehicle reactive power oscillation in phase with the line voltage and rotary converter speed indeed improves the situation compared with the unstable reference case.

The limiter is, in these cases, not active at all due to the small disturbance.

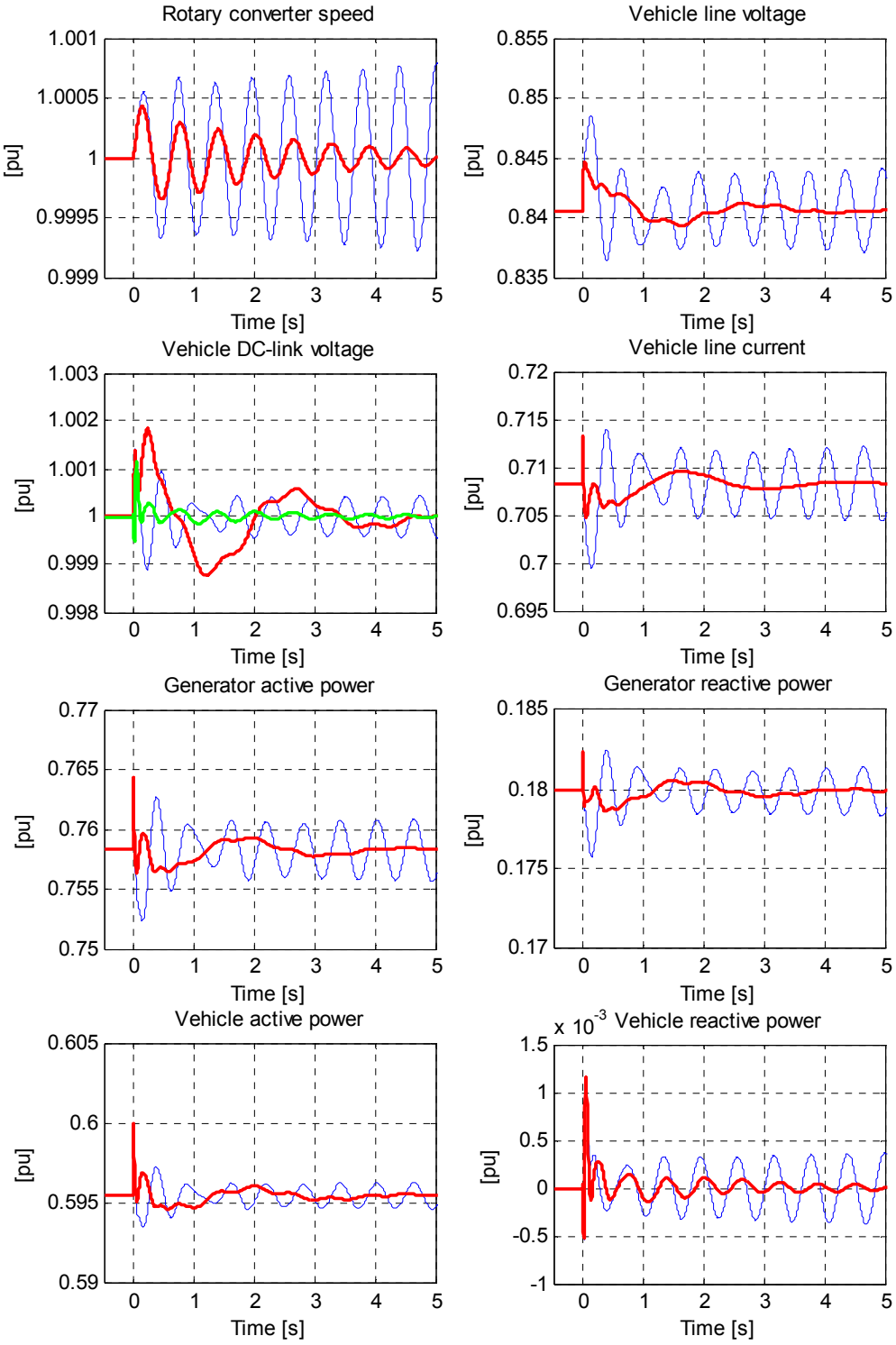

Figure 7-17: Simulated responses when POD1a is used. The unstable reference case (thin blue) is shown for comparison. The POD output signal (thick green) is shown as u_{POD}+1, together with the vehicle DC-link voltage.

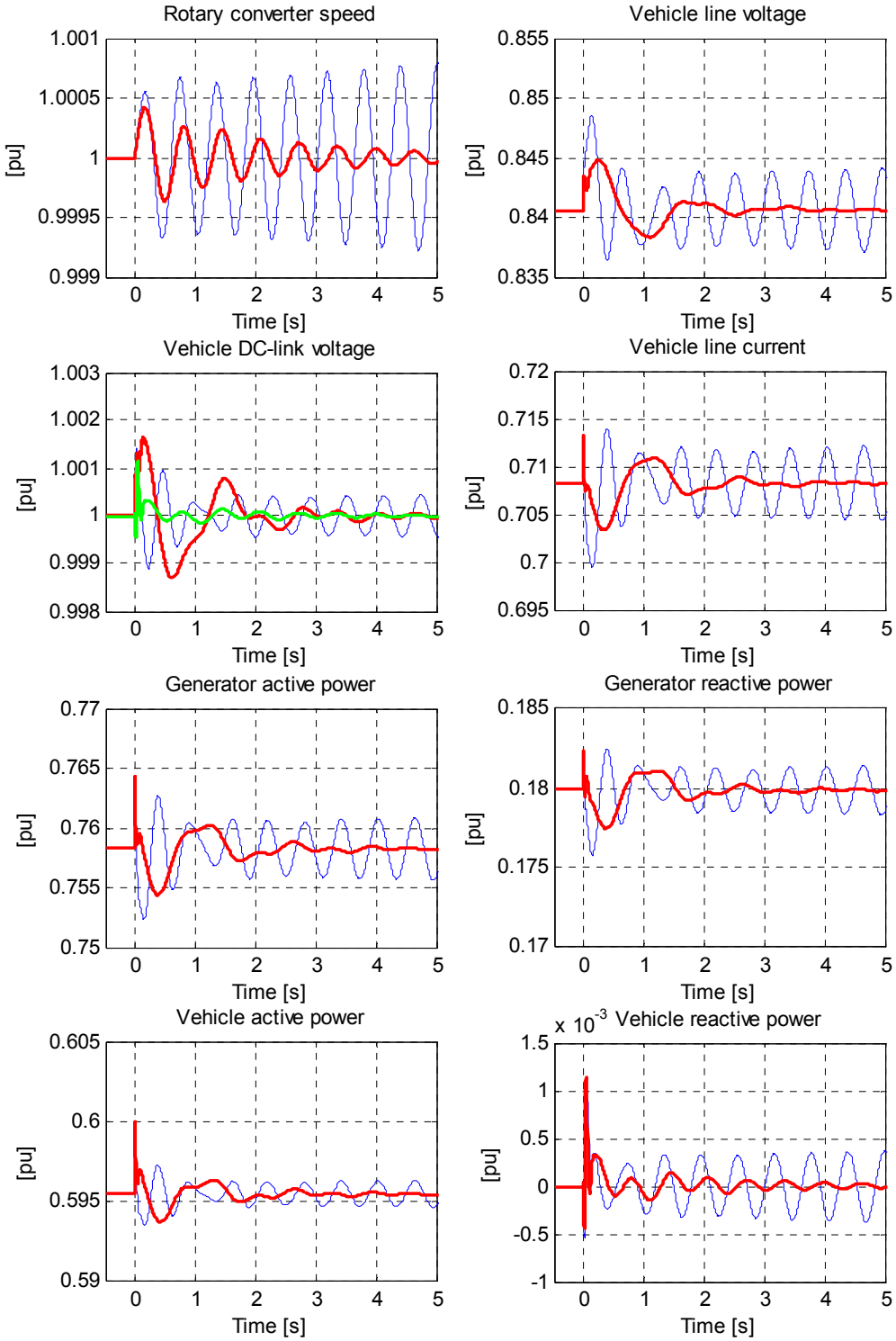

Figure 7-18: Simulated responses when POD1b is used. The unstable reference case (thin blue) is shown for comparison. The POD output signal (thick green) is shown as u_{POD}+1, together with the vehicle DC-link voltage.

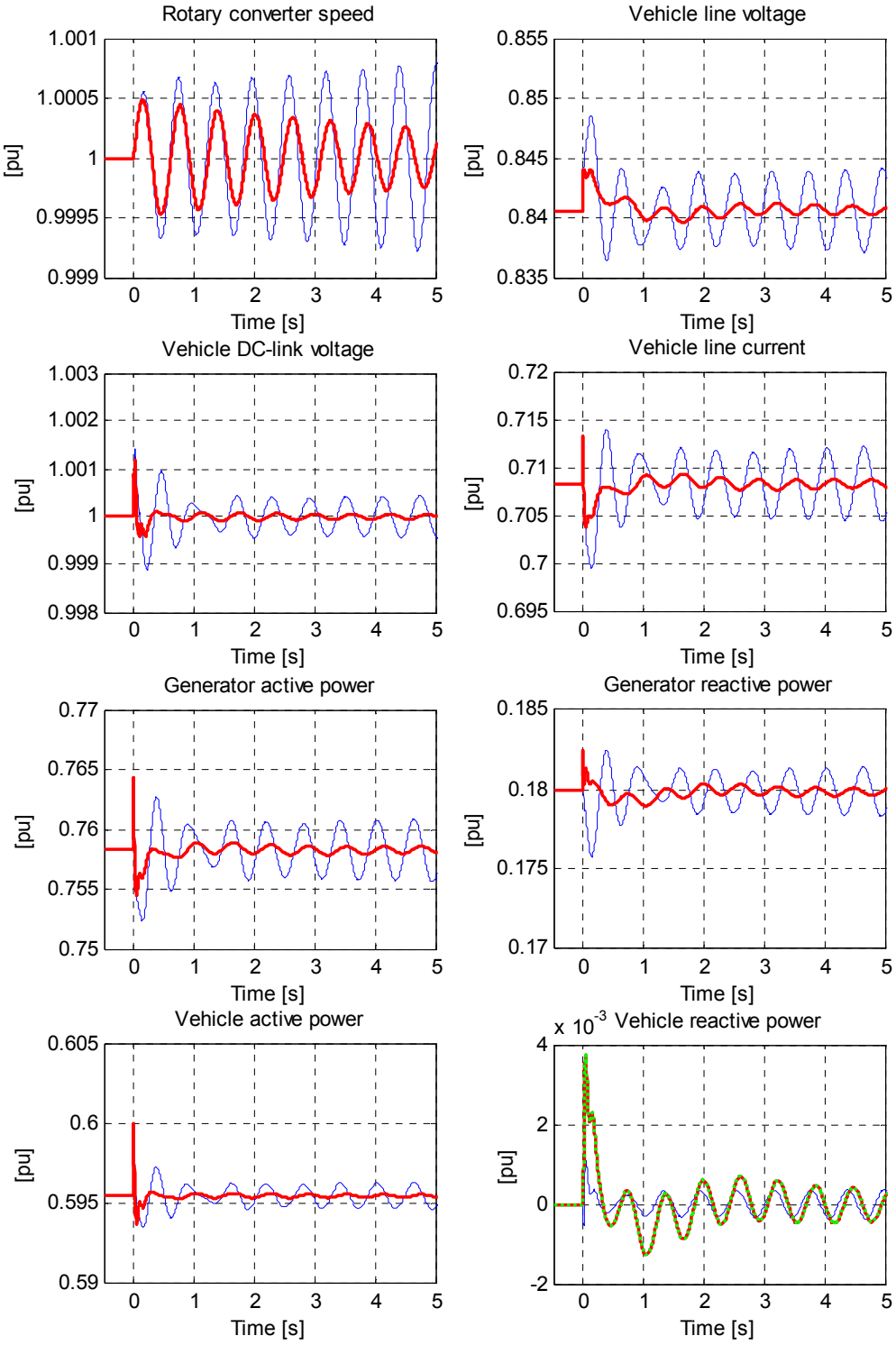

Figure 7-19: Simulated responses when POD2 is used (thick red). The unstable reference case (thin blue) is shown for comparison. The POD output signal (u_{POD}) (thick green) is shown together with the vehicle reactive power.

7.5 Measurements on a real-life vehicle

Measurements have been performed on the same real vehicle as described in Section 6.5. All measurements are performed when the vehicle is fed from one rotary converter only, as in the reference case for the simulations in present thesis. The rotary converter used and its AVRs are of the same type as in the simulations. Their three-phase network differs, however slightly, as it has a voltage level of 22 kV and not 66 kV. Overhead contact line impedance is previously measured to be $0.183 + j0.211$ Ω/km (referred to 20° C). Furthermore, the distance from the train to the rotary converter is significantly shorter than 60 km, as the train starts at 10 km and runs to 20 km.

In the measurements shown here, there is no intervention by the implemented line power/current limitation or the reactive power compensation. The vehicle is controlled to provide a unity power factor at the current collector.

7.5.1 Unstable system

The test vehicle is driven away from the converter station, resulting in increased line length. At a specific distance, the stability limit for the given power demand from the vehicle is reached. Excited low-frequency oscillations are not damped, but increase in amplitude as time passes, with one such situation shown in Figure 7-20.

This figure intends to imitate the simulated response of the unstable reference case in Figure 7-1 by means of combining measurements in the converter station with measurements on the vehicle, though rotary converter speed and voltage phases were not measured. The vehicle control system measurements are not included, except for the logging of the DC-link voltage.

The vehicle is running at 75 km/h and consumes 6.5 MW. The short distance to the converter station results in a vehicle line voltage of 15.5 kV.

Figure 7-20 reveals an essentially similar pattern as that shown in Figure 7-1. The rotary converter oscillations are visible in the line voltage, both at the generator and at the vehicle. The principal observation here is that the line voltage and line current oscillate opposite each other. The vehicle line active and reactive powers oscillate essentially in phase with the line current. This is interpreted as the vehicle attempting to keep the active power equal to its slightly increasing reference despite the line voltage amplitude oscillation, though it fails. How the DC-link voltage oscillates relative to the other variables is difficult to state.

By application of Equation (C.3) on the reactive power oscillation curve, an apparent eigenvalue of $+0.24$ [1/s] $\pm j1.81$ [Hz], as an average over ten oscillation periods, is calculated.

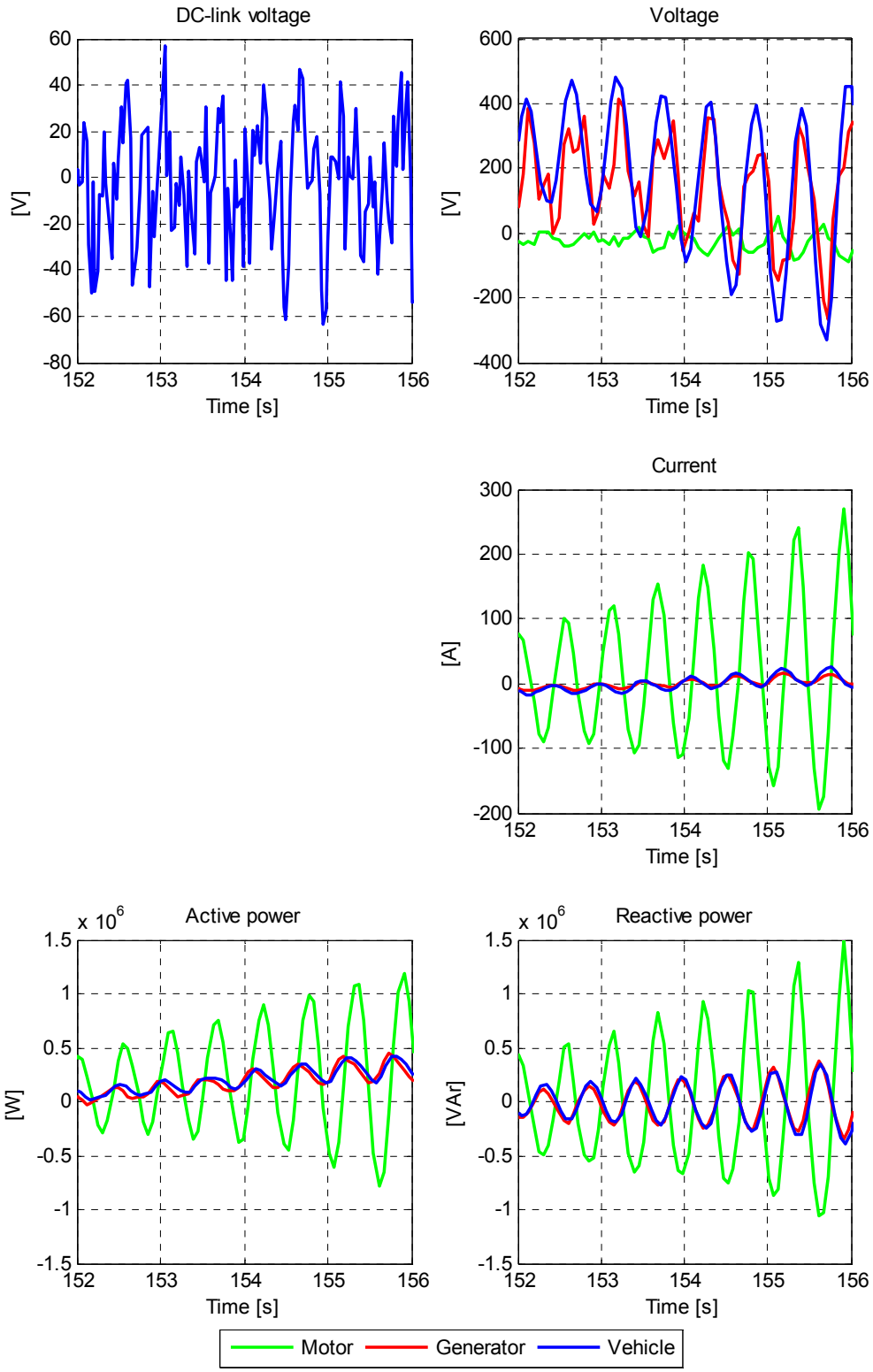

Figure 7-20: The measurement results from an unstable power system, with rotary converter and rail vehicle (ID004).

Still, there is one difference between the simulated and measured oscillation. For the simulation model, the reactive power oscillates in phase with the line voltage, as the measurement shows voltage and reactive power almost in anti-phase. This has an unfortunate impact as inductive behaviour when the voltage is low, and capacitive behaviour when the voltage is high amplifies the line voltage oscillations. This difference compared with the vehicle simulation model is further discussed in Section 7.7.1.

When creating and interpreting the figure there are several elements of uncertainty. First, there are three different measurement sets to synchronise (rotary converter measurements, vehicle measurements and vehicle control system registration). Second, it is difficult to find a real steady state. Third, it is believed that the measurement chain in the converter station has reduced accuracy. It should also be mentioned that the DC-link voltage registration sampling is below the Nyquist frequency, and consequently there is aliasing with the harmonics.

7.5.2 Stability improvement – Test of POD

A power oscillation damper is tested on the rail vehicle in order to investigate its influence on the system stability. Differences between the simulation model and the real vehicle apply since the real vehicle control system operates with parameters in physical units and not per-unit as the simulation model does. The damper algorithm's band-pass filter is designed according to Equation (7.7) with a bandwidth of 1 Hz. There is also a slightly different implementation of the measurement filters as the real vehicle does not utilise the SOGI, but instead uses a sliding RMS-calculation (Eisele [63]).

The tests are performed as a step disturbance in the line voltage when the test vehicle is consuming 150 A. The disturbance is created by a second locomotive (in the same test train) consuming 50 A. This extra load is suddenly removed by opening the second locomotive's main circuit breaker, consequently resulting in a line voltage jump.

As a reference, a similar load rejection is performed without the test vehicle in operation at all. Such a step to no-load is also studied and described in Section 3.5.6. This shows the system's original damping which the test-vehicle behaviour has to be compared with.

The test train is running along the line away from the rotary converter, i.e., the line length is increasing. First, a step test is performed without active power oscillation damp, i.e., the same configuration as in Section 7.5.1. Second, a test is performed with the originally proposed POD gain (K_{POD}), and finally, this gain was doubled.

Measured step responses in vehicle line voltage and current are compared for the four different tests in Figure 7-21. For the unstable configuration, the oscillations are essentially sustained. It is easy to observe that the vehicle current oscillates opposite to the line voltage. Application of the POD results in damping of the oscillations. The originally proposed damper gain results in a line current without oscillations, while the double gain results in a current oscillating in phase with the line voltage.

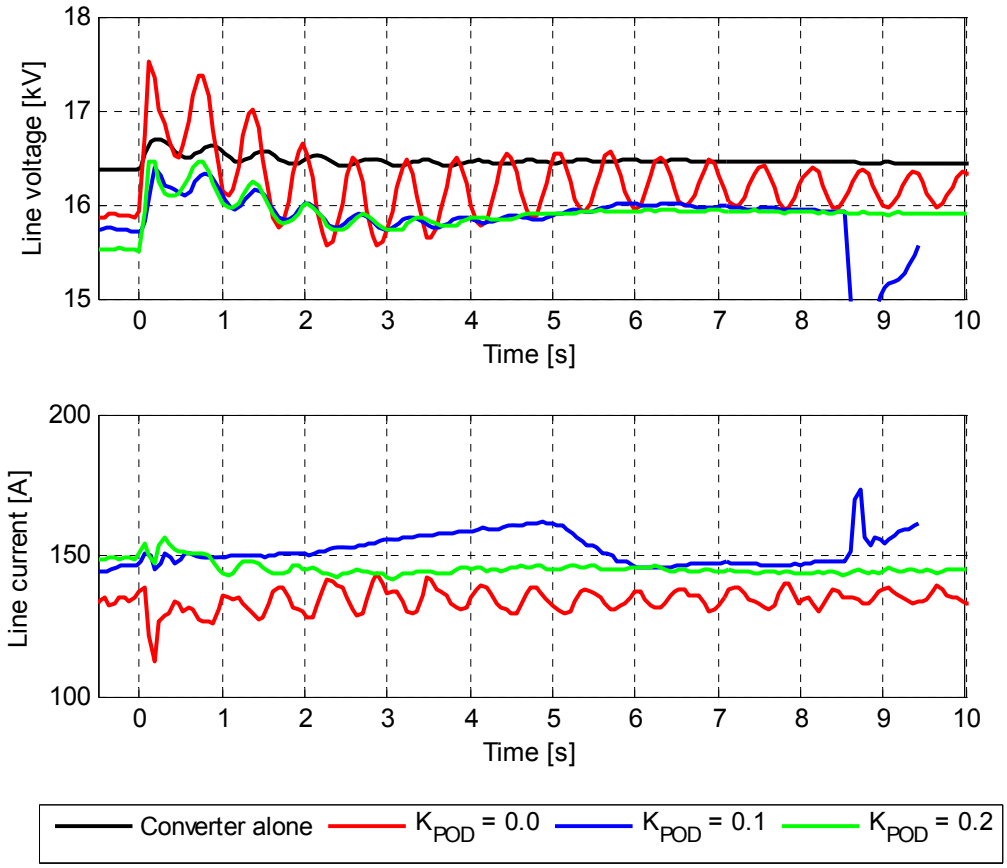

Figure 7-21: Step responses in vehicle line voltage and current (measurement IDs 002, 004, 006 and 007, respectively).

Directly after the step disturbance, an oscillation in the line current of approximately 4 Hz may be observed in all three of the loaded cases, which corresponds to the vehicle DC-link mode as measured in Section 6.5.

The step responses in the line voltage are analysed by use of a Prony Toolbox (Singh [157]) in Matlab software (Singh [158]) in order to calculate the apparent oscillating mode, and the results are shown for the rotary converter resonance in Table 7-5. The model order for the Prony analysis is a trade-off between accuracy for the mode of interest and the noise and non-linearities' influence.

Table 7-5: Results from a Prony analysis of step responses.

Case	**Electromechanical mode [1/s], [Hz]**	**Order**	**Classification**
Converter alone	$-0.37 \pm j1.6$	4	System original
$K_{POD} = 0.0$	$-0.08 \pm j1.6$	10	De-stabilising
$K_{POD} = 0.1$	$-0.34 \pm j1.6$	10	Neutral
$K_{POD} = 0.2$	$-0.46 \pm j1.5$	14	Damping

With reference to the rotary converter test which gives the system's original damping, the three different configurations of the test with the vehicle as load may be classified. Damping equal to the original damping is attained by a vehicle being neutral. Poorer damping is caused by a de-stabilising or negatively damping vehicle, while increased damping is a result of an actively damping vehicle. The situation with $K_{POD} = 0$ is considered practically unstable, despite the fact that the real part of the apparent eigenvalue is negative.

The line voltage measurements also show a damped oscillation at very low frequency, approximately 0.1-0.2 Hz. This mode has not been possible to identify by Prony analysis, and it is believed that this mode corresponds to the generator and exciter mode at 0.3-0.6 Hz in the simulation model. It is here, however, far from the poor damping shown in the simulation model.

7.6 Comparison with traditional power system modelling

The simulation studies and linear analysis performed in this chapter utilise the enhanced RMS modelling concept introduced in Chapter 4. This implies taking the fast current dynamics into account and includes the modelling of the vehicle current controller. According to the study of the vehicle model in Chapter 5, these dynamics demonstrate an influence on low-frequency stability, and should be included in stability studies. Traditionally, power system modelling for the study of low-frequency dynamics often disregards these dynamics.

In Table 7-6, the low-frequency eigenvalues of interest in the reference case are compared for enhanced RMS with the vehicle current control (CC) loop to standard RMS without the current control loop. Note that the DC-link voltage regulator (VC) and phase-locked loop (PLL) are still in use. In addition, the load rejection disturbance test performed in Sections 7.4.1.3 and 7.4.2.6 is repeated here for comparison between the various RMS models, with the results shown in Figure 7-22.

Table 7-6: A comparison of low-frequency modes for different methods of modelling in the reference case. The units are [1/s] and [Hz].

Model	**Converter mode (25,26)**	**Vehicle mode (21,22)**	**Vehicle mode (17,18)**
Enhanced RMS with CC	$+ 0.06 \pm j1.64$	$- 1.45 \pm j2.29$	$- 21.0 \pm j6.15$
Standard RMS without CC	$- 0.27 \pm j1.59$	$- 5.57 \pm j1.94$	$- 46.0 \pm j5.37$

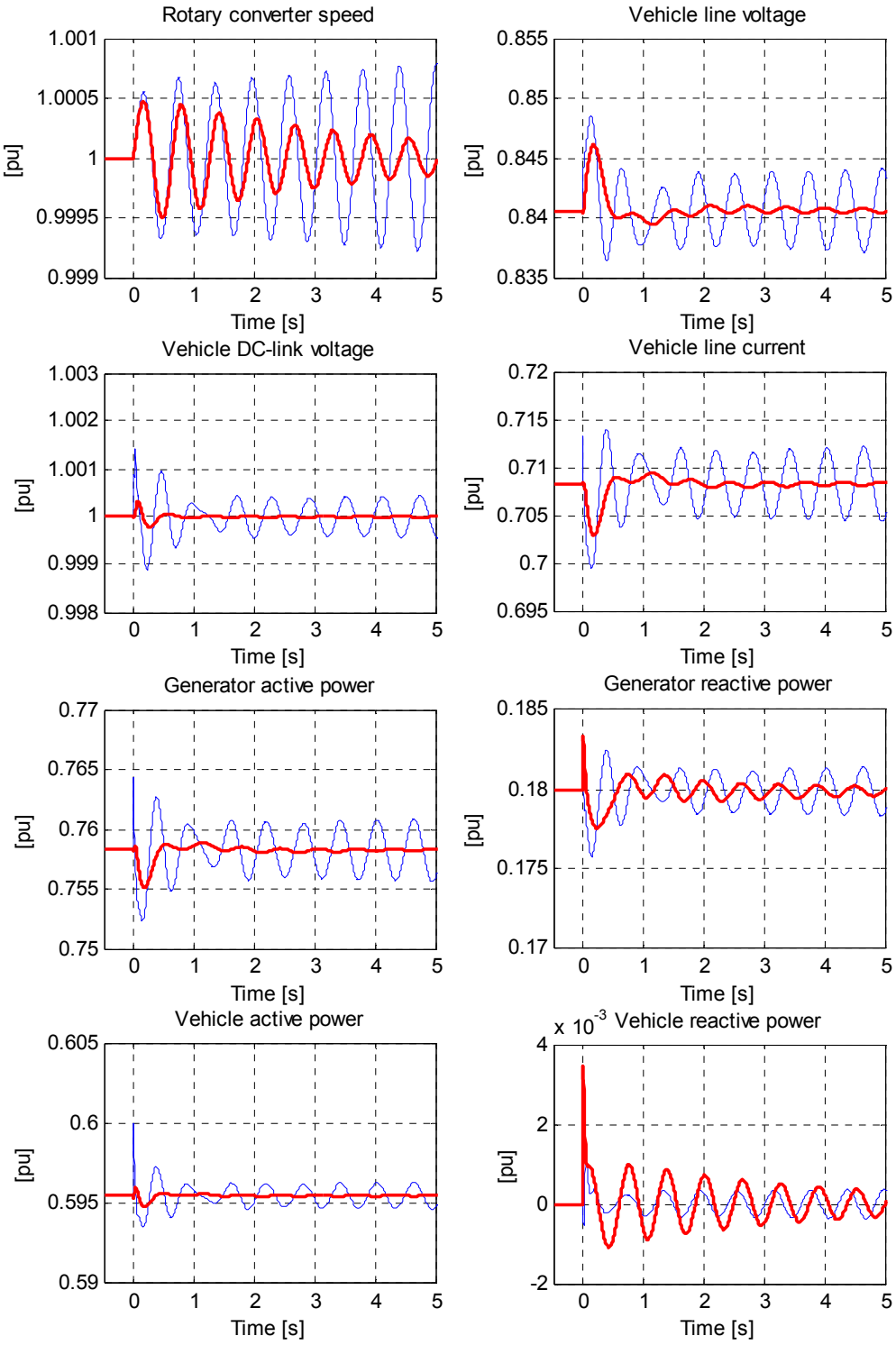

Figure 7-22: Simulated responses when traditional power system modelling (standard RMS without CC) is used (thick red). The unstable reference case using enhanced RMS with CC (thin blue) is shown for comparison.

Both eigenvalue analysis and time simulation show that the rotary converter electromechanical mode is better damped in standard RMS mode than in the enhanced RMS mode. The damping in standard RMS mode is reduced compared with the converter no-load damping, although better than in Case 6 with the non-dynamic constant power load in Section 7.3.4, which at first glance may be surprising. A reason for this is proposed in the following.

The DC-link voltage controller keeps the DC-link voltage essentially constant after the first dip given by the disturbance. This results in corresponding constant active power consumption. The constant power load behaviour emerges as the vehicle current oscillates opposite the line voltage. The improved damping compared with a pure constant power load is explained by the reactive power oscillation which is in phase with the line voltage and converter speed. Its amplitude is higher than in the reference case with the enhanced RMS model. When the current controller is neglected, there is no closed reactive current control loop. The active current is controlled by the outer DC-link voltage control loop.

The phase of the resulting current is given by the phase provided by the PLL, whose dynamics give a phase error during the oscillation as described in Section 7.4.1.4. The phase error when the rotary converter accelerates results in a line current lagging the line voltage and hence inductive power factor. Because of this, reactive power consumption reduces the line voltage increase which has a damping impact. Similarly, when the rotary converter decelerates, the line current will lead the line voltage.

This is a different impact from the PLL on the power flow compared with what was found when the closed current control loop was modelled. Therefore, the type of modelling has significant influence on the results.

It can also be observed that standard RMS modelling increases the damping of the vehicle modes when compared with the enhanced RMS model, with their oscillation frequencies showing a slight decrease.

7.7 Discussion and conclusion

7.7.1 Discussion

7.7.1.1 Model proximity to real-life system

When studying the vehicle-rotary converter interaction, it is important to remember that the diagrams shown and the numbers listed relate to the specific rail vehicle model developed in this thesis. Other vehicles having different control system structures and parameters may behave differently, which has been noted for example when comparing the simulation model to the measurements of the real rail vehicle.

It has also been observed that the power system behaves slightly differently. The 0.1-0.2 Hz oscillation that is observed for the voltage jump tests in Section 7.5.2 is not found among the eigenvalues in Table 7-1, and instead, there is a 0.3-0.6 Hz oscillation. This

observation is not studied further in this thesis, but confirms the fact that the simulation model and the real system are not completely equal. Further studies should also include an improvement of the generator exciter in this view.

Nevertheless, such a comparison as was performed with one vehicle also confirms that the modelled vehicle's reaction to or interaction with the rotary converter is essentially realistic. The oscillations are showing a similar pattern in several measurement variables. The operating points are however different, the vehicle model operates at half load (3.8 MW) at long line length (60 km) while the real vehicle operates on high power (6.5 MW) at short line (10-20 km). Figure 6-8 shows the simulation model's rotary converter mode for different operating points and indicates that also the combination of high power consumption and short line length reduces the stability margins and may result in instability.

There is one variable that differs though: the reactive power oscillation. The modelled vehicle shows a reactive power oscillation giving a damping impact, while measurements on the real vehicle show the opposite. The focus in the vehicle modelling in this thesis has been on the active power control, but further studies should be performed in relation to the control of the reactive vehicle power.

One reason that the vehicle model behaves differently in regard to reactive power is discovered to be the current measurement. The SOGI is used in this model as described in Section 5.4, and has a higher bandwidth than a DFT, which is more commonly used. A decrease of the current measurement bandwidth reduces the damping of the rotary converter mode as seen in Figure 7-5. For example, $Ki_{SOGI} = 1$ results in an eigenmode of +0.10 [1/s] ± j1.63 [Hz]. A time simulation (not shown in this thesis) shows that this change results in a non-oscillating reactive power at 1.6 Hz.

While real vehicles with a low semiconductor switching frequency often have a passive shunt filter for harmonic current reduction, this is not included in the developed simulation model. Qualitatively speaking, a shunt capacitor should increase the reactive power production at a higher voltage, though the quantitative contribution from a realistic filter is not considered.

Despite these differences, the stability criterion established for the rotary converter is equal for all vehicles. It is shown that the proposed power oscillation damper improves damping on the rotary converter eigenfrequency for both the simulation model and the real vehicle. This supports the proximity of the developed vehicle model to reality, together with the power supply modelling.

7.7.1.2 Reason for instability

The rotary converter and the vehicle were both initially stable before being modelled together in the reference case. It is the combination of these two components into one system that leads to instability since they both show low-frequency dynamics. In this case, their eigenfrequencies are not equal, but in the vicinity of each other, i.e., within the same decade. Several time constants are observed within this range. Participation

factors show that the vehicle and the rotary converter participate in each other's modes, though to a limited extent. The sensitivity analysis shows that the vehicle control system parameters exert an influence on the damping of the rotary converter. The system can easily become more unstable by control system parameter altering. From this, it is concluded that the vehicle dynamics can have a negative impact on the system's stability.

This instability is reached even when the vehicle is modelled with only the primary controllers necessary for operation, i.e., the DC-link voltage controller (VC), the AC current controller (CC) and the line voltage phase synchronisation controller (PLL). The most important controller in this view is the VC. Additional controllers such as reactive power control and line power limitation, as a function of line voltage, were never modelled nor in intervention in the real vehicle tests, and should be included in further work.

The participation factors however are not able to explain all the negative influences the vehicle has on the rotary converter, since their values are too small. There must be something more that influences the stability. The primary control objective for the vehicle is to supply the traction motors with the required power. From a power system point of view, the vehicle behaves like a constant power load. Such a load has itself a de-stabilising impact on the rotary converter resonance as shown in Section 3.4.5 since the rotary converter stability criterion is principally violated. Still, the vehicle dynamic results in a more unstable system than a non-dynamic constant power load does under the same conditions (see Section 7.3.4).

The constant power load characteristic leads to another observation. When the product of voltage and current is to be kept constant, the current has to increase when the voltage decreases, and vice versa. This leads to line active power losses oscillating in anti-phase to the voltage and converter speed. Accordingly, the violation of the stability criterion increases when both line length and power consumption increase. In this traction power system the line resistance cannot be neglected, as it is significant.

The constant power load behaviour alone is not able to explain the instability of the real rail vehicle. The line length between the rotary converter and the vehicle is too short, and observations (not referred to earlier in this thesis) of rail vehicles at a standstill or in coasting oscillating against the rotary converter cannot be explained. Details of these remain for further investigation.

Changing the vehicle model characteristics by damping its eigenmode and changing its characteristic into not acting as a constant power load have shown a positive stabilising impact, confirmed by real life measurements. However, the reason for instability may be different from the reasons suggested here. A change in the vehicle characteristic to be voltage dependent such as a resistor at the oscillation frequency might prove to be effective enough to make the system stable, even if the original reason has not been solved. Details in these remain for further investigations.

7.7.1.3 Stability improvements

In this thesis, system stability is improved by changes in the vehicle line-side converter control in two ways: parameter tuning and active damping.

The proposed improvement of the control parameters implies a reduced phase-locked loop bandwidth. In order to accept this reduction, the PLL must not be considered as a phase-tracking device that has only one single task, but rather as a synchronisation controller that can be tuned like the other controllers in the system. The tuning of the PLL is essential to increase damping as shown in Section 7.4.1.4, since tuning of the VC and CC by itself cannot achieve this result. However, the PLL must not be slowed down to the point that it cannot track the phase satisfactorily during disturbances. Problems with phase tracking have not been observed in this simulation model, most likely due to the relatively small parameter change (47 %).

Improving the stability by parameter change seems to imply that the reactive power originally oscillates in anti-phase to the line voltage, which damps the voltage oscillations. The study of the PLL phase lagging in Section 7.4.1.4 proposes that the reactive power should oscillate opposite what is observed for the full model. It might well be that the impact of the PLL is not large enough to override the inherent characteristic of the full model. This is not investigated further in present work.

If a vehicle is designed and tuned to have perfect active power control at the rotary converter eigenfrequency, it still reduces the system's damping since it violates the stability criterion. It may be better to concentrate in making the control principle of the vehicle neutral or damping, instead of focusing on such a perfect tuning. It is as studied in Chapter 3 and important characteristic of the rotary converter that electromagnetic torque imbalance results in acceleration or deceleration of its rotor. This surplus or deficit in kinetic energy can be observed in change in the synchronous generators' voltage amplitude and phase. The vehicle should act according to this characteristic, and does so regarding the phase due to the PLL lagging. Similar investigation should be done in view of the voltage amplitude. Harnefors, et al. [74] propose a three-phase general voltage source converter controller tuning to avoid instability by decreasing the VC, PLL and voltage measurement bandwidth as low as possible, preferably below critical power supply resonances. In order to ensure fast enough transient response, a change of parameters when a disturbance is detected is proposed. This proposal is not investigated any further for the traction power system in this thesis, as instead, active damping has been studied. However, it might be interesting for further work.

Both the parameter tuning and the power oscillation damper implementation indicate that the potential increase in damping of the rotary converter mode is not unlimited. The parameter tuning suffers from a reduction in damping of the two other vehicle modes. The active damping solutions reduce the damping of a power supply resonance at even lower frequencies than 0.1 times the fundamental frequency. In this thesis, the improvement of rotary converter mode damping is stopped when other eigenmodes show a damping ratio of approximately 15 %. Modelling the power supply and rail

vehicles together as is done here allows for the possibility to discover such unexpected disadvantages. Improvement can be performed on the system as whole and not on a sub-system level only.

The parameter improvement performed on the vehicle model studied here may not be transferable in detail to other vehicles with other control structures. The practical experience from Buhrkall, et al. [35] is that 'conventional' controller tuning is insufficient to ensure stability with rotary converters at long feeding distances. However, the basic idea of improvement by damping vehicle dynamics at the rotary converter eigenfrequency and avoiding the constant power load characteristic is expected to be valid for all vehicles, with the latter confirmed by tests on real vehicles (Buhrkall, et al. [34]; Buhrkall, et al. [35]).

Zhe, et al. [185] proposes to modulate the DC-link voltage of a full-scale back-to-back power converter for grid connection of a variable-speed wind turbine in order to mitigate flicker due to time-periodic wind turbine speed given by wind-shear and tower-shadow effects. The solution is essentially equal to POD1a proposed in this thesis and is reported to be effective in distribution grids where the X/R ratio is small, i.e., a considerable resistance. Flicker mitigation by reactive power control is reported to be less effective in such a grid, which is a conclusion that is interesting regarding the proposed POD2 in present thesis which shows a limited damping impact in a grid with small X/R ratio. This is however not studied further in the present thesis.

7.7.2 Conclusion

In this chapter, the interaction between the initially stable but poorly damped rotary converter together with the initially stable rail vehicle model has been investigated. The system, when these two components are combined, is unstable for the specific case. This instability is found to be caused by three main circumstances:

1. The vehicle controls its active power consumption from the line to be constant by changing the line current opposite to the line voltage oscillation. This constant power load characteristic principally violates the stability criterion for the rotary converter electromechanical mode as discussed in Section 3.4.6. An increase of power consumption and impedance between the rotary converter and the constant power load reduces converter damping due to line loss oscillations which additionally violate the stability criterion. The constant power load characteristic is found to be an important factor for the instability, but is in the studied case only able to reduce the system's damping and is not enough to cause instability alone.

2. The low-frequency vehicle mode studied in Chapter 6 results in vehicle dynamics at the rotary converter's eigenfrequency, and vehicle active power is not necessarily kept constant. The vehicle's low-frequency dynamics have a significant influence on system's stability due to the vicinity to the rotary converters' eigenfrequency. These dynamics and consequently the damping of the rotary converter can be changed by altering the vehicle control system

structure and parameter values. From Section 6.3.3 it is known that vehicle mode typically shows a reduction in damping and oscillation frequency when power consumption and outer impedance are increased, which is in Section 7.3.3.2 shown to worsen the situation. Only small amplification of the rotary converter's oscillations is enough to cause instability since the stability margins are generally small.

3. The vehicle's control of the reactive power may increase or decrease its stability margins depending on its oscillation relative to the line voltage. Oscillation in phase results in damping, while oscillation in anti-phase decreases damping.

It is possible to improve the stability of the system by changing the vehicle dynamics at the rotary converter eigenfrequency. One approach is to reduce the vehicle's influence by damping and increasing the frequency of its own low-frequency DC-link voltage control eigenmode(s), i.e., move the vehicle mode away from the rotary converter mode in the complex plane. This however might not be sufficient; as the constant power load characteristic of the vehicle can still be present. Additionally reducing the phase-locked loop's bandwidth may improve the system's damping. A second method is implementation of a power oscillation damper in the vehicle that neutralises this constant power load characteristic. Damping by means of active power modulation is experienced more effective than reactive power modulation. However, the model studies reveal that damping of the rotary converter's eigenmode in either way may be limited by reducing the stability margins for other eigenmodes in the system.

This conclusion is based mainly on an analysis on the simple vehicle model developed in Chapters 5, but important aspects are confirmed by observations on a real rail vehicle.

The observed instability is only possible to recreate by use of the enhanced RMS model that includes the fast network dynamics and the vehicle current controller. Neglection of the closed current control loop changes the behaviour of the vehicle since the PLL angle then is giving the displacement of the line current relative the line voltage instead of the actuated PWM voltage relative the line voltage.

7.7.3 Further work

The work in this chapter brings up several questions and observations. Hence, there is a great need for further study:

- The present study focuses on the behaviour of the vehicle's active power, while it has been observed that the reactive power has a significant influence on the stability margins as well. It is important to understand why the reactive power flow oscillates as observed and why there is a difference between measurements taken from the simulation model and the real life vehicle.

- The improvements by both the tuning of parameters and the design of power oscillation dampers are in present work performed at a relatively high level.

More detailed studies are needed to understand the detailed consequences of both approaches, as maybe some of the proposed improvements are not practically feasible or violate other stability criterions, or performance requirements for the system. Another approach to be investigated is the reduction of controller bandwidth and change of parameter set during a disturbance as proposed by Harnefors, et al. [74]. Can this be applied to a rail vehicle without comprising requirements for fast transient response and general performance?

- An instantaneous value model of the rotary converter would in view of this be useful. Different vehicle control system solutions may then be tested using this more realistic model and uncertainties introduced by simplification into a rotating reference frame are omitted.

- A more analytical and systematic optimisation of the vehicle line-side converter control should be performed, and relevant dynamics from the motor side should be included as well. Moreover, the line-side converter control parameters should be coordinated with both the line-side power oscillation damper and the motor-side DC-link voltage damping.

- Better damping of the rotary converter itself is expected to improve the system stability as well, and should still be focused on. This includes both improvement of present excitation system and possible implementation of power system stabilisers. More study of the excitation systems influence on the system stability should be carried out.

- Both the rotary converter and the vehicle eigenmodes showed reduction in damping when the system's power transfer capacity was approached. For the sake of understanding, it could be interesting to investigate if there is a correlation between the damping and derivative of the line voltage with respect to power consumption (dU/dP).

8 Vehicle and rotary converter admittance and impedance considerations

This chapter introduces considerations in the frequency domain of system stability based on input admittance of the rail vehicle and output impedance of the rotary converter. Simplified analytical frequency responses are discussed in view of a derived stability criterion. Input admittances of the full vehicle simulation models are also calculated and discussed.

8.1 Introduction

8.1.1 Insufficiency of eigenvalue calculations

In previous chapters in this thesis, eigenvalues of the complete power system, including the power supply infrastructure and the electric vehicle has been focused on. The eigenvalues' real part has been monitored in order to investigate system stability with regard to the damping of low-frequency oscillations.

It is rare, however, that the complete power system can be studied together based on a state-space model as has been performed in present thesis. The rotary converter may be implemented in a real-time simulator, but vehicle dynamics are seldomly represented in a rotating reference frame in power system analysis software. Real-time simulations may be of value if adequate power supply models can be provided, though they will still not provide explicit information of eigenvalues as they are performed in a stationary reference frame and are hence time variant. Advanced control systems may be difficult to represent sufficiently in a rotating reference frame, thus eigenvalue analysis are not appropriate as a method for stability investigation.

In addition, it cannot be expected that vehicle manufacturers will be willing to reveal enough inside information concerning their vehicles for complete modelling, since such information are normally treated as a company secrets. For electrical resonance instability, it has become praxis to provide information about the rail vehicle by use of a frequency response characteristic as defined on the interface between the vehicle and the rest of the power supply. This is introduced in the section 8.1.3 as input admittance.

The benefits of such 'impedance-based approach' over the traditional 'state-space approach' for small-signal analysis of AC distributed power systems in general are summarised by Sun [174].

8.1.2 Power system representation

In this chapter, the power system shown in Figure 1-1 is devided into a source and a load representing the power supply (rotary converter and overhead contact line) and the electric rail vehicle, respectively. The interface between them is located at the vehicle's connection to the rest of the power system, i.e., at its current collector, as shown in Figure 8-1.

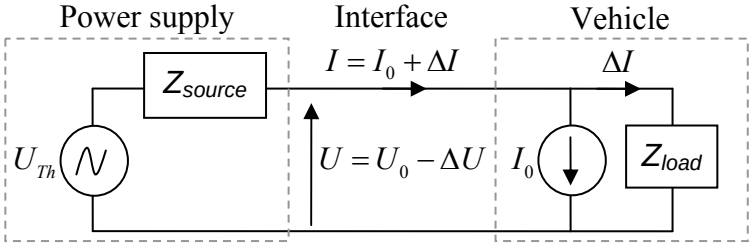

Figure 8-1: A power supply (source) and vehicle (load) combined as a power system.

The output from the source is the sum of the steady-state voltage U_0 and a voltage variation ΔU and is given by the Thèvenin voltage source U_{Th} and voltage drop over the Thévenin-equivalent source impedance Z_{source}. The current drawn from the source is represented by the sum of a steady-state current I_0 and a current variation ΔI given by the Norton-equivalent impedance Z_{load}. These impedances are frequency dependent, which will be explained further in the next sections.

The negative sign in front of ΔU is chosen due to pedagocial reasons since increased current leads to increased voltage drop over Z_{source} and consequently decreased interface voltage U if Z_{source} is understood to be positive. This is further discussed in Section 8.1.4. Strictly matemathically, however, it may be more convenient to include this negative sign into Z_{source}.

The voltages and currents are assumed to be represented by time domain signals, scalar or phasors depending on the application and question in study. The equivalent impedances may be represented by admittances when useful ($Z = 1/Y$), and vice versa.

8.1.3 Power system representation for electrical resonance instability

Electrical resonance instability in traction power systems is introduced in Section 2.4.5.1. For the study of stability margins against electrical resonances in the traction power system, the vehicle's input admittance is used as judgement of its qualitative and quantitative contribution (Lörtscher, et al. [114]; Meyer and Schöning [122]).

Figure 8-2 shows a simplified sketch of a vehicle's admittance, together with an admittance representing the rest of the power system (source). The input admittance criterion (IAC) proposed by (Paice and Meyer [135]) requires that the frequency response of the total network admittance ($Y_{network} = Y_{source}+Y_{load}$) should not cross the negative real axis, that is, that the phase remains between –90 and 90 degrees for all frequencies. This criterion has commonly been mentioned as the 'ESCARV' criterion after the project in which it was developed.

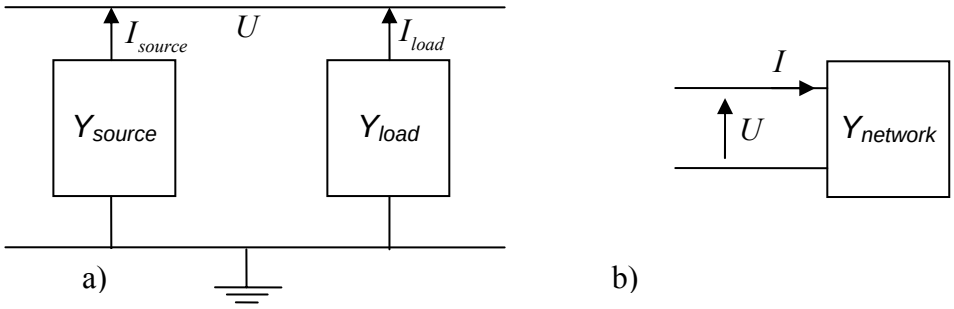

Figure 8-2: A power supply (source) and vehicle (load) represented by their admittances as a), and the total network admittance as b).

A vehicle's frequency response expressed via its input admittance reflects the change in current when the voltage changes, i.e., $Y = \Delta I/\Delta U$, seen from the current collector into the vehicle. From the IAC mentioned above, it is commonly derived (e.g. Meyer, et al. [120] ;Wallnberger, et al. [182]) that if the input admittance has a negative real part at any frequency, the vehicle is capable of causing instabilities combined with critical resonances in the power system at this frequency. The qualitative input-admittance criterion is hence that the vehicle's input admittance should have a positive real part at frequencies in which resonances may occur. Such a positive real part is commonly mentioned as being 'passive' for this frequency, while the opposite, having a negative real part is described as being 'active'.

From a practical viewpoint, stability is preferably ensured by defining a frequency range in which power supply resonances are allowed to occur, e.g. above 150-200 Hz, and another frequency range in which a negative real part is allowed, e.g. below 90 Hz as in Norway and Sweden (Banverket/Jernbaneverket [17]). If such a qualitative approach where the vehicle and power supply characteristics are separated in frequency cannot be applied, a detailed complete approach with modelling of the complete power system must be carried out. A vehicle having negative input admittance at a power supply resonance does not necessarily result in system instability if the system's damping is still sufficient. This complete power system modelling is then performed by representing the vehicles as black boxes where the frequency response of their input admittance describes each vehicle's interface attributes.

8.1.4 System representation for low-frequency instability

A similar input admittance approach for low-frequency instability as for electrical resonance instability is desirous. The power supply can be understood as a voltage source, while the vehicle (load) can be modelled as a current source. Figure 8-1 illustrates how these two components connect via the voltage and current. The line voltage is the power supply output signal, as well as the vehicle input or disturbance signal. The current is the vehicle output and the power supply input or disturbance. The power supply transfer function can hence be represented by the voltage change given by the current change, i.e., impedance Z_{source}. Correspondingly the vehicle transfer function can be represented by the current change given by the voltage change, i.e., admittance Y_{load}.

Figure 8-3 expresses the system as a closed control loop. Since the Z_{source} is assumed to be positive, the change in voltage is subtracted from the U_{Th} as chosen in Section 8.1.2. Both power supply and vehicle are assumed to be separately stable, which is not unreasonable based on the previous studies in Chapters 3, 5 and 6.

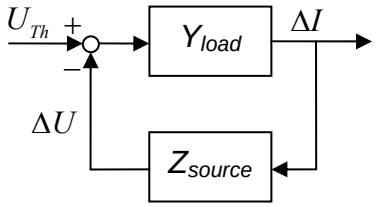

Figure 8-3: A power supply (source) and vehicle (load) combined as a closed loop control system.

The ratios between the electrical components' output and input signals describe how the components influence the voltage or current change during an oscillation at a given frequency. A common expression for the vehicle transfer function is the 'input admittance', which henceforth will be used (Harnefors, et al. [74]), and the rotary converter transferer function is referred to as the 'output impedance'[18].

In the following sections of this chapter, a stability criterion based on the dynamical admittance seen from the rotary converter into the line and vehicle is first proposed and discussed. Further on, simplified analytical expressions for the rotary converter output impedance and vehicle input admittance are derived the voltage and current amplitudes only and only active power are considered. This is of course a simplification, but the intention is to understand some basics before the considering the more complex AC power system.

Two methods for the frequency domain analysis of low-frequency instability in AC traction power systems have already been proposed by Pröls and Strobl [148] (where voltage and current are instantaneous time domain signals) and Menth and Meyer [116] (where voltage and current are phasors). These are further discussed in Section 8.4.

8.2 Analytical considerations

8.2.1 Rotary converter load input admittance criterion

In Section 3.4.6 a stability criterion, Equation (3.27), for the single-phase load voltage characteristic was developed in order to prevent instability at the rotary converter's eigenfrequency $\omega_{res} = 2\pi \cdot f_{res} \approx 2\pi \cdot 1.6$ [rad/s]. The rotary converter generator is a voltage source and the feedback from the single-phase system is the line current. It is therefore of interest to express the stability criterion related to voltage and current, i.e., as an input admittance criterion for the load seen from the rotary converter.

[18] But the ratio/transfer functions can also be observed termed as 'small-signal', 'incremental' or 'dynamical' admittance or impedance in different publications.

$$\mathrm{Re}\left(\frac{\Delta\tau_{eGpu}(s)}{\Delta\omega(s)}\right)\geq 0,\ s=j\omega_{res} \tag{3.27}$$

Such a criterion is derived from Equation (3.27) by the assumption of:

- The electrical power $P_{elGpu} \approx \tau_{elGpu}\cdot\omega_{pu}$, which when assuming no losses equals:
- The electrical power $P_{elGpu} \approx U_G\cdot I_G = U\cdot I$ where I_G is the generator current, which means that the unity power factor is taken for simplicity's sake.
- The relation between the speed and generator voltage oscillation according to Equation (3.20), resulting in Equation (8.1).
- The relation between the generator voltage and speed oscillation $k_u > 0$ as confirmed by the time simulations in Figure 7-1.

$$\Delta\omega_{pu}=\frac{\Delta U_G}{k_u}=\frac{\Delta U}{k_u} \tag{8.1}$$

Given the above assumptions, a relation between the change in torque and change in generator current can be found as expressed in Equation (8.2).

$$\Delta\tau_{elGpu}=k_u\Delta I_G=k_u\Delta I \tag{8.2}$$

Inserting Equations (8.1) and (8.2) into Equation (3.27) results in a ratio between a change in voltage and a change in current as described by Equation (8.3). A negative ratio will violate the stability criterion. For this reason, the load's input admittance should have a zero-valued or positive real part at the rotary converter's eigenfrequency in order to not reduce the system's damping, i.e., an increase in voltage should not lead to a decrease in current.

$$\mathrm{Re}\left(\frac{\Delta I(s)}{\Delta U(s)}\right)=\mathrm{Re}\big(Y(s)\big)\geq 0,\ s=j\omega_{res} \tag{8.3}$$

Since only the amplitude change of voltage and current is taken into account only, the dynamics of the AC system is only expressed in *d*-axis as discussed in Section 4.4.2. The corresponding voltage on the current change ratio is often mentioned as the DC impedance for AC system (Nousiainen [132]). Buhrkall, et al. [34], however, mention this simplification as the 'RMS-domain'. Since it is based on the ratio between the current and voltage amplitude modulation and the descriptive term 'low-frequency envelope' admittance is observed in use as well (Nousiainen [132]).

The corresponding impedances, however, do not necessarily conform to the standard definition of impedances and consequently do not have the properties of impedances (Chen and Sun [42]). One such property is that the property of two elements in series is equal to the sum of the impedance of the two elements. The conformity depends on the calculation method and what aspects that are considered.

8.2.2 Load voltage characteristic influence

For an electric power load, the relation in Equation (8.4) applies when voltage U and current I are still assumed to be in phase. P_0 is the initial power given by the product of I_0 and U_0. Furthermore, the steady-state voltage U_0 is assumed to be 1 pu for simplicity.

$$P = U \cdot I = U_0 \cdot I_0 \left(\frac{U}{U_0} \right)^{MP} = P_0 \cdot U^{MP} \tag{8.4}$$

An electric rail vehicle can as described in Section 8.1.4 be considered as a current source. Solving Equation (8.4) for the current I results in Equation (8.5).

$$I = P_0 \cdot U^{MP-1} \tag{8.5}$$

The partial derivation of Equation (8.5) for U based on Taylor's first-order representation of the non-linear exponential, results in the load input admittance Y in Equation (8.6).

$$Y = \frac{\partial I}{\partial U} = \frac{\Delta I}{\Delta U} \approx P_0 \cdot \left(MP - 1 \right) \tag{8.6}$$

This linearisation shows that a constant power load (MP = 0) results in a negative input admittance, i.e., a decrease in voltage (negative ΔU) will result in an increase of current (positive ΔI). A constant current load (MP = 1) represents no change in current and thus a zero valued input admittance. A constant resistance load (MP = 2) represents a positive input admittance. In complex form, the sign of the input admittance may be seen by value of the polar coordinate angle ($\arg(Y)$) where a 180 degree phase shift represents a negative real part ($\mathrm{Re}(Y) < 0$).

This sign is also reflected in Z_{load} in Figure 8-1 such that a constant power load will result in negative input impedance.

Comparing Equation (8.6) to Equations (3.22), (6.7) and (8.3), it can be concluded that a negative input admittance of a load has a destabilising impact, while a positive input admittance has a stabilising impact, and a zero valued input admittance is neutral. This corresponds to the general understanding of constant power loads in direct current systems as explained by Jusoh [96].

As discussed in Section 5.2.2, the vehicle power is originally given by the mechanical speed and torque demand, independent of the line voltage in steady state. In the following sections it is investigated whether this constant power load characteristic also holds for disturbances in the low-frequency range of interest in this thesis.

8.2.3 Vehicle input admittance

A simplified analytical expression of the input admittance for the second-order vehicle model illustrated by the block diagram in Figure 6-3 is here derived. The DC-link voltage control open loop transfer function A(s) in Equation (8.7) is obtained from Equation (6.2) when $T_{eq} = 0$ and $K_{eq} = 1$. In this case, the response to a change in the current into the DC-link is of interest. The corresponding closed loop transfer function $H(s) = A(s)/(1+A(s))$ is unaffected by where it is observed in the closed control loop (Equation (8.8)). For the sake of simplicity, the motor DC-link voltage dependency is chosen to be neutral, $MP = 1$, and can according to Equation (6.7) be neglected.

$$A(s) = \frac{Kp_{VC}\left(1 + Ti_{VC}s\right)}{Ti_{VC}s} \cdot \frac{1}{T_C s} \tag{8.7}$$

$$H(s) = \frac{Kp_{VC}Ti_{VC}s + Kp_{VC}}{Ti_{VC}T_C s^2 + Kp_{VC}Ti_{VC}s + Kp_{VC}} \tag{8.8}$$

The vehicle converter is assumed to be lossless and operating with unity power factor, i.e., the vehicle's main transformer is temporarily disregarded. The relation between the DC-side voltage and current (U_{dc} and I_{dc}) and the AC-side voltage and current ($U_{ac} = U$ and $I_{ac} = I$ as shown in Figure 8-1) is then given by simplification of the power balance Equation (5.2) into Equation (8.9).

$$U_{ac} \cdot I_{ac} = U_{dc} \cdot I_{dc} \tag{8.9}$$

By division of U_{ac}, this leads to an expression for the AC side current as in Equation (8.10).

$$I_{ac} = \frac{U_{dc} \cdot I_{dc}}{U_{ac}} = \frac{P_{dc}}{U_{ac}} \tag{8.10}$$

A partial derivation of Equation (8.10) with regard to the AC side voltage results in an expression of the input admittance as in Equation (8.11).

$$Y_{CPL} = \frac{\Delta I}{\Delta U} = \frac{\Delta I_{ac}}{\Delta U_{ac}} = \frac{\partial I_{ac}}{\partial U_{ac}} = -\frac{P_{dc0}}{U_{ac}^2} \tag{8.11}$$

This equation corresponds to Equation (8.6) for a constant power load when $U_0 = 1$. The DC-link power P_{dc0} equals the motor side power P_{m0} in Section 6.2.3.2. It is important to understand that the outer active control loop of the vehicle, i.e., the DC-link voltage control loop, has an objective that is independent of the vehicle motor voltage characteristic. That means that even if $MP > 0$ for the motor-side inverter as studied in Section 6.2.3.2, the DC-link voltage control loop with constant DC-link voltage reference will show constant power load behaviour to the power supply as shown.

If the vehicle keeps the power constant and independent of the voltage disturbance frequency, i.e., no low-frequency dynamical behaviour, then the input admittance will always be negative, which corresponds to Equation (8.6). However, the vehicle active power control has a limited bandwidth, with the studies in Chapters 5 and 6 showing a dominating low-frequency eigenmode. The vehicle's closed loop dynamics are therefore represented by the closed loop transfer function $H(s)$ in Equation (8.8). For the sake of simplicity here, the frequency-dependent low-frequency input admittance for the vehicle is described by Equation (8.12) as a product of the non-dynamic input admittance and the closed loop dynamics.

$$Y_{vehicle}(s) = Y_{CPL} \cdot H(s) = -\frac{P_{dc0}}{U_{ac0}^2} \cdot \frac{Kp_{VC}Ti_{VC}s + Kp_{VC}}{Ti_{VC}T_C s^2 + Kp_{VC}Ti_{VC}s + Kp_{VC}} \tag{8.12}$$

It should be noted though that the direct mathematical connection between Equations (8.11) and (8.8) is difficult to establish as the AC-side variables in the closed-loop expression are disregarded due to the simplification of $I_{dc} = I_{dc}^{ref}$. However, Harnefors, et al. [74] have developed an analytical expression for the corresponding input admittance for a general three-phase VSC without these simplifications. The basics of the constant power load input admittance in Equation (8.11) multiplied with the dynamics as represented by Equation (8.12) are recognised in their Equation (40).

Figure 8-4 shows a comparison of the load input admittance for the second-order vehicle model (Equation (8.12)) and the non-dynamic constant power load (Equation (8.11)) for the parameter values explained and derived in Chapter 6.

Based on these expressions, it is observed that the value of the vehicle's input admittance as seen from the AC side increases with an increased initial power demand, and increases as the operating point voltage decreases. The vehicle model and the constant power load show an equal behaviour below 0.5-1.0 Hz.

The calculated eigenfrequency for this second-order model in Section 6.2.5 at 2.62 Hz can be observed in the diagram at which the magnitude increases and the phase starts to shift. This is therefore the active power control loop bandwidth. A reduced damping of the vehicle mode will result in a larger overshoot around the eigenfrequency. The impact of these characteristics on the system stability is investigated further in Section 8.2.5.

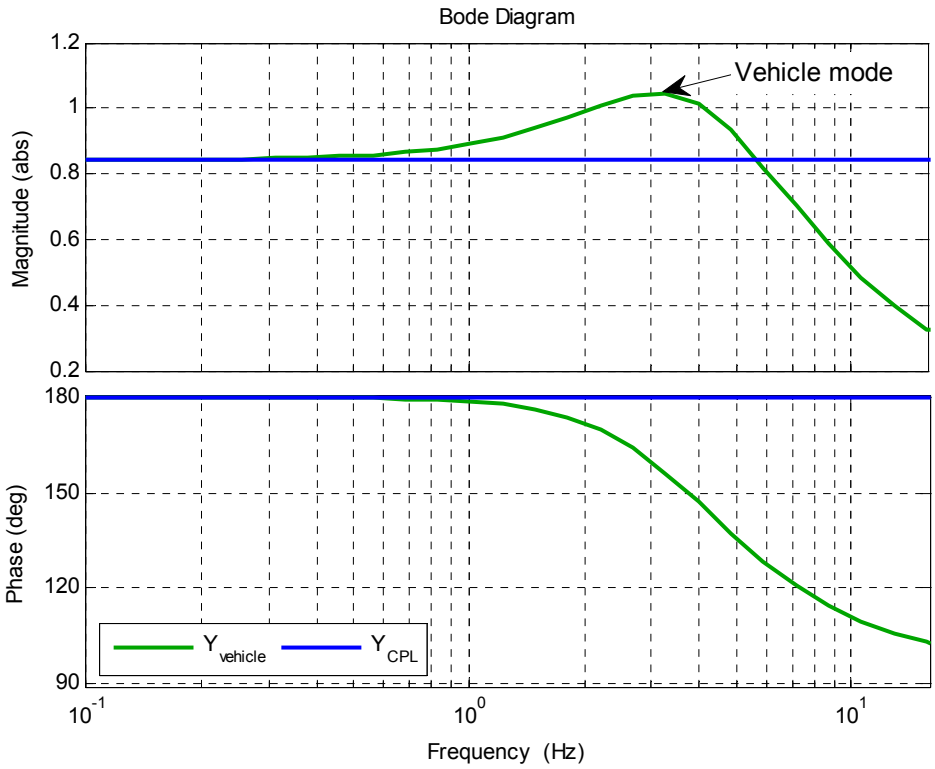

Figure 8-4: A comparison of input admittance for the dynamical vehicle model and the non-dynamical constant power load, with the magnitude in pu.

A line current/power limitation function in the vehicle may reduce the current/power at low line voltages. Consequently, it will influence on P_{dc0} and U_{ac} and limit the possible amplitude of the input admittance given by Equation (8.11). If and how it will also change the dynamics of the vehicle is not considered in this thesis.

8.2.4 Rotary converter output impedance

An analytical expression for the output impedance of the second-order rotary converter model in Chapter 3 is here developed. The converter is considered to be operating in single-phase side island mode. The output impedance is the ratio between the voltage amplitude given by the converter relative to the current amplitude given by the load, i.e., $Z_{rotary\_converter} = \Delta U/\Delta I$.

Based on the block diagram for this operating condition in Figure 3-5, the transfer function from the generator electromagnetic torque variation to the rotary converter speed variation is found. By application of the same assumptions as in Section 8.2.1, an expression for the output impedance such as in Equation (8.13) is obtained. Its frequency response is shown in Figure 8-5.

$$Z_{rotary\_converter}(s) = \frac{\Delta U(s)}{\Delta I(s)} \approx \frac{\Delta \omega(s)}{\Delta \tau_{eGpu}(s)} = \frac{k_u s}{2H_{MG}s^2 + D_M \omega_{sM} s + K_{1M} \omega_{sM}} \tag{8.13}$$

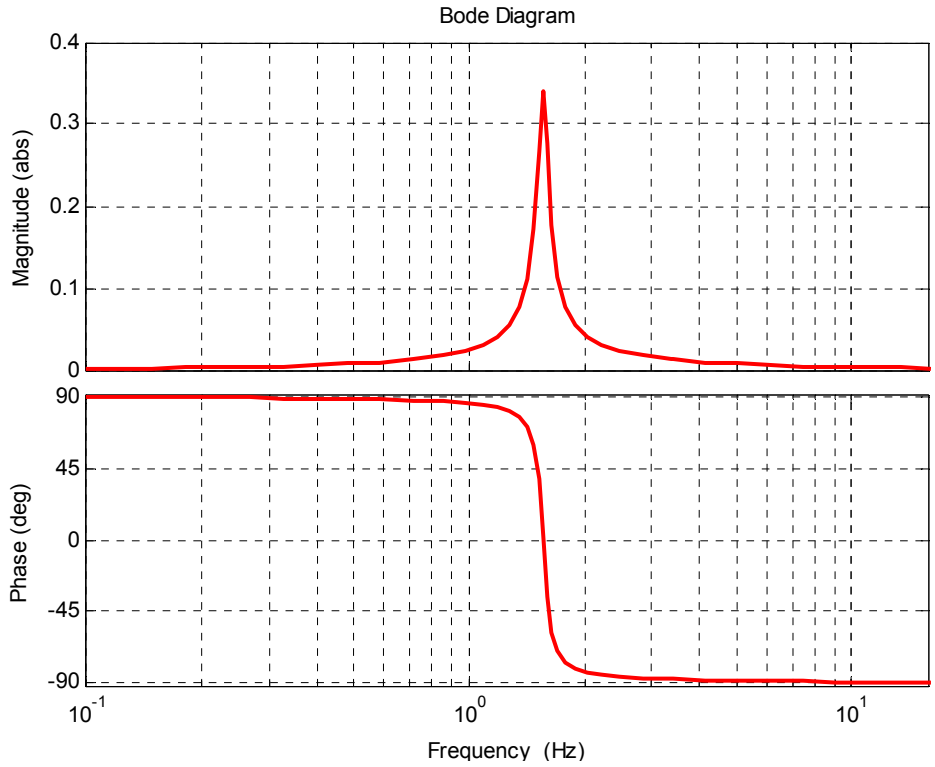

Figure 8-5: A rotary converter output impedance given by the electromechanical eigenmode.

The transfer function is a second-order band-pass filter where the poor rotary converter damping gives amplification at its eigenfrequency while other frequencies are attenuated. As a result the output impedance shows a considerable peak at the eigenfrequency. This means that if a given disturbance in the current is applied with this frequency, the speed oscillation will result in a large voltage amplitude oscillation. Such a large current on voltage ration represents large impedance. When the current is increased, the voltage will decrease and vice versa as can be observed both in the simulation of the complete model in Figure 7-1 and in the measurements in Figure 7-20.

This output impedance is here given by the electromechanical eigenmode only. For load changes at lower and higher frequencies, the electromechanical mode is not continuously excited, and these other changes in output voltage due to current change are not included. The impacts of the internal stator impedance and the automatic voltage regulator have to be added, though a part of the AVR influence is represented by the factor k_u. In this simplified approach, this representation is considered to be sufficient.

8.2.5 Stability consideration

The load input admittance and power supply output impedance developed in Sections 8.2.3 and 8.2.4 are in this section combined into one system as shown in Figure 8-3.

In addition to the output impedance given by the rotary converter's electromechanical eigenmode, the power supply also includes the overhead contact line, transformer and generator impedances. For the sake of simplicity is the vehicle transformer also included in the source output impedance, i.e., the interface between source and load is moved to the vehicle PWM terminals. These four series impedances are lumped into the total resistance and inductance $Z_{line} = R + j\omega_{osc}L$. This representation of the line impedance is chosen based on two conditions. It corresponds to the *d*-axis direct coupling impedance Z_{dd} that will be explained in Section 8.4.2, and with this choice, the impedance conforms to the standard definition as discussed in Section 8.2.1.

The total source output impedance is the sum of the rotary converter output impedance and the total line impedance as in Equation (8.14).

$$Z_{source} = Z_{rotary\_converter} + Z_{line} \tag{8.14}$$

The total system open loop transfer function is $Z_{source} \cdot Y_{load}$. The system will be unstable if the Nyquist contour of this transfer function encircles the critical point (-1,0) in the complex plane. This corresponds to a loop gain larger than unity when the phase shift is 180 degrees at a certain frequency. Middlebrook [126] showed that stability can be guaranteed for a DC system if the magnitude of Z_{source} is always less than the magnitude of $Z_{load} = 1/Y_{load}$. This corresponds to a loop gain always less than unity, i.e., a positive gain margin.

Figure 8-6 shows the frequency response of the source output impedance (Equation(8.14)) and the inverse of the vehicle input admittance (Equation (8.12)). In addition, the inverse of the non-dynamic constant power load input admittance (Equation (8.11)) is shown for comparison. The parameters that are used correspond to the numbers used in Sections 3.5 and 6.2.5, respectively, and the operating conditions correspond to the reference case.

The rotary converter eigenmode at 1.6 Hz is easily observable as a peak increase in the source impedance, while the vehicle low-frequency mode is observable as a reduction in Z_{load}. The constant power load characteristic of the vehicle gives a phase shift of 180 degrees below the vehicle's eigenfrequency. Consequently there is a 180 degree phase shift of the system's open loop transfer function giving potential for instability.

Figure 8-7 shows the open loop transfer functions $Z_{source} \cdot Y_{load}$ as illustrated in Figure 8-3 for the same system.

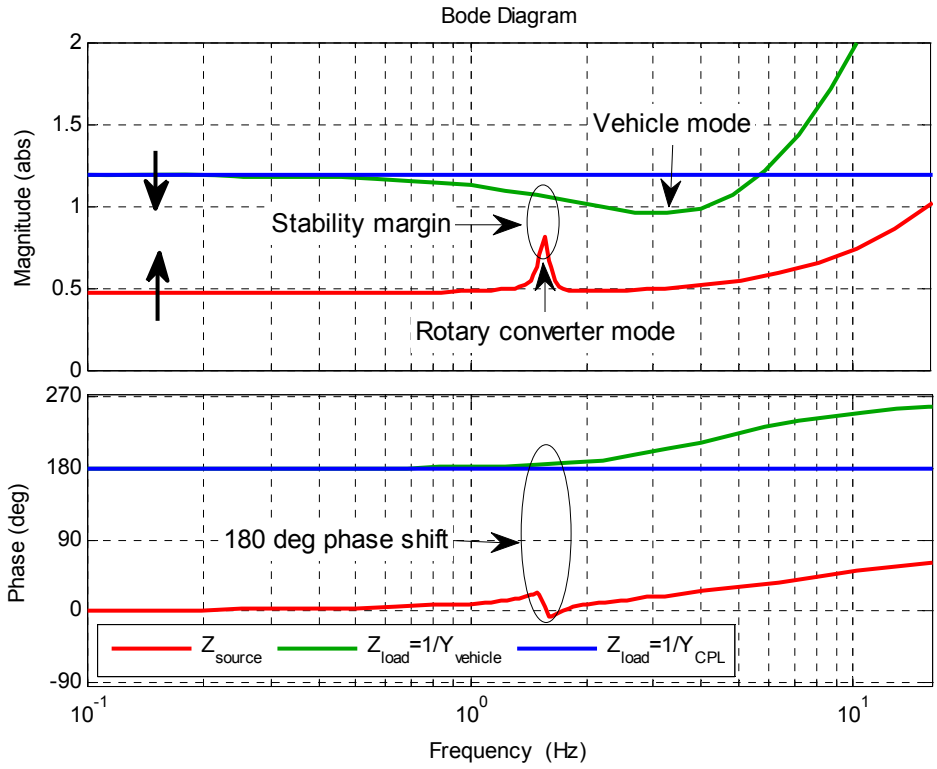

Figure 8-6: The power supply (source) output impedance and vehicle and constant power load (load) input impedance.

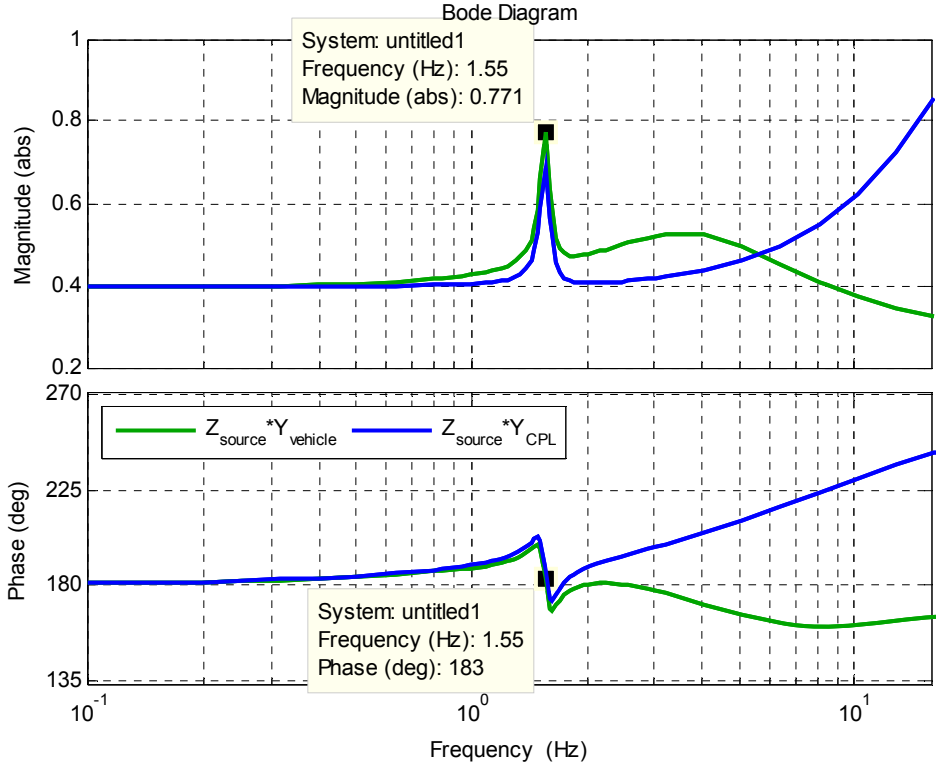

Figure 8-7: Open loop transfer functions (see Figure 8-3) for the source and dynamical vehicle model and the source and the constant power load.

The system as it appears here, given the simplifications described earlier and the chosen parameters, is stable as $|Z_{source}| < |1/Y_{load}|$ and $|Z_{source} \cdot Y_{load}| < 1$. Since the phase is 180 degrees, there is only a gain margin as indicated in Figure 8-6 by the distance between the source impedance and the load impedance. From Figure 8-7 it is derived that the gain margin is approximately -12 dB. However, the following changes may be applied to the system:

- Changed line length shifts $|Z_{source}|$ upwards or downwards as indicated by the lower the arrow on the left hand side in Figure 8-6. Therefore, the margin between $|Z_{source}|$ and $|1/Y_{load}|$ will be influenced.
- Changed line length changes the line voltage drop and hence changes the voltage operating point U_0 as indicated by the arrows on the left hand side in Figure 8-6. This, according to Equation (8.12), changes $|Y_{load}|$ and consequently shifts $|Z_{load}|$ upwards or downwards and influences the stability margin.
- Changed initial vehicle power P_{dc0} will, according to Equation (8.12), change $|Y_{load}|$ and consequently shift $|Z_{load}|$ upwards or downwards and influence the stability margin.
- The vehicle mode damping and/or frequency can be changed due to for example control system parameter altering or the load operating point P_{dc0}. This will influence the stability margin.
- Changed damping D_M of the rotary converter electromechanical mode will change the impedance peak of Z_{source} at 1.6 Hz and consequently influence the stability margin.

The roots of the closed loop transfer function $H(s) = Y_{CPL} \cdot Z_{source} / (1 + Y_{CPL} \cdot Z_{source})$ can be calculated. In order to avoid a third state variable, the term $j\omega_{osc}L = sL$ in Z_{line} is neglected. Hence the line impedance equals R only. An analytical expression for the eigenvalues is shown in Equation (8.15) and it can be observed how the line impedance and the load operating point influence the damping of the rotary converter electromechanical eigenmode. The impact corresponds to the above considerations.

$$\lambda_{1,2} = -\frac{D_M \omega_{sM} - \dfrac{k_u \cdot P_{dc0}}{U_0^2 - R \cdot P_{dc0}}}{4H_{MG}} \pm \sqrt{\left(\frac{D_M \omega_{sM} - \dfrac{k_u \cdot P_{dc0}}{U_0^2 - R \cdot P_{dc0}}}{4H_{MG}} \right)^2 - \frac{K_{1M} \omega_{sM}}{2H_{MG}}} \qquad (8.15)$$

The conclusion from this is that an increased line length and vehicle power will reduce stability margins. This is supported by the operating point sensitivity study in Section 7.3.3.2. The operating point directly influences the gain margin. The fact that the vehicle has a low-frequency eigenmode worsens the condition compared with a constant power load without dynamics, so at a given operating point, the system may become unstable. The resulting oscillation frequency is given by which eigenmode has the poorest damping, either the rotary converter or the vehicle.

Similar low-frequency interaction between the source's and the load's eigenfrequency is observed by Hoff and Mulukutla [85] for uninterrupted power supplies (UPS) and active power factor correction (PFC) power supplies used in computers.

8.2.6 Qualitative stability considerations for system without a rotary converter

The principle of the stability considerations in Section 8.2.5 can be extended to a power system without the poorly damped rotary converter. Even then, the traction power system may become unstable for a given combination of vehicle(s), line length and power demand. As a result, the undamped oscillation frequency is likely to be given by the vehicle low-frequency eigenmode as the 1.6 Hz source impedance peak is not present, though the influence from a change of line length and operating point remains. In Equation (8.16), the roots of the closed loop transfer function $H(s) = Y_{vehicle} \cdot Z_{line} / (1 + Y_{vehicle} \cdot Z_{line})$ is calculated in the same way as Equation (8.15). Increased the line length and load operating point decrease the system's damping. The sensitivity to line length and operating point is studied for the full vehicle model in Section 6.3.3 and supports this interpretation, e.g. the instability indicated for the 1-MW load when the line length increases over 180 km.

$$\lambda_{1,2} = -\frac{Kp_{VC}\left(1-\frac{R \cdot P_{dc0}}{U_0^2}\right)}{2T_C} \pm \sqrt{\left(\frac{Kp_{VC}\left(1-\frac{R \cdot P_{dc0}}{U_0^2}\right)}{2T_C}\right)^2 - \frac{Kp_{VC}\left(1-\frac{R \cdot P_{dc0}}{U_0^2}\right)}{Ti_{VC}T_C}} \quad (8.16)$$

Similarly, parts of the instability observed for the long line stability test in Section 5.7 may be qualitatively explained by an extension of the aforementioned considerations. This may also be interpreted as the 'depot problem' described in Section 2.4.5.2. In these cases, the vehicle attempts to keep its power demand equal to zero. This means that the PWM has to invert a voltage equal to the line voltage in amplitude and phase in order to result in no current into the DC-link (as support, see input admittance Y_{dd} calculated for the full vehicle model in no-load in Figure F-1):

- At a low disturbance frequency, e.g. below 0.1 Hz, it is easy for the vehicle control system to follow the line voltage to maintain this power balance since the disturbance is below the system's bandwidth. As a consequence, the resulting current is low, the input admittance is small (almost zero) and the phase is zero.
- At a high disturbance frequency, e.g. above 10 Hz, it is difficult for the vehicle control system to follow the disturbance in order to maintain the power balance as the controllers' bandwidths are limited. The input admittance shows a significant phase shift (above 360 degrees).
- In the low-frequency range between these two frequencies shows the vehicle its dynamical behaviour of interest. Any disturbance results in excitation of the DC-link voltage control mode. The vehicle is partially able to follow this

disturbance, but not without amplification or attenuation. At a given frequency the phase shift is 180 degrees. This is the frequency where the DC-link voltage controller overshoots in its effort to keep the DC-link voltage constant and the power consumption equal to zero. This results in a positive feedback loop and the system is prone to instability depending on the gain margin given by the source impedance and the vehicle input admittance magnitude.

The simplified second-order model used here fails however to recreate this long-line instability as the measurement filters and PLL are not included. It is believed that the dynamics of these filters plays an important role in vehicle mode instability, as they have their bandwidth in the same frequency range and exert an influence on the vehicle's ability to follow a line voltage variation, i.e., the transfer function from u_{ac1} to u'_{ac}. Stability in systems without rotary converters should be topic for further study.

8.3 Full vehicle model input admittance numerical example

The input admittance for the full vehicle model developed in this thesis has been derived as a numerical example as well as for a comparison with both time simulations and linear analysis of the enhanced RMS model. The input admittance under study is the change in current amplitude over the change in voltage amplitude ratio seen from the source-load interface as defined in Section 8.1.2. Five input admittances are compared in this section:

- the reference case with the original control parameters studied in Sections 7.2 and 7.3;
- the improved control parameters studied in Section 7.4.1;
- the two active power oscillation dampers (POD1a and POD1b) studied in Section 7.4.2; and
- the reactive power oscillation damper (POD2) studied in Section 7.4.2.

This study is performed with the enhanced RMS model only.

8.3.1 Simulation model

The input admittances are calculated by use of the power system shown in Figure 8-8, with the vehicle directly connected to an ideal voltage source. Its steady-state output voltage corresponds to the line voltage in the reference case, i.e., $|U_0| = |U_{ac1}| = 12.6$ kV $= 0.84$ pu.

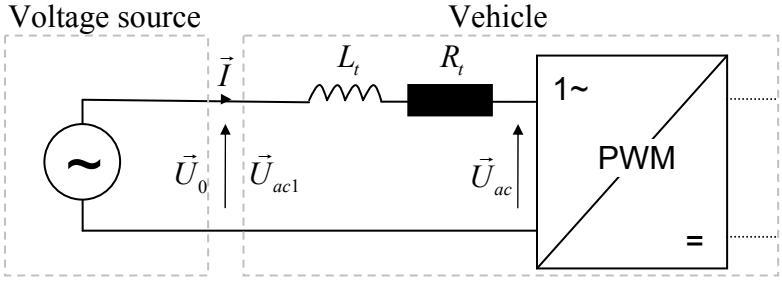

Figure 8-8: The electrical AC circuit in which the vehicle model is tested. The vehicle model includes the DC-link and motor side, even if it is not shown in the figure.

8.3.2 Admittance calculation

For the enhanced RMS model, the admittance is calculated by use of a so-called 'frequency scanning' ([3]). The system is linearised at the given steady-state operating point, and all time derivatives (d/dt) are replaced by $j\omega_{osc}$. A perturbation signal ΔU containing magnitude 1 and phase 0 is added to the steady-state voltage U_0. The perturbation frequency is increased from 0.1 Hz to 16 Hz with a resolution of 0.01 Hz. This corresponds to an amplitude modulation at the low frequencies of interest, $\omega_{osc} = 2\pi f_{osc}$. The response in the line current magnitude and phase is recorded as ΔI. The frequency dependent admittance Y seen from the converter rotor is hence calculated by Equation (8.17).

$$Y(j\omega_{osc}) = \frac{\Delta\left|\vec{I}\right|(j\omega_{osc})}{\Delta\left|\vec{U}\right|(j\omega_{osc})} = \frac{\Delta\left|\vec{I}\right|(j\omega_{osc})}{1} = \Delta\left|\vec{I}\right|(j\omega_{osc}) \tag{8.17}$$

The perturbation and calculation include amplitude modulation only, i.e., no phase/frequency modulation is taken into account.

8.3.3 Input admittance frequency responses

Figure 8-9 shows the corresponding frequency responses for the five different control system versions of the vehicle. Based on the input admittance magnitude and phase, its real part is calculated. The yellow areas in the diagrams show the range where the $\mathrm{Re}(Y) < 0$ for easier comparison to the criterion in Equation (8.3).

At very low frequencies such as below 0.1 Hz, the vehicle shows essentially no dynamical behaviour. Its control system compensates for the line voltage oscillations by changing the line current. The input admittance is negative and equals the value given by a non-dynamical constant power load. When the oscillation frequency is high, such as above 10 Hz, the vehicle active power control is not able to react on the line voltage oscillation without a phase shift. The input admittances' magnitude close to the fundamental frequency has not been further investigated in this thesis. These observations are common for all five models.

The dynamics in the low-frequency range of interest are discussed in the next section, together with a comparison with the time simulations and linear analysis for the corresponding models.

8.3.4 Comparison to linear analysis and time simulation

When the oscillation frequency in Figure 8-9 increases, the vehicle exposes its dynamical behaviour. A 2-3 Hz vehicle eigenmode (mode (12,13) in Table 6-1) in the original reference case (black curve) is clearly visible as an amplification and start of phase shift of the line current response, and essentially corresponds to the linear analysis in Chapter 6. Amplification is noticeable at the rotary converter eigenfrequency as well. The vehicle compensates for the line voltage oscillation by changing the line current in order to keep its power consumption constant.

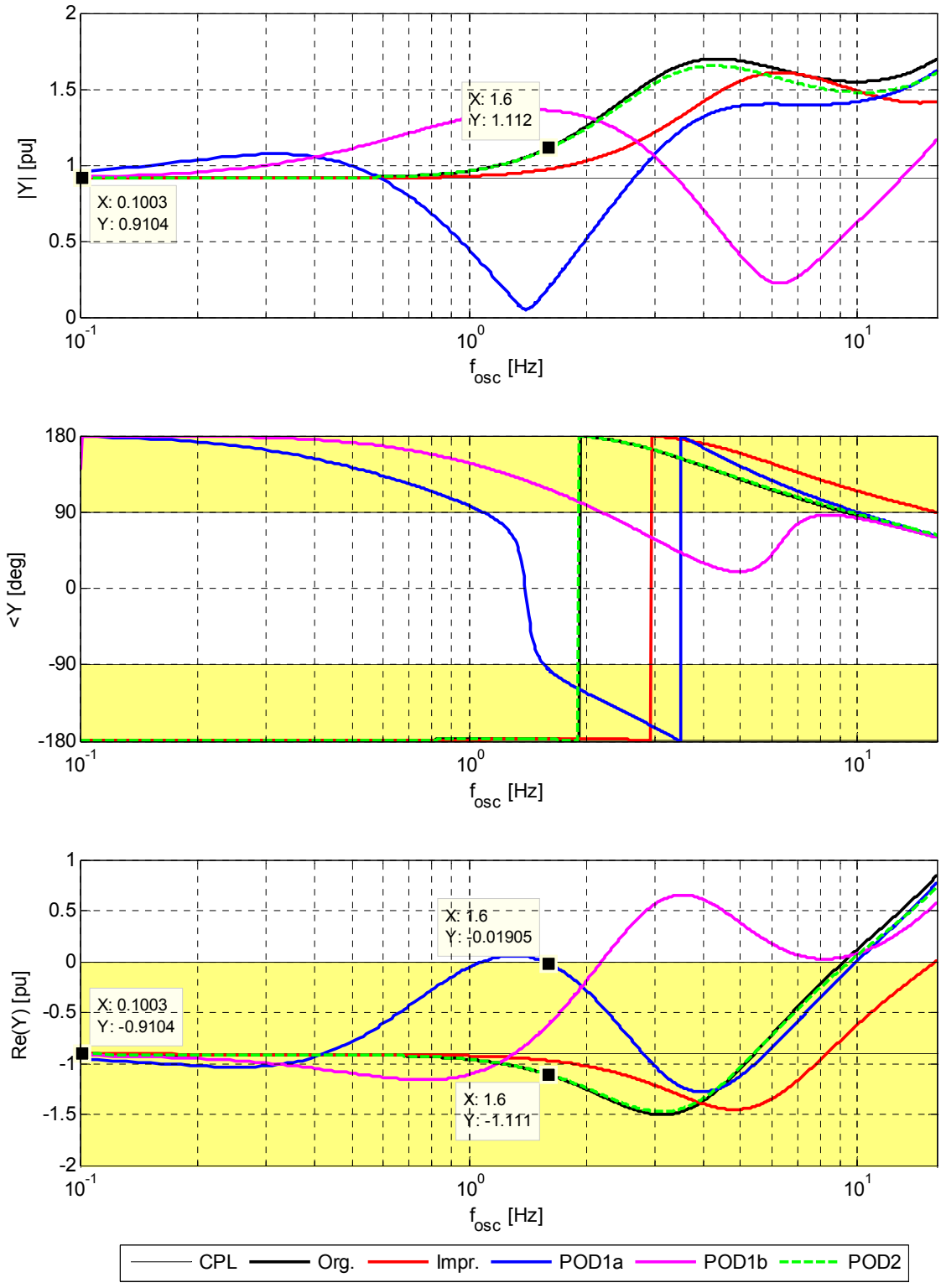

Figure 8-9: Vehicle model input admittance frequency responses in amplitude and phase together with the admittance's real part ('CPL' is a non-dynamic constant power load, 'Org.' is the original (Step 0) and 'Impr.' is the improved (Step 4) parameters). Yellow area: Re(*Y*) < 0.

The input admittance shows that due to the vehicle dynamics, the current is changed 20 % more than a non-dynamic constant power load will do at 1.6 Hz. The vehicle overshoots as observed in the time simulation in Figure 7-1. This overshooting depends on the vehicle mode damping which in Section 6.3 was shown to depend on control system parameters and structure together with the operating point.

One of the results from the improvement of the control system parameters in Section 7.4.1 was a change in the vehicle's dominating eigenfrequency. This is confirmed by the frequency response (red curve) in which the mode (21,22) (referred to Table 7-2) at 2-3 Hz is hardly visible compared to the other vehicle mode (13,14) at 6-7 Hz. The control system's bandwidth has increased and the input admittance at 1.6 Hz is still negative. The improved parameters result in less amplification at 1.6 Hz compared to a non-dynamic load than the original parameters. The frequency response resembles a constant power load having small dynamics at 1.6 Hz while the time simulation also resembled a constant current. This should then be reflected by a zero valued input admittance, which is not observed. This inconsistency shows that changes in the control system parameters are not reflected correctly in this calculated input admittance. The reason for this is assumed to be that the impact of the PLL that was found to be important is not considered when amplitude modulation is studied only.

The first active power oscillation damper, POD1a (blue curve), was designed to increase the active line current in phase with the line voltage amplitude oscillation at 1.6 Hz enough to neutralise the negative damping impact from the vehicle. Figure 8-9 shows a low admittance magnitude with zero phase at a centre frequency close to 1.6 Hz. The input admittance essentially reflects the time simulation, but further tuning of the closed loop system is needed to ensure an accurate behaviour as intended. Two vehicle eigenmodes, one below and one above POD1a's pass band, may be observed in the input admittance; this is according to the eigenvalues shown in Figure 7-16.

The input admittance seen for the case with POD1b (magenta curve) shows a positive real part in the frequency range where it was intended to damp oscillations. The current leads the voltage at 1.6 Hz as expected by the phase of the band-pass filter seen in Figure 7-15. The 0.6 Hz oscillation which is seen as a dominating mode in the time simulation and linear analysis is visible in the input admittance as well.

Both the time simulation and input admittance calculation using POD2 (green curve) show that the current amplitude oscillates opposite to that of the voltage amplitude. The difference between the input admittance without POD and with POD2 is small and cannot explain the improved damping seen in study of the complete system with the rotary converter. It is not possible to distinguish between active and reactive current by the present method, i.e., the current phase is not taken into consideration.

These results are further discussed in Section 8.6.1.

8.4 Admittance and impedance studies for AC systems

Previously in Section 8.2, the power system was, for the sake of simplicity, treated by voltage and current amplitudes only. In this section, two proposed methods for AC traction power system considerations are introduced, one in the stationary reference frame and one in the rotating reference frame. For the latter, the corresponding input admittances of the full vehicle model developed in this thesis are calculated for both the instantaneous value model and the enhanced RMS model, which also enables a comparison between the two.

8.4.1 Stationary reference system

Pröls and Strobl [148] propose a method for low-frequency stability investigations of AC railways by use of input admittances in the stationary reference frame, i.e., instantaneous values of single-phase voltage and current. This approach is based on the method used for the stability analysis of electrical resonance instability as described in Section 8.1.3. For low-frequency instability, the proposed method focuses on frequency components close to the fundamental frequency, i.e., the side bands described by Equation (3.21) rather than the amplitude and frequency modulation. The ESCARV input admittance criterion is extended to also include control loops as described in Section 8.1.4.

This method may also take frequency couplings as described by Möllerstedt [130] into account. This is further explained by Strobl [170], and will not be treated in the present thesis. Several details of the method are still under investigation and hence not published. More experience is necessary in order to completely understand this proposed methodology and to apply it in stability studies.

8.4.2 Rotating reference system

8.4.2.1 Introduction

All the considerations in Sections 8.2 and 8.3 assume voltage and current to be in phase. In an AC system, however, active power may be transferred due to differences in both voltage amplitude and voltage phase (see Equation (7.3)). The reactive power flow influences both the voltage drop and active power losses in the system. Moreover, there is frequency/phase modulation of the voltage due to the rotary converter oscillations as described in Equation (3.21). Menth and Meyer [116] propose an approach for AC railways that intends to take these phenomena into consideration.

This approach can be understood if the simplified system explained in Section 8.2 and illustrated by Figure 8-3 is used as a basis. In previous sections, the voltage and current are expressed as scalars. However, in an AC system the voltages and currents at the fundamental frequency are commonly expressed as phasors, such as in the complex *dq* system introduced in Section 4.3. This rotating reference frame is chosen so that the *d*-axis is oriented in phase with the vehicle line voltage ($\vec{U}_{ac1}$) as shown in Figure 5-2. For small-signal studies, a change in *d*-axis voltage reflects a change in line voltage amplitude, and a change in *q*-axis voltage reflects a change in the line voltage phase.

Figure 8-3 is hence replaced by Figure 8-10[19]. This decomposition results in a multiple-input multiple-output (MIMO) system since both load and source models both have two input and two output signals. There are furthermore two feedback loops, one for each axis, as will be explained in the following.

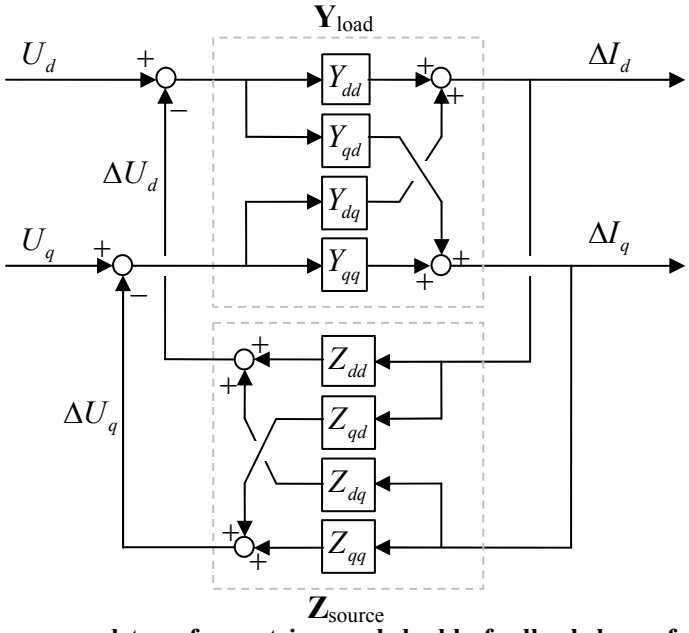

Figure 8-10: The proposed transfer matrices and double feedback loops for AC system stability studies.

The source and the load are no longer represented by single transfer functions, but rather by transfer matrices (Harnefors [72]) in which the *d*- and *q*-axis can be cross coupled to each other. Instead of one transfer function, such as Equation (8.12), the vehicle is now represented by four transfer functions, Y_{dd}, Y_{dq}, Y_{qd} and Y_{qq}, as shown in Equation (8.18).

$$\begin{bmatrix} \Delta I_d(s) \\ \Delta I_q(s) \end{bmatrix} = \begin{bmatrix} Y_{dd}(s) & Y_{dq}(s) \\ Y_{qd}(s) & Y_{qq}(s) \end{bmatrix} \begin{bmatrix} \Delta U_d(s) \\ \Delta U_q(s) \end{bmatrix}, \; s = j\omega_{osc} \tag{8.18}$$

If the source impedance is a line only as described by Equation (4.12), it can be included in the loop as shown by Equation (8.19). For a rotary converter, the transfer matrix has to include the impact of the electromechanical eigenmode as well, i.e., Z_{dd} must correspond to the proposal in Equation (8.13). Further derivations are necessary in order to determine Z_{qd}, Z_{dq} and Z_{qq}.

$$\begin{bmatrix} \Delta U_d(s) \\ \Delta U_q(s) \end{bmatrix} = \begin{bmatrix} R+Ls & -\omega_s L \\ \omega_s L & R+Ls \end{bmatrix} \begin{bmatrix} \Delta I_d(s) \\ \Delta I_q(s) \end{bmatrix} = \begin{bmatrix} Z_{dd}(s) & Z_{dq}(s) \\ Z_{qd}(s) & Z_{qq}(s) \end{bmatrix} \begin{bmatrix} \Delta I_d(s) \\ \Delta I_q(s) \end{bmatrix}, \; s = j\omega_{osc} \tag{8.19}$$

[19] The notation, for example '*qd*', is to be read as *q*(*d*) ('*q*-of-*d*'), i.e., change in *q*-axis output as function of *d*-axis input.

The interpretation of these vehicle frequency responses is 'possible, but difficult and still needs more experience' (Menth and Meyer [116]). Furthermore, Sun [173] claims that in many cases there is no clear physical interpretation. Nevertheless, these four load admittances are analytically derived for a controlled three-phase voltage source converter by Harnefors, et al. [74]. They are expressed in terms of initial power flow, filter inductance and controller bandwidths. Harnefors, et al. [74] further perform a stability study in which the Y_{dd} and Y_{qq} and their negative real values are emphasised. Belkhayat [19] derives stability criteria for three-phase systems based on a similar *dq*-approach, but concentrates on frequencies above the fundamental frequency. Huang, et al. [86] propose a method for the measurement of load input impedances in a single-phase system. A similar approach for the rotating reference system transfer function representation of a thyristor-controlled series capacitor is performed by Persson [141].

8.4.2.2 Example and interpretation

The vehicle input admittance for the enhanced RMS model is calculated by frequency scanning (see Section 8.3.2 for the principle). For the instantaneous value model, all the input admittances are calculated based on time simulations. Each oscillation frequency is investigated in the instantaneous value model by a quasi-stationary simulation for six seconds. A modulation of the source voltage $\vec{U}_{ac1}$ is performed by the use of Equation (3.21). The oscillation frequency f_{osc} is changed from 0 to 16 Hz by increments of ⅓ or 1 Hz and the current on voltage ration is found by use of Fast Fourier Transform (FFT). The method used in this calculation is described in Appendix A. As a matter of form, the corresponding input admittance in no-load is uncommented shown in Appendix F.

The frequency responses for the vehicle model in the present thesis have been calculated for all of the four input admittances representing the load in Figure 8-10. The following may be commented on:

- Y_{dd} represents the transfer function from a change in voltage amplitude to a change in current amplitude. The enhanced RMS model response corresponds to the Y calculated in Section 8.3.3. Both instantaneous value model and enhanced RMS model responses show the 180 degree phase shift given by the constant power load characteristic and further, the limited bandwidth of the active power control loop. The enhanced RMS model however is slightly better damped than the instantaneous value model, which is also observed in the comparison of time simulations performed in Section 5.6.3.

- Y_{qd} represents the transfer function from a change in voltage amplitude to a change in current phase. Its magnitude is low compared with Y_{dd}, although the differences between the instantaneous value model and the enhanced RMS model are noticeable. A dynamic discrepancy between the two models, for example, in a time simulation together with a rotary converter must thereby be expected. It is not known why they do not show equal phase at very low frequencies. One explanation for this is that maybe the correct phase is difficult to detect in an FFT analysis due to the low magnitude.

- Y_{dq} represents the transfer function from a change in voltage phase to a change in current amplitude, and its magnitude is in the same range as Y_{qd}. There are noticeable differences between the instantaneous value model and the enhanced RMS model. Hence, a dynamic discrepancy between the two models, e.g. in a time simulation together with a rotary converter must be expected. As the vehicle does not have any reference for the voltage phase angle, the input admittance phase at very low frequencies should therefore be zero.

- Y_{qq} represents the transfer function from a change in voltage phase to a change in current phase. The instantaneous value model and the enhanced RMS model responses correspond well. The vehicle does not have any reference for the absolute voltage phase angle; it synchronises the phase angle of the current according to the change in voltage phase angle by use of the PLL. Accordingly, the phase of Y_{qq} at very low frequencies should be zero as indicated by the step response test of the synchronisation system in Section 5.4.5. When the phase angle oscillation increases in frequency, the PLL angle lags the voltage angle it is supposed to track as studied in Section 7.4.1.4; this lagging can be seen in the phase response as a deviation from zero.

The interpretation of the complete double feedback loop system in Figure 8-10 is still an unsolved task. Even so, a qualitative judgement of each of the four isolated closed loops may be performed, i.e., assuming all other elements being zero, and when the source impedance is a line only:

- The loop given by $Y_{dd} \cdot Z_{dd}$ corresponds to the control loop studied in Section 8.2.5. This can result in a positive feedback due to the 180 degree phase shift in Y_{dd} given by the constant power load characteristic.

- The loop given by $Y_{qd} \cdot Z_{dq}$ can result in positive feedback depending on the sign of $\mathrm{Re}(Y_{qd})$. For the vehicle model here, the plot in Figure 8-10 indicates that this sign is not given, as in the frequency range of interest it may be approximately 90 degrees. $\mathrm{Re}(Z_{dq}) < 0$ as seen from Equation (8.19), so consequently, the loop's stability margins are reduced if $\mathrm{Re}(Y_{dq}) > 0$. This means that the stability margins are probably smaller for the instantaneous value model than for the enhanced RMS model.

- The loop given by $Y_{dq} \cdot Z_{qd}$ can result in positive feedback, depending on the sign of $\mathrm{Re}(Y_{dq})$. For the vehicle model here, the plot in Figure 8-10 indicates that this sign is not given, as in the frequency range of interest; it may be roughly 90 degrees. $\mathrm{Re}(Z_{qd}) > 0$ as seen from Equation (8.19) and as a consequence, the loop's stability margins are reduced if $\mathrm{Re}(Y_{dq}) < 0$. This means that the stability margins are probably larger for the instantaneous value model than for the enhanced RMS model.

- The loop given by $Y_{qq} \cdot Z_{qq}$ is not likely to contribute to instability, as both $\mathrm{Re}(Y_{qq})$ and $\mathrm{Re}(Z_{qq})$ are positive in the frequency range of interest.

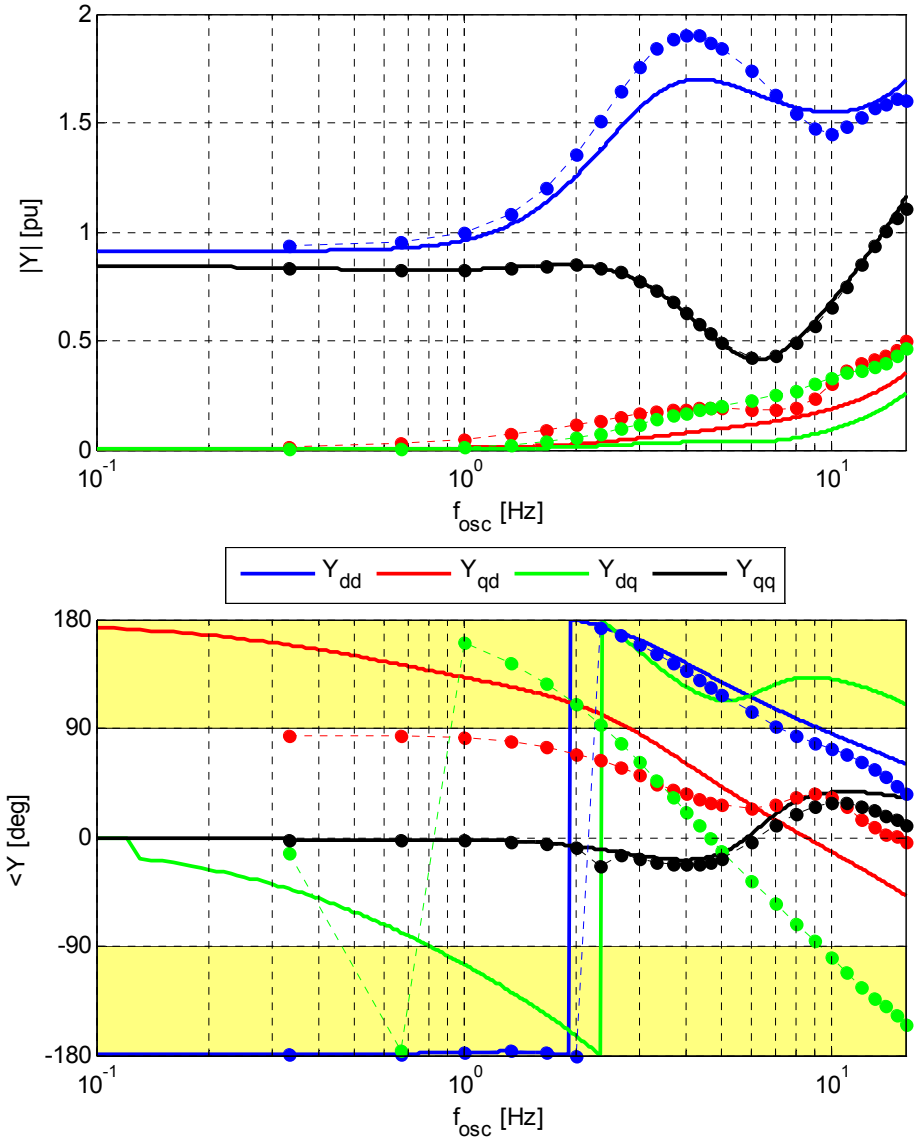

Figure 8-11: The full vehicle model input admittances in the rotating reference frame. Thick lines represents the enhanced RMS model, while the thin dotted lines with markers represent the instantaneous value model.

Since the vehicle input admittance cross couplings show a magnitude approximately one decade lower than the direct couplings, it is reasonable to believe that it is the direct-coupling loops which dominate the vehicles dynamic response. The *d*-axis loop has essentially positive feedback, while the *q*-axis loop shows essentially negative feedback. Hence, the *d*-axis direct loop will be the one that contributes the most to instability. The parallell loop given by $Y_{qd} \cdot Z_{dq}$ may have the most influence on the stability margins, and should therefore be focused on as the next step in further work.

A similar investigation with the full rotary converter model output impedance also remains for further study. It cannot be excluded that other loops and transfer functions than the '*dd*' as studied here have significantly influence on the closed loop stability.

8.5 Input admittance for a real-life vehicle

The input admittance of the real vehicle observed in Sections 6.5 and 7.5 are determined by real-time simulations (Eisele [64]; Buhrkall, et al. [34]; Danielsen, et al. [51]). The case is essentially equal to the calculations for the simulation model in Section 8.3 and 8.4.

The vehicle is directly supplied by a voltage source at 16.5 kV as shown in Figure 8-8, and this voltage source can be manipulated to create amplitude oscillations in the line voltage. The amplitude of the disturbance is 500 or 1000 V and the frequency step size is ⅓ Hz. The FFT analysis period is 3 s and a rectangular window is used. The vehicle is operating at full power (one DC-link only) at speed of 70 km/h.

The resulting input admittances are shown in Figure 8-12 for the three configurations introduced for the measured step-response in Figure 7-21, i.e., K_{POD} = [0.0, 0.1, 0.2].

At the rotary converter eigenfrequency (1.6 Hz), the original configuration without the POD shows negative input admittance. The admittance magnitude is increased roughly 20 % at 1.6 Hz compared with its magnitude at very low frequencies, but the real part of the input admittance is essentially unchanged. Increasing the oscillating frequency increases the admittance magnitude and introduces a shift in the phase response. This phase shift indicates an eigenfrequency in the 2-3-Hz range, while measurements in Section 6.5 are showing a 4-Hz oscillation. The motor DC-link voltage damping as studied in 6.2.3.2 may be a reason for this discrepancy.

Activating the POD with K_{POD} = 0.1 essentially neutralises the input admittance at 1.6 Hz due to an almost zero magnitude. Increasing to K_{POD} = 0.2 results in a positive input admittance. This behaviour is essentially confirmed by the step-response measurements in Section 7.5.

At the vehicle's DC-link controller eigenmode itself at 2-4 Hz, the amplitude of the input impedance is reduced when the POD is used compared to without POD.

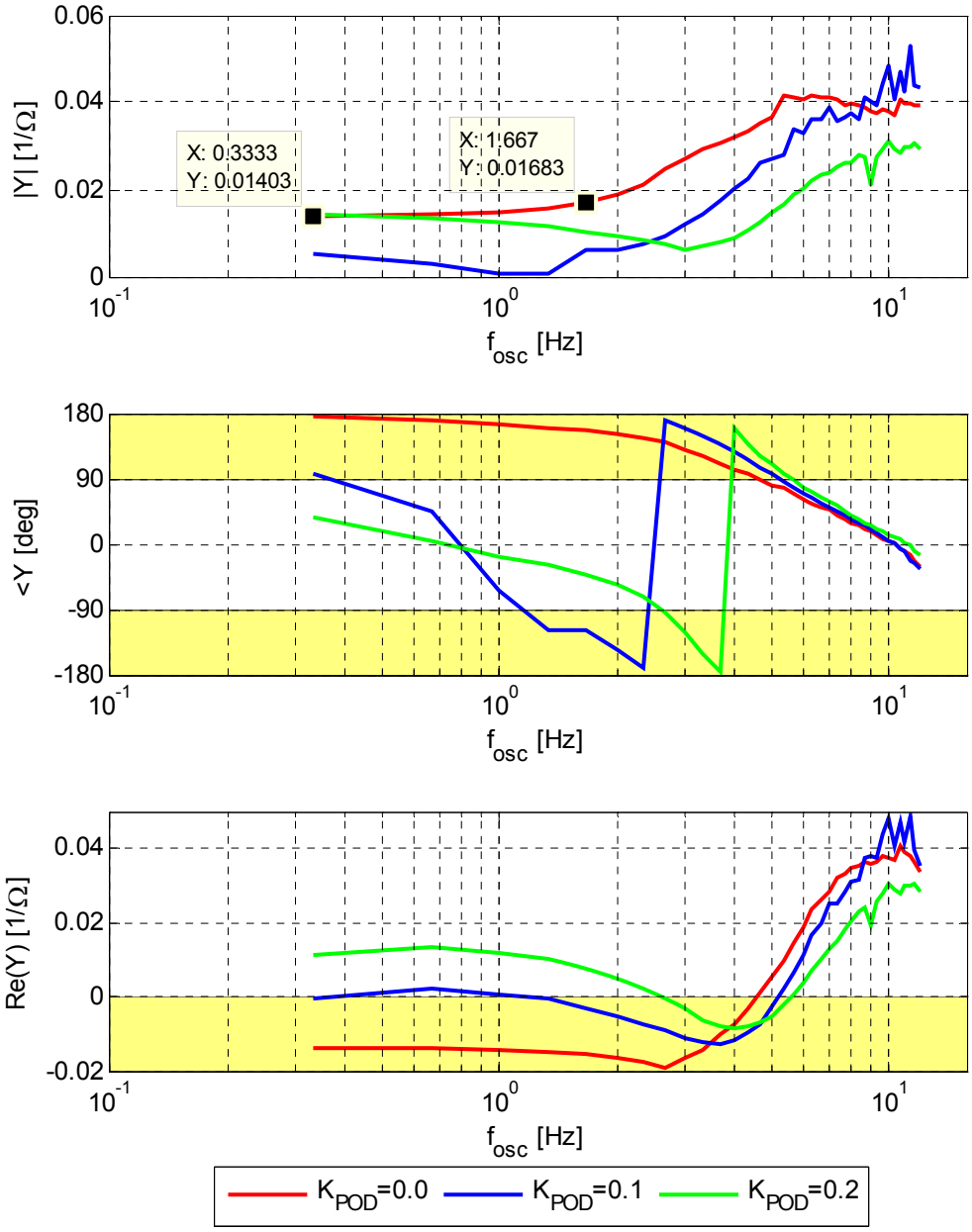

Figure 8-12: The calculated input admittances for a real vehicle based on real-time simulations.

8.6 Discussion and conclusion

8.6.1 Discussion

8.6.1.1 Analytical simplifications

This chapter introductorily investigates and discusses the usefulness of input admittance and output impedance considerations for low-frequency stability studies. The initial and analytical considerations are based on the second-order rotary converter and vehicle models that are developed in previous chapters of this thesis. These considerations are supported by physical explanations and the results are compared with previously performed time simulations. This is believed to be sufficient for understanding the basics of the impact from the constant power load behaviour on the converter oscillations.

On the other side, the analytical considerations performed imply several simplifications and hence have limitations. They only take into account active power changes during voltage amplitude modulation. The fact that the rotary converter oscillations result in frequency/phase modulation of the voltage is not included. In addition, the reactive power flow and inductive voltage drop ($j\omega_s L$) are not considered at all. Studies in previous chapters of this thesis show that both phase modulation and reactive power and voltage drop indeed have an influence on stability margins. Here, these phenomena are sacrificed as a first step in understanding what is believed to be the main driving force for instability. Further work should also include these phenomena.

The choice of this degree of simplification also makes the interface between the power supply and vehicle non-consistent compared to the definition in Figure 8-1. This means that it is chosen to include the vehicle transformer impedance in the power supply impedance and locate the interface at the line-inverter AC terminals where there is also a reactive power exchange. Alternatively, the expression for vehicle input admittance would have been more complex. This further reduces the accuracy of simplified calculations in present chapter.

It is important to note, that despite of the above simplifications, the system must be treated as an AC system when the initial conditions are calculated, i.e., by use of the complex AC system equations in Chapter 4. The simplifications only apply to the dynamical stability considerations as discussed in Sections 4.4.2 and 6.2.6.

For the complete vehicle model, however, the interface is according to Figure 8-1 and all calculations are performed with the complex AC system equations.

8.6.1.2 Stability criterion and considerations

Several of the simplifcations of the approach used for the analytical considerations are transferred to the study of the full vehicle model as well. The most important simplification is how the interface between the rotary converter and the rail vehicle is defined. Here, only the amplitude of the line voltage and current has been emphasised

and voltage and current are assumed to be in phase, i.e., there is no reactive power flow or oscillation. Is this sufficient for stability considerations?

Even if the stability criterion and the corresponding influence from the vehicle are easy to understand, this interface is not sufficient for a complete description of the interaction. When focusing on the active power exchange, the calculated input admittance frequency responses for the full vehicle model are plausible, i.e., the original parameters and POD1a and –b. But when the interaction tends to be more complex, such as for the improved parameters of the PLL and the reactive power modulation by POD2, the calculated input admittance fails to reflect the time simulations and the linear analysis of the full system. The simplified input admittance, $Y=\Delta I/\Delta U$, shows, despite of being a practical and useful characteristic (Buhrkall, et al. [35]), to be not precise enough and can therefore not be used in detailed stability studies.

On the other hand, this simplified input admittance describing the constant power load is still believed to be important. It is one of four input admittances proposed by Menth and Meyer [116] for AC system studies, and is an approach that is proposed by several others as well. Parts of the calculated four input admittances for the vehicle model developed in this thesis can be recognised in the analytical expressions developed by Harnefors, et al. [74]. And still, this simple input admittance is the only one which obviously leads to a positive feedback loop and violates the stability criterion. It could be, as indicated in Section 8.4.2.2, that a stability criterion has to be developed for each of the three other input admittances as well or one overall criterion for the complete double feedback loop system.

In general as a first approach, it might be of interest to distinguish between a qualitative criterion and a quantitative criterion. The open loop transfer function shows 180 degrees phase shift at the frequency where the rotary converter reveals poor damping. Consequently, the gain margin is small as indicated in Figure 8-7.

- The quality is related to the phase of the open loop transfer function which is given by the sign of the vehicle input admittance. The sign of the real part of the vehicle's input admittance tells *if* the qualitative stability criterion as suggested in Equation (8.3) is violated or not.
- The quantitative requirement may be interpreted as the magnitude of the admittance's real part which in this case results in the small gain margin. This magnitude tells *how much* the vehicle influences the stability given the quality discussed in above.
- A zero-valued real part may however be considered as either of the two above since neutral is also an important quality.

This quantity is often considered since the qualitative aspect might be too restrictive, resulting in stability margins that are too large and expencive (Sudhoff, et al. [172]). In the given traction power system, however, the rail vehicle is supposed to operate under a wide variation in conditions. From the considerations in Section 8.2.5 it is shown that the vehicle's operation point (power consumption, line voltage level and distance to the rotary converter) has large influence on the gain margin. Hence, a finite quantitative

requirement for the input admittance may be difficult to establish without limiting the range of operation.

If a qualitative requirement is generally satisfied, any quantitative change due to operating conditions is of minor importance, and the system becomes more robust. Thus, it is of interest to further investigate how much the dynamics of the vehicle changes under different operating conditions, i.e., how non-linear the vehicle is.

In the limited number of simulation model cases investigated in this thesis, there has not been any case observed in which the input admittance stability criterion is satisfied but where the system is unstable. In Section it 9.1.3 will be further discussed if this criterion is necessary or sufficient. As the power system (rotary converter) has some damping itself that increases stability margins, it is not given that every violation of the criterion results in an unstable system.

8.6.2 Conclusion

Based on the simple second-order models developed for the rotary converter and rail vehicle previously in this thesis, the basics of the vehicle constant power load influence on low-frequency stability are studied and discussed. The constant power load characteristic of an electric load generally reduces stability margins as it leads to a positive feedback loop. This characteristic can be described by a negative input admittance that increases in value as both power consumption increases and line voltage decreases. Moreover, the vehicle low-frequency eigenmode caused by the DC-link voltage control loop worsens this situation further by increasing this negative input admittance.

In a similar manner, stability margins decrease when the power supply becomes weaker, i.e., shows larger output impedance given by the impedance between the ideal voltage source and the interface to the rail vehicle. The poorly damped rotary converter electromechanical eigenmode adds an additonal resistance peak to the power supply output impedance at 1.6 Hz. This makes the system prone to instability at that specific frequency.

These analytical considerations are suitable for explanation of the basics of the instability phenomenon. An input admittance criterion is proposed based on assumptions when considering the amplitude of the AC voltage and current only. This criterion is also tested for the detailed vehicle model in present thesis. It is experienced that the vehicle may be stable, together with the rotary converter, despite a violation of this criterion. In spite of quantitative discrepancies, the qualitative damping impact of the vehicle models with active power oscillation damper is reflected by this input admittance. However, the simplified input admittance consideration fails when reactive power and frequency/phase modulation are taken into account.

These latter phenomena are attributes of AC systems and is in Chapter 7 shown to influence the stability margins. It is important to derive a qualitative input admittance

criterion that is also takes all the AC system phenomena into account. Such a work remains to be completed.

8.6.3 Further work

Based on the work presented in this chapter, the following topics for further study are proposed:

- It is of importance to understand and take into consideration the impact of reactive power, inductive voltage drop and frequency/phase modulation. Therefore more advanced methodologies for stability investigations for AC power systems are proposed and should be followed up on. It is in that context also of interest to understand if and how the power supply and vehicle transformer reactance $X = \omega_s L$ (in the cross couplings of Equation (8.19)) should be taken into account in Equations (8.15) and (8.16), which as presented in this thesis only include the resistance R. This is may be of even larger importance in networks with higher X/R ratio, e.g. 25-kV 50-Hz systems.

- It is especially of interest to attain an understanding of how the two coupled feedback loops in Figure 8-10 influence each other. Is it sufficient to treat each control loop in isolation as in Section 8.4.2.2, or is it necessary to consider all four at the same time?

- In order to gain deeper understanding of the four input admittances in the rotating reference frame, it is of interest to investigate if they could be expressed analytically for a rail vehicle in a similar way as they are derived for a three-phase voltage source converter by Harnefors, et al. [74]. These expressions could may be used understand how the input admittances change under different operating conditions.

- To complete the closed control loop system shown in Figure 8-10, the output impedance from the rotary converter should be established. Once this has been accomplished, then the possible qualitative and quantitative influence by the control loops other than $Y_{dd} \cdot Z_{dd}$ can be investigated. The operating point's influence on the rotary converter output impedance should be investigated more in detail. Ideally, the operating point for both source and load should correspond in the interface between them when the stability of the complete system is performed. A further question is: Does the load model used for establishing the rotary converter output impedance influence on the result?

- Based on the required understanding mentioned above is it necessary to create stability criteria and a methodology for low-frequency stability investigations of AC traction power systems. This means a system with more than one source and one vehicle as studied in this thesis. The vehicles should preferably be represented by black boxes that reflect the vehicles' dynamical characteristics, e.g. by input admittances. Hence, a format of data exchange is needed as well,

and a method for the measurement/verification of real vehicles' low-frequency input admittances should be developed.

- In a longer perspective, if small-signal instability is sufficiently treated by such input admittance considerations, it could be of interest to investigate whether large-signal instability can be treated in the same way, which means that possible discontinuous controllers, such as line power limitation functions in rail vehicles, can be included in the analysis.

9 Discussion and conclusion

This chapter includes a discussion of the results obtained in the previous chapters and presents answers to the research questions, conclusions and suggestions for further work.

9.1 Discussion

This section includes a discussion of the overall results gained and the methodology and approach used in the present thesis. More detailed discussions of specific phenomena, models and results are found in their respective chapters.

9.1.1 Relevance of system modelling

9.1.1.1 In this thesis

In this thesis, it has been chosen to study the experienced low-frequency oscillations and instability from a traditional power system point of view. This includes modelling in a rotating reference frame, linearisation and eigenvalue analysis. The rotating reference frame is closely connected to three-phase systems in which transform to and from the stationary reference frame can be done at any instant. In a single-phase system, an instant transform from a stationary to rotating reference frame is not possible. An orthogonal phase has to be artificially created, and the averaging of voltages and currents over a fundamental frequency period is needed.

Rotating reference frame modelling for single-phase systems thus represents a simplification and adaptation to three-phase systems. The second-harmonic power pulsation due to time-variant power availability is filtered. There are also control system components that work on the instantaneous values of voltage and current, e.g. the AC voltage and current measurements. Representation of these in the rotating reference frame imply simplifications as well, though these simplifications have shown to have only minor influence when the rail vehicle was studied supplied from an ideal voltage source via a line. Hence, it is reasonable to conclude that the main reason for the observed instability is caused essentially by time-invariant phenomena. Harmonics and time-variant power availability must however be taken into consideration when the vehicle model is designed, e.g. the controller's and measurement's bandwidths, so its basis is grounded in reality for single-phase systems.

These simplifications into a rotating reference frame give several benefits. It is possible to utilise tools, such as linear analysis, which are not commonly available for single-phase instantaneous-value systems. In addition, both amplitude and phase of voltages

and currents are directly accessible without measurment filters. In that way, it is possible to observe the quantitative impact of filtering components in the frequency range of interest, for example the impact of the phase-locked loop. It is also possible to compare vehicle dynamic behaviour to ideal constant power loads without dynamics, though such a load does not exist in a single-phase instantaneous-value system.

From a power system point of view, vehicle models in rotating reference frame would hence be of desire when studying low-frequency oscillations and instability, although the power system analyst normally has no access to detailed information concerning specific vehicles to make such models. This is further discussed in Section 9.1.5. The vehicle manufactures, however, use detailed real-time simulations which ensure inclusion of most of the relevant non-linear and discontinuous phenomena. One such phenomenon is the activation and deactivation of limiters. Such limiters are not included in the studies covered by the present thesis and are impossible to treat with linearisation as used here.

In the present study, the system which contains both the vehicle and the rotary converter is studied in the rotating reference frame only. Proposals for improved stability have been made, both by tuning of the vehicle model's controllers and by additional active damping controllers. The proposals are not tested in a real single-phase system to prove that they actually operate. In order to test the proposals, an instantaneous value model of a single-phase synchronous generator is needed. The input admittance comparison between the instantaneous value model and the enhanced RMS model in Section 8.4.2.2 shows differences in the frequency responses and hence different dynamical behaviour between these two different models must be expected. How large this difference will be and how it will influence the proposed improvements is however not known. One of the proposed power oscillation dampers has however been tested on a real vehicle with the expected results.

It has been shown in the present thesis that the traditional way of power system modelling for low-frequency oscillation studies is insufficient. The closed current control loop given by the vehicle current controller and the network impedance has to be taken into account in order to correctly represent the instability phenomena, which has been considered in the enhanced RMS model. The most obvious illustration of this is the long line stability test in Section 5.7, with another example being the influence of the PLL. In Section 7.4.1.4, it was proposed that the PLL in enhanced RMS modelling damps the rotary converter oscillations due to active power flow. In contrast, it was proposed in Section 7.6 how the PLL damps the same oscillations due to reactive power flow when the same case is modelled in standard RMS without this inner and closed current control loop.

9.1.1.2 In the future

Even if real-time simulations are probably the most accurate method, such an approach is presumed not to be usable for large power systems. Today's real-time simulators commonly include one vehicle of one type only. Furthermore, the inner details of a vehicle are commonly kept as a company secret by the manufacturer. A simulation

study with several different vehicle types from different manufacturers that are physically modelled is thus not feasible. Therefore a method has to be developed for future AC traction power system low-frequency stability studies.

A more common way to study such interaction phenomena in electric traction power systems is due to the above reasons the use of black-box representation. One such approach for low-frequency dynamics is proposed by Menth and Meyer [116]. This method implies the numerical linearisation of the vehicle into the rotating reference frame taking the present non-linear phenomena at the specific operating point into account. From the point of view of modelling of traditional three-phase power systems, this complex *dq* decomposition represents interesting features. First, these four input admittances are easy to calculate if a physical model in the rotating reference frame already exists. For principal studies, these admittances can then be obtained faster by linear analysis than with several time consuming real-time simulations including post-processing. Second, such a black box might replace a physical vehicle model in a power system study, as the proposed approach corresponds to the common way of power system modelling. For example, this has been tested for a thyristor controlled series capacitor by Persson [141] with promising results. This proposed methodology should be topic for further research.

The damping of the rotary converter covered by this study is poor, acheiving only a 3 % damping ratio in no-load. The stability margins are small and hence accurate models are needed to estimate the condition of the power system in detail. It may be difficult to find a method that is both accurate and feasible at the same time and thus it is of importance to find a qualitative and robust stability criterion as will be discussed in Section 9.1.3.

9.1.2 Relevance of developed vehicle model

A large part of this thesis is about the development of an advanced electric rail vehicle simulation model. This model is based on what is believed to be a typical state-of-the-art structure. Several resources, including text books, support the understanding of the main components, which includes the motor-side and line-side converters connected back-to-back by the intermediate DC-link. The use of a DC-link voltage proportional-integral controller also seems common. Yet, when starting to study details of these, one might discover that there are several approaches and solutions that all have their advantages and disadvantages. When making a concrete model, choices between these have to be made, which changes the vehicle model from being general to being specific.

Thus, the question is: How transferable are the observations made for this particular vehicle model to any advanced electrical rail vehicle in general, i.e., to which extent does this model reflect the possible general dynamic behaviour of a real-life vehicle and what is model specific? All vehicles work under the same physical laws and with the same overall control objective. Time-variant electrical power has to be converted into mechanical power in order to move the train. As long as the main components and the main structure are common, the main behaviour should be expected to be common as well. This includes a constant power load behaviour at low frequencies and a low-frequency eigenmode. However, filtering time constants, disturbance feed-forward

solutions, control-loop bandwidths and tuning, damping of resonances and so on may differ due to different methods, conditions, constraints, designs, knowledge and solutions. Consequently, details in the dynamical behaviour will differ as well.

The parallel modelling of the vehicle in stationary and rotating reference frame has introduced some constraints. One requirement was that the chosen solutions had to be possible to implement in both frames with a reasonable amount of effort and in a way that can easily be compared. This was the reason for choosing the synchronous rotating current controller. It was also a weighty decision as to whether one should utilise the SOGI instead of a DFT, which is more commonly used for voltage and current measurement. The SOGI can be (and is here) given a bandwidth that is higher than the DFT. This has an influence on low-frequency dynamics, i.e., the voltage measurement by SOGI gives a 12 degree phase lag at 1.6 Hz, while the DFT based on half a fundamental-frequency period sliding delay, gives 17 degrees.

The simulation model's reactive power oscillation observed in Section 7.2 is essentially in phase with the line voltage and has a damping impact on the oscillations when fed from the rotary converter. Additionally, the investigations in Section 7.4.1.4 indicate that the phase lagging of the PLL also has a damping impact. This narrows the possible causes for the instability seen in the simulation model. The constant power load behaviour, together with the vehicle low-frequency active power control loop dynamics has, in this thesis, been pointed out as an important reason for the instability. The active power control loop clearly shows positive feedback.

This constant power load characteristic is supported by the negative input admittance calculated for the real vehicle in Section 8.5. The study of the developed model shows a similar instability phenomenon as reported in the literature and important similarities to the real vehicle tested have been found. Additionally, one proposed solution for improving stability (POD1b) has a corresponding positive impact on both the model and real-life vehicle at the rotary converter's eigenfrequency, even though the control system structures are known to be slightly different.

Comparing details in the time simulation comprising the rotary converter performed with the developed model to measurements on the real vehicle, however, reveals some similiarities and some differences. The active power and current oscillate in a similar way relative to the line voltage, but the reactive power oscillations are different. The detailed reason for the instability caused by the real vehicle may hence be different from the simulation model's, since the stability limit is reached at a much shorter line length in reality than in the simulation model. For the time being, there have not been published enough characteristics and measurement results to say what is typical low-frequency behaviour for an advanced electric rail vehicle and what is not. There has also not been found any other descriptions for reactive power control in the literature other than the solution that has been implemented in the developed simulation model.

One identified important reason for the instability are the bandwidths of the active and reactive power control loops. A possible lower bandwidth reduces the constant power

load behaviour of the vehicle and shifts the focus to other reasons for the observed instability. When the typical behaviour is known, it will be possible to better quantify the relevance of the developed model. Based on this, it can be then judged how much weight should be given to the proposed constant power load explanation.

The future development of vehicles will of course change the view of what a typical or state-of-the-art structure is. Heising, et al. [80] propose a multi-variable line-side converter control system without the conventional integral part of the DC-link voltage controller. Glinka and Marquardt [71] propose a multi-level line-side converter that eliminates the need for the DC-link second-harmonic resonance tank. Moreover, the semiconductors' switching frequency limits the bandwidth of the AC current control loop, but the development tends towards a higher switching frequency and hence this constraint is lifted. These developments might exert an influence on low-frequency vehicle behaviour.

9.1.3 Necessary or sufficient stability criterion

The vehicle line-side converter has two primary tasks: It shall keep the DC-link voltage at reference value independent of motor power, and it shall control the line-side power factor. The first task implies a constant power load behaviour that has been emphasised in this thesis. This behaviour, together with the low-frequency DC-link voltage control eigenmode, has been used to explain how the vehicle may result in an unstable system in conjunction with the rotary converter. Active power oscillation has been in focus and a simple and qualitative stability criterion is expressed as an input admittance requirement in Section 8.2.

It is shown in Chapter 8 that the stability criterion for the rotary converter is violated by both the simulation model and the real vehicle. It has also been observed that fulfilment of the criterion improves the system stability due to application of the power oscillation damper. This experience tells that a positive input admittance is advantageous for stability and support the basic theory in Chapter 3.

It is, however, reasonable to believe that the influence and importance of the reactive power oscillations and line voltage frequency/phase modulation are larger than what is experienced and emphasised in this thesis. Neither damping by use of the PLL nor by reactive power is reflected well by the simple input admittance studied as shown in Section 8.3. It is not quantified how much these qualities increase or decrease the stability margins of the system from the proposed input admittance only.

This is the reason for the double feedback loop approach proposed by Menth and Meyer [116] as described in Section 8.4, which intends to include both the constant power load behaviour and the mentioned additional phenomena. The necessity and sufficiency of the proposed input admittance criterion is difficult to say for sure, since only one single loop in the double feedback loop in Figure 8-10 is studied in present thesis. Consequently, more experience and investigations are needed to assert this safely.

If the simple input admittance criterion is not guaranteed to be sufficient and is also not shown to be necessary, it might be too stringent to use this as an absolute criterion for the acceptance of a vehicle in a network with rotary converters. On the other hand, this criterion is simple to understand and might be a good target for the design of the vehicle low-frequency behaviour anyway.

9.1.4 System stability in a wider perspective

The classic understanding of low-frequency oscillations as described in Section 2.4 is only related to the synchronous-machine power angle oscillations. Van Cutsem and Vournas [179] refer to the oscillations as being 'generator driven' while voltage stability is 'load driven', though they pointed out that there is not a clear separation between these two in the short term. In the case investigated in the present thesis, the rotary converter power angle oscillations are clearly load driven and results in voltage amplitude oscillations.

Kundur [106] extends the oscillatory power system instability to also include a 'control mode' associated with poorly tuned exciters, speed governors, HVDC converters and static VAR compensators. This control mode may include the vehicle mode being investigated in the present thesis.

It was explained in Chapter 2 that the use of controlled power electronics in railways increases, both on the vehicle and infrastructure side. This, however, is not only the case for railways, as a similar development can also be observed in other power systems. Sun [173] describes how an AC power system until recent years was:

> *'largely an electromechanical system where power was almost exclusively generated by large synchronous generators and mostly consumed by linear and passive loads (...). This, however, is changing rapidly in recent years due to the proliferation of renewable energy and distributed generation technologies on the source side, and energy-efficient technologies such as solid-state lightning and variable-speed drives on the load side. (...). As a result, there is a great demand for the understanding of stability (...) in AC power systems, as well as methodologies and tools that can be applied to analyse and integrate such complex systems.'*

Both the work performed and referred to in this thesis confirm that stability in power systems dominated by power electronic components represent a challenging topic. The load, here represented by the vehicle, indeed has low-frequency dynamic behaviour. It has been shown that the dynamic load is able make a power system low-frequency oscillatory unstable, together with a line and an ideal voltage source only. Together with the rotary converter, the load is able to reduce the system damping, resulting in instability at the converter's electromechanical eigenfrequency. Neither of these instability cases are easy to put in the class defined by Kundur, et al. [107], and are indeed load-driven. The constant power load characteristic is widely known as a cause for voltage instability, but not explicitly and previously expressed for low-frequency

oscillations in AC systems. The classification of power system (in)stability should be extended to include both load dynamics and constant power characteristics more clearly.

Despite similarities to other power systems regarding the introduction of power electronic solutions as previously mentioned, traction power systems may also be special. Most AC railways are single-phase systems. The time-variant electrical variables in such a system often require filtering. To a large extent, these filters' bandwidths are given by the system's fundamental frequency, and they all introduce dynamics in the same frequency area. In addition, the transmission of 5-15 MW via high impedance lines is rarely seen in other single-phase systems. The moving loads result in large and rapid changes in operating points for the system and operating conditions for the vehicles. For this reason, the vehicles must show a qualitatively robust behaviour for all interaction phenomena which is valid over the entire range of operating conditions.

On the other side, even if passive behaviour is found to be of advantage, it cannot be expected that a vehicle should show a positive real value of the input admittance for all frequencies. The input admittances calculated for the simulation model and for the real vehicle shows a negative real value for very low frequencies even when the active damping controller is applied. A long-term passive characteristic is not even seen on old tap-changer vehicles: If the voltage drops enough for power consumption to be reduced and the train's speed decreases, the locomotive driver simply compensates by changing the transformer step.

The experience gained from the power oscillation dampers (POD) designed in this thesis is that new dynamical behaviour is introduced on an even lower frequency. This means that the vehicle dynamics seen from the network are shifted down in frequency. Similar experience comes from work with electrical resonance instability as well: When a particular control is applied in order to act passive above the given frequency limit, i.e., 90 Hz in Norway and Sweden, dynamics and active behaviour may result directly below this frequency.

But does this shift of dynamics also imply that the observed instability problems in railway networks without rotary converters will be shifted down in frequency as well if all vehicles are equipped with such a POD? The improved design of power oscillation dampers should aim to make the transition between constant power load behaviour and neutral or damping smoother without such amplification below 1 Hz as shown in Figure 8-9 for the simulation model. Different damping algorithms should be coordinated with the rest of the control parameters. Saying that, it is in this thesis not investigated if such a POD even is a usable remedy in the other stability cases reported in Table 2-2, for example the 'depot problem'. Solving these instability problems is a task for the near future.

9.1.5 Available information

The development of the vehicle model in this thesis is mainly based on available literature resources such as text books and scientific papers. Put together, their fragmental contribution results in an open and complete vehicle model which can be studied and criticised. The model can be used for principal studies and as a stepping stone for further investigations.

None of these resources found discuss the complete vehicle in terms of low-frequency behaviour, which has several probable reasons. First, the low-frequency instability phenomena that occur are still young. Second, most of the development and research are performed inside the vehicle manufacturer's companies and not in universities. Control structures, solutions and so on are often treated as company secrets. And third, the number of engineers working within this technical field is limited, which has resulted in a scarcity of published material.

The lack of available information about complex power system components is not specifically a railway problem. Persson, et al. [144] describe difficulties experienced by a utility company in performing a stability analysis of their power system with windmills from various manufacturers. There is no standardisation of windmill models, details about the simulation models are normally not given and different default models in simulation software give different results and stability margins.

If a methodology for an impedance-based approach for system stability can be established, the need for detailed information about the system's components compared to a state-space approach can be reduced.

One disadvantage of the developed model is that there is always an uncertainty with regard to whether the model is representative enough or not as discussed in Section 9.1.2. For more detailed studies, it is recommended to work in closer collaboration with a vehicle manufacturer. But as power system stability is a result of several interacting components, openness about technical problems and solutions is important.

9.2 Answer to research questions

Four research questions were listed in Section 1.3.3. Next follows short answers to these questions as a summary of this work:

- *Is it possible to use traditional power system analysis tools and methods to study the low-frequency instability in traction power systems?*
  Yes, both time simulation and linear analysis of the developed vehicle model are able to reflect the experienced instability phenomena, though a condition is that the vehicle's current control loop dynamics have to be taken into account. This means that it is necessary to include both the network dynamics and vehicle current controller in the model. This loop is commonly neglected in traditional power system analysis. The usability of such state-space based methods is however in practice limited due to the available information about the rail

vehicles and the difficulties in exact representing some single-phase and time-variant components in the rotating reference frame.

- *How and what influences the synchronous-synchronous rotary frequency converter's low-frequency electromechanical swing equation?*
  The swing equation for a rotary converter is an extension of the similar equation for a single synchronous machine infinite bus system. The converter's motor is stiffer connected to the three-phase equivalent network than the generator is connected to the single-phase equivalent network since the three-phase network fundamental frequency is higher than the single-phase network frequency. Hence, it is the motor synchronising torque coefficient and damping that dominate the low-frequency electromechanical eigenmode.

- *How does an advanced rail vehicle work in view of the observed low-frequency instability?*
  Seen from the power supply, the vehicle controls the active and reactive power at its current collector to be constant for the given operating point. The vehicle shows a dominating eigenmode in the low-frequency range due to the state-of-the-art DC-link voltage control and bandwidth of measurement filters. The active power control may react on a low-frequency line voltage amplitude oscillation by controlling the current opposite. The vehicle's low-frequency dynamics may cause an amplification of the oscillation resulting in system instability or damp the oscillation depening on the configuration of the line-side converter control system. The study of reactive power control is a task for future.

- *How do input admittance considerations work in terms of low-frequency instability?*
  Together, the vehicle input admittance and power supply output impedance form a closed control loop. Due to the vehicle's objective to control the power independent of line voltage amplitude changes, its input admittance relative to the line current amplitude shows a negative real part that results in a positive feedback loop. This relation can be simply studied by considering the amplitude of voltage and currents only. In an AC system, however, there are several circumstances, such as phase angles and reactive power, that influence the stability margins and the final method for a complete analysis remains for further study.

9.3 Conclusions

In this thesis, stability in electric traction power systems has been studied. Reported cases of instability have been surveyed and discussed in view of traditional power system stability classification. The overall technical development generally introduces more and more power electronic components into power systems. This changes the characteristics of the power system and introduces new dynamical phenomena. Therefore, traditional power system stability classification have to be extended in order to include and categorise these new phenomena.

One such instability phenomenon is the low-frequency power oscillation observed in several different railway networks. A typical oscillation frequency is 10-30 % of the system's fundamental frequency. New advanced electric rail vehicles which utilise power electronic converters are an essential part in this phenomenon. The unstable interaction experienced between these vehicles and the poorly damped rotary frequency converters used for the electric traction power supply in Norway have been further focused on.

In order to acquire knowledge about this low-frequency oscillation phenomenon, a large part of this work has been to develop a simulation model of such a rail vehicle based on available resources. The model is thoroughly described and discussed in order to compensate for the limited amount of information available on this topic. The simulation model shows essentially similar dynamical behaviour and instability phenomena as reported from real railways. One condition though is that network and vehicle current dynamics are included in the model. This closed current control loop has a large influence on the stability margins, but is commonly neglected in traditional power system stability studies for this frequency range.

The low-frequency dynamics in such a traction power system are studied by use of a traditional power system time-invariant method. This includes state-space modelling in a rotating reference frame and performing a linear eigenvalue analysis together with time simulations. These methods have been found to yield useful insight into the basics of the vehicle model's low-frequency behaviour and its interaction with the rotary converter, though impedance-based methods may be more practically usable than state-space based methods. A comparison between a rotating reference system model and a stationary reference system model show essentially the same low-frequency behaviour. Even so, it is important to understand that such a rotating reference frame modelling of a single-phase system represents a simplification with fewer constraints and several phenomena neglected compared with real life.

Study of the developed model indicates that one important reason for instability in conjuction with the rotary converter is the vehicle's characteristic to control the active power to be constant independently of the supply voltage. In principle, this constant power load characteristic reduces the stability margins of the system. A vehicle low-frequency oscillatory eigenmode due to several time constants in the same range may reduce the margins even more. The dynamics of the DC-link voltage control loop is shown to be important in that respect.

These observations are supported by simplified basic analytical calculations such as dynamical impedance and admittance considerations. A constant power load characteristic basically results in a negative input admittance for the vehicle, which again results in a positive feedback loop. The stability margins are further reduced since the rotary converter electromechanical eigenmode results in a peak increase in the power supply output impedance and consequently increased loop gain at its eigenfrequency.

The poor system stability that has been experienced in both the simulation model and real life can be improved by reducing the constant power load behaviour of the vehicle at the rotary converter eigenfrequency. Such a characteristic can be reached by introducing a power oscillation damper function in the vehicle's control system. The damping impact of such a function is in principle verified by measurements on a real vehicle, though the proposed power oscillation dampers are shown in the simulation model to introduce new dynamics at lower frequencies.

As the vehicle model is based on fragments of information from different sources, it is appropriate to question its general validity. That includes the low-frequency dynamics and the proposed hypothesis regarding the main reason for system instability. An instantaneous value model of the rotary converter is at present missing, and obstructs study of the system interaction and proposed improvements in a real single-phase system.

9.4 Further work

There are still open questions that require further work within the field of low-frequency stability in traction power systems. In each chapter in present thesis, proposals for further work are given within the respective topic. See Sections 3.7.3, 5.8.3, 6.6.3, 7.7.3 and 8.6.3. Next follows the superior and main proposals for further work:

- The present work focuses mainly on the interaction between the electric rail vehicle and the rotary converter, but instability is experienced and described also in systems without this machines. It is not considered in detail whether the proposed vehicle input admittance stability criterion regarding the rotary converter's electromechanical eigenmode (Equation (8.3)) is also feasible for a system without such specific power supply resonances, i.e. where the low-frequency dynamics are dominated by the rail vehicles only. This dynamic may be caused by the vehicle itself or other vehicles in the system. And, will the instability when applying a POD, then, only be shifted to another frequency? It is important to address these questions in a further work. Furthermore, a deeper understanding of the 'depot problem' and possible remedies is needed.

- The present thesis focuses on the active power control of the vehicle. However, the results indicate that the reactive power flow may have a large influence on stability margins too. Further work is needed in order to understand how the reactive power in a vehicle is controlled and participates in low-frequency oscillations.

- Furthermore, it is necessary to study the tuning of the vehicles' different controllers in terms of low-frequency stability. The present thesis only considers one controller at a time, which may not result in the optimal global low-frequency behaviour. A global optimisation study of the vehicle should therefore be carried out. Trade-offs between stability and other performance requirements should be more clearly stated so it is known where possible contradictions are.

- Additionally, all damping algorithms have to be coordinated against each other as well as to the rest of the vehicle's control system. In the present thesis, it has been observed that active damping at one frequency may increase the dynamics on another frequency, and that different damping algorithms may influence each other in an unfavourable way.

- The focus of the present thesis has been on the vehicle in no-load or power consumption (traction) mode only, as this is the basic operating mode in which most instability is experienced. A further study of the dynamical behaviour in regenerative braking mode should also be carried out. Different outer control loops (open or closed) such as reactive power compensation and line power limitation may exert an influence on dynamical behaviour. Such operating modes are common in weak networks in which the stability margins are already small and should be addressed in further work.

- The traditional state-space approach to study small-signal low-frequency stability in power system is difficult to apply to the complex single-phase power electronic components in practice. Therefore an impedance-based approach for more detailed analysis should be developed. The input admittance considerations in the present thesis simplify the AC system by only taking the voltage and current amplitudes into account. This approach is insufficient for more detailed stability investigations of the complex AC system. Frequency domain methods for AC systems are proposed by Menth and Meyer [116] and Pröls and Strobl [148], and it is recommended to continue with further work in this direction. Specifically, the understanding of how a reactive power and inductive voltage drop can be included in the analysis is of importance as a first step. Further, the influence from the phase oscillations has to be taken into consideration. This need is valid for all operating modes and the control system tunings mentioned above. This work should include both development and an understanding of the method, the establishment of stability criterion/criteria, and agreement on a format for information exchange.

- If the AC system frequency domain *dq* approach is widely understood and accepted, a method for the representation of the vehicle as a black box in traditional power system analysis software should be developed. The black box should include the four frequency responses that are intended to describe the vehicle's low-frequency dynamics. Persson [141] proposes and thoroughly describes in this context an approach that is of interest and has shown good results. This approach is temporarily adapted and suggested for an electric rail vehicle and shown in Figure 9-1 based on the vehicle model sketched in Figure 8-1. The vehicle is divided into a steady-state model (for example Equation (8.5)) and a linear dynamical model (for example $\boldsymbol{Y}_{load}$ in Figure 8-10) by low-pass filters. The Park's transform and its inverse are used for transforming phasors from the power system global rotating (*DQ*) reference system to the vehicle specific rotating (*dq*) reference system and vice versa. Unfortunately, the

study of this idea is not completed within the present thesis. If an electric vehicle is modelled by this approach in a complete system, perhaps use of linear analysis, such as in present thesis, can help understanding of the four transfer functions and how each of them interact with the rest of the system. It is however still an open question whether the non-linearity of the vehicle will limit the validity of one set of such frequency responses or if several sets at different operating points are needed. Further studies regarding this should also address the matter of necessity of including the $L \cdot di/dt$ voltage term in the rest of the power system model.

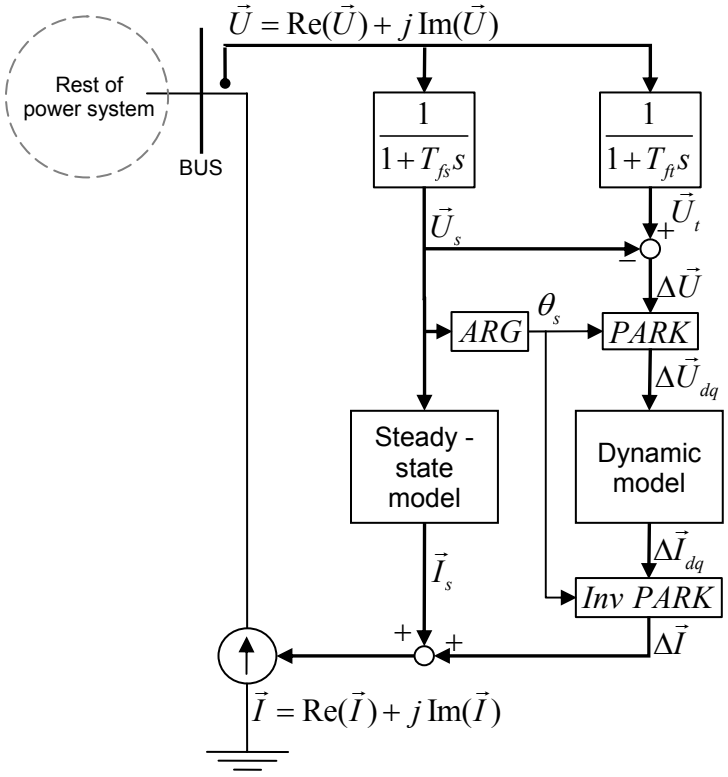

Figure 9-1: A temporarily adapted interface for the black box-modelling of an electric rail vehicle in power system studies. Subscript 's' denotes steady-state voltage and current while subscrip 't' denotes transient voltage and current. All signals are phasors except the phase angle θ_s.

- Further, if or when the theory for stability analysis of AC power system by frequency response representation as introduced above proves useful, methods for determining the vehicle input admittance and power supply output impedance from real-life measurements should be developed. Huang, et al. [86] may be useful in that context.

- The present thesis focuses on the interaction between electric rail vehicles and the synchronous-synchronous motor-generator sets. Increase in number of static frequency converters must however be expected in future. Low-frequency

oscillations in traction power systems fed by static frequency converters has also been observed (Meyer and Thoma [124]), which should be included in further studies. In this respect, also any implemented current limiter should be considered since they may influence the output voltage from the converter.

- Modelling in the rotating reference frame implies simplifications for single-phase systems. In order to check the validity of rotating reference frame model simulations in present thesis and how realistic the proposed improvements are, an instantaneous value model of the rotary converter should be developed. Such a model will be useful for the vehicle manufacturers as a basis for implementation of a more accurate power system infrastructure model in their vehicle real-time simulators.

- The classification of power system (in)stability should be extended to include both load dynamics and constant power characteristics more clearly.

10 References

[1] IEEE Std 421.5 - 2005 IEEE Recommended Practice for Excitation System Models for Power System Stability Studies, *IEEE Std 421.5-2005 (Revision of IEEE Std 421.5-1992)*. pp. 0_1-85, 2006.

[2] Rätselhafte Lokomotivstörungen im Raum Zürich, *Schweizer Eisenbahn-Revue*. 5 1995.

[3] *Simpow User Manual*, STRI AB, Ludvika, 2004.

[4] A. Abelsen, S. Bekkevold and T. Stensvold, Tough trains treaten the power supply (Original title in Norwegian: Tøffe tog truer kjørestrømmen), *Teknisk Ukeblad*. 145 (31), pp. 10-12, 1998.

[5] M. A. Abido, Analysis and assessment of STATCOM-based damping stabilizers for power system stability enhancement, *Electric Power Systems Research*. 73 (2005) pp. 177-185, 2004.

[6] M. E. Aboul-Ela, A. A. Sallam, J. D. Mccalley and A. A. Fouad, Damping controller design for power system oscillations using global signals, *Power Systems, IEEE Transactions on*. 11 (2), pp. 767-773, 1996.

[7] L. Abrahamsson, Railway Power Supply Models and Methods for Long-term Investment Analysis, Licentiate thesis, Department of Electrical Engineering, Royal Institute of Technology, 2008.

[8] M. Aeberhard, J. Duron, M. Lörtscher and M. Meyer, Stabilitätsundersuchungen im 132-kV-Netz der SBB, *Elektrische Bahnen*. 107 (6), pp. 267-273, 2009.

[9] M. Aeberhard and M. Lörtscher, Nachweis der mittleren nutzbaren Spannung auf der NBS Mattstetten - Rothrist, *Elektrische Bahnen*. 105 (1-2), pp. 62-66, 2007.

[10] E. Andersson, M. Berg and S. Stichel, *Rail vehicle's dynamics (Original title in Swedish: Spårfordons dynamik)*, Stockholm, Sweden, 2002.

[11] P. M. Andersson and A. A. Fouad, *Power System Stability and Control*, The Iowa State University Press, 1977.

[12] P. Appun and W. Lienau, Der Vierquadrantsteller bei induktivem und kapazitivem Betrieb, *EtzArchiv*. 6 (1984), pp. 3-8, 1984.

[13] B. Aschenbrenner, Verification and extension of a linear model of a rotary converter, Master thesis, Dept. of Engineering Cybernetics, Norwegian University of Science and Technology, 2007.

[14] H. Y. Assefa, S. Danielsen and M. Molinas, Impact of PWM switching on modeling of low frequency power oscillation in electrical rail vehicle. *Power Electronics and Applications, 2009. EPE '09. 13th European Conference on*. pp. 1-9, 2009.

[15] C. Bajracharya, M. Molinas, J. A. Suul and T. M. Undeland, Understanding tuning techniques of converter controllers for VSC-HVDC. *NORPIE*. Helsinki, Finland, 2008.

[16] M.-M. Bakran, A power electronics view on rail transportation applications. *Power Electronics and Applications, 2009. EPE '09. 13th European Conference on*. pp. 1-7, 2009.

[17] Banverket/Jernbaneverket, Requirements on rolling stock in Norway and Sweden regarding EMC with the electrical infrastructure and coordination with the power supply and other vehicles (BVS 543.19300/JD 590), 2007

[18] R. Bartelt, C. Heising, V. Staudt and A. Steimel, PLL and DFT feed-forward control for railway single-phase line-converter synchronisation. *Compatibility and Power Electronics, 2009. CPE '09.* pp. 217-223, 2009.

[19] M. Belkhayat, Stability criteria for AC power systems with regulated loads PhD thesis, Purdue University, 1997.

[20] P. Berggren, Synchronous condenser utilizes redundant equipment (Original title in Swedish: Synkronkompensator utnyttjar övertallig utrustning) *Tåg (Magazine for Swedish Railway Club)*. (2/08), 2008.

[21] R. E. Best, *Phase-Locked Loops: Design, Simulation and Applications*, Mc Graw Hill, 2007.

[22] N. Biedermannn, Criteria for the voltage in railway power supply systems, Master degree thesis, School of Electrical Engineering, KTH Royal Institute of Technology, 2010.

[23] H. Biesenack, Parallellbetrieb mit Synchron-Synchron-Umformern, *Deutsche Eisenbahntecknick*. 18 (2), pp. 82-83, 1970.

[24] H. Biesenack, Theorie und Betriebsverhalten von Synchron-Synchron-Umformern, Doktor Ingenieur thesis, Fakultät für Technik und Naturwissenschaft, Hochschule für Verkehrswesen 'Friedrich List', 1972.

[25] H. Biesenack and P. Schmidt, Die dezentrale Bahnenergieversorgung von 16 2/3-Hz-Einphasen-wechselstrombahnen über Synchron-Synchorn-Umformer, *Elektrische Bahnen*. 89 (11), 178-181, 1991.

[26] G. Bizjak, P. Zunko, E. Lerch and P. Zaherdoust, Use of rotating frequency converter in industrial networks-digital simulation study. *Stockholm Power Tech International Symposium on Electric Power Engineering*. pp. 414-19 vol.3, 1995.

[27] P. E. Bjorklund, K. Srivastava and W. Quaintance, Hvdc Light® Modeling for Dynamic Performance Analysis. *Power Systems Conference and Exposition, 2006. PSCE '06. 2006 IEEE PES*. pp. 871-876, 2006.

[28] C. S. Blacutts, L. Abrahamsson and T. Schütte, Bahnenergie-Primärerzeugung 16 2/3 Hz in Norwegen und Schweden, *Elektrische Bahnen*. 108 (1-2), pp. 80-85, 2010.

[29] T. J. Blalock, The frequency changer era-interconnecting systems of varying cycles, *Power and Energy Magazine, IEEE*. 1 (5), pp. 72-79, 2003.

[30] K. Bonfert, *Betriebsverhalten der Synchronmachine - Verhalten im Normalbetrieb und bei Störungen: Näherungen für die Praxis Zweiachsenteorie*, Springer-Verlag, Berlin/Göttingen/Heidelberg, 1962.

[31] B. Brogliato, R. Lozano, B. Maschke and O. Egeland, *Dissipative Systems Analysis and Control - Theory and Applications*, Springer-Verlag London, 2007.

[32] L. Buhrkall, AC Line Power Oscillations - Current and Power in the Time and the Frequency Domains, 2005-05-03 Available from Internet:http://www.buhrkall.dk/Power%20Oscillation%20In%20Time%20And%20Frequency%20Domain.pdf, Accessed at 2009-07-01, Published by L. Buhrkall Freelance Electrical Engineer

[33] L. Buhrkall, Traction system case study, Revision 7, 2004-09-13 Available from Internet:http://www.buhrkall.dk/Buhrkall%20L%20-%20Traction%20System%20Case%20Study%20rev.%207.pdf, Accessed at 2009-11-14, Published by L. Buhrkall Freelance Electrical Engineer

[34] L. Buhrkall, S. Danielsen, A. Eisele, M. Bergman and J. Galic, Low-frequency oscillations in the Scandinavian railway power supply - Part 1: Basic considerations, *Elektrische Bahnen*. 108 (1-2), pp. 56-64, 2010.

[35] L. Buhrkall, S. Danielsen, A. Eisele, M. Bergman and J. Galic, Low-frequency oscillations in the Scandinavian railway power supply - Part 2: Tests of traction units, *Elektrische Bahnen*. 108 (3), Accepted for publication 2010.

[36] E. J. Burnham, Application of Large Frequency Converters to Power Systems, *Journal of the American Institute of Electrical Engineers (continuation of Proceedings of the American Institute of Electrical Engineers)*. 47 (Oct 1928), pp. 744-748, 1928.

[37] B. Busco, P. Marino, M. Porzio, R. Schiavo and F. Vasca, Digital control and simulation for power electronic apparatus in dual voltage railway locomotive, *Power Electronics, IEEE Transactions on*. 18 (5), pp. 1146-1157, 2003.

[38] S. Buso and P. Mattavelli, *Digital Control in Power Electronics*, Morgan and Claypool publishers, 2009.

[39] A. Bülund, P. Deutschmann and B. Lindahl, Schaltungsaufbau im Oberleitungsnetz der schwedischen Eisenbahn Banverket *Elektrische Bahnen*. 102 (4), pp. 184-194, 2004.

[40] Cenelec, EN 50163 Railway applications - Supply voltages of traction systems, 2004

[41] Cenelec, EN 50388 Railway applications - Power supply and rolling stock - Technical criteria for the coordination between power supply (substation) and rolling stock to achieve interoperability, 2005

[42] M. Chen and J. Sun, Low-Frequency Input Impedance Models for Boost Single-Phase PFC Converters. *Power Electronics Specialists Conference, 2005. PESC '05. IEEE 36th*. pp. 1062-1068, 2005.

[43] M. Ciobotaru, R. Teodorescu and B. Blaabjerg, Improved PLL structures for single-phase grid converters. *PELINCEC'05*. Paper ID 106, 2005.

[44] M. Ciobotaru, R. Teodorescu and B. Blaabjerg, A New Single-Phase PLL Structure Based on Second Order Generalized Integrator. *PESC 2006*. Jeju, Korea, pp. 1511-1516, 2006.

[45] C. Courtois, E. Carpentier, D. Frugier and P. Mannevy, Low frequency instability and oscillation in French Railway Network. *Interaction Workshop 2009*. Thun, Switzerland, 2009.

[46] O. G. C. Dahl, *Electric Power Circuits, Theory and Applications - Volume II Power System Stability*, McGraw-Hill Book Company, Inc., New York and London, 1938.

[47] P. Dahler, G. Knapp and A. Nold, New generation of compact low voltage IGBT converter for traction applications. *Power Electronics and Applications, 2005 European Conference on*. pp.-P.9, 2005.

[48] S. Danielsen, Interaction between a synchronous-synchronous rotary frequency converter and surrounding grids. Document number 200703701-3X at Norwegian National Rail Adminitration (Jernbaneverket), Oslo, Norway, 2009.

[49] S. Danielsen, Low-frequency instability and oscillations in railway power systems. *Interaction Workshop 2009*. Thun, Switzerland, 2009.

[50] S. Danielsen, Vehicle related low frequency oscillations in the Norwegian rail traction power system with rotating converters. *Interaction Workshop 2006*. Thun, Switzerland, 2006.

[51] S. Danielsen, A. Eisele and L. Buhrkall, Report from LFSTAB tests at Hønefoss-Nesbyen with ... 2009-04-25/26. Document number 200800495-16X (Restricted) at Norwegian National Rail Administration (Jernbaneverket), Oslo, Norway, 2009.

[52] S. Danielsen, O. B. Fosso, M. Molinas, J. A. Suul and T. Toftevaag, Simplified models of a single-phase power electronic inverter for railway power system stability analysis – development and evaluation, *Electric Power System Research*. 80 (2), pp. 204-214, 2010.

[53] S. Danielsen, O. B. Fosso and T. Toftevaag, Use of participation factors and parameter sensitivities in study and improvement of low-frequency stability between electrical rail vehicle and power supply. *Power Electronics and Applications, 2009. EPE '09. 13th European Conference on*. pp. 1-10, 2009.

[54] S. Danielsen, M. Molinas, T. Toftevaag and O. B. Fosso, Constant Power Load Characteristic's Influence On The Low-Frequency Interaction Between Advanced Electrical Rail Vehicle And Railway Traction Power Supply With Rotary Converters. *MET2009 9th International Conference 'Modern Electric Traction'*. Gdansk, Poland, pp. 89-94, 2009.

[55] S. Danielsen, M. Molinas, T. Toftevaag and O. B. Fosso, Constant Power Load Characteristic's Influence On The Low-Frequency Interaction Between Advanced Electrical Rail Vehicle And Railway Traction Power Supply With Rotary Converters, *Invited for publication in Electromotion*. 17 (1), pp. 2010.

[56] S. Danielsen and T. Toftevaag, Experiences with respect to low frequency instability from operation of advanced electrical rail vehicles in a traction power system with rotary converters. *MET2007 8th International Conference 'Modern Electric Traction'*. Warsaw, Poland, pp. 51-57, 2007.

[57] S. Danielsen, T. Toftevaag and O. B. Fosso, Application of linear analysis in railway power system stability studies, *Invited for publication in 'Power Supply, Energy Management and Catenary Problems'*. 2009.

[58] S. Danielsen, T. Toftevaag and O. B. Fosso, Application of linear analysis in traction power system stability studies. *Computers in Railways XI: Computer System Design and Operation in the Railway and Other Transit Systems*. Toledo, Spain, pp. 401-410, 2008.

[59] S. Danielsen, T. Toftevaag and O. B. Fosso, Swing equation for synchronous-synchronous rotary frequency converters, *Submitted to Electric Power System Research in 2009*.

[60] M. Debruyne, Low frequency instability in the Amtrak's 12kV-25Hz network. *Interaction Workshop 2006* Thun, Switzerland, 2006.

[61] R. C. Dorf and R. H. Bishop, *Modern Control Systems*, Pearson Prentice Hall, Upper Saddle River, 2008.

[62] U. Ehrler, Traction Propulsion Control Development, ABB, Turgi, Switzerland. *Personal communication 2009*.

[63] A. Eisele, BR 185 under Nordic power supply conditions. *Interaction Workshop 2009*. Thun, Switzerland, 2009.

[64] A. Eisele, Propulsion & Controls, Bombardier Transportation Oerlikon, Switzerland. *Personal communication 2009*.

[65] M. A. Eitzmann, J. J. Paserba, J. M. Undrill, C. Amicarella, A. L. Jones, E. B. Khalafalla and W. Liverant, Model development and stability assessment of the Amtrak 25 Hz traction system from New York to Washington DC. *Railroad Conference*. pp. 21-28, 1997.

[66] A. Emadi, Modeling of power electronic loads in AC distribution systems using the generalized State-space averaging method, *Industrial Electronics, IEEE Transactions on*. 51 (5), pp. 992-1000, 2004.

[67] H. R. Fankhauser, K. Aneros, A. A. Edris and S. Torseng, Advanced simulation techniques for the analysis of power system dynamics, *Computer Applications in Power, IEEE*. 3 (4), pp. 31-36, 1990.

[68] C. P. Fowler, Synchronous Converters Versus Motor Generators, *Electrical World*. 47 (26), pp. 1078-1080, 1906.

[69] F. M. Gardner, *Phaselock Techniques*, Wiley Interscience, 2005.

[70] T. H. Garten, Linear Model of Rotary Converter in Traction Power System, Master thesis, Dept. of Engineering Cybernetics, Norwegian University of Science and Technology, 2006.

[71] M. Glinka and R. Marquardt, A new AC/AC multilevel converter family, *Industrial Electronics, IEEE Transactions on*. 52 (3), pp. 662-669, 2005.

[72] L. Harnefors, Modeling of Three-Phase Dynamic Systems Using Complex Transfer Functions and Transfer Matrices, *Industrial Electronics, IEEE Transactions on*. 54 (4), pp. 2239-2248, 2007.

[73] L. Harnefors, On Analysis, Control and Estimation of Variable-Speed Drives, PhD thesis, Royal Institute of Technology, 1997.

[74] L. Harnefors, M. Bongiorno and S. Lundberg, Input-Admittance Calculation and Shaping for Controlled Voltage-Source Converters, *Industrial Electronics, IEEE Transactions on*. 54 (6), pp. 3323-3334, 2007.

[75] L. Harnefors and H. P. Nee, Model-based current control of AC machines using the internal model control method, *Industry Applications, IEEE Transactions on*. 34 (1), pp. 133-141, 1998.

[76] J. F. Hauer, C. J. Demeure and L. L. Scharf, Initial results in Prony analysis of power system response signals, *Power Systems, IEEE Transactions on*. 5 (1), pp. 80-89, 1990.

[77] C. Heising, M. Oettermeier, M. Gorski, V. Staudt and A. Steimel, Implications of Resonant Circuit Adjustment Errors to the DC-link voltage in Single-Phase 16.7-Hz-Railway Applications. *Compatibility and Power Electronics, 2009. CPE '09.* Badajoz, Spain, pp. 210-216, 2009.

[78] C. Heising, M. Oettmeier, R. Bartelt, V. Staudt and A. Steimel, Integrated control of single-phase four-quadrant line-side converter and machine-side inverter for railway traction applications. *Power Electronics and Applications, 2009. EPE '09. 13th European Conference on*. pp. 1-10, 2009.

[79] C. Heising, M. Oettmeier, R. Bartelt, V. Staudt and A. Steimel, Single-phase 50-kW 16.7-Hz PI-controlled four-quadrant line-side converter lab model fed by rotary converter. *Compatibility and Power Electronics, 2009. CPE '09.* pp. 232-239, 2009.

[80] C. Heising, M. Oettmeier, V. Staudt, A. Steimel and S. Danielsen, Improvement of Low-Frequency Railway Power System Stability Using an Advanced Multivariable Control Concept. *35th Annual Conference of the IEEE Industrial Electronics Society (IECON)*. Porto, Portugal, pp. 560-565, 2009.

[81] U. Henning, D. Würgler, W. Graupner, A. J. Petersen, V. Staudt and P. Pozzobon, Elektrische Kompatibilität im System Bahn-Ergebnisse des ESCARV *Elektrische Bahnen*. (6-7), pp. 284-291, 2001.

[82] J. Hill, Sustainable growth for Europe's railways, *IEE Review*. 48 (5), pp. 37-40, 2002.

[83] N. G. Hingorani and L. Gyugyi, *Understanding FACTS - Concept and Technology of Flexible AC Transmission Systems*, IEEE Press, New York, 2000.

[84] T. K. Ho, Y. L. Chi, J. Wang, K. K. Leung, L. K. Siu and C. T. Tse, Probabilistic load flow in AC electrified railways, *Electric Power Applications, IEE Proceedings-*. 152 (4), pp. 1003-1013, 2005.

[85] C. M. Hoff and S. Mulukutla, Analysis of the instability of PFC power supplies with various AC sources. *Applied Power Electronics Conference and Exposition, 1994. APEC '94. Conference Proceedings 1994., Ninth Annual*. pp. 696-702 vol.2, 1994.

[86] J. Huang, K. Corzine and M. Belkhayat, Single-Phase ac Impedance Modeling for Stability of Integrated Power Systems. *Electric Ship Technologies Symposium, 2007. ESTS '07. IEEE*. pp. 483-489, 2007.

[87] K.-E. Högberg, Dämpregulator för järnvägsomformare i Norska Jernbaneverket. Document number 200500583-20 ('Teknisk meddelande' from STRI AB (Proinr 81757) 2007-12-21) at Norwegian National Rail Administration, 2008.

[88] F. Irgens, *Dynamics (Original title in Norwegian: Dynamikk)*, TAPIR Forlag, Trondheim, 1999.

[89] M. Jansson, A. Danielsson, J. Galic, K. Pietiläinen and L. Harnefors, Stable and Passive Traction. *NORPIE 2004: 4th Nordic Workshop on Power and Industrial Electronics*. Trondheim, Norway, 2004.

[90] X. Jian, A. Zynovchenko, L. Feng, H. J. Haubrich and P. Treige, Converter control and stability of the 110-kV railway grid increasing use of the static frequency converters. *Power Electronics and Applications, 2005 European Conference on*. pp.-P.8, 2005.

[91] F. Johannessen and P.-C. Bruu, Stability in the electrical grid of NSB Master Degree thesis, Department of Electrical Power Engineering, Norwegian University of Science and Technology 1996.

[92] E. Johansson, Detailed Description of Synchronous Machine Models Used in Simpow, Master thesis, Department of Electrical Engineering, Royal Institute of Technology, 2002.

[93] E. Johansson, J. Persson, L. Lindkvist and L. Söder, Location of Eigenvalues Influenced by Different Models of Synchronous Machines. *6th IASTED International Conference on Power and Energy Systems*. Marina del Rey, California, USA, pp. 352-145, 2002.

[94] S. G. Johansson, G. Asplund, E. Jansson and R. Rudervall, Power System Stability Benefits from VSC DC-Transmission Systems. *CIGRE Session 2004*. B4-204, 2004.

[95] F. Johnsen and M. Nyebak, Schaltungsaufbau im Oberleitungsnetz der norwegischen Eisenbahn Jernbaneverket *Elektrische Bahnen*. 102 (4), pp. 195-200, 2004.

[96] A. B. Jusoh, The instability effect of constant power loads. *Power and Energy Conference, 2004. PECon 2004. Proceedings. National*. pp. 175-179, 2004.

[97] M. Jänecke, Steuerverfahren und Steueranordnung für einen Wechselrichter, ABB Patent DE 41 10225 A1, 1992.

[98] K. Kaberere, K. Folly, M. Ntombela and A. Petroianu, Comparison of Industrial-Grade Analytical Tools Used in Small-Signal Stability Assessment,. *AUPEC 2005*. Hobart, Tasmania, Australia, pp. 147-152, 2005.

[99] M. Kaeser, F. Menius and M. Meyer, SBB-Flirt in Norwegen, *Schweizer Eisenbahn-Revue*. (4), pp. 169-171, 2009.

[100] W. Kaiser, G. Punz and G. Wallnberger, Softwaretools zur Simulation des 16 2/3-Hz-Bahnstromnetzes bei den ÖBB, *Elektrische Bahnen*. 101 (1-2), pp. 52-62, 2003.

[101] M. Karimi-Ghartemani, A distortion-free phase-locked loop system for FACTS and power electronic controllers, *Electric Power Systems Research*. 77 (8), pp. 1095-1100, 2007.

[102] F. Kiessling, R. Puschmann and A. Schmieder, *Contact Lines for Electric Railways*, Publicis Corporate Publishing, Munich, Erlangen, 2001.

[103] B. Kindell, Line Converter Control, Master thesis, Department of Signals, Sensors and Systems, Royal Institute of Technology 2003.

[104] P. Kraniauskas, *Transform in Signals and Systems*, Addison-Wesley Publishing Company, 1991.

[105] M. Kratz and J. Pawlak, Ein Jahr Traxx-Lokomotiven in Skandinavien, *Eisenbahn-Revue International*. (2), pp. 74-77, 2009.

[106] P. Kundur, *Power System Stability and Control*, McGraw-Hill California, 1994.

[107] P. Kundur, J. Paserba, V. Ajjarapu, G. Andersson, A. Bose, C. Canizares, N. Hatziargyriou, D. Hill, A. Stankovic, C. Taylor, T. Van Cutsem and V. Vittal, Definition and classification of power system stability IEEE/CIGRE joint task force on stability terms and definitions, *Power Systems, IEEE Transactions on*. 19 (3), pp. 1387-1401, 2004.

[108] B. Landström, *Email 'RE: Et spørsmål til angående eldre spenningsregulatorer...' sent to Ø. Stensby 2008-10-09*.

[109] B. T. Leclair and A. J. Krupy, Frequency Changers Also Have Stability Limits, *Electrical World*. 98 (26), pp. 558-561, 1931.

[110] Y. F. Lin, Z. Xu and Y. Huang, Power oscillation damping controller design for TCSC based on the test signal method. *Power Engineering Society General Meeting, 2005. IEEE*. pp. 1671-1675 Vol. 2, 2005.

[111] C. Linder and R. Heinze, Umstellung der Sollfrequenz im Zentralen Bahnstromnetz von 16 2/3 Hz auf 16,70 Hz, *Elektrische Bahnen*. 100 (12-2002), pp. 447-454, 2002.

[112] M. Liserre, R. Teodorescu and F. Blaabjerg, Stability of photovoltaic and wind turbine grid-connected inverters for a large set of grid impedance values, *Power Electronics, IEEE Transactions on*. 21 (1), pp. 263-272, 2006.

[113] R. Lundberg, *Textbook in electrical engineering in Swedish State Railways. Part IV Converter stations (Original title in Swedish: Lärobok i Elektroteknik för Statens Järnvägars personal. Del IV Omformarstationer)*, Svenska tryckeriaktiebolaget, Stockholm, 1959.

[114] M. Lörtscher, M. Meyer, A. Schneeberger and B. Hemmer, Kompatibilitätsuntersuchungen am sweizerischen 16,7-Hz-Bahnstromnetz, *Elektrische Bahnen*. (6-7), pp. 292-300, 2001.

[115] J. Machowski, J. B. Bialek and J. R. Bumby, *Power system dynamics and stability*, John Wiley & Sons, 1997.

[116] S. Menth and M. Meyer, Low frequency power oscillations in electric railway systems, *Elektrische Bahnen*. 104 (5), pp. 216-221, 2006.

[117] M. Mermet-Guyennet, Heavy and light train technologies. *Power Electronics and Applications, 2009. EPE '09. 13th European Conference on*. pp. 1-10, 2009.

[118] M. Meyer, Netzstabilität bei Wechselstrombahnen - Systemkompatibilität auf dem Weg nach Europa. *VDE-Tagung 2002*. Dresden, Germany, 2002.

[119] M. Meyer, Wechselwirkungen Energieversorgung-Triebfahrzeug bei AC-bahnen, *Elektrische Bahnen*. 103 (4-5), pp. 213-218, 2005.

[120] M. Meyer, M. Aeberhard, L. Germann, R. Suter and P. Dähler, Messung des Frequenzgangs von TriebFahrzeugen, *Elektrische Bahnen*. 105 (10), pp. 521-528, 2007.

[121] M. Meyer and C. Ljunggren, Schwere Züge auf schwachen Netzen - Elektrischer Betrieb auf der schwedisch-norwegischen Erzbahn, *Eisenbahn-Revue*. 1/2003 (1), pp. 16-21, 2003.

[122] M. Meyer and J. Schöning, Netzstabilität in grossen Bahnnetzen, *Schweizer Eisenbahn-Revue and Eisenbahn-Revue International*. (7-8), pp. 312-317, 1999.

[123] M. Meyer, M. Stadelmann and R. Kernen, Auswirkung der Netzresonanzen im Lötschberg-Basistunnel, *Elektrische Bahnen*. 105 (11), pp. 521-527, 2007.

[124] M. Meyer and M. Thoma, Netzkompatibilitätsstudie und -messungen für die Umrichteranlage Wimmis, *Elektrische Bahnen*. 104 (12), pp. 567-574, 2006.

[125] M. Meyer and G.-J. Van-Alphen, Netzresonanzmessungen auf HSL Zuid and Betuweroute, *Schweizer Eisenbahn-Revue*. (12), 2006.

[126] R. D. Middlebrook, Input Filter Considerations in Design and Application of Switching regulators. *IEEE Industry Applications Society Annual Meeting 1976*. pp. 366-382, 1976.

[127] M. Mikus, Untersuchung und Vergleich von zwei Regelverfahren für Vierquadrantsteller für Wechselstrom-Umrichter-Triebfahrzeuge, Master thesis, Lehrstuhl für Erzeugung und Anwendung elektrischer Energie, Ruhr-Universität Bochum, 1997.

[128] N. Mohan, T. M. Undeland and W. P. Robbins, *Power Electronics - Converters Applications and Design*, John Wiley & Sons, Inc, 1995.

[129] H. Mosskull, Robust Control of an Induction Motor Drive Automatic Control, PhD thesis, Department of Automatic Control, Royal Institute of Technology, 2006.

[130] E. Möllerstedt, Dynamic Analysis of Harmonics in Electrical Systems, PhD thesis, Department of Automatic Control, Lund Institute of Technology, 2000.

[131] E. Möllerstedt and B. Bernhardsson, Out of control because of harmonics-an analysis of the harmonic response of an inverter locomotive, *Control Systems Magazine, IEEE*. 20 (4), pp. 70-81, 2000.

[132] L. Nousiainen, Single-phase electronic load interactions with supply network, Master of Science thesis, Degree Programme in Electrical Engineering, Tampere University of Technology, 2009.

[133] M. Olofsson, Investigation of transient stability in railway power supply (Original title in Swedish: Undersökning av transient stabilitet i matningssystem för elektrisk tågdrift), Master degree thesis, Department of Electric Power Engineering, Royal Institute of Technology, 1989.

[134] M. Olofsson, Optimal operation of the Swedish railway electrical system - An application of optimal power flow, PhD thesis, Department of Electric Power Engineering, Royal Institute of Technology, 1996.

[135] A. D. B. Paice and M. Meyer, Rail network modelling and stability: the input admittance criterion. *MTNS*. 2000.

[136] M. K. Pal, Lecture Notes on Power System Stability, Available from Internet:http://www.mkpalconsulting.com/Stability_book.html, Accessed at 2008-12-16, Published by 2008

[137] A. Palesjö, Model of a rotary converter, for analysis of power-frequency phenomena in an electrical system. Document number TR H 52-107 at ABB Power Systems, 1998.

[138] A. Palesjö, Model of a rotary converter, for analysis of power-frequency phenomena. Implementation in SIMPOW and input data. Document number TR H 52-108 at ABB Power Systems, 1998.

[139] J. Pechlaner, M. Pröls and M. Meyer, Weiterentwicklung des Gesamtsystems Bahn im Zusammenwirken von Netz und Fahrzeug, *ZEVrail - Zeitschrift für das gesamte System Bahn, Sonderheft Tagungsband Moderne Schienenfahrzeuge 38. Tagung Technische Universität Graz 14.bis 17.September 2008*. 132 (November 2008), pp. 81-87, 2008.

[140] I. J. Perez-Arriaga, G. C. Verghese and F. C. Schweppe, Selective Modal Analysis with Applications to Electric Power Systems, PART I: Heuristic Introduction, *Power Apparatus and Systems, IEEE Transactions on*. PAS-101 (9), pp. 3117-3125, 1982.

[141] J. Persson, Bandwidth-reduced Linear Models of Non-continuous Power System Components, PhD thesis, Department of Electrical Engineering, Royal Institute of Technology, 2006.

[142] J. Persson, Linear Models of Non-linear Power System Components, Licentiate thesis, Department of Electrical Engineering, Royal Institute of Technology, 2002.

[143] J. Persson, Reference manual for the Fast Fourier Transform-Algorithm in SIMPOW. Document number TR POW /H 51-106A at ABB Power Systems, Västerås, Sweden, 1998.

[144] J. Persson, U. Axelsson, D. Wall and P.-O. Lindström, Need for Standardization of Wind Power Models for Stability Studies. *Wind Power to the Grid - EPE Wind Energy Chapter – 2nd Seminar*. The Royal Institute of Technology, Stockholm, Sweden, 2009.

[145] J. Persson, J.-P. Hasler and K. Aneros, Switching a Large Power System between Fundamental Frequency and Instantaneous Value Mode. *3rd International Conference On Digital Power System Simulators, ICDS'99*. Västerås, Sweden, pp. 1-6, 1999.

[146] J. Persson and L. Söder, Linear Analysis with Two Linear Models of a Thyristor-Controlled Series Capacitor. *IEEE Bologna Power Tech Conference 2003*. Bologna, Italy, 2003.

[147] A. Pfeiffer, W. Scheidl, M. Eitzmann and E. Larsen, Modern rotary converters for railway applications. *Railroad Conference, 1997., Proceedings of the 1997 IEEE/ASME Joint*. pp. 29-33, 1997.

[148] M. Pröls and B. Strobl, Stabiltätskriterien für Wechselwirkungen mit Umrichteranlagen in Bahnsystemen, *Elektrische Bahnen*. 104 (11), pp. 542-552, 2006.

[149] S. Sabery, FEM modelling of converter type Q48/Q49 and tension, fracture and fatigue analysis of rotor pole interface (Original title in Swedish: FEM-modellering av omformare typ Q48/Q49 och spännings-, sprick- och utmattningsanalys av laxhalsen), Master of Science thesis, Department of Solid Mechanics, Royal Institute of Technology, 2002.

[150] O. Samuelsson, Load modulation for damping of electro-mechanical oscillations. *Power Engineering Society Winter Meeting, 2001. IEEE*. pp. 241-246 vol.1, 2001.

[151] O. Samuelsson, Power System Damping - Structural Aspects of Controlling Active Power, Doctoral thesis, Department of Industrial Electrical Engineering and Automation, Lund University, 1997.

[152] H. Sandberg, Nonlinear Modeling of Locomotive Propulsion System and Control, Master thesis, Department of Automatic Control, Lund Institute of University, 1999.

[153] Sbb/An, Der Blackout bei den SBB, *Eisenbahn-Revue*. (8-9), pp. 373-379, 2005.

[154] S. Schmidt, D. Wuergler, P. Terwiesch and U. Henning, Electrical System Compatibility for Advanced Rail Vehicles: a survey. *8th International Conference on Harmonics And Quality of Power 1998. Proceedings*. pp. 623-629 vol.2, 1998.

[155] N. I. Selenochat, A. M. Djakow and H.-G. Dunkel, Betrachtung der statischen Stabilität einer galvanisch entkoppelten Energieübertragung mit Synchron-Synchron-Umformer, *Technish-Wissenschaftliche Zeitschrift für Energietechnik*. 29 (12), pp. 454-457, 1979.

[156] N. I. Selenochat, H.-G. Dunkel and A. M. Djakow, Über die Untersuchung von Ausgleichsvorgängen in Elektroenergiesystemen mit Synchron-Synchron-Umformer, *Technish-Wissenschaftliche Zeitschrift für Energietechnik*. 29 (9), pp. 394-398, 1976.

[157] S. Singh, Application of Prony analysis to characterize pulsed corona reactor measurments, Master of Science thesis, Department of Electrical and Computing Engineering, University of Wyoming, 2003.

[158] S. Singh, Prony Toolbox, Available from Internet:http://www.mathworks.com/matlabcentral/fileexchange/3955, Accessed at 2009-06-26, Published by Mathworks Matlab Central 2003

[159] H. Slootweg, J. Persson, A. M. Van Voorden, G. C. Paap and W. Kling, A Study of the Eigenvalue Analysis Capabilities of Power System Dynamics Simulation Software. *14th Power Systems Computation Conference 2002*. Sevilla, Spain, pp. 1-8 (Session 26, paper 3), 2002.

[160] G. Stanke, Untersuching von Modulationsverfahren für Pulsstromrichter mit hohen dynamischen Anfordrung bei beschränkter Schaltfrequenx, Doktor-Ingenieurs thesis, Der Fakultät für Elektrotechnik, Rheinisch-Westfälischen Technischen Hochschule Aachen, 1987.

[161] V. Staudt, C. Heising and A. Steimel, Advanced simulation concept for the power train of an AC locomotive and its verification. *Power Electronics, 2007. ICPE '07. 7th International Conference on*. pp. 866-870, 2007.

[162] A. Stefan, OpenPowerNet - Simulation of railway power supply systems. *Computers in Railways XI: Computer System Design and Operation in the Railway and Other Transit Systems*. Toledo, Spain, pp. 449-459, 2008.

[163] A. Steimel, *Electric Traction - Motive Power and Energy Supply*, Oldenbourg Industrieverlag, München, 2008.

[164] A. Steimel, Institute for Electrical Power Engineering and Power Electronics, Ruhr Universität Bochum, Bochum, Germany. *Personal communication March 2009*.

[165] A. Steimel, Power-Electronics Issues of Modern Electric Railway Systems. *To be presented on the 9th International Conference on Development and Application Systems*. Suceava, Romania, 1-6, 2010.

[166] C. P. Steinmetz, Instability of electric circuits, *Journal of the American Institute of Electrical Engineers (continuation of Proceedings of the American Institute of Electrical Engineers)*. 88 (Jan 1914), pp. 18-29, 1914.

[167] Ø. Stensby, *Email 'SV: Et spørsmål til angående eldre spenningsregulatorer...' 2008-10-15*.

[168] Ø. Stensby, Low frequency oscillations in traction power systems, Master of Science thesis, Department of Electrical Power Engineering, Norwegian University of Science and Technology 2006.

[169] T. Stoltze, Dynamisches Verhalten von Synchron-Synchron-Umformern, Doktor Ingenieur thesis, Fakultät für Elektrotechnik, Telekommunikation und Prozessautomatisierung, Hochschule für Verkehrswesen 'Friedrich List', 1992.

[170] B. Strobl, Analysis of stability for networks including converters. *Power Electronics and Applications, 2007 European Conference on*. pp. 1-10, 2007.

[171] S. D. Sudhoff, K. A. Corzine, S. F. Glover, H. J. Hegner and H. N. Robey, Jr., DC link stabilized field oriented control of electric propulsion systems, *Energy Conversion, IEEE Transactions on*. 13 (1), pp. 27-33, 1998.

[172] S. D. Sudhoff, S. F. Glover, P. T. Lamm, D. H. Schmucker and D. E. Delisle, Admittance space stability analysis of power electronic systems, *Aerospace and Electronic Systems, IEEE Transactions on*. 36 (3), pp. 965-973, 2000.

[173] J. Sun, AC power electronic systems: Stability and power quality. *Control and Modeling for Power Electronics, 2008. COMPEL 2008. 11th Workshop on*. pp. 1-10, 2008.

[174] J. Sun, Small-Signal Methods for AC Distributed Power Systems - A Review, *Power Electronics, IEEE Transactions on*. 24 (11), pp. 2545-2554, 2009.

[175] J. M. Sølvberg, Mathematical modelling of current collector and overhead contact line (Original title in Norwegian: Matematisk modellering av strømavtaker og kontaktledning), Master thesis, Department of Physics, University of Oslo, 2008.

[176] P. Terwiesch, T. Keller and E. Scheiben, Rail vehicle control system integration testing using digital hardware-in-the-loop simulation, *Control Systems Technology, IEEE Transactions on*. 7 (3), pp. 352-362, 1999.

[177] W. T. Thomson, *Theory of Vibration with Application*, George Allen & Unwin, Sydney, 1981.

[178] T. Toftevaag and M. T. Pálsson, Low frequency oscillations in the Norwegian electric traction power supply caused by interaction between the supply system

and propulsion machinery – analysis and consequences. *MET'05 7th International Conference 'Modern Electric Traction in Integrated XXI st Century Europe'*. Warsaw, Poland, pp. 137-142, 2005.

[179] T. Van Cutsem and C. Vournas, *Voltage Stability of Electric Power Systems*, Kluwer Academic Publishers, 1998.

[180] G. Varju, Further investigation of AT-system for the Norwegian railway, Part 1. Amended version - Short-circuit impedance seen by the protection relay. Document number at Varju EMC Bt, 2005.

[181] V. Venkatesh, S. Rao, B. S. Gupta and V. T. Ranganathan, Single Phase Front End Converter for Traction Drive, *IE(L) Journal-EL*. 87 (June 2006), 2006.

[182] G. Wallnberger, G. Punz, H. Pechlaner and M. Meyer, Untersuchungen zu Überspannungen im Oberleitungsnetz bei den ÖBB, *Elektrische Bahnen*. 104 (11), pp. 536-541, 2006.

[183] X. Yanhong and C. Shaotang, Instability issues for control system in induction generator. *Industry Applications Conference, 2001. Thirty-Sixth IAS Annual Meeting. Conference Record of the 2001 IEEE*. pp. 110-117 vol.1, 2001.

[184] H. D. Young and R. A. Freedman, *University Physics*, Addison-Wesley Publishing Company, Inc, 1996.

[185] C. Zhe, W. Yue, H. Weihao and W. Zhaoan, Flicker Mitigation by Active Power Control of Variable-Speed Wind Turbines With Full-Scale Back-to-Back Power Converters, *Energy conversion, ieee transactions on*. 24 (3), pp. 640-649, 2009.

[186] D. N. Zmood, D. G. Holmes and G. H. Bode, Frequency domain analysis of three phase linear current regulators, *IEEE Transactions on Industry Applications*. 37 (2), pp. 601-610, 2001.

[187] A. Zynovchenko, G. George and H. Olsen, Elektrifizierung von Eisenbahnstrecken mit Autotransformatoresystemen, *Elektrische Bahnen*. 107 (4/5-2009), pp. 233-239, 2009.

[188] S. Östlund, *Electric Traction (original title in Swedish: Elektrisk Traktion)*, School of Electrical Engineering, Electrical Machines and Power Electronics, Royal Institute of Technology (KTH), Stockholm, Sweden, 2005.

Appendix A Instantaneous value model input admittance calculation method

This appendix describes the method that is used for the calculation of the input admittance for the instantaneous value vehicle model in Section 8.3.

A.1 Test bench

The vehicle is directly connected to an AC voltage source as shown in Figure A-1, i.e., there is no line impedance in between. Even if it is not explicitly shown in the figure, the vehicle model still includes the DC-link, motor side and control system. The source and vehicle line voltage and current are measured and used for the input admittance calculation.

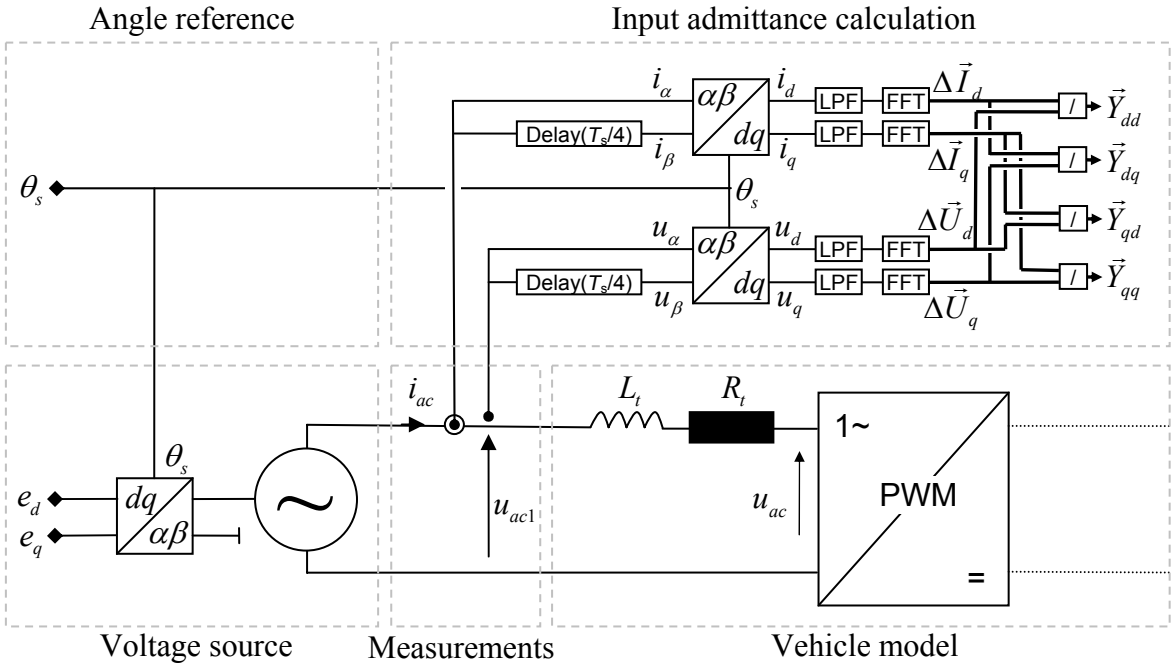

Figure A-1: A signal flow diagram for the testbench. The thin lines are instantaneous value scalars and the thick lines are phasors.

The source voltage $u_{ac1}(t)$ is an initial 15-kV 16 ⅔-Hz single-phase AC source, of which the voltage amplitude and phase can be manipulated by controlling the *d*- and *q*-axis voltages e_d and e_q in the synchronously rotating reference frame. The voltage phasor

$\vec{U}_{ac1}$ is originally aligned along the real complex axis such that $\vec{U}_{ac10} = |\vec{U}_{ac10}| + j0 = |\vec{U}_{ac10}| \angle 0° = e_{d0} + je_{q0}$. Small changes (Δ) in e_d and e_q, leads to a change in voltage amplitude and phase, respectively, as shown in Figure A-2 and Equation (A.1).

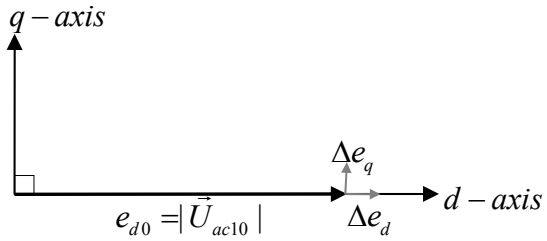

Figure A-2: Voltage components in the rotating reference frame.

$$\begin{aligned} e_d &= e_{d0} + \Delta e_d = |\vec{U}_{ac10}| + \Delta e_d \\ e_d &= e_{q0} + \Delta e_q = 0.0 + \Delta e_q \end{aligned} \tag{A.1}$$

A transformation from the synchronously rotating reference frame is done by Equation (A.2) ($dq/\alpha\beta$). This is the first row in the inverse Park's transform (inverse of Equation (4.7)). θ_s is the angle for orientation of the global complex synchronously rotating frame for the system given by Equation (A.3) where ω_s is the system fundamental angular frequency ($=2\pi f_s$). See Figure 4-1 b).

$$u_{ac1} = e_d \cos\theta_s - e_q \sin\theta_s \tag{A.2}$$

$$\theta_s = \int_0^t \omega_s dt = \omega_s t \tag{A.3}$$

As we are interested in the *d*- and *q*-axis currents as well as the voltages, these must be calculated. A simple and direct transform from a stationary reference frame to a rotating reference frame for the single-phase system does not exist such as for a three-phase system. An artificial second phase therefore has to be created. In this case, a time delay of a quarter of the fundamental period time ($T_s/4$) is used to establish an orthogonal (β) signal that is 90 fundamental degrees lagging physical signal (α). This is a simple way of orthogonalisation, but it has two disadvantages:

- It has a filtering impact as illustrated in Figure A-3 and shown in Equation (5.10).
- It produces harmonics, especially when the signal frequency is not exactly according to the tuning of the delay.

The low filtering impact from the delay on the measured *d*- and *q*-axis currents are compensated for by applying the same method and filtering to the voltage measurements. The cross couplings between the axes are weak and hence neglected.

The influence from harmonics are not specifically reduced, but an anti-aliasing low-pass filter (LPF) (Butterworth of the 7th order) avoids the folding of harmonics into the Fast Fourier Transform (FFT) analysis. This filtering is thoroughly described by Persson [141] (Section 4.8.1).

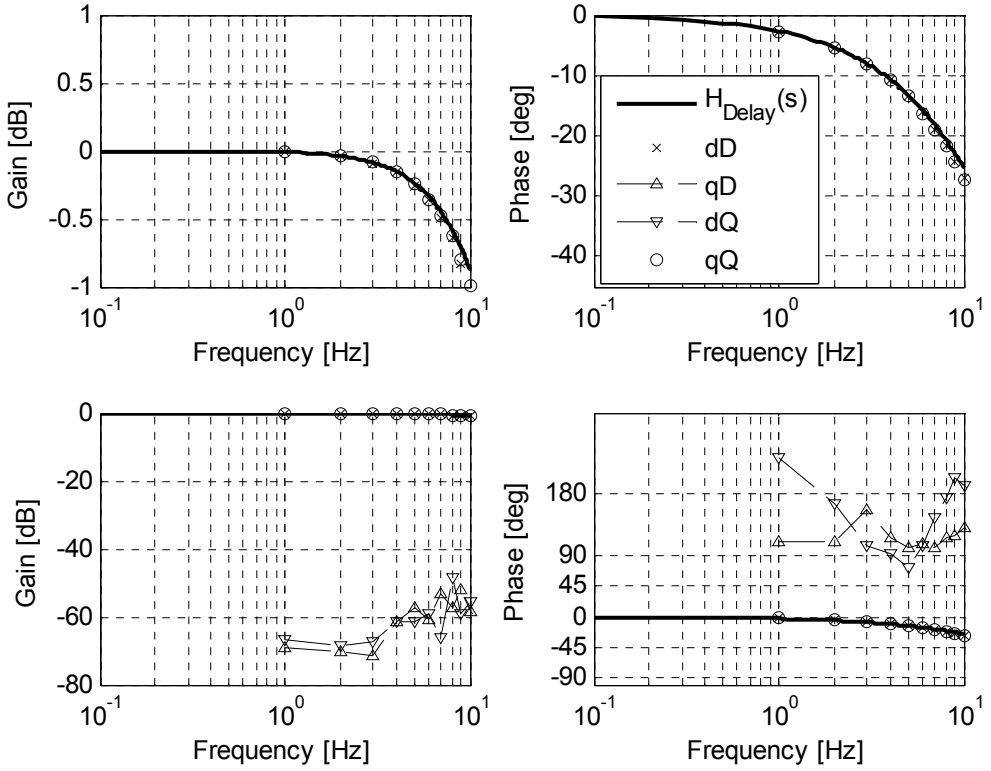

Figure A-3: The frequency response of the instantaneous value model of delay compared with the low-pass filter transfer function in Equation (5.10).

Huang, et al. [86] use the Hilbert transform for orthogonalisation instead. The Hilbert transform is a mathematical transform that shifts every input signal component 90 degrees lagging relative to the component's own frequency. However, this transform is difficult to implement and a good qualitative description of the benefits over a single delay as used in the present thesis has not been found.

For the transformation from a stationary reference frame to the rotating reference frame ($\alpha\beta/dq$), the angle for orientation of the global complex synchronously rotating fram, θ_s, is used as the angle for Park's transform.

A.2 Frequency sweep

Disturbances in the source voltage $u_{ac1}(t)$ amplitude and phase are imposed by overlaying a sinusoidal voltage with an amplitude of 0.1 pu on the synchronous rotating source voltages e_d and e_q, respectively. The overlaying signal is periodic with the oscillation frequency f_{osc}. The voltage source output is given by Equation (A.4) combined with Equation (A.2), which is essentially represented by Equation (3.21).

$$\begin{aligned} e_d &= e_{d0} + 0.1\sin(2\pi f_{osc} t) = |\vec{U}_{ac10}| + 0.1\sin(2\pi f_{osc} t) \\ e_d &= e_{q0} + 0.1\sin(2\pi f_{osc} t) = 0.0 + 0.1\sin(2\pi f_{osc} t) \end{aligned} \quad \text{(A.4)}$$

The amplitude and phase of u_{ac1} is disturbed one at a time by a periodic signal, i.e., when the amplitude is changed, the phase change is 0 and vice versa. Huang, et al. [86] though change both the *d*- and *q*-axis component of the source voltage at the same time.

The amplitude of the disturbance (here: 0.1 pu = 1.5 kV) can be discussed. The amplitude has to be large enough to ensure proper results for the FFT analysis, but it should be limited depending on what degree of system non-linearity the results should include. The 10 % amplitude used here is in the range used by Persson [141] for a similar system identification.

The frequency sweep performed in the present thesis includes the following frequencies:

- Every 1/3 Hz from 1/3 to 5 Hz
- Every 1/1 Hz from 5 to 16 Hz

An FFT analysis is performed for six seconds of the time simulation result by using a rectangular window. The chosen period allows both an integer number of fundamental frequency periods and oscillation frequency periods to be included. The analysis period starts after the system has come to a quasi-stationary state, i.e., when all transients are vanished and only the forced oscillations from the periodic change are left. Details about the FFT algorithm used in this thesis are described by Persson [143].

The results from the FFT analyses are four phasors, ΔI_d, ΔI_q, ΔU_d and ΔU_q, that represent the *d*- and *q*-axis voltage and current components at the imposed oscillation frequency. A change in voltage ΔU may lead to a change in the current ΔI. This is enough information to calculate the corresponding magnitude and phase shift from the disturbance in voltage to the response in current. In the field of electrical engineering, the current on voltage ratio is called admittance *Y*. Altogether, this relieves four admittances (Menth and Meyer [116]):

- $Y_{dd} = \Delta I_d / \Delta U_d$ – current amplitude change given by voltage amplitude change
- $Y_{qd} = \Delta I_q / \Delta U_d$ – current phase change given by voltage amplitude change
- $Y_{dq} = \Delta I_d / \Delta U_q$ – current amplitude change given by voltage phase change
- $Y_{qq} = \Delta I_q / \Delta U_q$ – current phase change given by voltage phase change

There are two direct terms, *d-of-d* and *q-of-q*, and two cross-coupling terms, *q-of-d* and *d-of-q*. When the four admittances are found for all the frequencies in the list above, the vehicle input admittance frequency response can be plotted as shown in Figure 8-11.

Appendix B Simulation model parameters

B.1 Reference case

Throughout this thesis, several numerical examples are provided. Many of these examples are related to a reference case that is selected as follows.

A transportable synchronous-synchronous rotary frequency converter type ASEA Q38, as shown in Figure 2-2 having a continuous rating of 4 MVA, is feeding a single-track railway and one single rail vehicle as shown in Figure 1-1. A single-line diagram in Figure B-1 shows the steady-state power flow for the reference case.

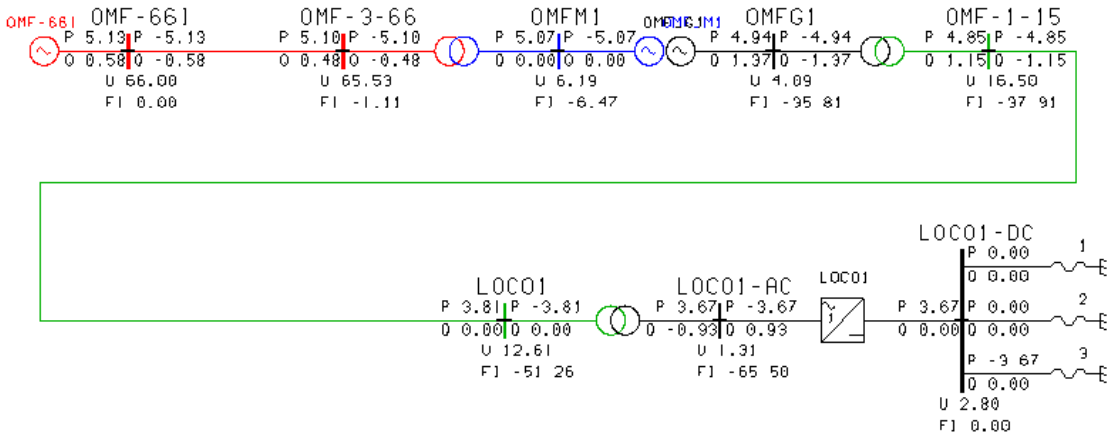

Figure B-1: A single-line diagram for the reference case. Active and reactive power is given in MW and MVAr, and voltage's magnitude and angle in are given in kV (phase to phase voltages) and degrees, respectively.

The converter may be overloaded to 5.8 MVA for one hour or 8 MVA for six minutes according to Lundberg [113]. It is fed from a 66-kV three-phase system representing a short-circuit capacity of 250 MVA at the converter three-phase transformer upside. This converter and three-phase network are most commonly found in Norway (Banverket/Jernbaneverket [17]). Both the motor and generator include exciters and automatic voltage controllers (AVR). The motor excitation adjusted so the reactive power at its terminal equals zero, which gives the reference voltage for the AVR. Furthermore, if necessary (here it was not) the three-phase transformer tap-changer may be adjusted (in increments of 300 V) in order to keep the motor voltage as close as possible to 6.3 kV. The line voltage at the single-phase transformer 15-kV side is controlled to be 16.5 kV with a zero load-depending slope by use of the AVR. Data for the converter, the transformers and the regulators are given in Appendix B.1.

Between the rotary converter and the rail vehicle, there is 60 km of overhead contact line. This length was chosen since it is the length of line for which a vehicle is required to operate stably in order to be accepted for operation in Norway and Sweden (Banverket/Jernbaneverket [17]). The line impedance is $(0.19 + j0.21)\ \Omega/\text{km}$.

The rail vehicle is based on exercise 17.8 by Steimel [163] and is further introduced and explained in Chapter 5. It represents a 6.4 MW universal locomotive measured on wheel. This results in an electrical rating of 7.35 MW. The vehicle is operated on half of the rated power, i.e., 3.67 MW. This power demand results in a line voltage of 12.6 kV at the train's current collector. The line losses increase the total load of the converter to 5 MVA. The detailed load flow is shown in the single-line diagram.

Figure B-2 shows the steady state nose curves (P-V curves) for various loads with unity power factor fed from a voltage source at 16.5 kV over an overhead contact line. The reference case operating point is specially marked. It has been observed that the reference case has a stability margin for a voltage collapse of more than 1 MW (~25 %) and 15 km (~25 %).

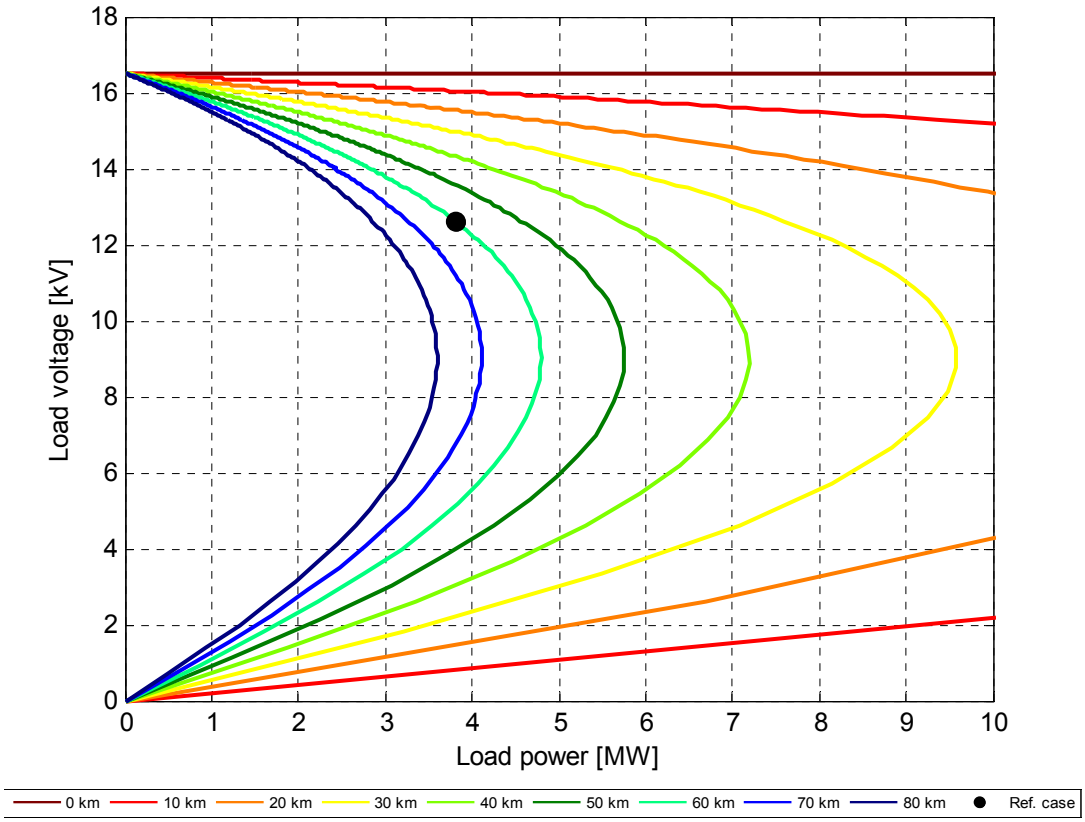

Figure B-2: Nose curves (P-V curves) for power transfer over an overhead contact line for a load with unity power factor.

B.2 Rotary converter parameters

B.2.1 Synchronous machines

The rotary converter synchronous-machine parameters used in this thesis are given in Table B-1. They have all been received from the former manufacturer of these machines, but the following changes, as described in Section 3.5.3, apply:

- The inertia constant is increased by 5% to take the exciters into account.
- The motor q-axis sub-transient reactance is increased by 42% in order to adapt to the poor damping observed in reality (see Section 3.5.3).

Table B-1: Rotary-converter synchronous-machine parameters.

Parameter	Unit	Motor	Generator
S_N – Rated power	MVA	4.4	4.0
U_N – Rated voltage	kV	6.3	4.0
X_a – Stator leakage reactance	pu	0.11	0.096
R_a – Stator resistance	pu	0.0033	0.00175
X_d – D-axis synchronous reactance	pu	0.90	1.02
X_d' – D-axis transient reactance	pu	0.24	0.12
X_d'' – D-axis sub-transient reactance	pu	0.165	0.10
$X_q = X_q'$ – Q-axis synchronous reactance	pu	0.40	0.47
X_q'' – Q-axis sub-transient reactance	pu	0.34	0.11
T_{d0}' – D-axis transient time constant	s	4.0	8.6
T_{d0}'' – D-axis sub-transient time constant	s	0.04	0.08
T_{q0}'' – Q-axis sub-transient time constant	s	0.10	3.4
H – Inertia constant	MWs/MVA	1.70	1.87

The reactances are unsaturated and saturation in is not included in the model.

B.2.2 Transformers

The parameters for the transformers connecting the rotary converter to the respective grids used in this thesis are given in Table B-2. The data are found in test protocols.

Table B-2: Rotary-converter transformer parameters.

Parameter	Unit	Motor	Generator
S_N – Rated power	MVA	4.4	4.0
U_{N1} – Rated voltage first winding	kV	66	4.0
U_{N2} – Rated voltage second winding	kV	6.3	16.6
ER_{12} – Short-circuit resistance	pu	0.0054	0.014
EX_{12} – Short-circuit reactance	pu	0.079	0.034

B.3 Automatic voltage regulator parameters

The parameters for the exciters and ASEA YGUA automatic voltage regulators used in this thesis are given in Table B-3. The standard excitation system model IEEE Type DC1A 'Excitation system with DC commutator exciter' ([1]) is used. The background for the different parameter values are:

- T_R is assumed to be half of the rectifier diode-bridge switching frequency equal to a quarter of a fundamental period.
- K_A is calculated by Stensby [167] based on measurements from Landström [108].
- T_A and T_F are measured in Landström [108].
- K_E is according to Högberg [87], zero due to rheostat adjustment.
- T_E, VR_{MIN} and VR_{MAX} are found for the motor exciter by Stensby [168]. Similar measurements and calculations are performed for generator exciter.
- K_F is assumed to be equal to typical values as given by Andersson and Fouad [11], page 300.

Table B-3: Rotary-converter exciter and automatic voltage regulator parameters.

Parameter	Unit	Motor	Generator
T_R – Regulator input filter time constant	s	0.005	0.015
K_A – Regulator amplifier gain	pu	382	382
T_A – Regulator amplifier time constant	s	0.11	0.11
K_E – Exciter constant related to self-excited field	pu	0.0	0.0
T_E – Exciter time constant	s	0.46	0.53
K_F – Regulator stabiliser circuit gain	pu	0.04	0.04
T_F – Regulator stabiliser circuit time constant	s	0.7	0.7
VR_{MIN} – Min value of regulator output	pu	-2.9	-3.5
VR_{MAX} – Max value of regulator output	pu	2.9	3.5

No current (power) dependent voltage charateristic is used ($R_C = X_C = 0\%$).

B.4 Vehicle model parameters

B.4.1 Electrical component values

The vehicle's nominal power is 6.4 MW measured on wheel, which is used as the base power for the per unit system. Taking losses and 5 % overload into account as shown by Steimel [163], the rated power is 7.35 MVA. The line-side converter's switching frequency is 250 Hz.

The vehicle transformer and DC-link parameters are listed in Table B-4 and Table B-5, respectively.

Table B-4: Vehicle transformer parameters.

Parameter	Unit	Value	Source
S_N – Rated power	MVA	7.35	Calculated above
U_{N1} – Rated voltage first winding	kV	15	Steimel [163]
U_{N2} – Rated voltage second winding	kV	1.568	Steimel [163]
ER_{12} – Short-circuit resistance	pu	0.005	Steimel [163]
EX_{12} – Short-circuit reactance	pu	0.333	Steimel [163]

Table B-5: Vehicle DC-link parameters.

Parameter	Unit	Value	Source
U_{dcN} – Rated voltage	kV	2.8	Steimel [163]
C_d – DC-link capacitor	mF	24.4	= 0.026·7.35/2.8^2
C_2 – Second-harmonic filter capacitor	mF	16.52	Steimel [163]
L_2 – Second-harmonic filter inductor	mH	1.375	Steimel [163]
R_2 – Second-harmonic filter resistor	mΩ	30	Mikus [127]

According to Equation (6.1) the DC-link discharge time is:

$$T_C = \left(C_d + C_2\right)\frac{U_{dcN}^2}{P_{dcN}} = \left(0.0244 + 0.01652\right)[F]\frac{\left(2800[V]\right)^2}{7350000[VA]} = 0.0436[s]$$

B.4.2 Control system parameters

The vehicle control-system parameters used in the original model in this thesis are listed in Table B-6. The per unit values are related to S_{Base} = 6.4 MW and the transformer secondary side voltage U_{Base} = 1.558 kV.

Table B-6: Vehicle control system parameters.

Parameter	Unit	Value	Source
Ku_{SOGI} – Voltage measurement SOGI gain	pu	0.8	Selected
Ki_{SOGI} – Current measurement SOGI gain	pu	3	Selected
Kp_{PLL} – Phase-locked loop gain	pu	51	Based on Ciobotaru, et al. [43]
Ti_{PLL} – Phase-locked loop integration time	s	0.079	Based on Ciobotaru, et al. [43]
Kp_{VC} – DC-link voltage controller gain	pu	1.67	Section 6.2.2
Ti_{VC} – DC-link voltage controller integration time	s	0.06	Section 6.2.2
Kp_{CC} – AC current controller gain	pu	0.87	Based on Harnefors, et al. [74]
Ti_{CC} – AC current controller integration time	s	180	Stanke [160]
Tu_{DC} – DC-link voltage measurement filter bandwidth	Hz	100	Selected
Ti_{DC} – Motor current measurement filter bandwidth	Hz	100	Selected
Tf_{CPL} – Motor damping filter time constant	s	0.15	From a real locomotive, Eisele [64]

Appendix C Linear analysis and eigenvalue analysis introduction

A common way to study small-signal stability in electric power systems is by linear analysis and eigenvalue considerations (Kundur [106]). Such tools are used to a large extent in this thesis, and therefore it has a value to introduce these mathematical tools. A deeper description of linear analysis applied to electric power systems can be found in the thesis written by Persson ([142] and [141]).

Together with time domain simulations, linear analysis represents a powerful tool. A dynamical system may be systematically analysed instead of being done by trial and error only.

Even if linear analysis as described here and eigenvalue considerations are not often seen in traction power system stability studies, eigenvalue considerations are not new to railways. That is, it is used to study both the rail-wheel mechanical interaction as done by Andersson, et al. [10], or the overhead contact line-current collector mechanical interaction as done by Sølvberg [175].

C.1 Linearisation

A dynamical system may be described by a number of characteristic differential equations, normally based on the physics of the system to be studied. Based on these equations and information about the initial conditions, the state of the system can be determined and the system's response to a disturbance can be calculated.

If a system is non-linear, which a power system normally is (Kundur, et al. [107]), the system is commonly linearised around an operating point. Then so-called Δ-values that describe small deviations of the states from the linearisation point are used. In that way, the mathematical tools which are used for linear systems can be utilised for non-linear systems as well, such as traction power systems. The application of these tools is formally valid in the vicinity of the linearisation point only.

C.2 Eigenvalues

A common way to describe a linear or linearised system is by a state space model as shown in Equation (C.1). $\mathbf{x}$ is the state vector containing the state variables, i.e., the variables from which the time derivative is to be considered. $\mathbf{u}$ is the vector containing disturbance variables. $\dot{\mathbf{x}}$ is a vector containing the time derivative of the state variables, and $\mathbf{y}$ is called the output vector.

$$\begin{aligned} \Delta\dot{\mathbf{x}} &= \mathbf{A}\Delta\mathbf{x} + \mathbf{B}\Delta\mathbf{u} \\ \Delta\mathbf{y} &= \mathbf{C}\Delta\mathbf{x} + \mathbf{D}\Delta\mathbf{u} \end{aligned} \tag{C.1}$$

Matrix **A** is the state matrix and contains important information about the inherent qualities of the linear or linearised system. **B**, **C** and **D** will not be used further in this thesis. The roots of the characteristic Equation (C.2), λ, are called the eigenvalues of the system describing the system's so-called system modes. **I** is the identity matrix.

$$\det(\mathbf{A} - \lambda\mathbf{I}) = 0 \tag{C.2}$$

The number of eigenvalues for a system is equal to the dimension of **A** and the number of independent first-order differential equations describing the system. An eigenvalue is a complex number $\lambda = \sigma + j\omega_{res} = \sigma + j2\pi f$ describing a mode of the system in which the imaginary part describes the oscillation frequency and the real part describes the damping or time decay of the oscillation.

Complex eigenvalues appear as conjugate pairs. A negative real part identifies a damped and hence stable mode in which the amplitude of the oscillation will become zero as time increases after disturbance. A positive real part describes a negatively damped and hence unstable mode in which the oscillation amplitude will increase as time increases.

An example of a complex pair of eigenvalues $\lambda_{1,2} = -0.31$ [1/s] $\pm j1.55$ [Hz] plotted in the complex plane is shown in Figure C-1 together with the corresponding second-order system's impulse response in the time domain. The real parts of the eigenvalues represent the inverse of the envelope curve's decay time constant. After one time constant ($1/\sigma$), the envelope curve has decreased to $1/e$ times the initial value y_0.

Eigenvalues without imaginary part are non-oscillatory, and the envelope curve in Figure C-1 will then represent $\lambda_3 = -0.31$ [1/s].

Even if eigenvalues only formally describe linear and linearised systems, their real and imaginary part represents important attributes that can be used for a simple description of some transients or oscillations seen in non-linear dynamical systems. For example, when measuring an oscillation, it might be useful to describe it by its frequency and its damping or decay. Based on the time domain representation of an eigenvalue describing a harmonic oscillator (Irgens [88]), Equation (C.3) can be developed and applied on the curve in Figure C-1 in order to find the apparent or dominating eigenmode.

$$\lambda_{1,2} \approx \frac{1}{t_2 - t_1}\ln\left(\frac{y_2 - y_\infty}{y_1 - y_\infty}\right) \pm j\frac{1}{t_2 - t_1} \tag{C.3}$$

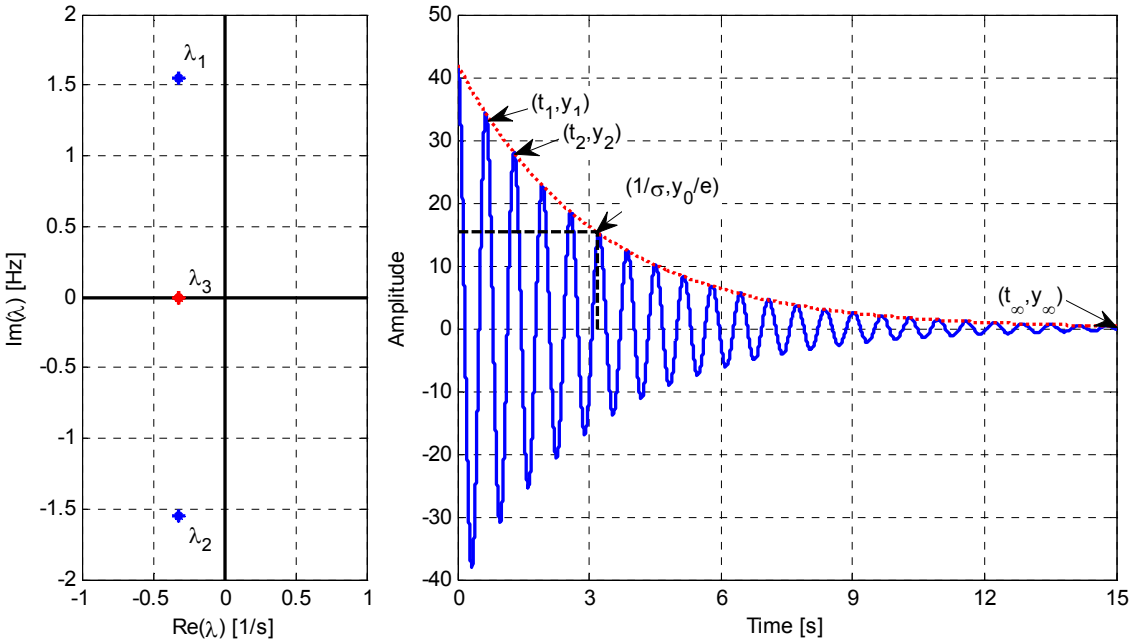

Figure C-1: A complex pair of eigenvalues and a real valued eigenvalue shown in the complex plane and their impulse response in time domain.

For more complex responses in which several modes are excited, for example from field tests or time domain simulations, Prony analysis may be used (Hauer, et al. [76]). Prony's method allows for the estimation of frequency, damping, amplitude and phase components of a uniformly sampled signal.

The damping ratio ζ determines the rate of decay of the amplitude of the oscillation, i.e., how effective the damping is, and is defined as in Equation (C.4).

$$\zeta = \frac{-\sigma}{\sqrt{\sigma^2 + \omega_{osc}^2}} \tag{C.4}$$

C.3 Participation factors

For every eigenvalue λ_i there exist two eigenvectors, the right eigenvector Φ_i and the left eigenvector Ψ_i. These can be calculated based on the state matrix **A** as in Equations (C.5) and (C.6), respectively. The superscript T denotes the transpose of the associated vector.

$$\mathbf{A}\boldsymbol{\Phi}_i = \lambda_i \boldsymbol{\Phi}_i \tag{C.5}$$

$$\boldsymbol{\Psi}_i^T \mathbf{A} = \lambda_i \boldsymbol{\Psi}_i^T \tag{C.6}$$

The right eigenvector describes the relative activity of the system's state variable in a particular mode i, also called the mode shape. The left eigenvector weights the state variables' contribution in the i^{th} mode. One problem in using the eigenvectors

individually for identifying the relationship between states and modes is that their elements depend on the state variables' units and scaling. However, calculating the participation factors $\boldsymbol{P}_i$ for the mode as in Equation (C.7) (Perez-Arriaga, et al. [140]), the eigenvectors are normalised so that the sum of participation factors associated with any mode or with any state variable is equal to 1. A participation factor is a measure of the relative participation of one state variable in one specific mode or vice versa. This means that it is possible to determine what state variables and hence components that participate in and dominate one system mode.

$$\mathbf{P}_i = \boldsymbol{\Psi}_i^T \boldsymbol{\Phi}_i \tag{C.7}$$

Participation factors are to be understood as indicative and not an exact numbers, i.e., they are not as formal as the eigenvalues.

C.4 Simulation tool used

Different power system analysis computer programs include tools for linear analysis and eigenvalue calculations (Slootweg, et al. [159]). One such program is SIMPOW (SIMulation of POWer system) that is used for the study of the complex power systems in this thesis.

SIMPOW is an integrated software for the simulation of power systems (Fankhauser, et al. [67]). It covers a wide range of network applications, but focuses mainly on dynamic simulation in time domain and analysis in frequency domain. The software includes an optimal power flow module that is the basis for further dynamical simulations. Time domain simulations can be performed in either instantaneous values or by RMS values. A linear analysis module allows for the linearisation of the system's differential equations for eigenvalue analysis (Slootweg, et al. [159]). The user is allowed to tailor his/her own models of almost all the system's components by a built-in programming language if the standard component library is inadequate.

SIMPOW is used for power system analysis by both the Norwegian and Swedish National Rail Administrations. The standard library includes a wide area of railway related components such as synchronous-synchronous rotary converters (Palesjö [137] and [138]) and various types of static converters ([3]). However, an instantaneous value model of a single-phase synchronous machine does not yet exist and is not developed in present thesis.

Appendix D Vehicle dynamical model source code

This appendix includes the Dynamic Simulation Language (DSL) code for modelling the advanced electrical rail vehicle in both standard and enhanced RMS modes (called TRANSTA in SIMPOW) and instantaneous values mode (called MASTA in SIMPOW). The initial load flow and the initialisation of the state variables for the dynamical simulation are not included in the code shown here:

```
!! Orthogonalisation (SOGI and SOGI imitation)

IF (ACTYPE.LT.0) THEN !!TRANSTA

  UA1T: 1/KUSOGI*(1/WREF+TDELAY)*.D/DT.UA1T = UPRE(AC1)/NTPU - UA1T
  UB1T: 1/KUSOGI*(1/WREF+TDELAY)*.D/DT.UB1T = UPIM(AC1)/NTPU - UB1T

  IAT: 1/KISOGI*(1/WREF+TDELAY)*.D/DT.IAT = -_PRE(IAC) - IAT
  IBT: 1/KISOGI*(1/WREF+TDELAY)*.D/DT.IBT = -_PIM(IAC) - IBT

  UA1 = UA1T
  UB1 = UB1T

  IA = IAT
  IB = IBT

ELSE !! MASTA

  UA1M: .D/DT.UA1M = WREF * (KUSOGI*(U0(AC1)/NTPU-UA1M) - UB1M)
  UB1M: .D/DT.UB1M = WREF * UA1M

  IAM: .D/DT.IAM = WREF * (KISOGI*(-I0(IAC)-IAM) - IBM)
  IBM: .D/DT.IBM = WREF * IAM

  UA1 = UA1M
  UB1 = UB1M

  IA = IAM
  IB = IBM

ENDIF
```

```
!! PARK Transform

UD1 = UA1*COS(TETA) + UB1*SIN(TETA)
UQ1 = -UA1*SIN(TETA) + UB1*COS(TETA)

ID = IA*COS(TETA) + IB*SIN(TETA)
IQ = -IA*SIN(TETA) + IB*COS(TETA)


!! PLL

X1: TIPLL * .D/DT.X1 = +UQ1

IF (ACTYPE.LT.0) THEN !!TRANSTA

  WT = KPPLL*(X1 + UQ1)
  TETAT: .D/DT.TETAT = WT

  W = (WT + WREF)/WREF
  TETA = TETAT

  TETAPLL: .D/DT.TETAPLL = WT
  IF (TETAPLL .GT. 2*PI) THEN
    TETAPLL = TETAPLL - 2*PI
  ENDIF
  PHASE = TETAPLL + TETAT0

ELSE !! MASTA

  WM = WREF + KPPLL*(X1 + UQ1)
  TETAM: .D/DT.TETAM = WM

  W = WM/WREF
  TETA = TETAM

  TETAPLL: .D/DT.TETAPLL = WM
  IF (TETAPLL .GT. 2*PI) THEN
    TETAPLL = TETAPLL - 2*PI
  ENDIF
  PHASE = TETAM - FI0

ENDIF


!! DC-link voltage measurement

UDCFIL: TUDC * .D/DT.UDCFIL = U(BUS2) - UDCFIL


!! Motor current measurement

IDCMFIL: TIDC *  .D/DT.IDCMFIL = (IDCM) - IDCMFIL
```

```
!! Power oscillation damper

UAC1 = SQRT( UD1**2 + UQ1**2 )
UAC1W: TW * .D/DT.UAC1W = TW * .D/DT.UAC1 - UAC1W
UAC1WC: TPOD * .D/DT.UAC1WC = UAC1W - UAC1WC

!! Limiting
IF (KPOD*UAC1WC .GT. UPODLIM) THEN
  UPOD = UPODLIM
ELSEIF (KPOD*UAC1WC .LT. -UPODLIM) THEN
  UPOD = -UPODLIM
ELSE
  UPOD = KPOD*UAC1WC
ENDIF

!! DC-link voltage controller

IF (PODNO .EQ. 1) THEN
  EPS = UDCREF + UPOD - UDCFIL
ELSE
  EPS = UDCREF - UDCFIL
ENDIF

X2: TIVC * .D/DT.X2 = EPS * KPVC
KSI = X2 + EPS * KPVC

IDCREF = KSI + IDCMFIL
IDREF = (IDCREF) * UDCFIL/UD1

IF (PODNO .EQ. 2) THEN
  IQREF = 0 - UPOD
ELSE
  IQREF = 0
ENDIF

!! AC current controller

DID = IDREF - ID
DIQ = IQREF - IQ

X3D: TICC * .D/DT.X3D = DID * KICC
X3Q: TICC * .D/DT.X3Q = DIQ * KICC

UDREF = UD1 - (X3D + DID*KICC) + IQ*XT
UQREF = UQ1 - (X3Q + DIQ*KICC) - ID*XT


!! Inverse PARK Transform

!!UAREF = UDREF*COS(-TETA) + UQREF*SIN(-TETA)
!!UBREF = -UDREF*SIN(-TETA) + UQREF*COS(-TETA)

UAREF = UDREF*COS(TETA) - UQREF*SIN(TETA)
UBREF = UDREF*SIN(TETA) + UQREF*COS(TETA)
```

```
!! PWM current injection

IF (ACTYPE.LT.0) THEN !!TRANSTA

  !! AC currents
  IF (CC .EQ. 1) THEN !! Use CC
    _PRE(IAC): UPRE(BUS1) = UAREF
    _PIM(IAC): UPIM(BUS1) = UBREF
  ELSE !! Bypass CC
    _PRE(IAC): _PRE(IAC) = -(IDREF * COS(TETA) - IQREF * SIN(TETA))
    _PIM(IAC): _PIM(IAC) = -(IDREF * SIN(TETA) + IQREF * COS(TETA))
  ENDIF

  !! DC current
  I(IDC): U(BUS2)*I(IDC) + _PRE(IAC)*UPRE(BUS1) + _PIM(IAC)*UPIM(BUS1) = 0

ELSE !!MASTA

  !! AC currents
  IF (CC .EQ. 1) THEN !! Use CC
    I0(IAC): U0(BUS1) = UAREF
  ELSE !! Bypass CC
    I0(IAC): I0(IAC) = -(IDREF * COS(TETA) - IQREF * SIN(TETA))
  ENDIF
  !! DC current
  IDC: U(BUS2)*IDC + 2*U0(BUS1)*I0(IAC) = 0  !!Active power balance

ENDIF
```

Appendix E Vehicle DC-link voltage control eigenvalues

Table E-1 lists the eigenvalues for the vehicle DC-link eigenmode found by time simulation and linearisation in Sections 5.5.4 and 5.6.4.

Table E-1: Dominant mode. Operation point: 3.67 MW load on a 60 km long line.

Case (model)	Current controller	Displacement angle [deg]	Eigenvalue [1/s] ± *j*[Hz]	Dominant mode from time plot [1/s] ± *j*[Hz]
Inst. value	No	0	+1.51 + *j*0.08 / Not identified	-9.06 ± *j*2.80
		45	-11.3 ± *j*2.47	-8.84 ± *j*2.87
		90	-22.4 ± *j*3.34	-8.99 ± *j*2.73
		135	-12.3 ± *j*3.37	-8.83 ± *j*2.77
RMS	No	N/A	-10.1 ± *j*2.53	-9.75 ± *j*2.52
RMS L·di/dt	No	N/A	-9.86 ± *j*2.76	-9.52 ± *j*2.67
Inst. value	Yes	0	+3.65 + *j*0.00 / Not identified	-4.84 ± *j*2.85
		45	Not identified	-4.71 ± *j*2.84
		90	Not identified	-4.85 ± *j*2.91
		135	-18.0 ± *j*1.49	-4.57 ± *j*2.90
RMS	Yes	N/A	-7.89 ± *j*2.56	-8.21 ± *j*2.58
RMS L·di/dt	Yes	N/A	-6.69 ± *j*2.90	-6.43 ± *j*2.91

Appendix F Vehicle no-load input admittance

Figure F-1 shows the vehicle no-load input admittance calculated by frequency sweeps of the enhanced RMS model (including the current controller) as described in Section 8.4.2.2. The motor power is zero and the line voltage is 16.5 kV as in the long line stability test in Section 5.7. The line length between the stiff voltage source and the vehicle is 0 km. Only the Y_{dd} is considered in this thesis in Section 8.2.6 and it shows a 180 degrees phase shift at 3.36 Hz. Further interpretation of these frequency responces is needed.

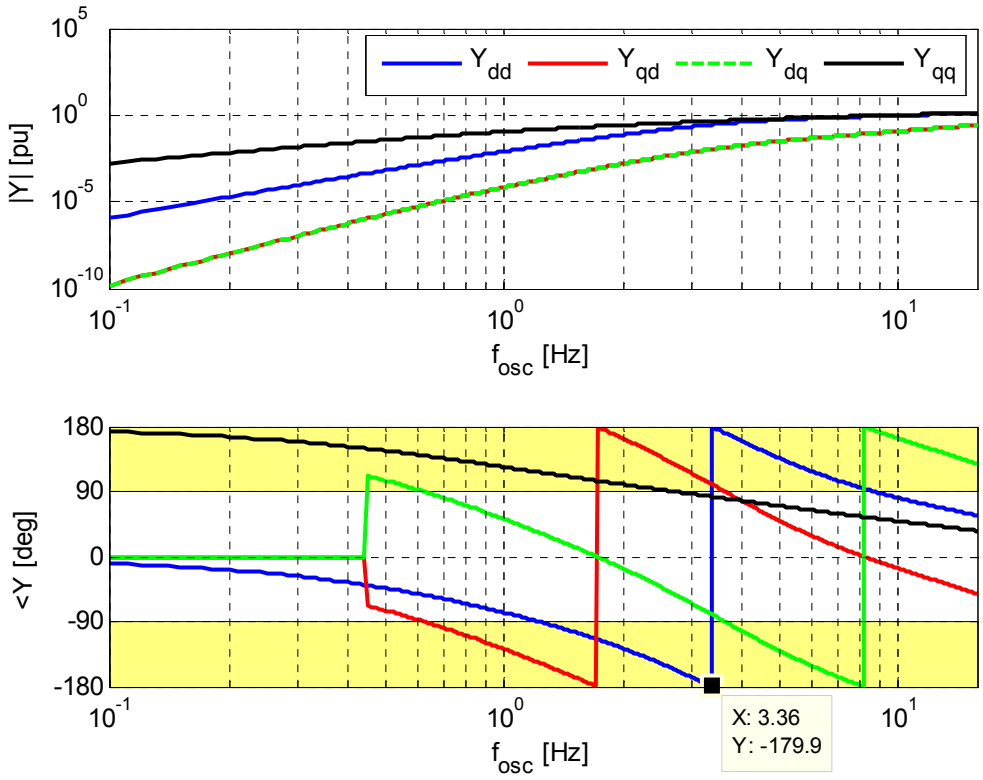

Figure F-1: Vehicle input admittance in no-load.